EPA U.S. Environmental Protection Agency
Office of Research and Development
Industrial Environmental Research Laboratory
Research Triangle Park, North Carolina 27711

EPA-600/7-77-066
June 1977

REVIEW OF LASER RAMAN AND FLUORESCENCE TECHNIQUES FOR PRACTICAL COMBUSTION DIAGNOSTICS

Interagency
Energy-Environment
Research and Development
Program Report

RESEARCH REPORTING SERIES

Research reports of the Office of Research and Development, U.S. Environmental Protection Agency, have been grouped into seven series. These seven broad categories were established to facilitate further development and application of environmental technology. Elimination of traditional grouping was consciously planned to foster technology transfer and a maximum interface in related fields. The seven series are:

1. Environmental Health Effects Research
2. Environmental Protection Technology
3. Ecological Research
4. Environmental Monitoring
5. Socioeconomic Environmental Studies
6. Scientific and Technical Assessment Reports (STAR)
7. Interagency Energy-Environment Research and Development

This report has been assigned to the INTERAGENCY ENERGY-ENVIRONMENT RESEARCH AND DEVELOPMENT series. Reports in this series result from the effort funded under the 17-agency Federal Energy/Environment Research and Development Program. These studies relate to EPA's mission to protect the public health and welfare from adverse effects of pollutants associated with energy systems. The goal of the Program is to assure the rapid development of domestic energy supplies in an environmentally--compatible manner by providing the necessary environmental data and control technology. Investigations include analyses of the transport of energy-related pollutants and their health and ecological effects; assessments of, and development of, control technologies for energy systems; and integrated assessments of a wide range of energy-related environmental issues.

REVIEW NOTICE

This report has been reviewed by the participating Federal Agencies, and approved for publication. Approval does not signify that the contents necessarily reflect the views and policies of the Government, nor does mention of trade names or commercial products constitute endorsement or recommendation for use.

This document is available to the public through the National Technical Information Service, Springfield, Virginia 22161.

EPA-600/7-77-066
June 1977

REVIEW OF LASER RAMAN AND FLUORESCENCE TECHNIQUES FOR PRACTICAL COMBUSTION DIAGNOSTICS

by

A.C. Eckbreth, P.A. Bonczyk, and J.F. Verdieck

United Technologies Research Center
East Hartford, Connecticut 06108

Contract No. 68-02-2176
Program Element No. EHE624

EPA Project Officer: William B. Kuykendal

Industrial Environmental Research Laboratory
Office of Energy, Minerals, and Industry
Research Triangle Park, N.C. 27711

Prepared for

U.S. ENVIRONMENTAL PROTECTION AGENCY
Office of Research and Development
Washington, D.C. 20460

FOREWORD

Under Contract 68-02-2176 sponsored by the Environmental Protection Agency, the United Technologies Research Center (UTRC) is conducting an analytical and experimental investigation aimed at developing non-perturbing, spatially precise, in-situ diagnostic techniques to measure species concentration and temperature in practical combustion flames, i.e., luminous, particle-laden, turbulent. Under Task I, a comprehensive review has been conducted and is reported herein of potential, nonintrusive laser light scattering techniques for thermometry and chemical composition measurements in hostile combustion environments such as furnaces and gas turbine combustors.

TABLE OF CONTENTS

TABLE OF CONTENTS (CONT'D)

LIST OF FIGURES

LIST OF TABLES

LIST OF SYMBOLS

A	(1) excited molecular state designation (2) aperture diameter
A_{ij}	Einstein coefficient for spontaneous emission
A_{ℓ}	(1) area of laser beam (2) area of lens
A_o	principal axis rotational constant
a	(1) molecular state designation (2) particle radius (3) lineshape parameter
α	bond angle
α_a	absorption coefficient
B	(1) excited molecular state designation (2) molecular rotational constant
B_{ij}	Einstein coefficient for stimulated absorption/emission
B_e	equilibrium rotational constant
B_o	principal axis rotational constant
b	molecular state designation
b_{ij}	stimulated absorption/emission rate
C	excited molecular state designation
C_o	principal axis rotational constant
C_∞, C_{2v}, C_s	point group symbols
c	speed of light
c_a	medium specific heat
c_s	particulate specific heat
Γ	Raman linewidth
D	(1) atomic state designation (2) lens diameter (3) particle diameter
D_∞, D_{3h}, D_{3d}	point group symbols
Δ	(1) molecular state designation (2) fractional population difference (c) change in associated parameter

Δ_j	population difference
$\frac{\partial\sigma}{\partial\Omega}$	differential scattering cross-section
δ	absorption parameter
E	(1) electric field intensity (2) energy
ϵ	light collection efficiency
F	(1) atomic state designation (2) lens f-number
f	(1) lens focal length (2) fraction of energy absorbed by particle
f^s	Stokes bandwidth factor
f^a	anti-Stokes bandwidth factor
$f_{v=0}$	fraction of species in v = 0
$f_{J=J_{MAX}}$	fraction of species in $J = J_{MAX}$
G	(1) atomic state designation (2) geometrical constant
g	(1) stimulated Raman gain factor (2) even inversion symmetry
g_i	(1) level degeneracy (2) susceptibility strength factor
η	photocathode quantum efficiency
H	atomic state designation
h	Planck's constant
I_i	(1) CARS intensity (2) laser intensity at frequency ω_i
I_A	A-axis moment of inertia
I_L	laser intensity
$I_{L\nu}$	laser spectral intensity
J	(1) sum of spin and orbital momentum (2) molecular rotational quantum number

K	Knudsen number
k	Boltzmann's constant
k_a	medium thermal conductivity
k^s	Stokes power calibration factor
k^a	anti-Stokes power calibration factor
L	total electronic orbital momentum
l	(1) Raman or fluorescence sample length (2) absorption path length
$\ell_{\|\|}$	coaxial light collection sampling extent
$\ell_{\perp}$	right-angle light collection sampling extent
Λ	projection of orbital momentum on molecular symmetry axis
λ	wavelength of light
M	number of populated rotational levels
M_{ij}	transition moment between i and j
m	refractive index
N	(1) number density (2) background luminosity
N^o	total equilibrium species number density
N_i	instantaneous number density in state i
$N_i{}^o$	total equilibrium species number density in state i
n	number density
n_p	particulate number density
n_n	number of noise photons
n_s	number of signal photons
ν_i	(1) frequency of light (2) normal mode vibrational frequencies
ν_S	frequency of Stokes light
ν_A	frequency of anti-Stokes light
ν_L	frequency of laser
O_h	point group symbol

P	atomic state designation
$^2P_{1/2,3/2}$etc	atomic state designation
P_i	(1) incident laser power (2) CARS power
P_r^s	Stokes power
P_r^a	anti-Stokes power
P_{nm}	induced electric moment matrix element
P_M	Mie power
Π	molecular state designation
π	pi
Q	Q-branch molecular transition
Q_{ij}	collisional relaxation rate between states i and j
R	saturation parameter
R'	saturation parameter
$\mathfrak{R}$	radiation energy density
r_o	bond length
ρ	laser energy density
ρ_a	medium mass density
ρ_s	particulate mass density
S	(1) atomic state designation (2) total electronic spin momentum (3) Raman signal power
S_s	signal channel signal
S_n	noise channel signal
S_F	fluorescence power
Σ	molecular state designation
σ_e	light extinction cross-section
σ_{abs}	absorption cross-section
T	temperature

T_d	point group symbol
τ_p	perturbation heat transfer time
τ_c	heat conduction time
u	odd inversion symmetry
V	sample volume
$V_{\|\|}$	coaxial light collection sample volume
$V_{\perp}$	right-angle light collection sample volume
v	molecular vibrational quantum number
ϕ	CARS interaction region diameter
X	molecular state designation
χ	molecular susceptibility
χ'	real part of susceptibility
χ''	imaginary part of susceptibility
χ^{nr}	non-resonant part of susceptibility
Ω	light acceptance solid angle
z	phase matching distance
ω	circular frequency (radians)
ω_i	circular frequency (radians)

INTRODUCTION

With the advent of laser light sources, light scattering spectroscopic diagnostic techniques are assuming an ever-increasing role in a broad spectrum of physical investigations. Of particular importance is the potential application of laser spectroscopy to the hostile, yet sensitive, environments characteristic of those in which combustion occurs. These diagnostic techniques should facilitate greatly improved understanding of a variety of combustion processes which, in turn, should lead to enhanced efficiencies and cleanliness in energy, propulsion and waste disposal systems.

Recently, exciting experimental demonstrations of the potential of a variety of Raman processes (spontaneous, near-resonant, coherent, stimulated) and laser fluorescence techniques have appeared in studies dealing primarily with laboratory flames. Unlike the situation prevailing in the field of remote detection of atmospheric pollutants, where several comprehensive reviews have appeared comparing the capabilities and systems aspects of various diagnostic approaches, little work of a similar nature has appeared in connection with the remote, localized probing of practical combustion devices, e.g. funaces, gas turbine combustors. Although the pollutant detection review studies can be drawn upon, the measurement requirements and potential problem areas in practical flame diagnosis are sufficiently different to require a fresh perspective and review of measurement techniques more aptly suited for the extraction of species and temperature information from combustion devices. The objective of this report is to provide such a review. Realistically, such a review of diagnostic techniques must focus keenly on the problems and sources of noise which must be circumvented for successful application to practical devices. Since it is unlikely that any one technique will provide the species and temperature measurements over the range desired, systems considerations become important in ascertaining how the various approaches can be integrated together with maximum measurement rate and minimal redundancy. Such systems studies should also illuminate the tradeoffs between systems complexity and cost on the one hand, and probability of successful measurements on the other.

In addition to the need for a comprehensive review of various practical flame diagnostic techniques, there is the important requirement that the various approaches undergo laboratory testing to realistically evaluate the assumptions of and explore new research avenues raised by the review. Under Contract 68-02-2176 sponsored by the Environmental Protection Agency, the United Technologies Research Center (UTRC) is conducting an analytical and experimental investigation aimed at developing nonperturbing, spatially precise, in-situ diagnostic techniques for species and temperature measurements in practical flames. Under Task I, the review described above has been prepared and is presented herein. Under Task II, laboratory investigations of the most promising diagnostic techniques will be conducted. Hence, another objective of this report is to provide recommendations for the Task II experimental development program.

In the next section of this report, various laser diagnostic techniques potentially suitable for "point" temperature and species concentration measurements in flames are reviewed. From this list, four techniques are selected for detailed evaluation including: (1) spontaneous Raman scattering, (2) near-resonant Raman scattering, (3) laser fluorescence and (4) coherent anti-Stokes Raman scattering (CARS). The spectroscopy of species of combustion interest is discussed and the applicability of the foregoing techniques to detection of the various species is examined. Practical device considerations are reviewed with emphasis on sources of noise (e.g., luminosity, particulates), medium perturbations, laser and signal transmission, and signal averaging in temporally fluctuating media. Each diagnostic technique is then addressed in some detail in the order previously stated. Basic physics, species sensitivity, thermometry applicability, signal to noise, problem areas, and new variations of the techniques are included in these treatments. Measurement systems approaches are described together with approximate cost estimates, probability of success assessments and risk assignments. An integrated measurement system is described. The report ends with a series of general conclusions suggestive of future research efforts required for the evaluation and development of the more promising diagnostic approaches.

REVIEW OF POTENTIAL IN-SITU, POINT, COMBUSTION DIAGNOSTIC TECHNIQUES

There are a large variety of diagnostic processes potentially applicable to the remote, nonintrusive, point probing of combustion phenomena. Here these various processes will be briefly reviewed and from them, a list of the most promising technqiues for flame probing will be selected for further detailed study. In this review, attention will be directed ultimately only to those laser techniques which permit the determination of local species concentrations and temperature. Velocity measurements and emission spectroscopy techniques will not be considered.

The subject of combustion diagnostics has received a great deal of attention in the past few years. In the summer of 1974, the American Physical Society conducted a one month summer study to evaluate the role of physics in combustion (Ref. 1). Diagnostics for experimental combustion research received considerable attention. In May 1975, Project SQUID conducted a several day workshop devoted exclusively to combustion measurements in jet propulsion systems (Ref. 2). In January,1976, the combustion sessions of the AIAA 14th Aerospace Sciences Meeting emphasized combustion diagnostics (Ref. 3).

In Table I potential flame diagnostic techniques are listed; these have been drawn from a listing of techniques applicable to air pollution measurements (Ref. 4) gasdynamics (Ref. 5), and analytical chemistry (Ref. 6). Image formation and tracer techniques (Ref. 1) will not be considered.

TABLE I

POTENTIAL COMBUSTION DIAGNOSTIC TECHNIQUES

Elastic Scattering Processes
- Rayleigh
- Mie

Linear Inelastic Scattering Processes
- Raman
- Near-resonant Raman
- Fluorescence

Absorption Processes
- Resonant, Line of Sight
- Differential Absorption

Nonlinear Optical Processes
- Inverse Raman Scattering
- Raman-Induced Kerr Effect (RIKES)
- Stimulated Raman Scattering
- Hyper-Raman Scattering
- Coherent anti-Stokes Raman Scattering (CARS)
- Higher-order Raman Spectral Excitation Spectroscopy (HORSES)

Elastic Scattering Processes

Rayleigh Scattering

The elastic scattering of light quanta from molecules is termed Rayleigh scattering (see Fig. 1) and is the phenomenon giving rise to the blue appearance of the sky. Because the scattering process is elastic, the scattered light is unshifted in frequency and, hence, not specific to the molecule causing the scattering. Thus the technique can be used for total density measurements but not for individual species concentrations. Temperature measurements can be made by resolving the Doppler linewidth of the scattering (Ref. 7). From a practical viewpoint, Rayleigh diagnostics suffer from Mie interferences and spuriously scattered laser light and have been employed in only very clean situations. The technique has seen very limited utilization and is not suitable for practical combustor device probing.

Mie Scattering

Elastic scattering of light quanta from particulate matter is termed Mie scattering. It is not dependent on molecular number density of temperature and, hence, cannot be used to provide such information. It is the basic effect underlying laser Doppler velocimetry and differential absorption backscattering (Ref. 4) measurements. It can be a very strong process depending on particle number density and particle size, and is a potential source of interference as will be described later.

Linear Inelastic Scattering Processes

Raman and Near-resonant Raman Scattering

Raman scattering is the inelastic scattering of light from molecules as illustrated in Fig. 1, and is termed rotational, vibrational or electronic depending on the nature of the energy change which occurs in the molecule. The process is essentially instantaneous occurring within a time of 10^{-12} sec or less. The molecule may either become excited or deexcited depending on its original state prior to the interaction. Raman scattering is ideally suited to combustion diagnostics and has been widely applied in clean flames (Ref. 8). Visible wavelength lasers are typically employed since the strength of the scattering scales as the fourth power of the Raman frequency, but no specific wavelength is required. Due to the quantization of the molecular energy states, the Raman spectrum resides at fixed frequency separations from the laser line characteristic of the molecule from which the scattering emanates. Thus the Raman scattering is species specific and linearly proportional to species number density. Furthermore, spectral interferences between vibrational Raman bands in gases are rare. Temperature measurements are readily made from the distribution of the scattering. Unfortunately, Raman scattering is very weak with cross sections typically around 10^{-30} cm^2/sr, resulting in a collected Raman to laser energy ratio of 10^{-14} in flames. In practical combustion

SCATTERING PROCESSES

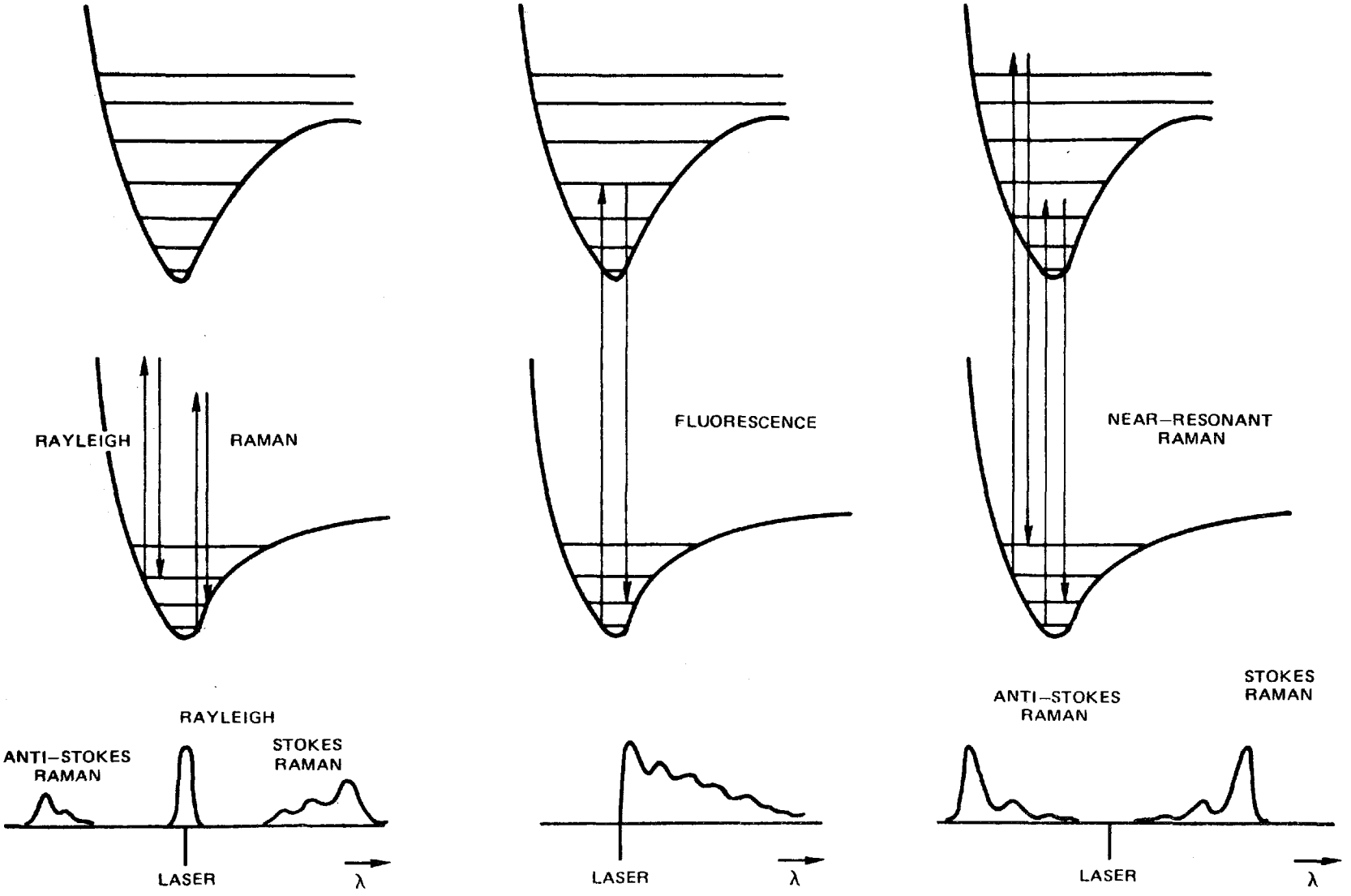

FIG. 1

situations, Raman scattering diagnostics are typically plagued by very low S/N ratios. Despite this fact, because of its many advantages, it will be given major consideration in this review.

If the incident laser wavelength is tuned near an electronic resonance of the molecule being probed, (Fig. 1), the Raman cross section can be resonantly enhanced perhaps by six orders of magnitude (Ref. 9). This process is termed near-resonant Raman scattering and deserves attention because of the greatly increased Raman signal strengths which may result. In the literature there is a great amount of discussion in regard to the distinction, if any, between resonance fluorescence and resonance Raman scattering. Most investigators now seem to agree that they are variations of the same physical process distinguishable by the proximity to resonance. It is generally believed that the nearly instantaneous process, insensitive to collisional quenching, which is characteristic of a Raman process, occurs off but near resonance. Consequently the terminology "near-resonant" Raman scattering is used here to distinguish it from fluorescence or resonance fluorescence which occurs on resonance, is longer-lived and subject to quenching. Unfortunately, many molecules of combustion interest do not contain electronic resonances accessible to currently available laser sources and hence are not amenable to near-resonant enhancement. In some instances, the sacrifices in laser characteristics which result in tuning to a certain resonance mitigate some or all of the enhancement achieved. Near-resonant Raman scattering will also be carefully considered.

Fluorescence and Resonance Fluorescence

Fluorescence is the emission of light from an atom or molecule following promotion to an excited state by various means: electron bombardment, heating, chemical reaction (chemiluminescence) or photon absorption (Fig. 1). Here only the last means will be considered (Ref. 10). The precise definition of fluorescence requires that emission occur between electronic energy states of the same multiplicity, i.e., same electronic spin states. Emission between states of different electronic spin is termed phosphorescence. In general, fluorescent lifetimes vary between 10^{-10} and 10^{-5} sec, much shorter than the phosphorescent lifetimes of 10^{-4} sec to seconds. The light emission may be shifted in wavelength from the incident light, fluorescence, or occur at the same wavelength, resonance fluorescence. In general it is desired to examine shifted emission to avoid potential interferences from particle (Mie) or spurious laser scattering. Fluorescence is of diagnostic interest since it is species specific, and the cross sections for fluorescence are generally many orders of magnitude stronger than Raman or near-resonant Raman scattering.

A molecule in an excited state may not necessarily emit radiation however; several other pathways of energy loss are available which may compete with fluorescence. Some of these are: dissociation, energy transfer to another molecule, energy transfer to other internal energy states within the same molecule, and chemical reaction. These processes competitive with fluorescence, termed quenching

processes, reduce the amount of fluorescence which can be obtained and obscure interpretation of the data. In principle, if all the quenching species densities are known and if all of the appropriate quenching rate data is available, analytical quenching corrections to the data would be possible. Because this is hardly ever the case, fluorescence techniques involving partial or complete saturation will be emphasized in this review since such approaches eliminate the problem of quenching or permit in-situ experimentally determined quenching corrections.

Absorption

Absorption techniques employing tunable lasers can provde very sensitive measurements of species concentrations using line-center techniques in flames (Ref. 11) or in the atmosphere (Ref. 4). They provde measurements averaged over a path and are not strictly point measurements. Mathematical inversion techniques can be applied to obtain spatial variations of properties generally in spatially symmetric situations but also in some nonsymmetric cases (Ref. 12). The results are, however, sensitive to the assumptions in the inversion process and may not always be rigorously accurate. Furthermore, the inaccuracy in the assumptions is often uncertain. Absorption techniques are not considered in this review because of these uncertainties and because they do not truly yield point,spatially precise measurements.

In differential absorption, one monitors radiation backscattered from distributed Rayleigh and Mie scattering and tunes the incident wavelength on and off the absorption line of interest. In this manner one measures the intial and final power over some pathlength, the attenuation resulting from absorption which permits determination of the species number density. Although differential absorption permits depth resolved measurements in pollutant detection (Ref. 4), it is unlikely to be successfully applicable to combustion diagnosis because of the short pathlengths involved (i.e., spatial resolution) and the spatial nonuniformity of scatterers (i.e., soot) from point to point in the combustor.

Nonlinear Optical Processes

Inverse Raman Scattering

Inverse Raman scattering is illustrated in Fig. 2 and is essentially an induced absorption process first disclosed by Jones and Stoicheff (Ref. 13). Physically the process originates through the imaginary component of the third order nonlinear susceptibility. As shown, two collinear beams, one a high intensity monochromatic source, the other a broadband continuum, traverse the medium under observation. Under high enough intensity, absorption of the continuum occurs at frequencies corresponding to the anti-Stokes Raman frequencies. Intensities just short of producing stimulated effects are required and the absorptions produced by low density

NONLINEAR OPTICAL PROCESSES

SPONTANEOUS RAMAN
(LINEAR, SHOWN FOR REFERENCE)

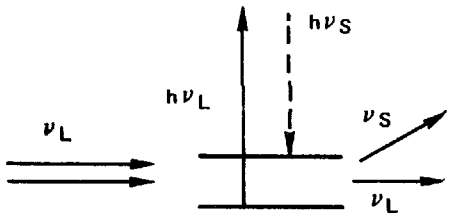

INVERSE RAMAN

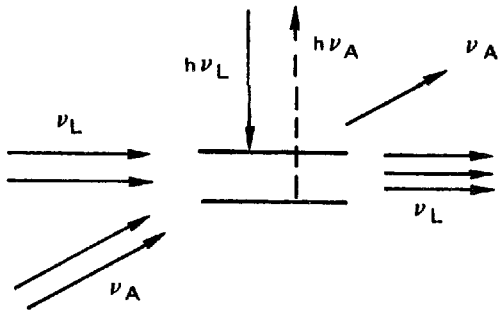

HYPER RAMAN

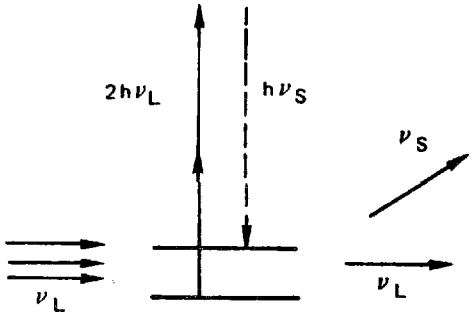

STIMULATED RAMAN

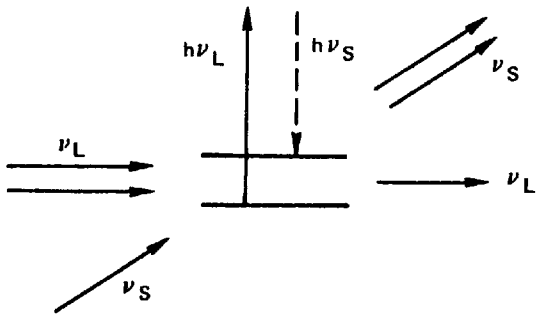

COHERENT ANTI–STOKES RAMAN

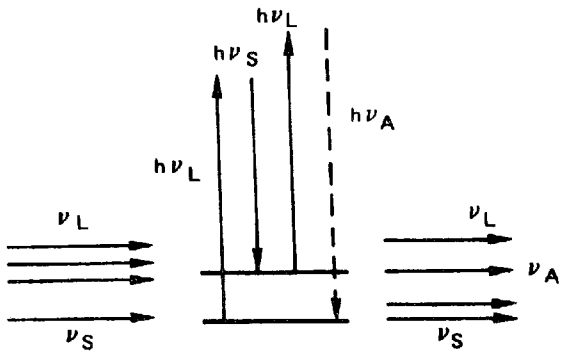

FIG. 2

gases are extremely weak. Clearly the absorption must be significantly larger than the anti-Stokes emissions produced by the intense source (Ref. 14). Inverse Raman scattering possesses all the difficulties of any weak absorption process, namely detecting a very small change in a strong signal. It does not appear to be a promising technique for combustion diagnosis.

Raman Induced Kerr Effect (RIKES)

This effect first disclosed in 1976 (Ref. 15) is remotely similar to the inverse Raman effect in that an intense monochromatic pump source interacts with a broadband probe source to produce a birefringence at the Raman frequencies. The effect is resonantly enhanced when the frequency difference between the pump and probe beams is tuned to the vibrational resonances of the molecule being probed. To avoid interferences from the optical Kerr effect, the pump beam is circularly polarized. The probe beam is linearly polarized and blocked by a crossed polarizer. In the presence of the pump source, the probe beam experiences birefringence at the Raman frequencies which are transmitted through the crossed polarizer to a suitable detector. The effect has yet to be demonstrated in gases. Practically, RIKES suffers from the rejection achievable with crossed polarizers which, at best, is about 10^{-6}. Due to slight birefringence in intervening optical elements, e.g., lenses, windows, practically achievable rejection is less. Turbulent fluctuations in combustion media may also produce undesired anisotropies. Clearly if the effect is not stronger than the best rejection achievable, no signal is observed which may well be the case in gases particularly at low concentrations. Until demonstrated to the contrary, this phenomenon does not appear promising for gas-phase combustion diagnostics.

Stimulated Raman Scattering

Stimulated Raman scattering (Ref. 16, 17) is illustrated in Fig. 2 and compared to spontaneous Raman scattering. Under intense laser radiation, the spontaneously generated Stokes photons experience exponential growth in the direction of laser propagation and emerge as a coherent beam. The technique, despite high conversion efficiencies in certain circumstances, is not promising for gas phase diagnostics for several reasons. It can only be generated in certain selected gases, e.g., N_2, H_2 and then only at many atmospheres of pressure with very high intensity laser pulses. Only selected lines of the Raman spectrum emerge which may make data interpretation ambiguous. The effect to date remains in the realm of nonlinear optics investigations and has not been applied for the above reasons to gas phase diagnosis.

Hyper Raman Scattering

Hyper Raman processes (Ref. 18) are illustrated in Fig. 2 and result in Raman spectra relative to the second harmonic of the exciting laser frequency. The scattering occurs into all solid angles and is very weak even at tens of atmospheres

of gas pressure with very high intensity laser sources. The technique is of no utility for combustion diagnosis.

Coherent Anti-Stokes Raman Scattering (CARS)

Coherent anti-Stokes Raman scattering (CARS) has received considerable attention over the past few years for combustion diagnosis based upon the pioneering investigations of Taran in France (Ref. 19). It is schematically diagrammed in Fig. 2. In brief two laser sources at ω_1 (pump) and ω_2 (Stokes) generate an intense coherent beam at $\omega_3 = 2\omega_1 - \omega_2$ (anti-Stokes or CARS) when the frequency difference $\omega_1 - \omega_2$ is tuned to a molecular vibrational resonance. The effect has no threshold per se and possesses two major advantages. The CARS signal produced is, first, many orders of magnitude stronger than conventional Raman scattering and, second, emerges as a coherent beam so that it can be completely collected. Since it is in the anti-Stokes region it resides in a region free of fluorescent interferences for the most part. The technique may well become to combustion thermometry what LDV has in combustion velocimetry. A major section of this report is devoted to CARS. Among its disadvantages are its double endedness (i.e., two opposed optical ports are required), its more complicated spectra and limited species concentration sensitivity. Several techniques have been proposed to circumvent this difficulty as will be seen.

Higher-Order Raman Spectral Excitation Studies (HORSES)

HORSES have been observed in connection with CARS experiments in liquids (Ref. 20). In addition to the CARS beam at $2\omega_1 - \omega_2$, higher order signals at $3\omega_1 - 2\omega_2$ and $3\omega_2 - 2\omega_1$ were observed corresponding to sequential four-wave mixing. These are very low intensity processes and it is unlikely that they offer any potential advantage to CARS particularly for gas phase diagnostics.

Selected Techniques

From this list of techniques, only four processes appear to offer potential promise for combustion diagnostics, namely: (1) spontaneous Raman scattering, (2) near-resonant Raman scattering, (3) laser fluorescence, and (4) coherent anti-Stokes Raman scattering (CARS). In subsequent sections of this report, the potential of these techniques will be examined in detail.

SPECIES SPECTROSCOPY

Spectroscopic data, which are available from the literature for those atomic and molecular species of interest in combustion processes are summarized in this section. A literature survey, hopefully complete but by no means exhaustive, up to December 1976 was performed. The data are presented in concise form in Tables II, III and IV, for atoms, diatomic molecules, and polyatomic molecules, respectively. An explanation of the often cryptic nomenclature used in molecular spectroscopy precedes each table.

In addition to the Tables, each atomic or molecular species is discussed individually with respect to spectroscopic (fluorescence, Raman, CARS, etc.) observation in a combustion or similarly hostile environment (e.g., electric discharge). Completeness has been attempted in the selection of combustion species included in the Tables. Even though there may be little interest in the measurement of some of the species considered, it is important to include them for consideration of potential interferences in Raman or fluorescence measurements. Atoms, diatomic molecules, and polyatomic molecules will be discussed respectively in the sections which follow.

Atomic Species of Interest in Combustion

Table II lists those atoms which may be found in a combusting chemical system, namely H, C, N, O, and perhaps S. The Table lists the electronic configuration of the valence shell, the electronic state, the J value for the electronic state and the term energy in wave numbers. Both forbidden and allowed transitions are indicated with their associated transition probabilities (in the form of the Einstein coefficient, A_{ij}).

The symbol for the electronic state gives the multiplicity of the state, $2S+1$ (where S is the total electronic spin) as a left superscript, and the orbital angular momentum, L, as a capital letter S, P, D, F, G, H, ... according to the values 0, 1, 2, 3, 4, 5, etc. for the orbital angular momentum. The possible values for J, often listed as a right hand subscript, are listed separately. J is the vector sum of the spin and orbital angular momentum. Atomic states are further classified as odd or even states according to whether the sum, $\Sigma\ell$, of the orbital angular momentum of all electrons in the atom is odd or even. These three quantities S, L, J, along with the energy of the state, completely define the state under the classification known as Russell-Saunders coupling (or LS coupling). Russell-Saunders coupling does not hold for high atomic weight atoms, which are of no concern here.

TABLE II

ATOMIC SPECIES OF INTEREST IN COMBUSTION[63,64]

Species	Configuration	State	J	Term Energy cm^{-1}	Transition	$A_{ij}(sec^{-1})$
H	$1s^1$	^2P	1/2	0.0		
	$2s^1$	^2P	1/2	82281.285	$2\ ^2P_{1/2} \rightarrow 1\ ^2S_{1/2}$	4.7×10^8
		^2S	1/2	82281.320	$2\ ^2S_{1/2} \rightarrow 1\ ^2S_{1/2}$	
		^2P	3/2	82281.650	Lyman 1215Å	
C	$2s^2 2p^2$	^3P	0	0.0		
			1	16.4		
			2	43.5		
		^1D	2	10193.7	$^3P \rightarrow {}^1D$ Spin Forbidden	< 1
		^1S	0	21648.4	$^3P \rightarrow {}^1S$ Spin Forbidden	< 1
		^3D	3	64088.0	$^3P \rightarrow {}^3D$ 1560Å	1.5×10^8
N	$2s^2 2p^3$	^4S	3/2	0.0		
		^2D	5/2	19223.0	$^4S \rightarrow {}^2D_{5/2,3/2}$	< 1
			3/2	19231.0	Spin Forbidden Laporte Forbidden	< 1
	$2s^2 2p^2 3s$	^4P	5/2 3/2 1/2	88135.0 AVE	$^4S \rightarrow {}^4P$ 1135Å	2.3×10^8
O	$2s^2 2p^4$	^3P	2	0.0		
			1	158.5		
			0	226.5		
O		^1D	2	15867.7	$^3P \rightarrow {}^1D$ Spin Forbidden	10^{-3}
		^1S	0	33792.4	$^3P \rightarrow {}^1S$ Spin Forbidden	10^{-4}
	$2s^2 2p^3 3s$	^3S	1	76795.0	$^3P \rightarrow {}^3S$ 1303Å	3.8×10^8
S	$3s^2 3p^4$	^3P	2	0.0		
			1	396.8		
			0	573.6		
		^1D	2	9239.0		
		^1S	0	22181.0		
		^3S	1	55331.0	$^3P \rightarrow {}^3S$ 1807Å	4×10^8

The selection rules for transitions between states are:

$\Delta S = 0$	no change in spin
$\Delta L = 0, \pm 1$	
$\Delta J = 0, \pm 1$	but J=0 to J=0 is forbidden
$\Delta \ell = \pm 1$	transition electron must change angular momentum

The two selection rules concerning L and ℓ may be summarized by stating that only odd and even states combine, i.e., odd → even or even → odd are allowed transitions but not odd → odd or even → even. This is termed the Laporte rule. Reference to Table II shows that the allowed transitions have transition probabilities on the order of 10^8 sec^{-1}, whereas forbidden transition possess rates several orders of magnitude lower. This discussion has been limited to a consideration of electric dipole allowed transitions only; magnetic dipole and electric quadrupole transitions have been omitted because of their low transition probabilities.

Detection of Atomic Species

For all of the atoms listed, detection by means of laser-induced fluorescence in the visible region of the spectrum is impossible because all of the strong atomic absorptions reside in the vacuum ultraviolet region of the spectrum.

Schlossberg has suggested that fluorine atoms may be detected and measured in operating chemical lasers by means of CARS (Ref. 21). The method is based upon an electronic Raman effect for the transition in the F-atom between the fine structure components of the ground state, $^2P_{3/2}$ and $^2P_{1/2}$. The separation of these two states is 404 cm^{-1}. Schlossberg has calculated the Raman scattering cross-section for this F-atom transition for incident radiation of 5000Å. A formula given by Vriens (Ref. 22) was employed which relates the Raman scattering probability to the transition frequency and the frequency of the first allowed transition. The value for the calculated cross-section is 3×10^{-31} cm^2/sr, which is comparable to that measured for diatomic molecules. To our knowledge, the detection of F-atoms by means of spontaneous Raman or CARS techniques has not been performed in a chemical laser or even under laboratory conditions.

Both the carbon atom and the oxygen atom have fine structure in the ground state, similar to the F-atom; unfortunately the nitrogen atom does not. The ground states of the C-atom and O-atom are both ^3P. The position of the triplet levels in C are 0, 16.4 and 43.5 cm^{-1} for $^3P_0$, $^3P_1$ and $^3P_2$ respectively. In the O-atom for $^3P_2$, $^3P_1$ and $^3P_0$ the levels are at 0, 158.5 and 226.5 cm^{-1}, respectively. The inversion of J occurs because the O-atom has the valence shell more than half-filled. Certainly the transitions $^3P_0 \rightarrow {}^3P_1$, $^3P_0 \rightarrow {}^3P_2$, $^3P_1 \rightarrow {}^3P_2$ for either atom could be resolved by a good Raman instrument, viz., a double monochromator with high resolution and high rejection of scattered Rayleigh light. The Raman cross sections for these transitions have not yet been calculated. A qualitative examination of the formula derived by Vriens and an inspection of the energy levels of C and O leads to the conclusion that the O- and C-atom Raman cross sections should

be comparable to that of the F-atom. An important difference is that, for both the O- and C-atom, there are real electronic states (see Table II) which are in the spectral regions accessible to argon ion lasers and dye lasers. This opens up the possibility of near-resonant enhancement of the electronic Raman scattering from O- and C-atoms. Near-resonance enhancement is not feasible for the F-atom as the first excited state lies too high, $\sim$ 100,000 cm^{-1} (1000Å). Unfortunately, this near-resonance enhancement for the O- and C-atom may not be very large, because the transitions mentioned are not very strongly allowed. Clearly, detailed calculations are required to assess the situation in order to decide if O- and C-atom detection is feasible by means of electronic Raman scattering and, of course, by CARS. In the latter case, sensitivity may be limited by nonresonant background contributions as will be explained later. For the case of the C-atom, the small electronic Raman shifts most likely would be obscured by rotational Raman scattering from molecules present in the flame.

N is an extremely difficult species to measure because the lowest allowed transitions are deep in the vacuum ultraviolet near 1200Å. Radiation from a microwave-driven hollow cathode lamp could, in principle, be used to excite resonance fluorescence from N atoms. However, both the incident and emitted radiation are likely to be strongly absorbed by other species. Raman scattering cannot be employed since the photon energy from any available UV laser source is considerably less than the excited state energy.

Diatomic Molecules

The available data for selected diatomic species are summarized in Table III. The species C_2, CH (radical), CN (radical), CO, H_2, CS, N_2, NH (radical), NO, O_2, OH (radical), and SO are listed. Although not technically radicals, C_2, CS and SO are short-lived molecules; technically NO is a radical, but is long-lived.

The data is presented in a fashion similar to that of Herzberg (Ref. 23). The term energy of the electronic state listed is given in wave numbers (cm^{-1}). The ground state is denoted by capital X (with the exception of C_2) and states which connect by spin-allowed transitions are denoted by capital letters A, B, C, etc.; lower case letters are used for systems of different multiplicity. The multiplicity of a state is given by 2S+1, as for atoms, by a left superscript on a Greek capital letter which accounts for the total orbital angular momentum of a state. States with 0, 1, 2 units of orbital angular momentum are termed Σ, Π, Δ states. Additionally, homonuclear molecules require a g or u label (gerade-even or ungerade-uneven) to designate whether the wave function is even or odd according to inversion symmetry, and a + or-label (right superscript) to designate the symmetry of the wave function with respect to reflection of the nuclei.

TABLE III

SPECTROSCOPIC DATA FOR DIATOMIC MOLECULES OF INTEREST [19,28,42,64]

Species Diss. Energy	Term Energy cm^{-1}	Electronic State cm^{-1}	Vibrational Frequency cm^{-1}	Anharmonicity cm^{-1}	Rotational Constant cm^{-1}	Major Electronic Transitions		Lifetime (sec)
C_2	0	X $^1\Sigma_g^+$	1854.8	13.4	1.82	Swan	X ← A' 4000 - 6000Å	185 x 10^{-9} (i)
	716	X $^3\Pi_u$	1641.3	11.7	1.63			
6.11 eV	6443	A' $^3\Sigma_g$	1470.4	11.2	1.49			
	8145	B' $^1\Pi_u$	1608.2	12.1	1.62			
	19988	A $^3\Pi_g$	1788.2	16.4	1.75			
	34240	C' $^1\Pi_g$	1809.1	15.8	1.78	Fox-Herzberg	X ← B 2300 - 3300 Å	
	40416	B $^3\Pi_g$	1106.0	39.3	1.19			
CH	0	X $^2\Pi_{1/2}$	2858.7	63.0	14.19			
Radical	17.9	$^2\Pi_{3/2}$						
3.45 eV	23217	A $^2\Delta$	2930.7	96.6	14.58	4315Å	X ← A 5000 - 4300Å	~ 0.5 x 10^{-6} (h)
	25698	B $^2\Sigma$	(2250)		13.64	3900Å	X ← B 4500 - 3600Å	~ 0.5 x 10^{-6} (h)
CN	0	X $^2\Sigma^+$	2071.1	13.8	1.899			
Radical								
7.69 eV	9117	A $^2\Pi$	1812.5	12.6	1.715	Red	X ← A 14000 - 5200Å	7 x 10^{-6} (h)
	25799	B $^2\Sigma^+$	2144.8	12.2	1.97	Violet	X ← B 4600 3500Å	60 x 10^{-9} (h)
CC	0	X $^1\Sigma^+$	2169.8	13.3	1.93			
11.09 eV	48474	a $^3\Pi$	1743.0	14.0	1.69	Cameron	X ← a 2000 - 2500Å	~ 10^{-3} (h)
	64746	A $^1\Pi$	1515.6	17.3	1.61	4th positive	X ← A 1500 - 2400Å	~ 1 x 10^{-9} (g)
H_2	0	X $^1\Sigma_g^+$	4405.3	125.3	60.87			
4.477 eV	91698	B $^1\Sigma_u^+$	1356.90	19.0		Lyman	X ← B 1200Å	
CS	0	X $^1\Sigma^+$	1285.1	8.5	0.8205			
(7.35) eV	38797	A $^1\Pi$	1072.3	10.0	0.78		X ← A 2500 - 2700Å	176 x 10^{-9} (i)
N_2	0	X $^1\Sigma_g^+$	2358.0	14.2	1.999			
9.76 eV	49756	A $^3\Sigma_u$	1460.6	13.9	1.454		A ← B 10000 - 5000Å	A $^3\Sigma$ ~ 1 sec (i)
	59310	B $^3\Pi_g$	1735.0	15.2	1.637			B $^3\Pi$ ~ 5 x 10^{-6} (i)
	68951	a $^1\Pi_g$	1694.0	13.9	1.615		X ← a Vac UV	a 100 x 10^{-6} (i)
NH	0	X $^3\Sigma^-$	3203.0	78.5	16.66			
3.2 eV	a	a $^1\Delta$	3231.0	6.3	16.44			
(Radical)	a+8502	b $^1\Sigma^+$	3355.0	74.4	16.73			
	29776	A $^3\Pi$	3188.0	87.5	16.32		X ← A 3360Å	A, 500 msec
NO	0	X $^2\Pi_{1/2}$	1904.0	14.0	1.7046			
	121	$^2\Pi_{3/2}$	1903.7	14.0	1.7046			
6.5 eV	44200	A $^2\Sigma$	2371.3	14.5	1.998	γ-system	X ← A	200 - 400 x 10^{-9} (h)
	45488	B $^2\Pi_{1/2}$	1036.9	7.5	1.076	β-system	X ← B	2 - 3 x 10^{-6} (h)
	44516	$^2\Pi_{3/2}$	1038.3	7.5	1.178			
O_2	0	X $^3\Sigma_g^-$	1580.2	12.0	1.4456			
5.115 eV	7882	a $^1\Delta_g$	1509.0	12.9	1.4264			
	13121	b $^1\Sigma_g^+$	1432.7	13.9	1.4004	Atmospheric	X ← b	10 sec (i)
	35006	A $^3\Sigma_u^+$	(805)	(13)	0.917	Herzberg Bands	X ← A	10^3 sec (i)
	49349	B $^3\Sigma_u^-$	700.4	8.0	0.8104	Schumann-Runge	X ← B	
OH	0	X $^2\Pi_{1/2}$	3725.0	82.8	18.871			
Radical	126	$^2\Pi_{3/2}$						
4.40 eV	32682	A $^2\Sigma^+$	3184.3	97.8	17.355	3064Å Syst.	X ← A 2400 - 4000 A	800 x 10^{-9} (i)
SO	0	X $^3\Sigma^-$	1149.0	5.63	0.72			
3.36 eV	10510	b $^1\Sigma^+$						
	38292	A $^3\pi_b$					A → X 2500 - 2600Å	12 x 10^{-9} (i)
	41629	B $^3\Sigma^-$					B → X 2400 - 4000Å	16 x 10^{-9} (i)

The fundamental vibration frequency is given in wave numbers as is the first anharmonic constant and the rotational constant. Higher order corrections to the vibrational-rotational energy terms are not given. The major allowed transitions are listed along with the lifetime of the upper electronic state.

The selection rules for allowed transitions in diatomic molecules are:

	$\Delta S = 0$	spin does not change
	$\Delta\Lambda = 0, \pm 1$	orbital angular momentum
thus,	$\Sigma \rightarrow \Sigma$, $\Sigma \rightarrow \Pi$, $\Pi \rightarrow \Sigma$, but $\Sigma \not\rightarrow \Delta$	
and	$g \rightarrow u$, $u \rightarrow g$	even to odd, odd to even
	$g \not\rightarrow g$, $u \not\rightarrow u$	(Laporte Rule)
and	$+ \rightarrow +$, $- \rightarrow -$	
	$+ \not\rightarrow -$	

It must be borne in mind that "forbiddenness" is a matter of degree and that transitions which are forbidden do occur to some extent, and are observable.

Individual molecules are discussed in the order given in the Table, with regard to detection by means of fluorescence, Raman or CARS techniques. As these techniques are discussed in detail in later sections, only an abbreviated treatment is given here.

C_2

The Swan bands, $A^3\Pi_g \rightarrow X\ ^3\Pi_u$, a strong emission found in flames, cover the range from 4000 to 6700Å with peak intensity at 5165Å the 0-0 band. Although the transition does not originate from the ground state, the lower state lies only 714 cm^{-1} above the ground state and has ample population in flames. Laser-induced fluorescence has been observed in flames by several workers (Refs. 24, 25, and 26). Both groups of workers claim that real time measurements of the C_2 concentration can be made in atmospheric pressure hydrocarbon flames. Jones and Mackie (Ref. 24) conclude that using a CW Argon ion laser yields marginal results. Baranavski and McDonald (Ref. 25) employed a saturation technique utilizing a pulsed dye laser; they claim concentration measurements of 10^{16} cm^{-3} and excited state lifetimes of 10^{-12} sec. The C_2 fundamental vibrational frequency of 1855 cm^{-1} is, of course, Raman allowed and, hence, could be detected by means of Raman scattering or CARS. C_2 measurements are precluded where soot is present because laser-generated C_2 would interfere.

CH

The methyne radical, CH, has two strong band systems in the visible and near UV with strong features at 4300Å and 3900Å respectively. For both transitions the lower state is the ground state, hence absorption of dye laser radiation is feasible and has been carried out in a flame environment by Barnes and coworkers (Ref. 27). A nitrogen laser pumped dye laser was employed to excite the (0,0) band at 4315Å in an oxy-acetylene flame, presumably operating at one atmosphere.

CN

This radical has two main emission systems, the so-called "red" A $^2\Pi \rightarrow X\ ^2\Sigma^+$ and the "violet" B $^2\Sigma^+ \rightarrow X\ ^2\Sigma^+$ transitions. Of the two, the violet system has the more intense emission (absorption), and hence would be the more favored system for laser excitation. Jackson (Ref. 28) has observed laser induced fluorescence from CN produced by photolysis of cyanogen, C_2N_2. Therefore, laser-induced fluorescence should be observable in flames.

CO, H_2, N_2, O_2

All of these molecules have strong allowed transitions in the vacuum UV and hence, cannot be excited with present technology dye lasers. The measurement of these species must utilize conventional Raman or CARS techniques. There are no strong interferences from other Raman lines from either diatomic or polyatomic molecules; however, there may be fluorescent interferences from hydrocarbons or radicals such as CH or NH. All of these have been monitored in numerous Raman and CARS investigations. For example, laser excited vibrational Raman spectra of CO, O_2, CH_4 and N_2 have been observed from a natural gas-air flame by Vear and colleagues (Ref. 29). Rotational Raman lines of H_2 were also observed. No estimates of sensitivity were given.

CS

Emission from CS has been observed in flames containing sulfur compounds (Ref. 30) and from the photolysis of CS_2 and OCS (Ref. 31). Laser-induced fluorescence would require absorption in the region of 2575Å (0,0), hence a frequency-doubled dye laser is mandatory. The lifetime of the A $^1\Pi$ state is 176 nanoseconds (Ref. 32).

NH

Emission from the imino radical NH is seen in flames of nitrogen-bearing compounds in the near UV with maximum intensity at 3360Å (Q0,0) (Ref. 33). The A $^3\Pi$ state has a lifetime of 455 nanoseconds (Ref. 32); hence, absorption is moderately strong. This wavelength region is accessible by means of frequency-doubled dye lasers.

NO

Until recently, nitric oxide has been a difficult molecule to excite with available laser sources and doublers because the strongly absorbing system, the γ-system (A-X) absorbs mainly below 2260Å. With the relatively new doubling crystal, potassium pentaborate (KBP) laser-induced fluorescence has now been observed by Zacharias and coworkers under laboratory conditions at low pressure, 0.03 Torr (Ref. 34). Doubling efficiencies into this region are relatively poor, however, about 0.5 to 1 percent. Because of the extreme interest in this particular molecule as regards pollution, it is important to find a reliable means of measuring its concentration. An alternative is to attempt laser-induced fluorescence from the β-band (B-X). The β-band (lifetime = 2-4 microseconds) (Ref. 32) is weaker than the γ-band (lifetime = 200-300 nanoseconds), (Ref. 28) but occurs in a wavelength region more amenable to efficient frequency doubling. This is true even though the B state lies higher than the A state. This arises due to large shift toward larger interatomic separations of the potential energy curve of the B state, causing a large Franck-Condon shift. Thus, the maximum intensity bands (in emission) are 0-10, 0-9, 0-8, etc. This in turn means that laser absorption would have to be from upper vibrational levels (hot bands) of the ground state. The low upper vibrational level populations would most likely mitigate against the frequency doubling efficiency gains.

Much of the work to date on NO has been performed using conventional light sources. Quenching studies have been carried out by numerous workers (Refs. 35, 36).

OH

The resonance fluorescence of the OH radical has been intensively studied by Wang and coworkers at the Ford Scientific Laboratory following the initial observation by Baardsen and Terhune (Ref. 37) of the same laboratory. Early efforts were directed toward measurement of the concentration of OH in the atmosphere (Ref. 38). That laboratory has also measured the ground state population distribution of OH in a methane-air Bunsen burner flame (Ref. 39). Quite recently (Ref. 40), a detailed study of the quenching effects of H_2O and N_2 on the OH radical was performed, along with the saturation behavior of the absorption transition under high laser flux.

These experiments employed a pulsed, tunable dye laser which is frequency doubled with ADP to the desired wavelengths at 2526Å and 2822Å, the $P_1(2)$ and $P_1(1)$ transitions respectively. Fluorescence is observed at 3145Å (1-0) and at 3090Å (0-0). Concentrations as low as 10^{+6} cm^3 have been measured in air. Becker's group at the University of Bonn has also measured OH concentrations produced by a chemical reaction in a flow tube, with a pulsed dye laser (Ref. 41). A sensitivity range comparable to that found by the Ford Scientific Laboratory was obtained. Additionally, the quenching rates for H_2O, H_2, N_2, He and Ar were measured. The water quenching rate was highest with a rate constant of 4.5×10^{-10} cm^3 $molecule^{-1}$ sec^{-1}, nearly gas-kinetic; however, the other quenchers were also quite efficient with the following values given: H_2, 66.5×10^{-11}; N_2, 1×10^{-11}; He, 1×10^{-12}; Ar, 5×10^{-12}.

SO

Emission from SO has been observed from sulfur containing fuels (Ref. 42). The detection and measurement of this particular species would appear to be important in unraveling the fate of sulfur in combustion. The main system, $B \rightarrow X$, occurs in the near UV from 3940Å to 2400Å. The strongest bands in emission are: 0-10, 0-9, 0-8; which again indicates a strong Franck-Condon shift. These bands may be more accessible than the NO β-bands, because of the smaller vibrational frequency (1150 cm^{-1} in SO compared to 1904 cm^{-1} in NO); hence, SO is more likely to have "hot band" transitions.

Polyatomic Molecules

Spectroscopic data for polyatomic molecules of importance in combustion studies are given in Table IV. The Table also includes some hydrocarbon fuel molecules. Because of the large number of vibrational modes they possess, these molecules could exhibit interferences with desired Raman frequencies. Additionally, representative aromatic ring hydrocarbons are given. These molecules are known to be formed in combustion processes and again may be potential interferences. In these cases, broadband fluorescence is produced from the aromatic hydrocarbons, which absorb over a very broad spectral region, cf., Table IV.

A considerable amount of information is given in Table IV. Note that under the species chemical symbol, it is indicated whether or not the molecule is a radical. If so, the lifetime of the ground state is of the order of 10^{-3} seconds. This fact doesn't preclude laser spectroscopic measurements, but it certainly mitigates against a conventional chemical method. The second column of the Table lists the electronic term energy in wavenumbers. The third column shows the electronic state as X, A, B; the ground state, first excited, second excited, etc., and the symmetry species of that particular state according to the symmetry point group (column 4) that the molecule belongs to. Also given with the electronic state symbol is the spin multiplicity as a left superscript, 1 for singlet (total spin = 0), 2 for doublet (total spin = $\frac{1}{2}$), 3 for triplet (total spin = 1), etc., just as for atoms and diatomic molecules.

The point group designation given in column 4 completely specifies the symmetry properties of all of the electronic states (as long as the point group doesn't change) and of all of the vibrational and rotational states of the molecule. The reader unfamiliar with group theory can still picture the molecular geometry by noting the following simplified rules: a C or D denotes an axis of rotational symmetry given by the subscript 2, 3, 4, etc. for a 2-fold, 3-fold, 4-fold symmetry axis, etc. The infinity symbols, D_∞, C_∞ are used for linear molecules (infinite-rotation axis). The difference between C_p and D_p is that the D symmetry has additionally, p-C_2 axes perpendicular to the main symmetry axis. The subscripts h and v denote horizontal and vertical (to the main rotation axis) planes of symmetry.

TABLE IV

SPECTROSCOPIC DATA FOR POLYATOMIC MOLECULES[66,67,68]

Species	Term Energy	Electronic State	Point Group	Normal Vibrational Frequencies	Raman or Infrared Active	Rotational Constants	Major Electronic Transitions
CH_2 (RAD)	0	X $^3\Sigma_g^-$	$D_{\infty h}$ (Linear sym)	ν_1 ν_2 UNK ν_3	R I,R I,R	A_o B_o 13.39 C_o r_o 1.079 α 180.0	B ← X 1415Å
	70637	B $^3\Sigma^-$	$D_{\infty h}$				
CH_3	0	X $^2A_2''$	D_{3h} (Planar trigonal)	ν_1 ν_2 ν_3 (580) ν_4	R I,R I,R I,R	A_o UNK B_o (9.57) C_o r_o 1.079 α 120.0	B ← X 2160Å
	46205	B $^2A_1$	D_{3h}				
CH_4	0	X $^1A_1$	T_d Tetrahedral Pyramid	ν_1 2916.5 ν_2 1533.6 ν_3 3019.5 ν_4 1306.2	R R I,R I,R	A_o B_o 5.2412 C_o r_o 1.094 α	A ← X (1455 - 1500Å)
	68730	A $^1F_2$					
C_2H_2 (acetylene)	0	X $^1\Sigma$	$D_{\infty h}$ (Linear sym)	ν_1 3372.6 ν_2 1973.5 ν_3 3294.8 ν_4 611.7 ν_5 729.1	R R I R I	A_o B_o 1.1766 C_o r_o CH, 1.058; CC, 1.208 α 180.0	A ← X 2370 - 2100A
	42197	A ^1A_u	C_{2h} (Bent)			α 120.0	
C_2H_4 (ethylene)	0	X ^1A_g	D_{2h} Planar sym	ν_1 (R) 3026.0 ν_7 (I) 949 ν_2 (R) 1622.0 ν_8 (R) 950 ν_3 (R) 1342.0 ν_9 (I) 3105 ν_4 neith 1027.0 ν_{10} (I) 810 ν_5 (R) 3102.0 ν_{11} (I) 2988 ν_6 R 1236.0 ν_{12} I 1443		A_o 4.83 B_o 1.001 C_o .828 r_{ch} 1.086; r_{cc} = 1.339 αHCH = 117.6°	
	< 28700	a $^3B_{1u}$	(D_{2d})				a ← X 2600 - 3400Å
	40015	A $^1B_{1u}$	D_{2d}				A ← X 1600 - 2100Å
C_2H_6 (ethane)	0	X $^1A_{1g}$	D_{3d} or D_{3h} 3-fold axis, sym staggered or eclipsed UNK	ν_1 R 2953.8 ν_7 I,R 2934 ν_2 R 1388.4 ν_8 I,R 1486 ν_3 R 944.2 ν_9 I,R 820 ν_4 neith (278) ν_{10} R 2963 ν_5 I 2895.7 ν_{11} R 1460 ν_6 I 1379.1 ν_{12} R (1155)		A_o 2.681 B_o 662.0 C_o r_{CC} = 1.536; r_{ch} = 1.091 αHCH = 108	A ← X 1350 - 1600 continuous ABSN
	6200	A					
C_6H_6 (benzene)	0	X $^1A_{1g}$	D_{6h} planar hexag.	ν_1 3162 ν_2 995 ν_3 3047	R R R	A_o B_o 0.1896 C_o r_{cc} = 1.397; r_{ch} = 1.084 α 120°	
	29510	a $^3B_{1u}$	only strong Raman modes listed				a ← X 3400 - 3000 Å
	38086	A $^1B_{2u}$					A ← X 2370 - 2070 Å
$C_{10}H_8$ (naphthalene)	0	X $^1A_{1g}$	D_{2h} planar sym				A ← X 3000 - 2400 Å
	~ 30300	A ?					A ← X 3000 - 3800 Å
$C_{14}H_{10}$ (anthracene)	0	X $^1A_{1g}$	D_{2h} planar sym				A ← X 3800 - 3000 Å
	26000	A ?					A ← X 3800 - 4800 Å
CO_2	0	X $^1\Sigma$	$D_{\infty h}$ Linear sym	ν_1 1388 ν_2 667 ν_3 2349	R I,R I,R	A_o B_o 0.3902 C_o r_o 1.161 α 180.0	A ← X 1400 - 1700 Å
	46000	A $^1B_2$	C_{2v}				A ← X 3100 - 3800 Å

TABLE IV (CON'T)

SPECTROSCOPIC DATA FOR POLYATOMIC MOLECULES

Species	Term Energy	Electronic State	Point Group	Normal Vibrational Frequencies	Raman Infrared Activity	Rotational Constants	Major Electronic Transitions
CH_2O (formaldehyde)	0	X $^1A_1$	C_{2v}	ν_1 2766 ν_2 1746 ν_3 1500 ν_4 1167 ν_5 2843 ν_6 1251	I,R I,R I,R I,R I,R I,R	A_o 9.405 B_o 1.295 C_o 1.134 r_o r(CH) = 1.102; r(CO) = 1.21 α(HCH)121.1°	
	25194	a $^3A''$	C_s				a ← X 4000 - 3600
	28188	A $^1A''$	C_s				A ← X 3400 - 5200Å
HCO	0	X $^2A'$	C_s	ν_1 (2700) ν_2 1083 ν_3 1820	R,I I,R I,R	A_o 22.36 B_o 1.494 C_o 1.400 r_o (HC) 1.08 (CO) 1.19 α 119.5	
	9294	A $^2A''$					X ← A 4600 8600Å
H_2O	0	X $^1A_1$	C_{2v} (bent)	ν_1 3657 ν_2 1594.7 ν_3 3755.7	R,I I,R I,R	A_o 27.877 B_o 14.512 C_o 9.285 r_o .956 α 105.2	
	53800	A $^1B_1$	C_{2v}				A ← X 1860 1450Å
HCN	0	X $^1\Sigma^+$	$C_{\infty v}$ (linear)	ν_1 3311.5 ν_2 713.5 ν_3 2096.7	R,I I,R I,R	A_o B_o 1.478 C_o r_o 1.064 (H-C); 1.156 (C-N) α 180	
	52256	A $^1A''$	C_s (bent)				A ← X (1915 - 1600Å)
NH_2 (RAD)		X $^2B_1$	C_{2v} (bent)	ν_1 ν_2 = 1497 ν_3	R,I I,R I,R	A_o 23.72 B_o 12.94 C_o 8.16 r_o 1.02 α 103.4°	
		A $^2A_1$	C_{2v}				A ← X 9000 - 4300Å
NH_3	0.0 0.0793 Inversion Splitting	X $^1A_1$	C_{3v}	ν_1 3337.2 3336.2 ν_2 968.3 932.5 ν_3 3443.9 3443.6 ν_4 1627.4 1626.1	R,I R,I I,R I,R	A_o B_o 9.444 C_o 6.196 r_o 1.0173 α 107.8	
		A $^1A_2''$	D_{3h}			r_o 1.08 α 120	A ← X 2170 - 1700Å
NO_2	0	X $^2A_1$	C_{2v} (bent)	ν_1 1319.7 ν_2 749.8 ν_3 1617.8	R,I R,I R,I	A_o 8.0012 B_o .4336 C_o .4104 r_o 1.1934Å α 134°	
	< 15000	A $^2B_1$	C_{2v}				A ← X 10000 - 3200Å
	40126	B $^2B_2$					B ← X 2580 - 2350Å
NO_3	0	X $^2A_2'$	D_{3h} (planar)	UNK			A ← X 6650 - 5000Å
	15089	A $^2E'$	D_{3h}				
SO_2	0	X $^1A_1$	C_{2v} (bent)	ν_1 1151.3 ν_2 517.6 ν_3 1361.7	R,I R,I R,I	A_o 2.027 B_o .3442 C_o .2935 r_o 1.43 α 119.5	
	25767	a $^3B_1$	C_{2v}				a ← X 3900 3400Å
	29622	A $^1B_1$	C_{2v}				A ← X 3400 - 2600Å
SO_3	0		Weak bands on a continuum 2483 to 2337				Goodeve, C. F. and Fajans, E., Trans. for Soc. 32, 511 (1936).

Two special point groups are T_d and O_h; the former is used for the symmetry of the regular tetrahedron (CH_4), the latter, for the regular octahedron (SF_6). A concise but complete description of point groups is given by Herzberg (Ref. 43). A very readable account of group theory and its applications is given by Cotton (Ref. 44).

The set of normal mode vibrational frequencies is given in the next column. The numbering of the particular vibrational modes for a given molecule follows that of Herzberg (Ref. 43) where one may find illustrations of the atomic motions. For example, the ν_1-mode is the totally-symmetric stretch of a given molecule and is always strongly Raman-active. This ν_1 mode is not observed in the infrared if the molecule has a center of symmetry because there is no induced dipole moment caused by the nuclear motion. This is an example of a general rule, the mutual exclusion rule, that for molecules with center of symmetry (inversion symmetry, x, y, z → -x, -y, -z), those modes which are Raman active are infrared inactive and vice versa. The Raman and/or infrared activity of the normal modes is indicated with an R or I, respectively, or both, if the mode is observed by both techniques. There are some vibrational modes which are inactive in both Raman and infrared, e.g., the torsional mode of ethane, ν_4. These modes are marked "neither."

The rotational constants along with bond lengths and angles are given in the next columns. The rotational constants are given by $A = h/8\pi^2 c I_A$, where h is Planck's constant and c, the speed of light. I_A is the principal moment of inertia about the A-axis. Similar definitions hold for B and C. The principal axes system is the cartesian coordinate system for which the moment of inertia tensor is diagonalized. For a linear molecule one is concerned with only the moment of inertia about an axis perpendicular to the molecular axis. A symmetric top molecule has two principal moments of inertia identical. A necessary and sufficient condition for this to be true is that the molecule have a 3-fold symmetry axis (or higher). A spherical top has all three principal moments equal, e.g., methane and CF_4. Because of these equalities, rotational constants which are equal are not repeated in the Table but so indicated by a blank.

The major electronic transitions are shown in the last column. Absorption is indicated by a right-to-left arrow, viz., B ← X, and fluorescence by the opposite. With polyatomic molecules, fluorescence is often considerably red-shifted (sometimes termed Stokes-shifted) from the position in the spectrum where absorption occurs. This effect is more pronounced with polyatomic molecules than for diatomic molecules because of the more rapid vibrational relaxation in the upper electronic state. For some very large molecules, such as the aromatic hydrocarbons, absorption and emission overlap very little, just at the 0-0 band. This phenomenon is indicated in the Table. Fluorescence is not always observed following absorption. The molecule may dissociate or predissociate, or fluorescent quenching may be so severe that few molecules radiatively relax.

CH_2

The methylene radical absorbs deep in the vacuum UV, precluding its measurement by means of laser-induced fluorescence. Since the vibrational frequencies are not known, conventional Raman scattering or CARS cannot be applied either at this time.

CH_3

The methyl radical has its strongest absorption bands in the vacuum UV; however, there are some bands in the region of 2160 Å. It would be difficult to reach these bands with a frequency doubled dye laser, but in principle it could be done. The frequency of the Raman active ν_1 mode is unknown, so that Raman/CARS cannot be used at this time.

CH_4

Laser-induced fluorescence is eliminated because of the deep UV absorption. Raman/CARS techniques could utilize the strong Raman active ν_1 mode. It should be noted that because methane is a spherical top it possesses no rotational Raman spectrum. CARS has been observed in the ν_1 band of CH_4 using CW lasers (Ref. 45).

C_2H_2

Acetylene is a linear molecule in the ground state, but bent in the first excited state. The absorption between these two states takes place between 2100 Å and 2370 Å which would be accessible to frequency-doubled dye lasers. Fluorescence has been observed from electric discharges in acetylene (Ref. 42). The ν_1 frequency at 3372 cm^{-1} is strongly Raman-allowed and should be easy to observe by conventional Raman or CARS spectroscopy.

C_2H_4

Ethylene has a double bond rather than a triple bond as in acetylene and absorbs further in the UV for the allowed singlet-singlet transition. Laser-induced fluorescence is doubtful at best. The ν_1 C-H symmetric stretch is amenable to Raman/CARS. It should be pointed out that for all carbon-hydrogen compounds the CH stretch occurs in the neighborhood of 2900-3100 cm^{-1} and there may be interferences with other hydrocarbons.

C_2H_6

Ethane is a saturated hydrocarbon and for this reason absorbs far in the vacuum UV, 1350-1600 Å. Moreover, the absorption is continuous, indicating dissociation, hence, fluorescence techniques are not applicable. Raman/CARS techniques can be used, however. In fact, the many Raman allowed frequencies could cause interferences with the measurement of some desired species.

C_6H_6, $C_{10}H_8$, $C_{14}H_{10}$

The aromatic hydrocarbons, benzene, naphthalene, and anthracene are listed to indicate the potential for interference for both fluorescence and Raman/CARS techniques. Note that the absorption and fluorescence of these species covers a large portion of the near UV and visible spectrum. The large number of normal modes are a source of interference for Raman/CARS methods. It should be pointed out that these hydrocarbons can be formed in combustion processes.

CO_2

Carbon dioxide absorbs in the vacuum UV, eliminating laser induced fluorescence. Raman or CARS methods are applicable to the detection of this molecule. Weber and co-workers (Refs. 46, 47) have performed high-resolution spectroscopy on CO_2 in the gas phase, including a measurement in a low pressure electric discharge.

CH_2O

Formaldehyde absorbs in the near UV as indicated in the Table. Laser-induced fluorescence has been detected in atmospheric air using a frequency-doubled dye laser in the region 3200-3450Å (Ref. 48). The sensitivity was of the order of 5 pphm. The estimated quantum yield under the conditions of the experiment (i.e., with quenching by H_2O and CO_2) was $\sim 10^{-4}$. NO_2 and SO_2 did not interfere. It is difficult to predict if a similar method would yield such good results in a flame environment.

HCO

Little is known about this radical except that emission (termed Vaidya's hydrocarbon flame bands) has been observed from hydrocarbon flames (Ref. 30). The broad emission range from this species is certainly a source of interference for both laser-induced fluorescence and Raman/CARS.

HCN

Hydrocyanic acid absorbs in the far UV in the region 1600-1900Å, as indicated. This fact precludes laser induced fluorescence. The ν_1 normal mode vibration, essentially the CH group vibrating against the N atom, is very strongly observed in the Raman spectrum, thus permitting conventional Raman or CARS methods to be attempted.

H_2O

Water does not absorb in the visible or near UV region of the spectrum. However, there are vibrational overtones which appear in the near IR in both emission and absorption. Laser-induced fluorescence is not applicable. The symmetric stretch vibration, ν_1, is strong in Raman scattering, and hence, is amenable to both Raman

and CARS techniques. Lapp and co-workers have performed extensive Raman scattering studies on water vapor (Ref. 49). The CARS method has been successfully applied to H_2O in the liquid phase (Ref. 50). The ν_2 and ν_3 vibrational modes are also Raman-allowed but weakly so. However, these modes, along with the allowed ν_1 mode, serve as potential interferences to measurements on other molecules.

NH_2

This radical absorbs in the visible region of the spectrum between 4300 Å and 9000 Å. Laser-induced fluorescence has been observed by Welge and co-workers (Ref. 51) using both a pulsed and CW dye laser. The NH_2 radicals were produced by the photolysis of ammonia. Quenching rates for several gases were measured to be of the order of 10^{-9} cm^3 $molecule^{-1}$ sec^{-1}, which is gas kinetic. The lifetime of the NH_2 radical is estimated to be several microseconds. Because of the very rapid quenching rates, laser-induced fluorescence measurements of NH_2 in an atmospheric pressure flame would be difficult to perform. However, the possibility of fluorescence measurement should be assessed experimentally. The ν_1 symmetric vibrational-mode, although not yet measured, should be strongly Raman allowed, hence amenable to Raman/CARS techniques.

NH_3

Laser-induced fluorescence in ammonia would be difficult to observe because there is only weak absorption in the quartz UV, wavelengths above 2000 A. The symmetric ν_1 vibrational mode is strongly allowed in Raman scattering, hence should be easily measured by Raman/CARS methods. Ammonia, like water, may serve to provide interferences to the measurement of other molecules.

NO_2

A great deal of work has been directed to the detection of NO_2 in the atmosphere by means of laser-induced fluorescence (Refs. 52, 53, 54). Although these attempts have met with some success, it is problematical that this technique can be applied to the hostile conditions existing in a hydrocarbon flame. NO_2 has been measured in a hydrogen-air flame, up to the position of the flame front (Ref. 55). Beyond this point, fluorescence was not detectable. The lifetime of the excited state is ~ 50 microseconds, hence is easily quenched by the major flame constituents. The strongly Raman-allowed ν_1 mode at 1319 cm^{-1} would be suitable to Raman/CARS techniques.

NO_3

Apparently very little is known about this molecule. Absorption has been observed in the region 5400 to 6600 Å. Nothing is known about the lifetime or the vibrational frequencies.

SO_2

Sulfur dioxide absorbs in the near UV starting at 3500 Å and extending to below 2000 Å. Fluorescence has been observed in air at atmospheric pressure; this is possible because the lifetime of the excited SO_2 is a few nanoseconds; hence, quenching is not too severe (Ref. 56). Fowler and Berger at UTRC performed an experimental study (Ref. 57) of laser-induced resonance fluorescence in SO_2 at 3000 Å with a view toward remote detection. A commercial instrument based upon the fluorescence caused by a pulsed, incoherent UV source is manufactured by Thermoelectron Corp. (Ref. 58). The instrument is stated to be sensitive to a few ppm of SO_2. Recently, Jahnke and co-workers at the Environmental Science Research Laboratory of EPA have assessed quenching effects in this instrument (Ref. 59) and found that the composition of the gas is quite important due to quenching by oxygen. This problem can be taken care of by means of suitable modifications. It is not obvious from the success of this technique if laser-induced fluorescence from SO_2 can be used to measure SO_2 concentration in the presence of more serious quenchers such as water, radicals, etc. SO_2 has been detected in a stack plume by means of laser Raman radar (Ref. 60). A Q-switched frequency-doubled Nd:YAG laser was employed and the scattered light collected from the test volume was passed through a narrow band filter. Photon counting with noise subtraction had to be employed. Similar techniques have been employed with good success to atmospheric measurements by Hirschfeld and associates (Ref. 61) and by Kobayasi and Inaba (Ref. 62).

Raman Cross Sections

Absolute differential Raman cross sections for many species of combustion interest are given in Table V. Values are given for excitation by three different wavelengths 3371 Å (nitrogen laser), 4880 Å (argon ion laser) and 5320 Å (frequency-doubled neodymium). The 5320 Å values were calculated from the 3371 Å measurements by scaling with the λ_R^{-4} relation. A few values are given for pure rotational scattering. In general, note that there is little difference between the magnitudes of the cross sections for a wide variety of molecular species.

Interferences

Table VI presents some possible interferences to the measurement of various species by means of Raman scattering or CARS. The Table presents the strongest Raman-allowed transition for a given species in wave numbers, and the Stokes and anti-Stokes Raman wavelengths relative to the frequency-doubled Nd laser line, 5320 Å. Interferences are then listed as Raman interferences or fluorescence interferences. For the former case, interference would originate from a similar Raman process with an interfering molecule of nearly the same vibrational frequency; hence, the interference would occur at both the Stokes and anti-Stokes wavelength.

TABLE V

RAMAN CROSS SECTION FOR MOLECULES OF INTEREST
(Units of 10^{-30} cm^2/sr)

Species		Vibrational Frequency	Vibrational $\frac{d\sigma}{d\Omega}(3371\text{Å})$[69]	Vibrational $\frac{d\sigma}{d\Omega}(5320\text{Å})$[70]	Vibrational $\frac{d\sigma}{d\Omega}(4880\text{Å})$[71]	Rotational $\lambda_{EXC} = 4880\text{Å}$ $zz_{J \rightarrow J'}$[d]
N_2		2330.7	3.5 2.8(Q)	.46 .37(Q)	.68	5.4 $(6 \rightarrow 8)$[71]
H_2		4160.2			1.32 .88(Q)	1.0 $(1 \rightarrow 0)$[72]
O_2		1556	4.6 3.3(Q)	.65 .47	.72	14.0 $(7 \rightarrow 9)$[71]
NO		1877	1.5	.2	.15	
NO_2	ν_1 ν_2	1320 754	51.0 24.0	7.37 3.63		
NH_3		3334	11.0	1.3	2.75	
CO		2145	3.6	.48		0.27 $(6 \rightarrow 8)$[72]
CO_2	ν_1 $2\nu_2$	1388 1285	4.2 3.1	.6 .45	.77 .49	53.0 $(16 \rightarrow 18)$[71]
H_2O		3651.7	7.8(Q)	.9	1.4[73]	
H_2S		2611	19.0	2.4	3.5	
SO_2		1151.5	17.0	2.5	2.9	
CH_4	ν_1 ν_3	2915 3017	21.0 14.0	2.6 1.7	3.3	
C_2H_4	ν_1 ν_2	3020 1623	16.0(Q) 5.4(Q)	1.9 .76		
C_2H_6	ν_3	993			.88	
C_6H_6	ν_1 ν_2	3070 991	30.0 44.0	3.7 5.6	3.8 5.0	
SF_6		775	12.0	1.8		
CCl_4		459	26.0	4.04		

TABLE VI

POSSIBLE INTERFERENCES FOR DETECTING DESIRED

SPECIES BY RAMAN/CARS METHODS

Species	Raman Shift (cm^{-1})	Stokes λ_{Raman}	Anti-Stokes λ_{Raman}	Raman Interferences	Fluorescence Interferences
C	43	5332	5308	---	---
O	226	5385	5257	---	NH_2(AS)
C_2	1832	5900	4847	HCO	CH(AS)
CH	2633	6186	4666	CH_2, CH_4	CN(S), CN(AS)
CN	2045	5969	4798	HCN	CN(AS), HCO(AS)
CO	2143	6004	4775	---	CH(AS), HCO(AS)
CS	1272	5706	4983	NO_2	---
H_2	4169	6836	4354	---	CH(AS)
N_2	2331	6073	4733	---	C_2(AS) C_2(S)
NH	3048	6349	4578	C_2H_4	CH_2O(AS)
NO	1876	5901	4837	CH_2O	CH(AS)
O_2	1556	5800	4913	CH_4	---
OH	3665	6609	4452	H_2O	CN(S), CH_2O(AS)
CH_4	2916	6297	4605	CH	CH(S), CN(AS)
C_2H_2	3372	6383	4510	NH_3	CN(AS)
C_2H_4	3026	6341	4582	C_2H_6	CN(AS)
C_2H_6	2953	6312	4598	C_2H_4	CN(AS), CH_2O(AS)
C_6H_6	3162	6396	4554	C_2H_6, C_2H_4	NO_2(S), CH_2O(AS)
CO_2	1388	5774	4954	C_2H_4,NO	CN(AS)
CH_2O	2766	6238	4638	---	NO_2(S)
HCN	3311	6457	4523	NH_3	C_2(S), NH_2(AS)
H_2O	3657	6605	4454	OH	CN(S), CH_2O(AS)
NH_2	(1497)	5780	4928	---	---
NH_3	3337	6468	4518	C_2H_2	C_2(S), NH_2(AS)
NO_2	1319	5721	4971	CS,CO_2	CN(S)
SO_2	1151	5667	5013	CH_2O	CN(AS)

λ_{Raman}^{Stokes} and $\lambda_{Raman}^{Anti\text{-}Stokes}$ are relative to λ_{EXC} = 5320Å

--- No entry indicates no obvious interference from other molecules from this Table.

(S) Stokes, (AS) Anti-Stokes

( ) Indicates doubtful value

For the case of fluorescence interference, the emission from molecules present in the flame which are excited by whatever means, i.e., laser irradiation or chemiluminescence, is taken into consideration. For either case, overlap was considered to occur if lines were within 20 to 30 cm^{-1} because of the broadening in the rotational wings.

The Table is by no means exhaustive and the reader is cautioned that interferences may exist where none is indicated. It should be noted that most of the fluorescent interferences come from CH, CN, NH_2 and formaldehyde, and a few other species. Obviously then, the extent to which these species interfere depends upon their concentrations in the flame. Unfortunately, for a given flame there is no way to control these concentrations. Hopefully, with suitably narrow slits and/or appropriate time gating, sufficient discrimination against these interferences can be obtained.

Applicability of Techniques

In Table VII, the applicability of the four potential measurement techniques, laser fluorescence, spontaneous Raman, near-resonant Raman and CARS, have been summarized for all of the species considered in the preceding text. Potential applicability is indicated by a scale ranging over excellent, good fair, poor and not applicable. Also appearing is the label indicating insufficient information, or an untried method. Detection of O and C atoms by means of the electronic Raman effect (discussed before in the section on atomic species) is listed as possible under Raman, near-resonant Raman, and CARS.

It must be pointed out that this assessment of applicability is not absolutely certain nor is it meant to be. Rather, the Table should serve as a guide to which method is most appropriate for the measurement of a given species. Various factors were considered such as absorption region, lifetime, concentration, etc.; interferences were not accounted for in this assessment since they were considered in Table VI and, depending on the circumstances, may not be troublesome.

TABLE VII

SUMMARY OF SPECTROSCOPIC APPLICABILITY OF TECHNIQUES

Species	Fluorescence	Raman	Near-Resonant Raman	CARS
C	NA	possible	possible	possible
H	NA	NA	NA	NA
O	NA	possible	possible	possible
N	NA	NA	NA	NA
C_2	E	E	E	G
CH	E	P	P	P
CN	E	P	P	P
CO	NA	E	NA	E
CS	F	P	P	P
H_2	NA	E	NA	E
N_2	NA	E	NA	E
NH	E	F	P	G
NO	E	G	P	G
O_2	NA	E	NA	E
OH	E	G	G	G
CH_2	NA	?	NA	?
CH_3	NA	?	NA	?
CH_4	NA	E	NA	G
C_2H_2	?	E	NA	G
C_2H_4	NA	E	NA	G
C_2H_6	NA	E	NA	G
C_6H_6	E	G	P	F
$C_{10}H_8$	E	G	F	F
$C_{14}H_{10}$	E	G	G	F
CO_2	NA	E	NA	E
CH_2O	E	G	NA	G
HCO	?	?	?	?
HCN	F	G	NA	G
H_2O	NA	E	NA	E
NH_2	F-G	G	G	F
NH_3	NA	E	NA	G
NO_2	P	G	G	G
NO_3	?	?	?	?
SO_2	G	E	P	G
SO_3	?	?	?	?

E	excellent	NA	not applicable
G	good	?	not enough information or untried
F	fair		
P	poor		

PRACTICAL CONSIDERATIONS

Practical combustion devices possess flames which, generally, from an instrumentation standpoint, differ markedly from flames often investigated in fundamental or laboratory devices. Many diagnostic approaches developed for use on relatively benign flames in ideal laboratory environments are often unsuited for practical application. Consequently, in evaluating any diagnostic approach, the ultimate environment of application must be factored into any decision concerning the feasibility of a given technique. The application of interest here is a research scale furnace. Like most practical combustors it contains flames which are highly luminous and particulate laden when burning a hydrocarbon fuel. The high luminosity levels preclude the use of a continuous wave laser source for most diagnostic applications. However, use of a pulsed laser source engenders a variety of laser induced particulate effects which can mask detection of the sought-for signal. In addition, practical flames are generally highly turbulent which leads to large temporal variations in medium properties. In measurement situations where signal averaging is required to enhance signal/noise ratios, averaging over these temporal fluctuations often introduces ambiguity into data reduction and interpretation. In addition there are other factors, such as the presence of windows with limited aperture, and large distances from the device periphery to measurement location, which constrain diagnostic freedom. These factors often decrease signal to noise by introducing additional noise, e.g., window fluorescence, and diminishing signal strength in intensity dependent processes. In addition, there are other effects common to both laboratory and practical devices, such as gas breakdown, which need to be considered and which limit laser source intensity. In this section these various considerations will be reviewed. In the sections which follow, these factors will be taken into account as the feasibility of the various diagnostic techniques is assessed.

Sources of Noise

Background Luminosity

The laser light scattering diagnostic techniques to be considered here are generally situated in the visible or near UV portion of the spectrum due either to cross section scaling or the location of electronic resonances. Consequently, concern is centered in flame source radiations in this spectral region, hence, the use of the photometric term luminosity. Luminosity in this region is comprised primarily of chemiluminescent emissions and the gray/blackbody continuum from soot and other particulates (Ref. 30). The former emissions arise from electronic states excited during chemical reactions. The emissions are generally narrowband although continuum radiations are also present. The narrowband emissions consist either of line (atoms) or band (molecules) structure, specific to the emitting species and in

distinct spectral regions. For certain diagnostic processes, their possible interference can be avoided by appropriate laser wavelength selection. In premixed, near stoichiometric flames these emissions are dominant. In hydrocarbon-fueled diffusion flames, however, their contribution to the total luminous intensity is generally small compared to the soot blackbody continuum. In certain instances (Ref. 30) some fine structure may exceed the soot continuum in certain spectral regions.

An extensive series of luminosity measurements have been performed on the EPA "Rainbow" furnace and reported in Ref. 74 as spectral radiance. A Gamma Scientific Model 2020 radiometer (Ref. 75) was employed to measure the spectral radiance at various locations in the furnace operating with various fuels and swirl vane combinations. For an optically thin flame, it is more appropriate to use spectral radiation energy densities to account for the actual volume subtended in a particular instrumentation approach in a manner to be illustrated shortly. The conversion to radiation energy density was made by dividing the spectral radiance by the depth of field of the radiometer as described in Appendix I. In Fig. 3, several converted measurements are displayed which illustrate the range of radiation energy densities one is likely to encounter. As may be seen, depending on the measurement location, fuel employed, and spectral region of interest, the radiation energy densities range from a few tenths to a several thousand nanowatts/cm^3 Å sr. Also shown in Fig. 3 is the radiation energy density emitted by a dispersion of 400 Å diameter soot particles at 2000°K, at a density of 10^8 cm^{-3}, corresponding to a rather modest mass density of about 7.6(10-9) grams/cm^3 or volume fraction of 3.4(10-9). This calculation was performed by merely summing the individual particle radiation contributions as calculated from the Planck radiation formula. Since the dispersion assumed can be shown to be optically thin, aggregate extinction effects, i.e., absorption and scattering, can be neglected. As seen the spectral variation of the measured radiation energy density is very nearly blackbody and is easily accountable in magnitude by a soot dispersion of moderate density. For a given mass density or volume fraction of soot, larger sized particles result in less luminosity due to a decreased surface/volume ratio. A more complete discussion of soot sizes is given in the next section. 400 Å was used in the Fig. 3 calculation for illustrative purposes, and because it corresponded to the average particle diameter obtained in measurements at UTRC on an air-sustained laminar propane diffusion flame using an absorption/Mie scattering technique, Ref. 76. For comparison with Fig. 3 it should be noted that a ten watt Argon ion laser will produce a Raman scattered power of about 10^{-11} watts/sr over a centimeter pathlength from flame nitrogen at atmospheric pressure and 2000°K. Roughly then, note that even for the lowest radiation energy density displayed in Fig. 3 that the background will exceed a high power, continuous wave laser Raman signal by at least an order of magnitude. This means that in luminous environments, pulsed laser sources are generally required to produce signal powers comparable to or preferably in excess of the background power.

The signal/noise ratio attained will actually depend on details of the optical collection system and bandwidth. To illustrate this point, consider the signal/noise for a Raman experiment in a luminous background for the optical collection

FIG. 3

BACKGROUND LUMINOSITY IN EPA RAINBOW FURNACE

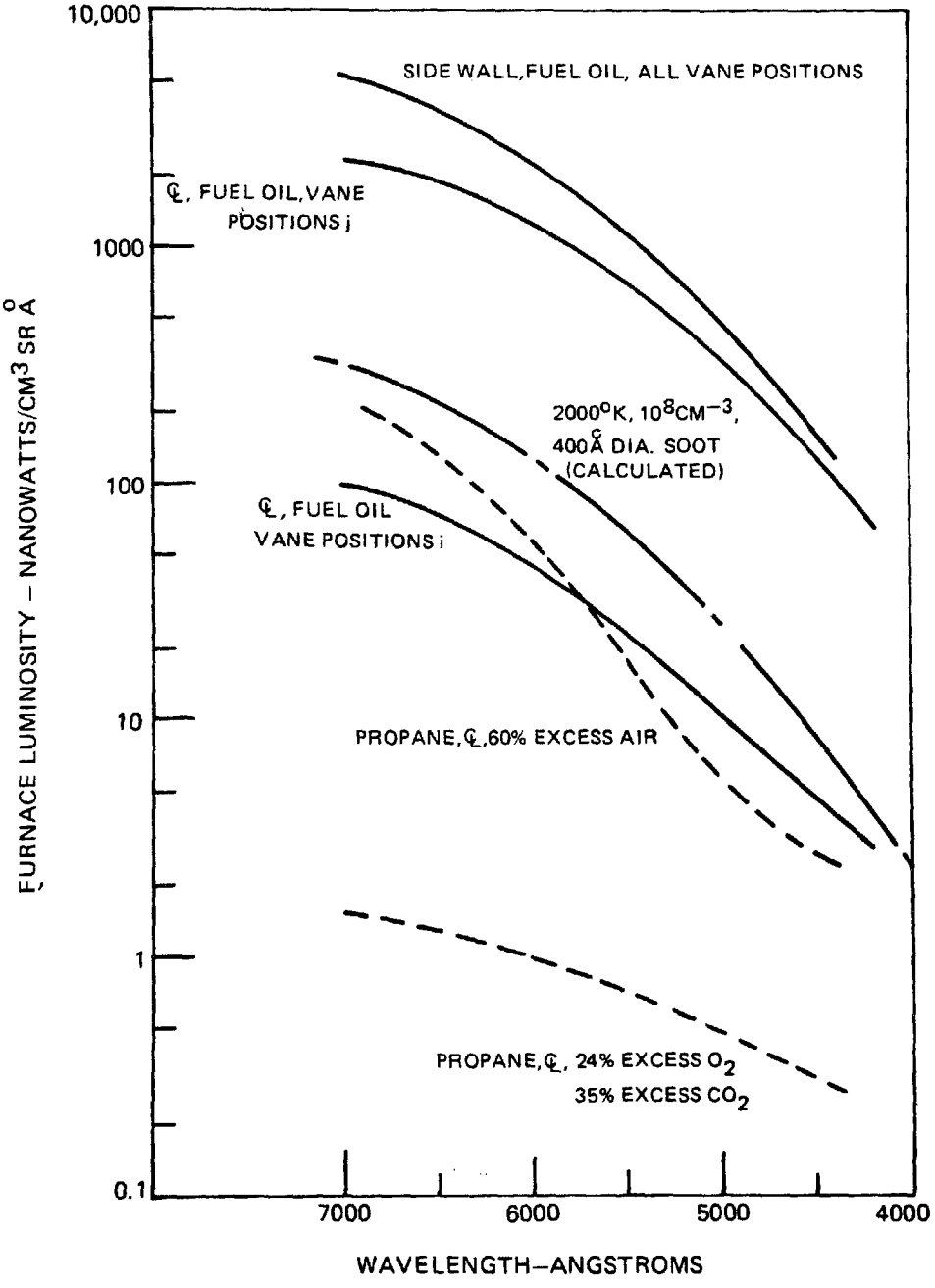

system of Fig. 4. There a double lens system is used to collect scattered light and focus it upon an aperture. The double lens system, as opposed to a single lens, possesses the advantage of being able to probe different sample volumes simply by translating the forward lens. The Raman signal power S is given by (Ref. 8)

$$S = P_i n \frac{\partial \sigma}{\partial \Omega} \Omega \epsilon \ell \tag{1}$$

where P_i is the incident laser power; n, the number density of scatterers in the appropriate initial quantum states; $\frac{\partial \sigma}{\partial \Omega}$, the Raman cross section; Ω, the solid acceptance angle; ϵ, the collection efficiency; and ℓ, the Raman sampling extent. For right angle scattering and a unity magnification optical collection system, $\ell_\perp$ is simply set by the aperture diameter, A. For coaxial or backscattering, $\ell_{||}$ is approximately equal to the depth of field 2AF where F is the f number of the individual lenses, i.e., f/D where f is the focal length, D the lens diameter. The background luminosity N collected is

$$N = \mathcal{R} \Delta\lambda \, \Omega \, \epsilon \, V \tag{2}$$

where $\mathcal{R}$ is the radiation energy density; $\Delta\lambda$, the optical bandwidth; and V the volume subtended by the optical system. V is approximately cylindrical with diameter A, and a length equal to the depth of field.

$$V = \frac{\pi}{4} A^2 \, 2FA \tag{3}$$

Substituting for A in terms of the Raman sampling extent, one finds

$$V_\perp = \frac{\pi}{2} F \ell_\perp^3 \qquad V_{||} = \frac{\pi}{6} \frac{1}{F^2} \ell_{||}^3. \tag{4}$$

Note that

$$\frac{V_\perp}{V_{||}} = 8F^3 \, \ell_\perp^3 / \ell_{||}^3 \tag{5}$$

i.e., for a given Raman sampling extent, the volume subtended in right angle scattering exceeds that "seen" in backscattering. For example, with F = 5 optics, this ratio is 10^3. This means a right angle scattering approach will collect three orders of magnitude more background than the equivalent coaxial approach. Physically, the reduction with backscattering occurs because the Raman scampling extent is matched to the optical system depth of field. Another point worth noting is that for any geometry, the signal/background noise scales as

LIGHT SCATTERING OPTICAL COLLECTION SCHEMATIC

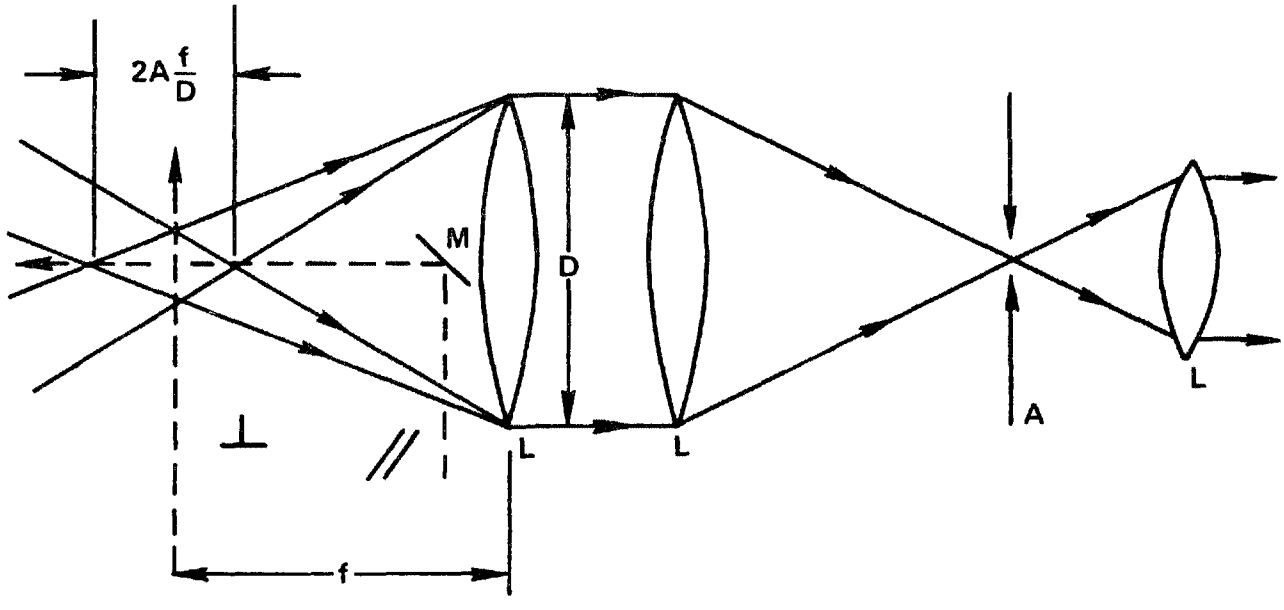

$$S/N \sim \frac{1}{\ell^2} . \qquad (6)$$

In any geometry it is thus desirable to maximize the spatial resolution. For example, a reduction in Raman sampling extent from 1 cm to 1 mm will result in a two order of magnitude increase in S/N. Of course, the sampling extent must be kept large enough to collect a statistically significant number of photons on a pulsed basis or expedite photon collection on a continuous wave basis. Similar conclusions would also apply to the case where the aperture A is rectangular, e.g., the entrance slit of a monochromator, although the results are analytically less tractable. Quantitative signal/noise calculations will be presented in later sections for each diagnostic technique. Background luminosity can also be suppressed, if, as is sometimes found (Ref. 77), it is slowly modulated by combustion instabilities, aerodynamic effects (e.g., swirl) or turbulent fluctuations. In these instances electronic filtering techniques can be used to suppress the gross excursions from entering the signal processing equipment. As a final note, for light scattering processes producing polarized signals, the background can be halved by use of a polarization filter.

Particulates

In the previous section, it was seen that particulates are primarily responsible for the large luminous backgrounds characteristic of hydrocarbon-fueled diffusion flames which loom as a major source of noise in laser light scattering diagnostics. Unfortunately, that is only part of the noise problem that particulates engender. In interacting with the signal producing laser source, particulates can fluoresce (Refs. 78, 79, 80, 81, 82), Raman scatter (Refs. 81, 83) and incandesce (Ref. 84). With pulsed laser sources, incandescence has been found to be especially severe.

Particulates may range in size from a few tens of Angstroms in diameter to several tens of microns. Particles a few hundred Angstroms in diameter (Ref. 76) to a few thousand Angstroms (Refs. 85, 86) appear typical in low molecular weight hydrocarbon-fueled diffusion flames. With higher molecular weight liquid fuels, size distributions skewed to larger particle sizes have been found. For example, measurements (Ref. 87) made in a model gas turbine combustor burning JP-4, indicated a particle size distribution which varied with particle radius as $r^{-0.36}$ over the diameter range from 0.01 to 10μ.

Fluorescence

Laser induced particulate fluorescence could pose a serious noise problem for laser light scattering diagnostics. Fluorescence generally occurs over a large wavelength extent on the Stokes side of the exciting laser source and is not easily avoided. In Raman probing of a gas turbine exhaust, Leonard (Ref. 78) encountered severe hydrocarbon fluorescences which precluded NO detection using a pulsed N_2 laser at 3371 Å. In fact, this phenomenon was utilized ultimately as a total hydrocarbon content diagnostic. However, Raman spectra from major species were generally

observable with the N_2 Raman signal-to-noise decreasing to unity as the hydrocarbon fraction reached 1000 ppm. Fluorescence excitation studies reported in Ref. 78 on jet oil indicated fluorescence could be significantly curtailed at laser wavelengths above 3750 Å. In Ref. 80, in combustor exhaust measurements at 5145 Å, strong fluorescence was found to swamp the Raman spectrum at exhaust temperatures below 1100°K. The fluorescence was believed due to incompletely burned pyrolyzed products of high molecular weight. Following the lead of Leonard, the authors also suggested the use of the laser induced fluorescence as a hydrocarbon probe. In Ref. 79 fluorescences from hydrocarbon aerosols excited at 4880 A interferred significantly with laser Raman studies of the exhaust of an internal combustion engine. The fluorescent interferences were on the same order as the major Raman signals in regard to signal intensity for hydrocarbon concentrations on the order of 5000 ppm (as CH_4), corresponding to a hydrocarbon mass density on the order of 10^{-6} gm/cm^3. Detailed excitation and fluorescence studies of a wide range of particulates are reported in Ref. 81 where a variety of fluorides, oxides, chlorides, sulfates, and phosphates were examined. In general, little fluorescence occurred for excitation wavelengths above 4500 Å. Fluorescence of unidentified atmospheric aerosols has also been studied in Ref. 82 using a continuous wave argon ion laser at 4880 Å. Based upon the above results, it appears that hydrocarbon fluorescences are probable for excitation wavelengths below 5000 Å; for mass densities corresponding to concentrations of 1000 to 5000 ppm, these fluorescences may be comparable in signal strength to Raman scattering from major constituents.

Raman Scattering

Unlike fluorescence, Raman scattering from particulates is spectrally specific and will not pose a problem unless the fundamental frequencies of the particulate molecules coincide with those of the particular gas species under investigation. Reference 81 contains Raman shifts and cross sections for a wide variety of particulates. With the general exception of the sulfates, most particulates (classes of oxides, sulfides, halides) have Raman shifts below 700 cm^{-1}. The sulfate bands are grouped in three regions: 400-500 cm^{-1}; 600-700 cm^{-1}; and 950-1200 cm^{-1}. Carbon has Raman bands at 1360, 1580 and 2140 cm^{-1} (Ref. 83) although the third band is only seen from sputtered carbon and may not exist in soot. In carbon black, the bands at 1360 and 1580 cm^{-1} are quite broad (hundred to several hundred cm^{-1}) and merge together. In comparison with other sources of noise from particulates, i.e., background luminosity, fluorescence and laser modulated incandescence, Raman scattering from the particulates is not anticipated to be a major problem and will not be belabored further.

Laser Modulated Particulate Incandescence

Laser modulated particulate incandescence occurs when the already incandescent soot particles absorb the incident light scattering laser radiation, heat to temperatures far above the ambient flame temperature and emit greatly increased

quantities of blackbody radiation. This phenomenon has been studied in some detail (Refs. 84, 88) and represents a very serious source of noise in laser light scattering diagnostics. This is particularly true for weak processes such as spontaneous Raman as will be apparent in a later section. For example, in an air sustained laminar propane diffusion flame, the N_2 Raman signal to laser modulated particulate incandescence noise ratio is below 10^{-4} for 400 kW laser excitation at 5900 Å. Being broadband, the laser modulated particulate incandescence is not easily avoided. Most solution approaches to this problem yield some improvement in signal/noise, perhaps two orders of magnitude, but the resultant signal/noise remains low generally necessitating signal averaging. As mentioned previously, for turbulent environments, this can lead to ambiguous data interpretation. Space does not permit a detailed exposition of laser modulated particulate incandescence here. Suffice it to say that depending on the laser flux, the irradiated soot particles are generally driven to or slightly above carbon vaporization temperatures as seen in Fig. 5. There the dashed curves are analytical predictions of particle surface temperature as a function of laser flux. It is quite apparent that at flame temperatures where the gaseous mean free path exceeds the soot particle diameter that heat conduction is insufficient to restrain the particle surface temperature from reaching the vaporization point. Consequently vaporization is the dominant heat transfer mechanism and the surface temperature displays a weak dependence on laser flux. Also shown are measured laser modulated soot temperatures (points) in an air-sustained laminar propane diffusion flame (Ref. 88). As seen the experimental results are in fair agreement with the theory and approximately 10-25 percent higher. The absolute amount of incandescence (noise), of course, depends not only on the temperatures to which the soot is driven but also on the soot number density which determines the number of particles irradiated. Signal to noise calculations for the various diagnostic techniques under consideration will be presented in their respective sections.

In addition to broadband incandescence, spectrally specific molecular emisssions may also be present. In studies of laser modulated particulate incandescence, Swan emissions at 5165 Å from laser vaporized C_2 were inferred to be present. In fact, the oscillator strength of the Swan system has been measured from studies of laser irradiated graphite (Ref. 89). There are other cases in the literature where C_2 Swan band radiation has been excited by ruby laser irradiated graphite (Refs. 90, 91). Besides incandescence, then, Swan (C_2) and other C_n interferences may thus also be present. In Table VIII, potential Swan and Comet Head (C_3) interferences in the N_2 Raman bands (typically used for thermometry) using various fixed frequency laser sources are shown.

Only the bandheads are listed. The Swan bands degrade to the violet, the Comet Head to the red. With the advantage of tunability, these specific emissions can be avoided vis-a-vis the Raman scattering with a dye laser appropriately tuned.

LASER IRRADIATED PARTICLE TEMPERATURES

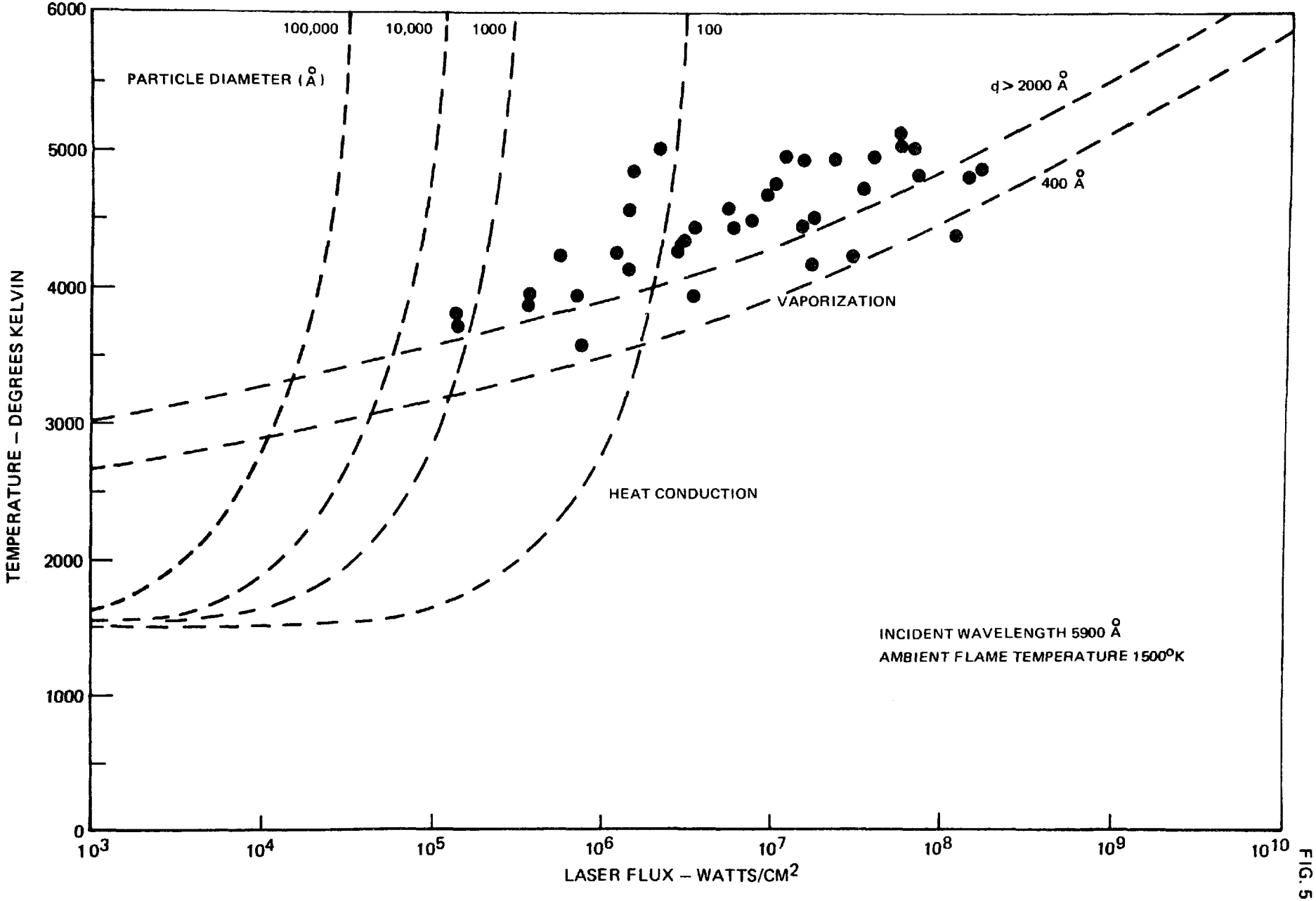

FIG. 5

TABLE VIII

POTENTIAL LASER VAPORIZED C_n INTERFERENCES (Ref. 42)

Laser, wavelength Angstroms	N_2 Raman Q Branch Wavelength, Angstroms	Band	
Ruby, 6943	8284		--------
	5976	C_2 Swan	6004.9 (3,5)
			5958.7 (4,6)
2x Neodymium, 5320	6073	C_2 Swan	6122.1 (1,3)
			6059.7 (2,4)
	4733		4737.1 (1,0)
2x Ruby, 3472	3777	C_3 Comet-Head	3793.5
	3212		--------
N_2, 3371	3658	C_3 Comet-Head,	3657
	3125		--------
Dye, 5877	6810		--------
	5169	C_2 Swan	5165.2 (0,0)

It is important to note that not all particles will pose a problem in light scattering diagnostics. For example, alumina possesses an imaginary refractive index component of 10^{-6} in the visible (Ref. 88), so that the visible light absorption coefficient varies from 10^{-5} to 10^{-3} times the geometric cross section for alumina particles in the 0.1 to 10.0μ range respectively. Consequently, very little incident laser energy is absorbed by an alumina particle and little heating occurs unlike the situation with carbonaceous particles (soot). Furthermore, the emissivity of alumina is a factor of two to three lower than that for carbon leading to reduced radiative output for whatever heating does occur. Actually, alumina particles appear to be an excellent seed for simultaneous LDV (laser Doppler velocimetry) - laser Raman work since laser induced alumina incandescent noise should be quite small. Thus, in regard to laser modulated particulate incandescence, not only are the number density and size of the particles important, but their chemical composition as well.

Mie Scattering

Particles can also elastically scatter the incident laser radiation and do so with cross sections much larger than those associated with fluorescence or Raman scatter as shown in Fig. 6. There scattering cross sections are displayed as a function of particle circumference to laser wavelength ratio and were calculated

FIG. 6

PARTICLE SCATTERING AND ABSORPTION CROSS SECTIONS

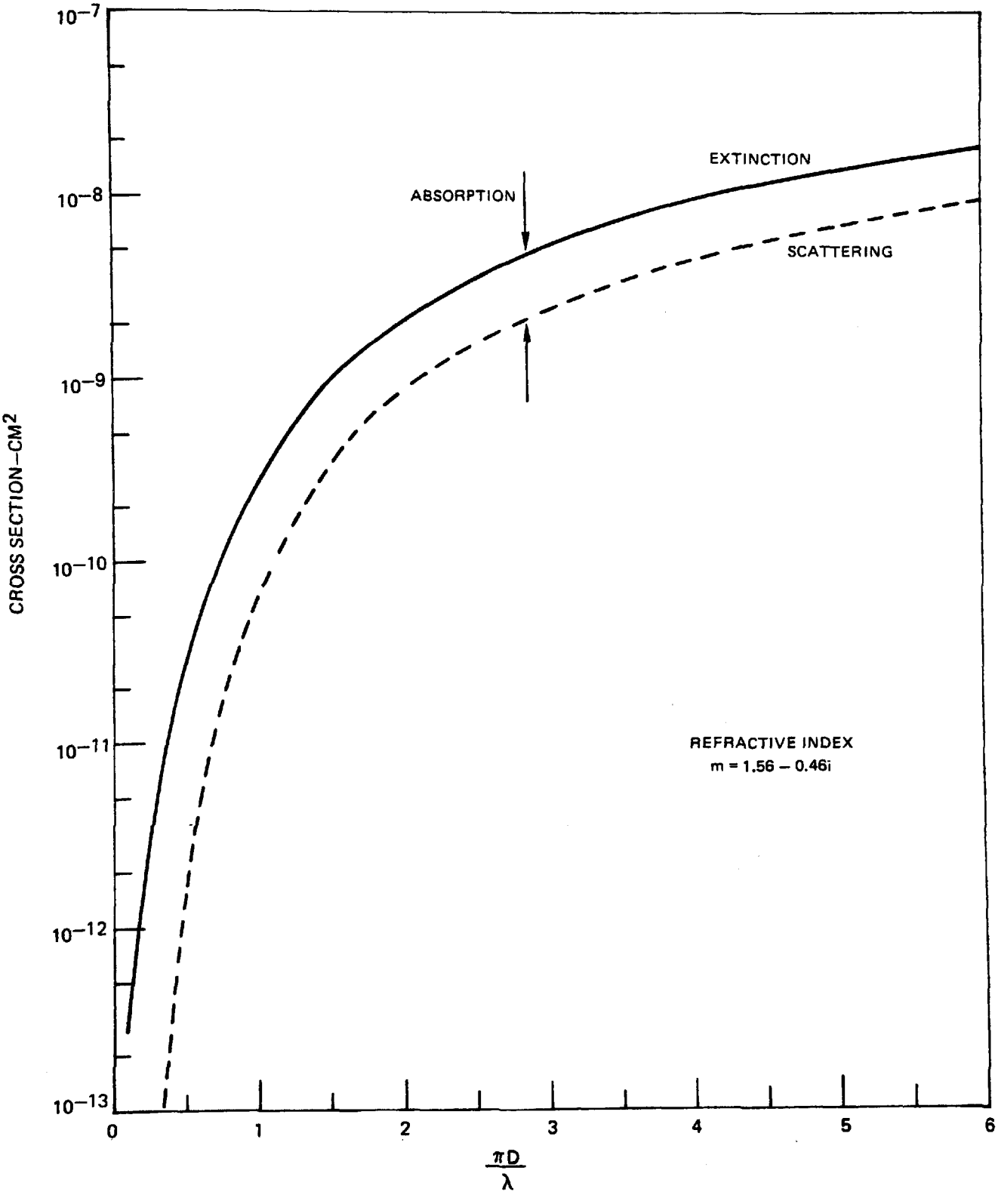

using the UTRC Mie scattering code. The extinction cross sections which are the sum of the scattering and the absorption cross sections will be discussed in a later section. As can be seen, the cross section for scattering from a 0.1 μ diameter particle is about twenty orders of magnitude greater than the N_2 Raman cross section. For a particle number density of 10^8 cm^{-3}, the N_2 number density in a flame would be about ten orders of magnitude higher. Hence the Mie scattering would be about 10 orders of magnitude greater than the N_2 Raman signal. Nominally this is not a problem when detecting inelastic scattering well shifted spectrally from the incident laser line. It is a problem, however, if the spectrally selective instrument being used does not have a high enough rejection outside the passband. Single monochromators have rejection ratios in the range of 10^4 to 10^6. If such an instrument were employed with no other prefiltering, the unrejected Mie signal would greatly exceed the Raman signal present. Consequently, care must be taken in the design of a light scattering experiment to ensure adequate rejection outside the passband region. Clearly such scattering precludes the diagnostic viewing of unshifted resonance fluorescence and can be problematical for rotational Raman scattering if a double or triple monochromator is not used.

Window Fluorescence

As seen previously, coaxial scampling approaches, i.e., 180° or backscattering, are preferable to right angle schemes from a signal to background luminosity noise standpoint. In experiments at UTRC on a model combustor, window fluorescence proved to be a problem with coaxial viewing for dye laser fluxes on the order of 10^6 W/cm^2 at 5900 Å. The fluorescence from the quartz window was approximately equal to the Raman Stokes signal from high temperature nitrogen in the combustor. The fluorescence prevented utilization of coaxial sampling and right angle viewing was instead attempted. However, the very high levels of background luminosity prevented successful diagnosis. Window fluorescence is a potential problem for laser Raman and laser fluorescence measurements; it should pose no difficulties for CARS however,

One solution to this problem involves the use of compound windows with opaque baffling to prevent fluorescence from entering the section of window used to view the scattering. Such a window is yet to be demonstrated on high temperature combustors and may prove either impractical or too expensive to implement.

Spuriously Scattered Laser Light

For weak signal processes, particularly Raman, the laser beam must be trapped with a very high capture efficiency after passing through the measurement location. If permitted to reflect diffusely and specularly in a random fashion in the combustor, very large unshifted radiations are likely to be incident on the spectral instrument used to detect the scattering. Very large rejection ratios would be required to preclude the detection of such spuriously scattered laser radiation. Worse yet such radiations may cause various optical elements, e.g., interference

filters, to fluoresce and incandesce in the spectral passbands of interest. Thus, in general, high efficiency beam traps should be an integral part of the measurement approach. These may range from highly absorbing spheres with an off-axis entrance, heavily baffled cylinders with absorbing glass endwalls oriented at Brewster's angle, Rayleigh horns, etc. A discussion of diffuse reflectivities and beam trapping is provided in Reference 92.

Perturbations

Although laser light scattering techniques are generally touted to be unobtrusive and nonperturbing this is not always the case. In this section, three potential perturbations, namely medium heating, stimulated Raman scattering, and optical breakdown will be considered.

Medium Heating

In the absence of particulates, most combustion media of interest are transparent to the incident laser radiation even when electronic resonances are being probed. Soot particulates, however, are highly absorbing over a wide spectral range and, in sufficient quantity, can absorb substantial fractions of the incident radiation. Of concern here is the thermal perturbation of the medium as heat is transferred from the particulates to the gas. The characteristic time for heat to be transferred a distance, L, within the medium is approximately

$$\tau_p = \frac{L^2 \rho_a c_a}{k_a} \tag{7}$$

where k_a is the medium thermal conductivity; ρ_a, the mass density of the medium; and c_a, its specific heat. For the medium to be perturbed, L must be of the order of half of the interparticle spacing, i.e., $\sim 0.5\ n_p^{-1/3}$ where n_p is the particulate number density. The above will apply as long as the time, τ_c, for heat conduction from the particle to the medium to become effective is less than τ_p. τ_c may be expressed as (Ref. 88)

$$\tau_c = \frac{a^2 \rho_s c_s\ (1+GK)}{3k_a} \tag{8}$$

where ρ_s is the individual mass density of the particulates; c_s, the particulate specific heat; G, a geometry dependent parameter; and K, the Knudsen number. The Knudsen number, i.e., the ratio of mean free path to particle diameter, enters since for small particles in high temperature flames, the gaseous mean free path (about 5000Å @ 1 atm, 2000°K) exceeds the particle size and continuum heat transfer is no longer applicable. In Fig. 7, τ_p and τ_c are tabulated for 2000°K, 1 atm pressure air for a soot dispersion of mass density 10^{-7} gms/cm^3.

FIG. 7

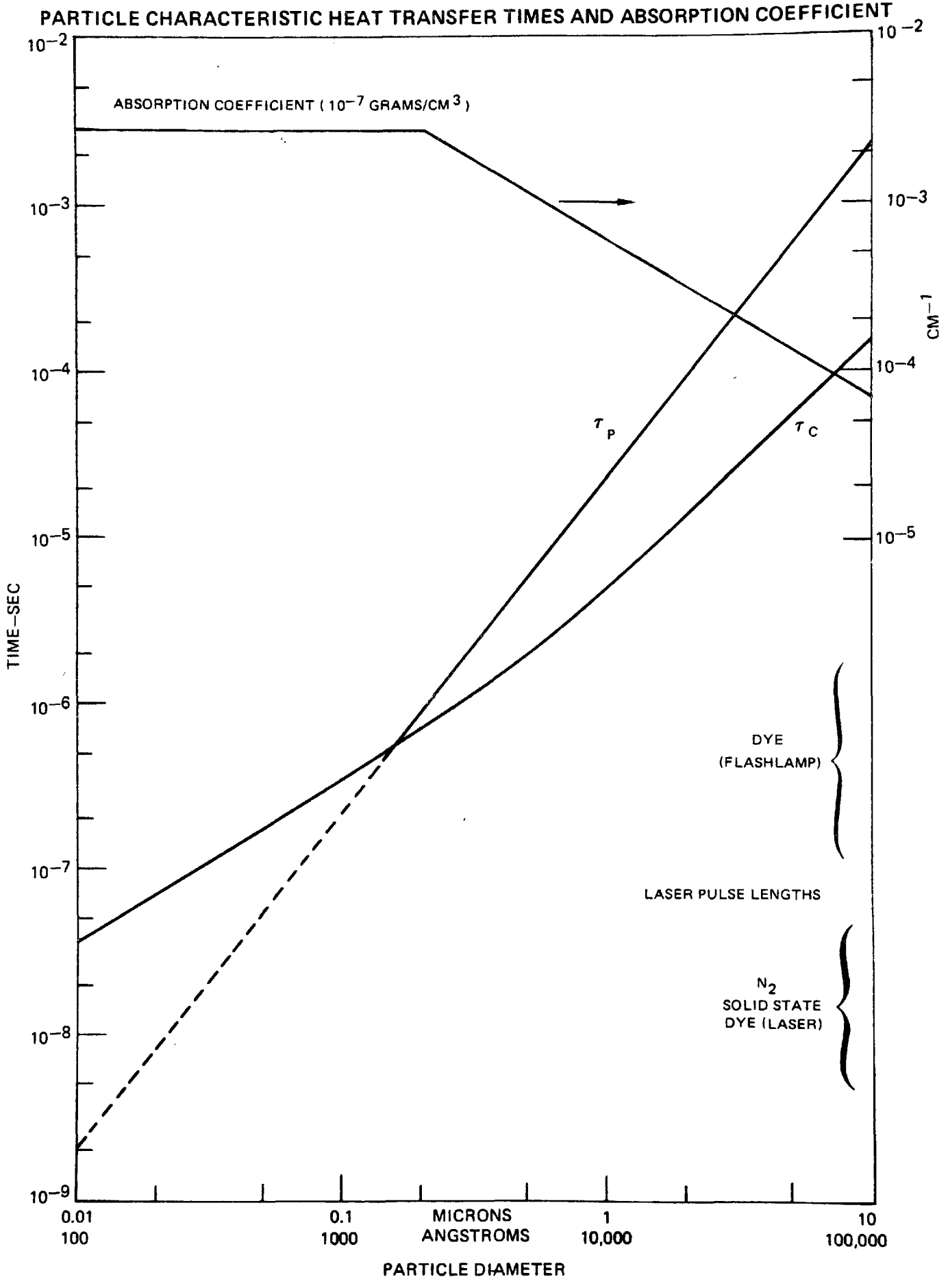
PARTICLE CHARACTERISTIC HEAT TRANSFER TIMES AND ABSORPTION COEFFICIENT
ABSORPTION COEFFICIENT (10^{-7} GRAMS/CM^3)
τ_P
τ_C
TIME–SEC
10^{-2}
10^{-3}
10^{-4}
10^{-5}
10^{-6}
10^{-7}
10^{-8}
10^{-9}
CM^{-1}
DYE
(FLASHLAMP)
LASER PULSE LENGTHS
N_2
SOLID STATE
DYE (LASER)
0.01
100
0.1
1000
MICRONS
ANGSTROMS
1
10,000
10
100,000
PARTICLE DIAMETER

For laser pulses of 10^{-6} seconds or less in duration, large particles ($>1\mu$) pose no perturbation threat. For short laser pulses, i.e., $\sim 10^{-8}$ seconds, no perturbation of the medium will occur. For intermediate length pulses of several hundred nanoseconds, typical of flashlamp-pumped dye lasers, perturbation of the medium with small particulates dispersed throughout could occur. Whether the medium will actually be perturbed depends on the amount of energy absorbed from the laser beam.

The incident laser beam will lose energy as it propagates through the combustor volume in accordance with the relation

$$I(x) = I_o \, e^{-\alpha_a x} \tag{9}$$

where I_o is the input intensity and $I(x)$ that after traveling a small distance, x. Assuming the absorption coefficient α_a to be small, the energy lost in traveling a small distance Δx is

$$\Delta E = \alpha_a E_o \Delta x \, . \tag{10}$$

The absorption coefficient, α_a, may be expressed as

$$\begin{aligned} \alpha_a = n_p \sigma_{abs} &= n_p \pi a^2 \qquad a > \delta \\ &= n_p \pi a^2 \frac{a}{\delta} \qquad a < \delta \end{aligned} \tag{11}$$

where σ_{abs} is the absorption cross section and δ an absorption parameter dependent on the particle indices of refraction. For soot particulates in the visible, $\delta \approx 0.1\mu$ (Ref. 84). In Fig. 7, the absorption coefficient has been calculated as a function of particle diameter for a soot mass density of 10^{-7} gm/cm^3. The largest value of absorption coefficient shown would lead to about a 15 percent decrease in laser intensity over a 50 cm path. If it is assumed that a fraction, f, of the energy absorbed by the particles goes into sample volume heating, and neglecting volume property changes with temperature, the temperature perturbation of the sample volume, V, can be calculated

$$\Delta T = \frac{\Delta E f}{\rho_a c_a V} = \frac{\alpha_a E_o f}{\rho_a c_a A_\ell} \tag{12}$$

where A_ℓ is the cross sectional area of the focused beam. Calculations (Ref. 88) indicate that $f \approx 0.1$, i.e., 10 percent of the absorbed energy is conducted away, while 90 percent is lost to vaporization losses. For a cylindrical sample volume of 10^{-2} cm^2 cross sectional area, a pulse energy of 1 joule and pulse duration of 0.5 μsec, a ΔT of 163°K is calculated, an error of about 8 percent for particles less than 0.1μ in diameter. From Fig. 7 it is seen that the larger particles pose no perturbation problems for pulse lengths below 10^{-6} sec.

Stimulated Raman Scattering

At high laser intensities, stimulated Raman scattering may occur (Refs. 16 and 17). By promoting molecules from the ground to the first vibrational state at a high rate, the species being probed may be perturbed resulting in erroneous density and temperature measurements. A Stokes input intensity of $I_s(0)$ will be amplified by stimulated Raman scattering according to the relation (Ref. 93)

$$I_s(\ell) = I_s(0) \exp (gI_L\ell) \tag{13}$$

where $I_s(\ell)$ is the amplified Stokes intensity after a distance, ℓ; I_L, the laser intensity; and g, the Raman gain factor which on line center is

$$g = \frac{16\pi^2 c^2 N\Delta}{\hbar\omega_s^3 n^2 \Gamma} \left(\frac{\partial\sigma}{\partial\Omega}\right) \tag{14}$$

where c is the speed of light; N, number density; Δ, the fractional population difference between the lower and upper states; $\partial\sigma/\partial\Omega$, the Raman cross section; $\hbar = h/2\pi$ where h is Planck's constant; ω_s, the Stokes radian frequency; n, the index of refraction which is nearly unity in gases; and Γ, the Raman linewidth. At 1500°K in N_2 the maximum population resides in J = 16 and Δ can be shown to be 0.04. Assuming $\Gamma = 0.1$ cm^{-1}, g can be evaluated for a laser wavelength of 5320Å and is found to be 5.94 (10^{-14}) cm/Watt. For a laser intensity of 10^{10} Watts/cm^2 and a 1 cm pathlength, the stimulated Raman gain is miniscule. This would also be true of 300°K, atmospheric pressure N_2. In Ref. 93, a gain of only 1.2 was found over a 10 meter path for a laser intensity of about 10^8 Watts/cm^2. Thus it may be concluded that stimulated Raman scattering is unlikely to perturb the populations being probed for typical combustor operating regimes, vis. pressures less than 100 atmospheres and spatial resolutions of a few centimeters.

Optical Breakdown

With the application of intense electric fields from high intensity laser radiation, the medium under examination may break down, i.e., become fully ionized. With plasma formation the medium is substantially altered, thus precluding diagnostic interrogation. A comprehensive review of laser radiation induced gas breakdown is presented in Ref. 94. Most work to date has been concerned with breakdown at 10.6, 1.06 or 0.6943μ where the breakdown thresholds roughly scale according to $1/\lambda^2$ as predicted by cascade ionization models. However, in the visible and, particularly, in the uv, multiphoton processes become important and the breakdown thresholds begin to decrease with decreasing wavelength. For example in Ref. 95, in examining air breakdown between 6500 and 5500Å, the threshold increased from ~ 1.5 (10^{11}) W/cm^2 at 6500 Å to a peak value of 8(10^{11}) W/cm^2 at 5500 Å. In Ref. 96, similar peaking

effects were observed in noble gas breakdown studies. In attempting to establish a breakdown threshold for a practical combustion device, the effects of particulates and number density must also be accounted for. Large particulates (i.e., greater than several microns in diameter) decrease clean air thresholds by about two orders of magnitude in general (Refs. 97 and 98). Smaller particulates generally have no effect due to very high electron diffusion losses. The pressure (i.e., density) dependence on the breakdown threshold is approximately inverse, i.e., 1/p. In an atmospheric pressure flame at temperatures on the order of 1500-2000°K, the breakdown threshold should be approximately 5-7 times higher than the clean air 1 atmosphere breakdown thresholds. Gas temperatures up to 2000-3000°K are not expected to affect the threshold values.

For an atmospheric pressure combustor operating at temperatures near 2000°K, breakdown will be assumed to occur at about 10^{10} W/cm^2 at 5000Å. To obtain this estimate the 10^{11} W/cm^2 atmosphere density value (Ref. 95) has been increased by an order of magnitude to account for density decreases at high temperature and reduced by about two orders of magnitude to account for particulates. The pessimistic assumption will be made that in a hydrocarbon fueled diffusion flame there will always be a few large particles, i.e., > few microns diameter, present in the laser focal volume. At shorter wavelengths, the threshold will decrease (Ref. 94) and breakdown will be taken to occur at 10^9 W/cm^2 at 2000Å and 5 (10^9) W/cm^2 at 3500Å. These values then represent the maximum focal fluxes tolerable for any diagnostic approach.

Laser/Signal Transmission

To perform spatially resolved measurements at a given location in the combustor, the laser beam must be transmitted reproducibly and with high efficiency to the desired measurement point. There are a number of factors which can influence the energy, intensity and even the actual measurement location pertaining in a given situation. Some of these considerations will be explored in this section.

Optical Component Damage

Experiments in the laboratory are often performed on flames devoid of enclosures and optical ports. This is generally not the case with practical device probing where the phenomenon under investigation is viewed through a window, often of limited aperture. With the device operating, the window is likely to become coated with particulates over a period of time. Quartz is commonly used for optical probing of combustors due to its high temperature capabilities. In Ref. 99, the optical damage threshold for bulk quartz at 6943Å for a single mode laser was found to be $28 \pm 5x(10^9)$ W/cm^2. Surface damage thresholds are generally lower than bulk values. In Ref. 100, a front surface damage threshold of 20.2 (10^9) W/cm^2 was reported at 6943 Å for X-cut crystal quartz. Exit damage thresholds are generally lower than entrance values due to Fresnel reflections; for glass with a refractive index of 1.55, the exit damage threshold is about 33 percent lower (Ref. 101). Furthermore cracks, pores, etc.

reduce the damage threshold between 2-5 for low index materials such as quartz (Ref. 1C2). Based on the foregoing, quartz may be assumed capable of transmitting fluxes on order of a few gigawatts/cm^2. If the optical surfaces become contaminated with dirt/soot, the threshold will be even lower. It should be noted that due to temporal variations in pulse shape and spatial variations in intensity, actual peak intensities in laser pulses may be a factor of five to ten higher than the calculated average flux level.

To minimize the probability of damage in optical materials, the laser flux should be kept as small as possible passing through the window. One way of achieving this is to place lenses as close to the window as possible. This then maximizes the distance between the laser focal point, the region of highest flux and the window. Another approach, of course, is to beam expand to decrease the laser intensity prior to transmission through the optical port. To avoid particulate deposition on ports, gas purging of the surface may be necessary. Measurements near a window , i.e., at the device periphery may be precluded, however, by optical damage.

Soot Extinction

As the laser beam propagates through the combustor, particulate matter, e.g., soot, will attenuate the beam due to scattering and absorption. The latter, of course, results in the laser modulated particulate incandescence phenomenon previously discussed. In Fig. 6, extinction and scattering cross sections are displayed for carbonaceous particles as a function of $\pi D/\lambda$. The difference between the extinction and scattering curves is due to particle absorption. Radiation propagating through such a dispersion will be attenuated as $\exp(-n_p \sigma_e \ell)$ where n_p is the soot density, σ_e, the extinction cross section, and ℓ, the path length. In Table IX calculations are presented as a function of particle size for an $n_p \sigma_e \ell$ of 0.1, corresponding to about 10 percent decrease in beam or signal transmission.

TABLE IX

PARTICULATE EXTINCTION EFFECTS

5000Å $n_p \sigma_e \ell = 0.1$ $\ell = 50$ cm

Diameter (μ)	$\pi D/\lambda$	σ_e(cm^2)	$n_p \ell$	n_p (cm^{-3})	ρ_{soot} (gm/cm3)
0.01	0.063	$1(10^{-13})$	$1(10^{12})$	$2(10^{10})$	$2.4(10^{-8})$
0.04	0.25	$3(10^{-12})$	$3.3(10^{10})$	$6.6(10^{8})$	$5.0(10^{-8})$
0.1	0.63	$6(10^{-11})$	$1.7(10^{9})$	$3.4(10^{7})$	$4.0(10^{-8})$
1.0	6.3	$2(10^{-8})$	$5(10^{6})$	10^{5}	$1.2(10^{-7})$
10.0	63	$2(10^{-6})$	$5(10^{4})$	10^{3}	$1.2(10^{-6})$

For the previously examined soot dispersion of 10^8 cm^{-3}, 400Å diameter particles, there would only be a beam attenuation of about 1.5 percent over a 50 cm pathlength. From Table IX it is clear that particulate extinction over a 50 cm path would become significant for small particles at mass densities above a few times 10^{-8} gm/cm^3. Hence, only at the highest background luminosities previously displayed in Fig. 3 might the potential for significant extinction be present.

Beam Steering/Defocussing

Turbulence and thermal gradient effects in the combustion medium may cause the incident laser beam to be defocused or steered due to refractive index gradients. This is a difficult phenomenon to analyze without detailed turbulence and temperature models. For small combustion devices operating at or near atmospheric pressure, it is not believed to be a serious problem. This is based upon steering experiments conducted at UTRC on the 12 cm dia. combustor described in Ref. 77 and experiments on the EPA Rainbow furnace described in Ref. 74. In the latter set of experiments, two laser beams were crossed in the furnace to produce an interference fringe pattern. The beams upon exiting the device were then imaged to form a second fringe pattern which could be probed with a tungsten whisker. Operation of the furnace produced no change in the fringe pattern. LDV measurements were also performed successfully. In LDV work at UTRC on the 12 cm dia. combustor previously mentioned, there is an interrupted data rate; whether the interruption occurs due to turbulence effects or lack of a scattering particle in the sample volume is not clear. Nevertheless LDV measurements have been successfully performed. In brief, then, it is believed that combustion turbulence in devices of small diameter (< 100cm) operating at atmospheric pressure will not be a serious problem. Whether it is a problem in large scale, high pressure devices is probably best determined via a series of relatively simple experiments.

Particulate induced thermal blooming of the incident laser beam (Ref. 103) is also anticipated to be unimportant for short laser pulse lengths. These effects would become important only on a time scale on the order of τ_p (Fig. 7) which is long compared to the pulse length of most high energy pulsed lasers. For long laser pulse lengths, convection effects would minimize blooming.

Signal Averaging

In instances where the single pulse signal to noise ratio is not sufficiently high to permit accurate measurements, signal averaging in conjunction with a noise sampling and subtraction approach, will be required to enhance signal to noise prior to further data treatment. In certain circumstances depending on the magnitude and correlation in medium property fluctuations, signal averaging may result in an accumulation of averages over these fluctuations. These residual terms cloud interpretation of the signal averages and introduce errors into the

measurements if the standard data reduction approaches are applied. Since each measurement technique differes in its functional dependences on density and temperature, more detailed assessments of signal averaging will be deferred to those sectionsin which each diagnostic approach is separately discussed. Suffice it to say here, that in general, signal averaging in temporally fluctuating media is not straightforward and should be carefully scrutinized.

Summary

In Table X, the various practical considerations discussed in this section are summarized. Many of the effects discussed can be dismissed as being unlikely, too weak or avoidable by proper design approaches. Those likely to be serious problems will be treated in the later sections in which each diagnostic approach is separately reviewed.

TABLE X

SUMMARY OF PRACTICAL CONSIDERATIONS

Item	Comment
Sources of Noise	
Background Luminosity	potentially serious interference
Laser induced particulate fluorescence	potentially serious interference
Particulate Raman scattering	interference unlikely
Laser modulated particulate incandescence	potentially serious interference
Mie scattering	avoidable with high rejection
Window Fluorescence	avoidable with compound window, or right angle viewing
Spurious laser scattering	avoidable with beam trapping
Perturbations	
Medium heating	generally unlikely
Stimulated Raman Scattering	very little liklihood
Optical Breakdown	maintain focal flux below 10^{9}-10^{10} W/cm^{2}
Laser/Signal Transmission	
Optical Component Damage	maintain window flux below 10^{9}W/cm^{2}
Soot Extinction	problematical in large (> 1 m dia), highly sooting combustors
Steering/Defocussing	unlikely in small (< 1 m dia) devices
Signal Averaging	with caution, only after analysis

RAMAN SCATTERING

Introduction

Laser Raman techniques offer a number of advantages for combustion and other diagnostics as described in detail in Refs. 8, 104, and 105. In brief, only a single laser is required to monitor all of the species of interest. The laser can operate at any wavelength without the necessity of being tuned to resonances of the molecule being probed. This is not true for near-resonant Raman scattering, whose discussion will be deferred to the end of this section. Here only spontaneous Raman scattering will be considered. Visible wavelengths are favored, however, because of the scaling of the Raman cross sections as λ_R^{-4}, where λ_R is the Raman scattering wavelength. With proper detection, several species can be monitored simultaneously. Quite importantly, the Raman scattered intensities are unaffected by quenching. Furthermore, absolute calibration is readily achieved by comparing the scattered signal from the species of interest with that of nitrogen. Unfortunately, spontaneous Raman scattering is very weak. Typical vibrational Raman cross sections (Table V) are on the order of 10^{-30} cm^2/sr. It is the weakness of the process, despite all of its other advantages, that makes spontaneous Raman scattering very difficult to apply to practical combustion devices, as will be shown later.

Most of the work on species measurements in flames utilizing Raman scattering has been directed toward detection of majority species such as N_2 (Refs. 106, 107, 108 and 109), O_2 (Refs. 106, 107, and 108), CO_2 (Refs. 104, 106, and 107), CO (Ref. 107), H_2O (Refs. 107, 108, and 109), and H_2 (Refs. 29, 109, and 110) to name a few. Leonard (Ref. 78) successfully monitored O_2 and CO_2 in a T53 engine exhaust, but was prevented from detecting NO because of hydrocarbon fluorescence interferences as mentioned before. CO and NO_2 detection were not attempted due to anticipated strong interferences from N_2 and CO_2, respectively. Much of the work on remote detection of pollutants carried out to date has been based on Raman scattering, although differential absorption backscatter is receiving much attention. Inaba and Kobayasi (Ref. 69) summarize much of the work to 1972. Of particular note (Ref. 61) is the detection of H_2O (10^4 ppm), CO_2 (310 ppm) and SO_2 (30 ppm), the latter from a range of 200 meters.

Thermometry has been performed by a number of investigators generally from analysis of the scattering from a dominant molecular constituent such as N_2. Raman temperature measurements have been made in flames (Refs. 104, 108, 109, 110, 111, 112 and 113), air in the atmosphere, wind tunnels, or shock tubes (Refs. 114 - 121), and electric discharges (Refs. 47, 122, and 123).

Most of the above referenced studies have been performed under relatively benign instrumentation circumstances, i.e., low background luminosity, particulate free environments. Spontaneous Raman scattering, despite its weak signal strengths, is ideally suited for diagnosis of such environments. Interpretation of the Raman spectra is relatively straightforward and for the most part free of spectral interferences (Table VI). However, for practical combustor diagnosis, the many sources of "noise" previously reviewed pose a formidable obstacle to successful implementation. In this section, the princples of Raman scattering will be briefly reviewed and its application to density and temperature measurements discussed. Its measurement capabilities in clean flames will be discussed and illustrated by sample calculations. Then, signal/noise calculations will be performed for various state-of-the-art laser sources for both background luminosity and laser modulated particulate incandescence. The effects of signal averaging Raman data in a turbulent medium will be reviewed. Costs and probability of success, i.e., risk, for practical applicability of Raman scattering will be discussed. Near-resonant Raman scattering will be examined at the conclusion of this section.

Theory

Raman scattering is the phenomenon of inelastic collision processes between photons of light and molecules in either solid, liquid, or gaseous phases. The effect was theoretically predicted by Smekal in 1923, but subsequently named in honor of its experimental discoverer, C. V. Raman, who first published his observations in 1928. Although the discovery of the effect is nearly fifty years old, its application to gas phase diagnostics awaited availability of powerful monochromatic light sources. With the advent of high power visible laser sources, Raman scattering is now being widely exploited for a variety of gas phase diagnostics studies as the foregoing references clearly indicate. Raman scattering has been physically understood for some time and detailed theoretical treatments are to be found in Refs. 8, 23, 124, and 125. For diagnostic purposes it suffices to know that the Raman scattered power is proportional to the incident light power and the number density of molecules in the appropriate initial quantum states for the scattering to be observed.

Photons of light colliding with molecules may either lose energy to or gain energy from the target molecules as shown in Fig. 8. In the former event, termed Stokes scattering, the molecule becomes excited, and, in the latter, termed anti-Stokes, the molecule is deexcited providing, of course, that it was in an excited state prior to the collision. The energy exchanges which occur are quantized in accordance with the allowable energy levels of the molecule, thusly,

$$h\nu + N(v,J) \rightarrow h\nu' + N(v',J')$$
$$h(\nu - \nu') = E(v', J') - E(v,J) \qquad (15)$$

RAMAN SCATTERING PROCESSES

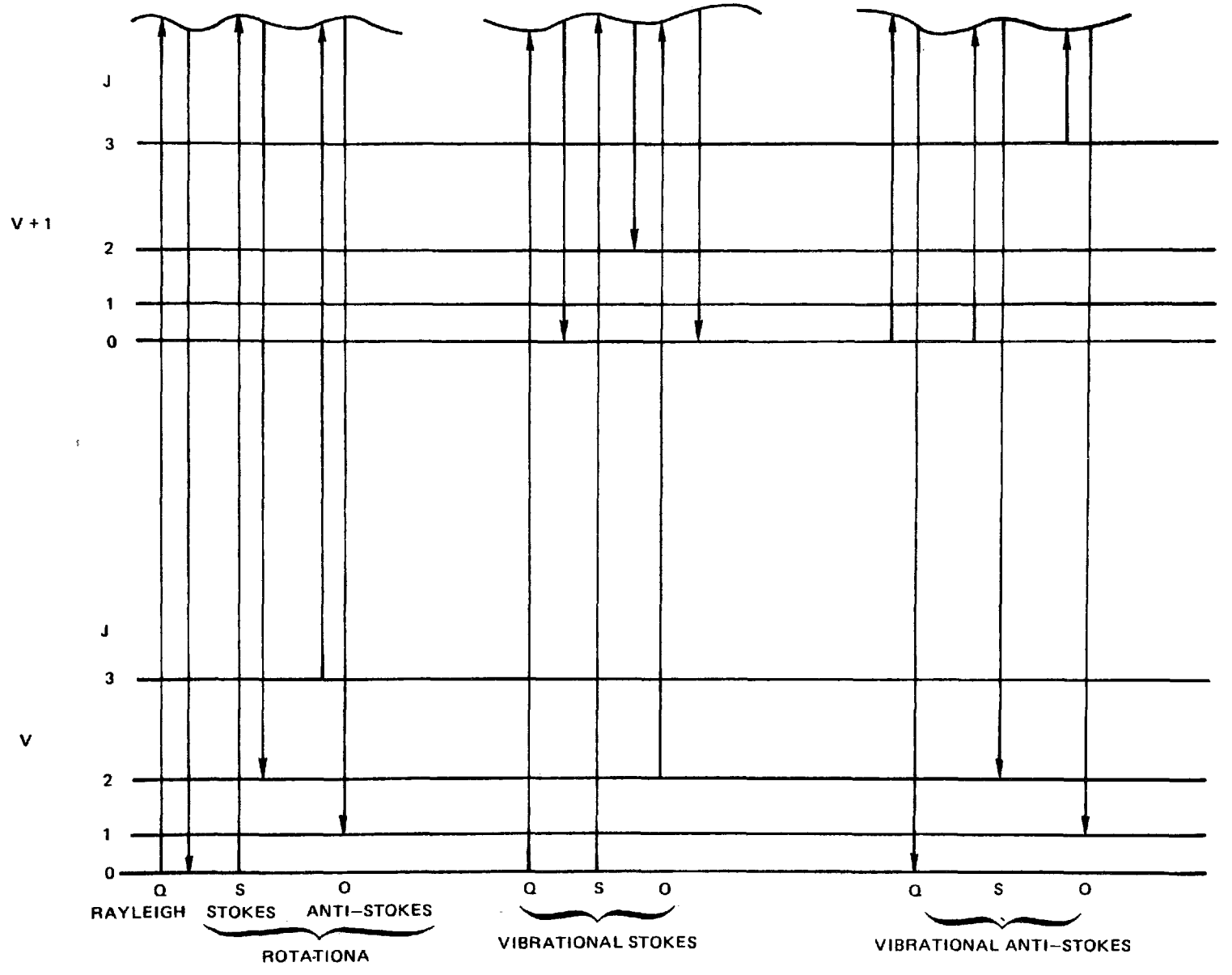

FIG. 8

where h is Planck's constant; ν, the frequency of incident photons; $N(v,J)$, the quantum energy state characterized by a vibrational quantum number, v, and rotational number, J; and E, the state energy. Primes denote the above quantities after the collision. Here v,J represent the totality of quantum numbers, dependent on the polyatomicity of the molecule. Since each molecular species possesses a characteristic set of energy states, the spectral distribution of Raman scattering is uniquely determined by the incident laser wavelength and the species from which scattering occurs. If no change in vibrational quantum number occurs, the scattering is termed rotational Raman, otherwise it is termed vibrational-rotational or vibrational for short. The allowed changes in quantum number are governed by certain selection rules for the process. For diatomic molecules vibrational quantum number changes are restricted to 0, ± 1 while rotational numbers changes of 0, ± 2 are permitted. If no change in rotational quantum number occurs, the Raman scattering is termed Q branch, while for ± 2 it is termed S and O. The scattering may be either upshifted (anti-Stokes) or downshifted (Stokes) in frequency depending on whether the state (v',J') resides below or above (v,J), respectively in energy.

Density measurements derive from the fact that the Stokes power, P_r^s, scales directly with incident power, P_i, and number density, n, as (rewriting Eq. (1))

$$P_r^s = k^s P_i n f^s(T) \tag{16}$$

$f^s(T)$ is termed the bandwidth factor and is a temperature dependent term which accounts for the fraction of scattering species in the appropriate initial quantum states for scattering to be observed. $f^s(T)$ depends on the spectral location, shape and bandwidth of the spectrometer or interference filters employed and on the laser "line" profile and bandwidth. It can be easily calculated employing detailed Raman codes (Refs. 109 and 113). k^s is a factor dependent on Raman cross section, wavelength, geometry, and optical collection efficiency and usually determined accurately by calibration. Having so determined k^s, and knowing or measuring P_i and T, n can be determined from the measured Raman scattering. To eliminate the requirement on temperature information in order to make density measurements, $f^s(T)$ can be made constant over a wide temperature range as shown in Fig. 9 by proper selection of bandwidth. Unfortunately the bandwidths required are large which decreases the S/N in the presence of spectrally broad sources of noise. In Fig. 9 bandwidth factors are displayed for varying bandwidths for Raman scattering from N_2 employing a 5320 Å laser source (e.g., frequency doubled neodymium) with infintesimally thin linewidth using a Raman code described in Ref. 113. Similar calculations have been performed, for example, in Ref. 109 with similar findings.

Because the spectral distribution of Raman scattering is essentially a display of state populations, temperature measurements can be performed in a number of ways, e.g., spectral band contours (Refs. 108, 110 and 112), peak height ratios (Refs. 111, 113 and 119), peak height shifts. A common technique is to ratio the anti-Stokes to Stokes vibrational scattering produced by a single pulse, i.e., from Eq. (16)

FIG.9

TEMPERATURE VARIATION OF STOKES BANDWIDTH FACTOR

LASER LINE 5320 Å

N_2 SCATTERING

FILTER CENTER AT 6073 Å

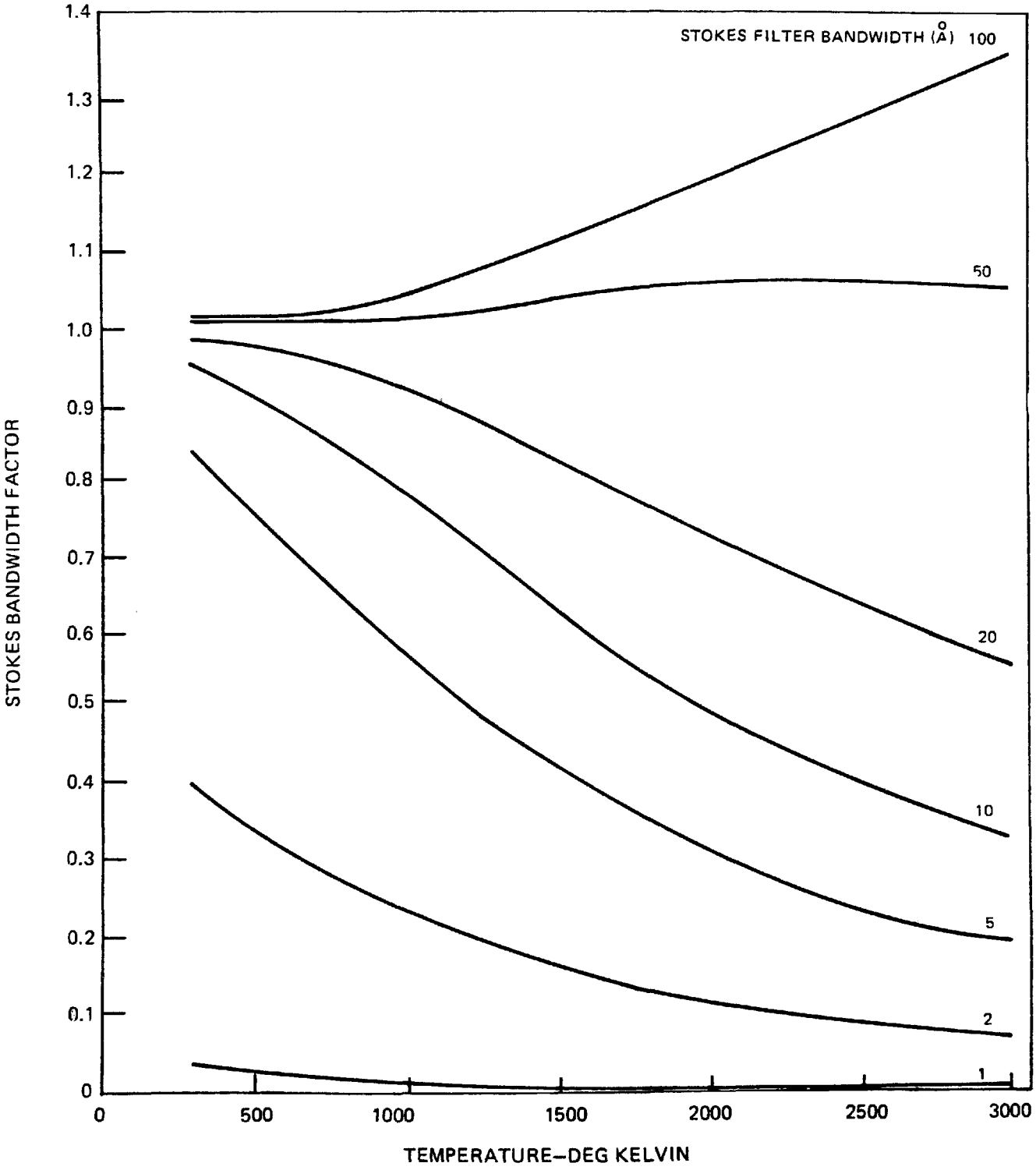

$$\frac{P_r^a}{P_r^s} = \frac{k^a f^a(T)}{k^s f^s(T)} \tag{17}$$

Note that the ratio is independent of the laser power and most importantly number density and solely dependent on temperature. In Fig. 10, anti-Stokes to Stokes bandwidth ratios are displayed for the previously illustrated case of an infinitesimally thin linewidth laser source at 5320 Å. In practice the factor k^a/k^s is obtained via calibration, e.g., from a tungsten filament lamp (Ref. 84).

Preferred Raman Approaches

Referring to Eq. (1) it is seen that the Raman scattered power scales as the product of the incident laser power, Raman cross section and molecular number density in the appropriate initial quantum states for scattering to be observed. With this in mind, preferred approaches to the implementation of Raman scattering diagnosis can be examined.

Raman Band Selection

Cross sections for rotational and vibrational-rotational scattering have been summarized in Table V. Of note is that only small differences exist in the scattering cross sections of the various molecules. This means that calculations performed for one species are fairly well exemplary of what can be expected for any other species. There is a substantial difference, however, between cross sections for pure rotational scattering and for vibrational/rotational scattering. For example, the cross section for a single line, $J = 6 \rightarrow J' = 8$, in the rotational spectrum of N_2 is nearly an order of magnitude greater than the entire vibrational Q branch cross section. This advantage is offset at high temperatures by the smearing of rotational level populations so that only a few percent of the molecules reside in the level from which scattering originates. Another problem with rotational scattering is that the energy exchanges involved are very small leading to small spectral displacements of the rotational Raman lines from the exciting laser line. The spectral displacement is given by:

$$\Delta\nu = \begin{cases} 2B(2J-1) & \text{O branch} \\ -2B(2J+3) & \text{S branch} \end{cases} \tag{18}$$

Since B for most molecules is only a few cm^{-1}, the rotational spectra from the various molecules overlap and interfere with one another. In addition discrimination against the nearby and much stronger Rayleigh , Mie and/or spurious laser scattering is very difficult.

FIG. 10

BANDWIDTH FACTOR RATIO VARIATION WITH TEMPERATURE

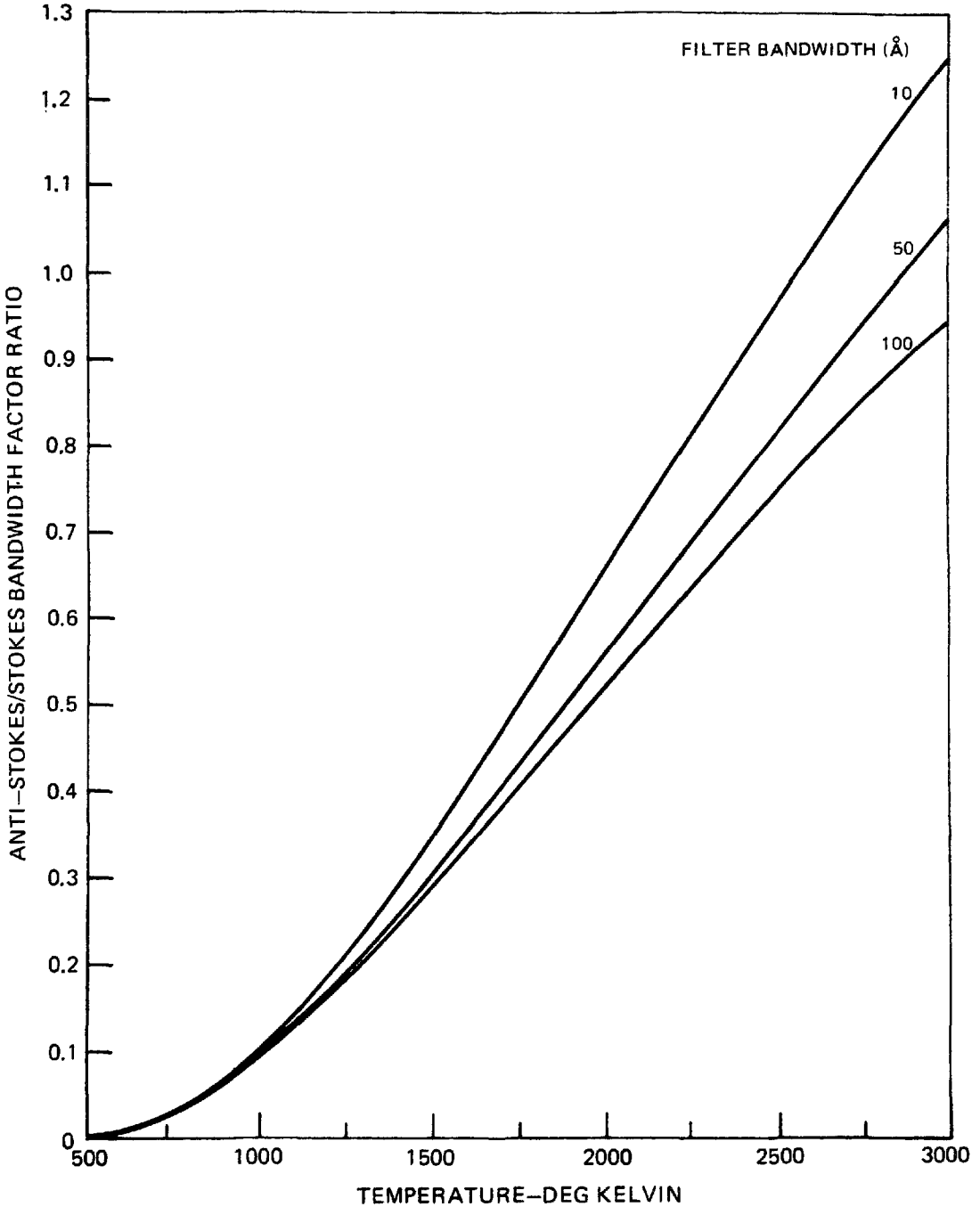

Some of these difficulties are overcome by the detection scheme devised by Smith (Ref. 126) in which a Fabry-Perot etalon with a free spectral range equal to the rotational Raman line spacing ($4B_o$) is employed. Properly tuned and with high finesse such an etalon simultaneously transmits all the rotational Raman lines of a particular molecule while discriminating against other molecules. However a Fabry-Perot etalon possesses a discrimination ratio of 10^4 to 10^5 at most, so that some light will be transmitted even though not resonant with the filter. Consequently, it would be extremely difficult to detect trace concentrations of species accurately due to incomplete discrimination of the rotational Raman scattering from major flame constituents, of the Rayleigh scattering and of the Mie scattering when particulates are present. In this light it is not surprising that rotational Raman has not been widely used in flames or multicomponent mixtures.

Despite the weakness of the cross section, vibrational Raman bands are well displaced spectrally from the exciting line, typically by 1000 cm^{-1} or more, and interferences between vibrational Raman spectra in flames are rare (Table VI). Furthermore for Q branch transitions, the scattering arising from the entire population of a given vibrational state can be monitored, partially offsetting the vibrational cross section disadvantage. Consequently, only vibrational Raman scattering will be considered in these diagnostic evaluations.

Continuous Wave or Pulsed Laser Excitation

Although many Raman studies have been conducted with continuous wave lasers in clean flames, it will be shown here that cw lasers are unacceptable for practical combustion device diagnostics. This will be done by considering the Raman signal/noise ratio in a luminous background. Combining Eqs. (1) through (3), the Raman signal to background luminosity noise ratio may be expressed as

$$\frac{S}{N} = \frac{2Pnf \frac{\partial\sigma}{\partial\Omega}}{\Re \Delta\lambda \pi F \ell^2} \tag{19}$$

Consider the situation for Raman scattering from N_2 using a 10 watt argon ion laser at 5145 Å. The Stokes scattering will reside at 5846 Å and the cross section (Ref. 127) appropriately scaled is 4.31 (10^{-31}) cm^2/sr. For a 2000°K flame the number density of molecules in the ground vibration state, n_o is 2.38 (10^{18}) cm^{-3}. For a 10 Å bandwidth, $f \cong 0.5$. F8 collection optics will be assumed typical of most monochromator acceptance solid angles. The sampling extent will be taken as 1 mm, chosen small to increase the S/N ratio. The calculated S/N are summarized in Table XI below as a function of the radiation energy density.

TABLE XI

CONTINUOUS WAVE LASER RAMAN/BACKGROUND LUMINOSITY NOISE RATIO

(Powers of Ten in Parentheses)

$\mathcal{R}\ \left(\frac{\text{nanowatts}}{\text{cm}^3\text{Å sr}}\right)$	.001	.01	.1	1	10	100	1000
S/N	4.1	4.1(-1)	4.1(-2)	4.1(-3)	4.1(-4)	4.1(-5)	4.1(-6)

As is apparent for radiation energy densities typical of a furnace (Fig. 3), the background luminosity exceeds the Raman scattered signal by several orders of magnitude. These noise calculations illustrate that, even with high power lasers, cw Raman scattering studies are applicable only in very low luminosity environments.

From Table XI and Eq. (19), it is clear that with a high peak power pulsed laser that the Raman signal to luminosity noise ratio will be considerably improved. For example with a pulsed laser with a peak power of 10^8 Watts, the foregoing S/N ratio will be increased by about seven orders of magnitude possibly permitting majority species studies in highly luminous environments.

Trace species detection is difficult, however, regardless of background considerations due to the smallness of the Raman cross sections. As mentioned earlier, because the Raman Q-branch cross sections are all nearly the same, detectability limits for one specie will be exemplary of the sensitivity levels that may be generally achieved. In the following, the detection limits for NO will be examined. The Raman scattered energy in the Stokes Q-branch, Q_r, induced by a pulsed laser with energy, Q_{in}, is given by (rewriting Eq. (1))

$$Q_r^{NO} = Q_{in}\, n^{NO}(v=0)\, \sigma_{NO}^{0\to 1}\, \Omega\, \ell\, \epsilon \tag{20}$$

where $n^{NO}(v=0)$ is the ground state number density. For simplicity the detector bandwidth is assumed broad enough so that the bandwidth factor is unity. The Q branch NO cross section appropriately scaled is 2.1 (10^{-31}) cm^2/sr. F5 collection optics corresponding to a 3.1 (10^{-2}) sr solid angle will be assumed; for a 1 meter diameter furnace, a 10 cm optical port would be required. The collection efficiency will be assumed to be 10 percent. The amount of ground state NO is given by

$$n^{NO}(v=0) = (1 - e^{-[E(1)-E(0)]/kT})nC \tag{21}$$

where E(1)-E(0) is the energy difference between the first and ground vibrational state, 1977 cm^{-1}; n, the total number density; and c, the fractional NO concentration. Assuming the scattering is induced by a pulsed, frequency-doubled, neodymium laser at 5320 Å, the center of the NO Stokes Q branch will reside at 5910 Å. Dividing

the Raman scattered energy by the individual photon energy yields the number of collected Raman photons, n_p. Ignoring background for this illustration, the S/N is limited by photocathode statistics (Ref. 128) and is given by

$$S/N = \sqrt{\eta n_p} \tag{22}$$

where η is the photocathode quantum efficiency, assumed to be 0.1. Assuming the detectability limit to be a single pulse S/N of unity, the minimum detectable concentration can be calculated. The accuracy of the measurement when shot noise limited can be improved by signal averaging. For example, averaging the above over 100 shots would provide a measurement accuracy of ± 10 percent. In Fig. 11, pulsed laser Raman detectability limits for NO are displayed as a function of laser pulse energy with gas temperature and spatial resolution shown parametrically. For a 1 Joule laser pulse at a high flame temperature, 2000°K and a 1 cm sampling extent, measurements are not possible below about 2000 ppm. Note that a 1 Joule laser pulse with a typical pulse length of 10^{-8} sec and focused to a 1 mm spot size, corresponds to an average focal flux of 10^{10} W/cm^2. Higher energies would most likely lead to gas breakdown as seen earlier. Although a 10 cm length lowers the sensitivity an order of magnitude, this hardly constitutes a "point" measurement. 10 cm can in effect be obtained with a 1 cm extent in a multipass cell with a gain of 10. Multipass cells have been successfully demonstrated in Raman studies using diffraction limited gas lasers on small burners (Ref. 129). Their applicability to poor beam quality pulsed lasers on a real furnace is highly doubtful however. The foregoing calculations are intended to illustrate that even in the absence of background noise effects, Raman detection of species in trace quantities is very limited even with high energy/pulse lasers and poor spatial resolution.

Pulsed Laser Raman Signal to Noise Calculations

In the preceding section, continuous wave lasers were shown to be incapable of Raman combustion studies except in very low luminosity environments. It was also indicated that pulsed lasers may lead to sufficiently high S/N ratios for majority species determinations in luminous environments. In this section, this conclusion will be more closely examined for a variety of pulsed laser systems. In addition to considering noise from background luminosity, laser modulated particulate incandescence effects need also be considered as described previously.

Laser Source Selection

Four state-of-the-art laser sources will be considered for the signal/noise calculations. These will include: (1) a 1 Joule per pulse frequency-doubled neodymium laser at 5320 Å with a 10 nanosecond pulsewidth; (2) a 0.5 Joule dye laser at 5900 Å with a 0.5 μsec pulsewidth; (3) a 1 Joule, 30 nanosecond pulsed ruby laser

PULSED RAMAN NO DETECTABILITY LIMITS

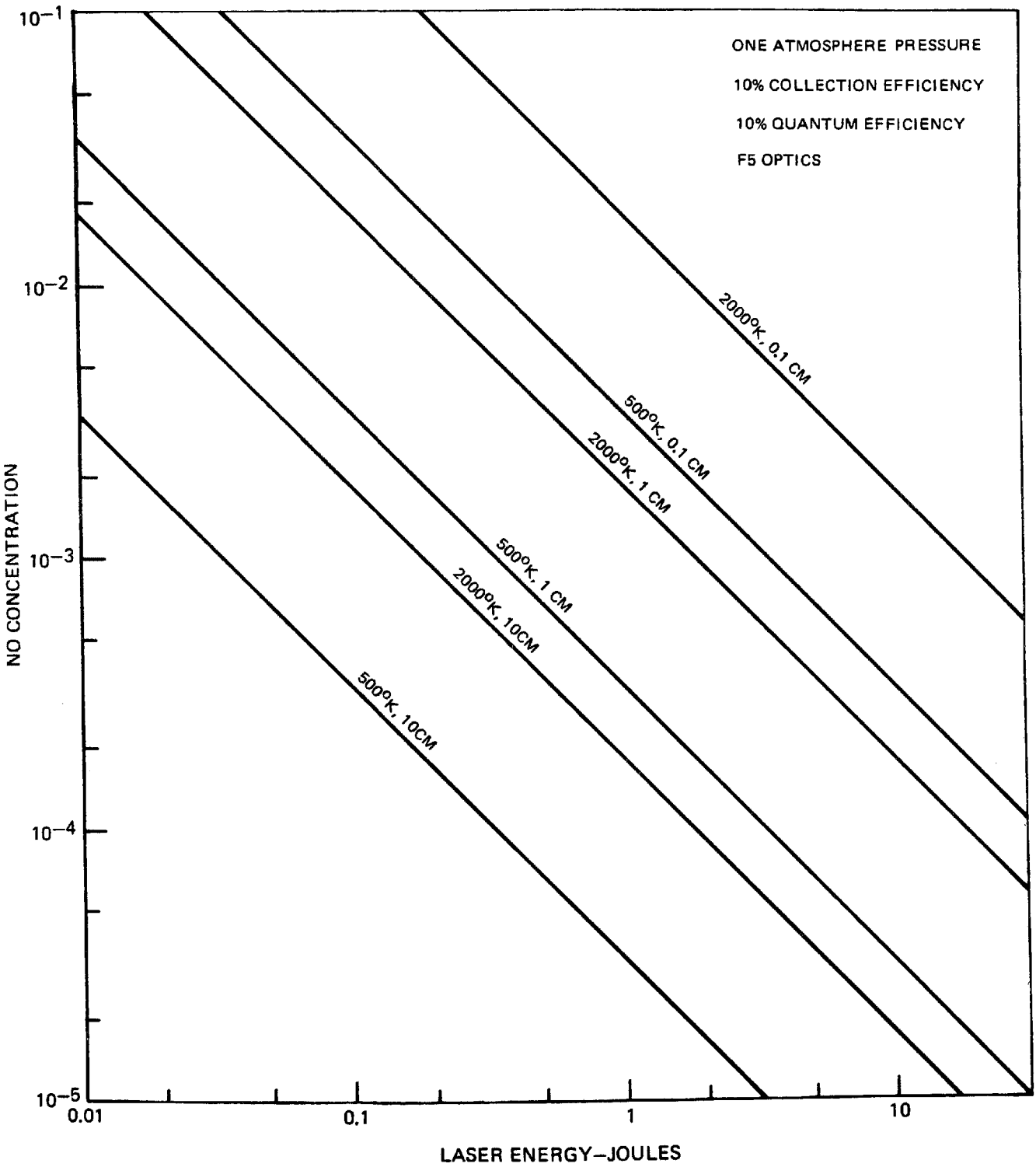

at 6943 Å and (4) the aforementioned ruby laser frequency doubled to 3472 Å with 50 percent doubling efficiency. Low energy pulsed N_2 lasers have been excluded from consideration since their Raman photon yields are generally quite low. With the high pulse energy lasers selected, adequately large numbers of Raman photons are collected, thus minimizing shot noise fluctuation effects and permitting single pulse thermometry in principle (Ref. 113).

Background Luminosity

First, "noise" from background luminosity will be treated. The calculations will be performed utilizing Eq. (19) for the following conditions: an atmospheric pressure, 2000°K flame; Raman scattering from N_2 assumed to constitute 70 percent of the combustion gas mixture; a 10 Å bandwidth and F5 optics. The radiation energy density will be assumed to be 130 (10^{-9}) watts/cm^3 sr Å corresponding to the particulate dispersion of 10^8 cm^{-3}, 400 Å soot particles (Fig. 3). In Table XII, the calculated S/N are displayed.

TABLE XII

N_2 RAMAN SIGNAL/BACKGROUND LUMINOSITY NOISE RATIOS

flame: 2000°K, 1 atm
particulates: 10^8 cm^{-3}, 400 Å

Laser	Power (W)	Wavelength (Å)	N_2 Raman (Å)	Sampling Extent 1 cm	Sampling Extent 1 mm
2X Nd	10^8	5320	6073	4.3	430
dye	10^6	5900	6840	.013	1.3
ruby	3.3 (10^7)	6943	8284	.086	8.6
2X ruby	1.7 (10^7)	3472	3778	600	60,000

In each case the scaling of the Raman cross section (λ_R^{-4}) and blackbody distribution (Fig. 3) with wavelength has been taken into account. From the Table, it is seen that the high peak power solid state lasers give good S/N at high spatial resolution. However in a more luminous situation, i.e., liquid fuel, where the luminosity is as much as a factor of thirty larger (Fig. 3) only the doubled neodymium or doubled ruby appear feasible. A similar conclusion in regard to the 2X ruby laser is the presence of intense background was reached in Ref. 105.

Although ruby lasers with tens of joules of energy per pulse exist, they have not been seriously considered in the above due to gas breakdown considerations. With the 1 Joule, 10 nanosecond doubled neodymium laser, breakdown may pose a problem. If the laser were focused to a 1 mm beam diameter, the average focal flux would be

on the order of 10^{10} Watts/cm^2. Due to spatial (intensity) and temporal (pulse shape) variations, the peak flux is probably a factor of four or more higher making gas breakdown a likely possibility. Consequently higher energy pulses than those selected have not been considered. If the neodymium pulse were stretched to decrease the intensity (say to 50 nsec) the peak power and, hence S/N, would be correspondingly decreased by a factor of five. Hence with proper laser selection it would appear that even the most intense background luminosity measured in the Rainbow furnace could be overcome. Of course this applies only to Raman scattering from the dominant molecular constituent and is not true of trace species concentrations, i.e., below 1000 ppm. For example, in attempting detection of a trace constituent at 1000 ppm in the highest luminosity case shown in Fig. 3, all the lasers listed would produce S/N ratios less than unity with the exception of the 2X ruby which would yield a S/N of about three. Actually for trace concentration levels and the high resolution (1 mm) required for good S/N, the photon yields would be extremely small as seen in Fig. 11.

Laser Modulated Particulate Incandescence

It has just been shown that with proper laser selection, background luminosity can be overcome by the spontaneous Raman scattering from a major flame constituent. Yet to be considered is the laser pulse particulate interaction which can lead to the variety of noise effects previously noted. Fluorescent interferences for laser wavelengths below 5000 Å appear to be of the same order as the Raman scattering from a dominant molecular constituent for hydrocarbon concentrations in the 1000-5000 ppm (as CH_4) range. Fluorescent interferences are difficult to predict quantitatively a priori without knowledge of the specific hydrocarbon species involved. Here only the distinctive liklihood of fluorescence interferences for laser excitation below 5000 Å will be noted.

Laser modulated particulate incandescence occurs when the already incandescent soot particles absorb the incident light scattering laser radiation, heat to temperatures far above the ambient flame temperature and, thereby, emit greatly increased amounts of blackbody radiation as described earlier. Unlike the situation with background luminosity where the Raman volume and total sampling volume can differ, laser modulated incandescence can occur only from the irradiated (i.e., Raman) volume. Consider the situation for the previously examined lasers when focused to a beam diameter of 1 mm. Assuming gas breakdown does not occur, the temperature to which the soot particles are heated can be found from Fig. 5 once the flux has been calculated. Using the Planck radiation expression, the single particle radiation per unit bandwidth per unit solid angle can be calculated. For a 1 mm Raman sampling extent, the irradiated and viewed volume will be 0.79 mm^3. Knowing the particulate number density, the total laser modulated incandescence can be calculated. For the previously examined soot dispersion, namely 10^8 cm^{-3}, 400 Å dia, and assuming a 10 Å bandwidth and a bandwidth factor of 0.5, the 2000°K N_2 Raman signal to laser modulated soot incandescence noise ratio has been calculated and is summarized below in Table XIII.

TABLE XIII

N_2 RAMAN SIGNAL/LASER MODULATED SOOT INCANDESCENCE NOISE RATIO

Laser	Flux (W/cm^2)	Particle Temperature (^oK)	S/N
2X Nd	10^{10}	6000	1.6
dye	10^8	4500	0.037
ruby	$3.3(10^9)$	5500	0.33
2X ruby	$1.6(10^9)$	5300	4.2

Compared with the 1 mm sampling extent results in Table XII it is clear that laser modulated particulate incandescence is a more serious problem than background luminosity. Despite fewer particulates being viewed relative to the normal background case, the noise increases significantly due to the high temperatures to which the particles are driven. Furthermore, due to the shift in the blackbody spectral distribution with temperature, the frequency doubled ruby laser is now only slightly better than the frequency doubled neodymium laser in contrast to the case of background luminosity. It should also be pointed out that these S/N ratios are about the best which can be expected since it was demonstrated in Ref. 84 that the Raman signal to laser modulated incandescence noise ratio increases with increasing focal flux.

Clearly, the S/N actually obtained will depend strongly on the properties of the soot dispersion present. As an example, in Fig. 12 (Raman) signal to (laser modulated particulate incandescence) noise ratio contours are mapped out over soot dispersion space. These contours were calculated for the previously examined case of the 1J frequency-doubled neodymium laser inducing Raman scattering from flame N_2 at 2000°K and atmospheric pressure. Also shown are soot dispersions characteristics of practical devices and sooting flames. Note that for a given mass density of soot, the calculated S/N increases linearly with particle size. This is due to the scaling of the particle surface area/volume ratio inversely with particle diameter. For larger size particles and a constant soot mass density, there is less total surface area available to radiate. Thus for a given soot mass density, distributions skewed toward larger particle sizes are less troublesome and lead to higher S/N ratios. However, a given radiation energy density, R, (Fig. 3) requires that the soot mass density increase linearly with particle diameter, again due to surface area/volume considerations. Thus for a certain level of radiation energy density, one finds the Raman signal to laser modulated soot incandescence noise ratio to be <u>independent</u> of particle size. Thus contours of constant S/N are contours of constant radiation energy density. This means that the S/N ratios calculated in Table XIII are valid independent of the specific soot dispersion characteristics assumed and would result for the calculated radiation energy density shown in Fig. 3, namely any dispersion producing an R of 130 (10^{-9}) Watts/cm^3 Å sr at 6000Å. For radiation energy densities an order of magnitude larger, e.g. liquid fuels (Fig. 3), the laser modulated soot incandescence would exceed the N_2 Raman signal in all of the laser cases examined. These calculations illustrate the serious noise problems facing spontaneous Raman diagnostics even for scattering from major species constituents. Thermometric

FIG. 12

RAMAN S/N MAP OVER SOOT DISPERSION CHARACTERISTICS FOR LASER MODULATED PARTICULATE INCANDENSENCE

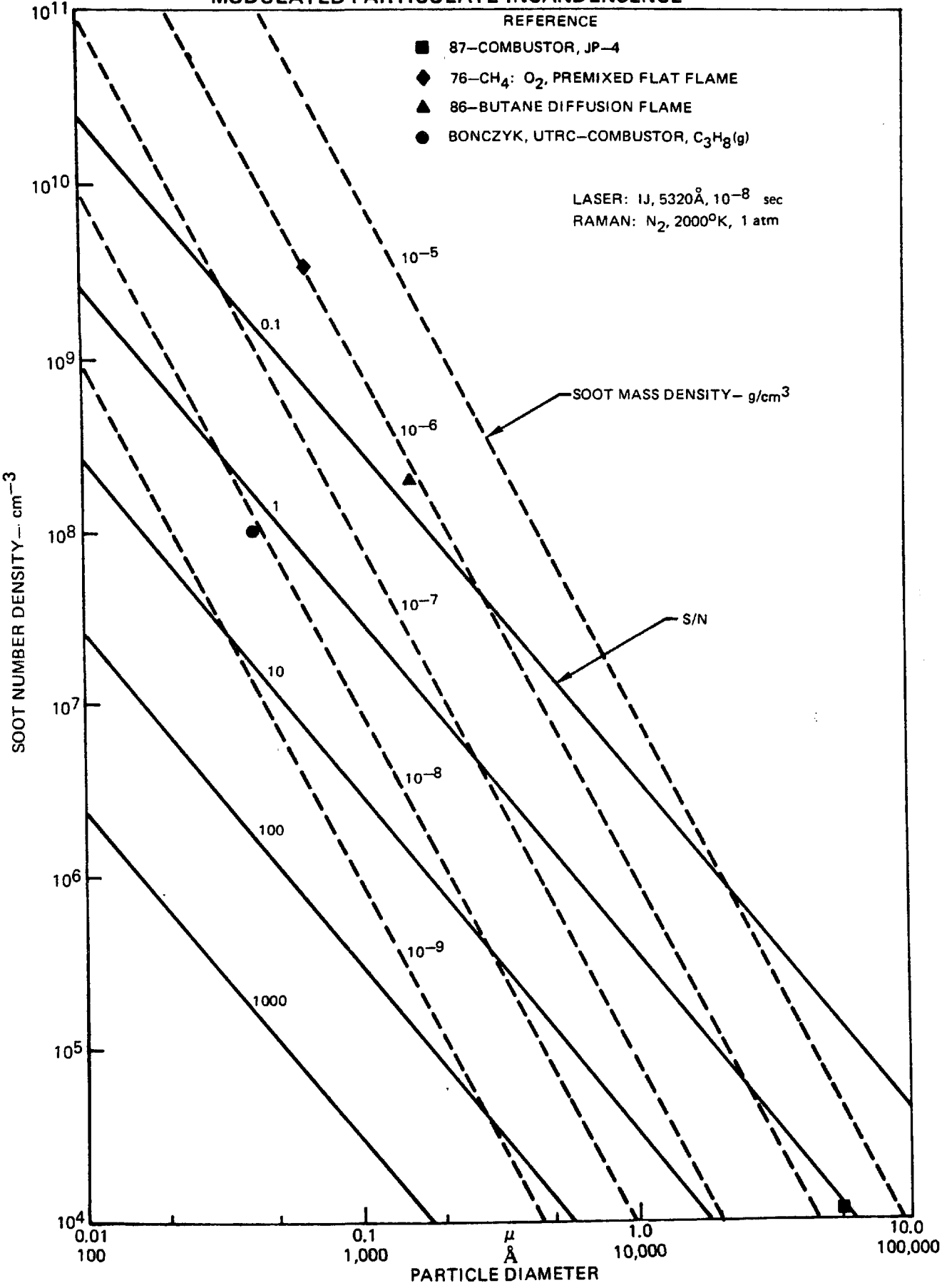

investigations from major species may be possible with proper laser selection but, probably, only at modest radiation energy densities, e.g. <10 (10^{-9}) Watts/cm^3 Å sr at 6000Å. Successful detection of minor species definitely appears unlikely. At very high focal fluxes, some decreases in noise may occur during the laser pulse due to particle shrinkage (Ref. 88). Such effects are not anticipated to greatly improve the S/N ratio, however.

Required S/N and Signal Averaging

The foregoing S/N ratios can be increased using a noise sampling and subtraction technique (Ref. 84) if the Raman photon count is high enough. In such an approach, the "noise" is sampled in a spectral region adjacent to the Raman bands simultaneously with the signal and then subtracted from the signal. In the following, the accuracy to which this can be done will be briefly explored. It will be assumed that both the "signal" and "noise" channels can be accurately calibrated relative to one another. The signals and relative errors on both the "signal" and "noise" channels can be written for photomultipliers with Poisson Statistics (Ref. 128) as

$$S_s = \eta(n_s + n_n) \pm \sqrt{\eta(n_s + n_n)} \tag{23}$$

$$S_n = \eta n_n \pm \sqrt{\eta n_n} \tag{24}$$

where η is the detector quantum efficiency; n_s, the number of signal photons; and n_n, the number of noise photons. The shot noise will actually vary from shot to shot; the relative error quantities shown correspond to the variance in the signal over a large number of shots and are taken to be representative of the error on any one shot. The subtraction can be performed to yield the true signal ηn_s, with a resultant signal to noise (S/N)* of

$$(S/N)^* = \frac{\sqrt{\eta n_s (S/N)}}{1+\sqrt{1+(S/N)}} \tag{25}$$

where S/N is the average single pulse S/N ratio, n_s/n_n. In Fig. 13, the signal to noise ratio after subtraction (S/N)* is displayed for various initial S/N ratios as a function of single pulse photon yield for photomultipliers exhibiting a 20 percent quantum efficiency. Note that, depending on the initial S/N and the photon yield, subtraction may actually decrease the signal to noise ratio! In regions where this can occur, the curves in Fig. 13 are shown dotted. A 1 joule pulsed laser will typically produce a Raman yield in the range of 10^3 to 10^4 photons/pulse depending on collection solid angle and collection efficiency from 2000°K, atmospheric pressure flame N_2. Since two channels need to be ratioed to make a temperature measurement (i.e., the respective relative error will double) a signal/noise after subtraction on the order of 30-50 would be required for temperature measurements to an accuracy

SINGLE PULSE S/N ENHANCEMENT VIA NOISE SAMPLING AND SUBTRACTION

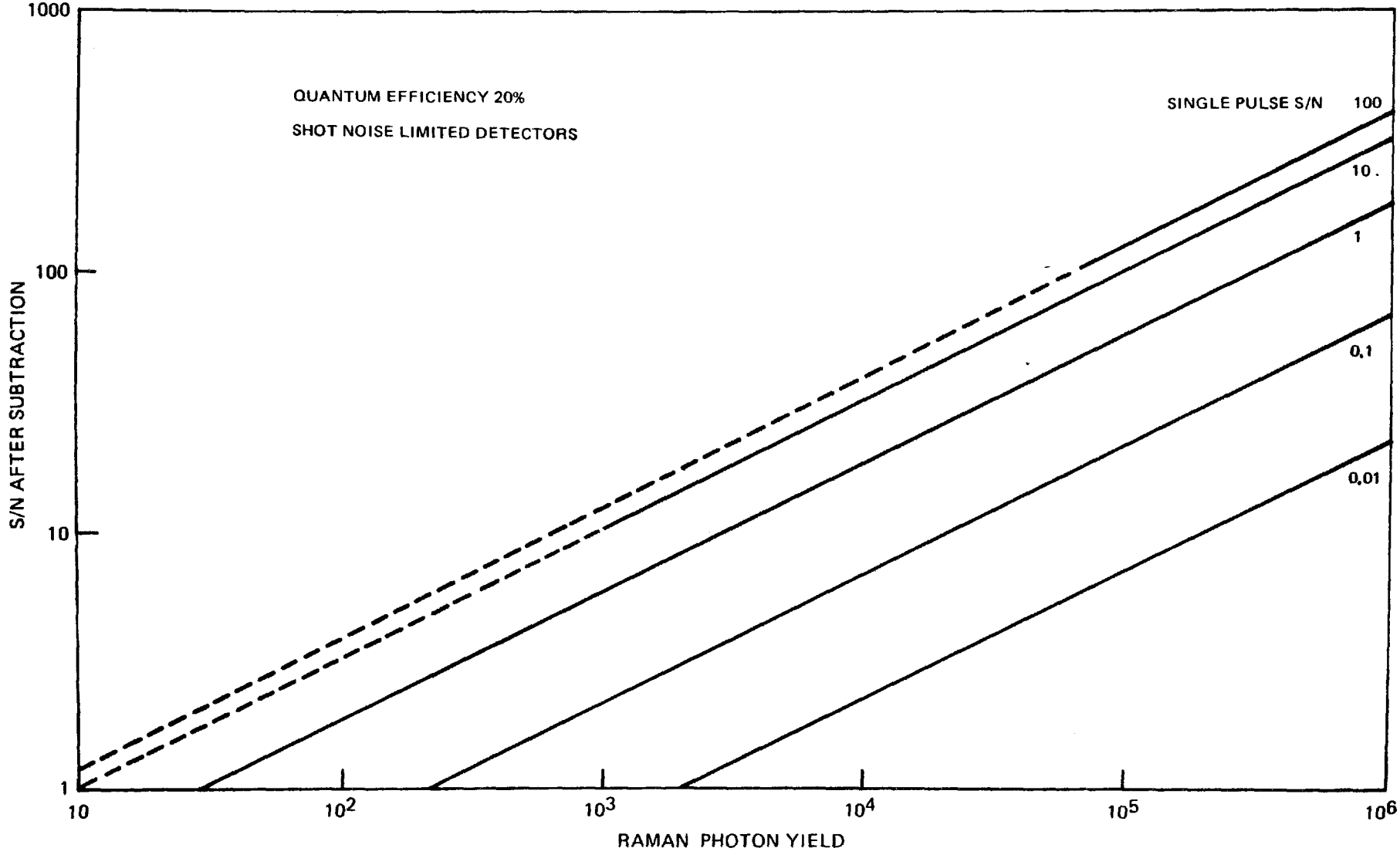

FIG. 13

of about ± 4 percent. This would require a minimum single pulse signal/noise on the order of 10. For density measurements to an accuracy of ± 10 percent, a S/N of unity would be tolerable since subtraction results in a large signal to noise improvement for photon yields on the order of several thousand. Thus for typical Raman photon yields, a minimum single pulse S/N in the range of from 1 to 10 is required for medium measurements with each pulse.

With signal averaging, the shot noise fluctuations can be averaged out completely in stationary media (Ref. 84) permitting measurements to be made. The effect of signal averaging is to increase the Raman photon count in essence permitting considerable enhancement in signal/noise as seen from Fig. 13. For example if a typical Raman yield was 10^3 photons, averaging over 100 pulses at a per pulse S/N of .01 would increase the S/N after subtraction from 0.7 to 7.

If the medium is fluctuating, however, averaging leads to an accumulation of terms involving the magnitude and correlation of fluctuations in density and temperature as demonstrated in Refs. 84, 109. In Appendix II, an analysis is presented which details the consequences of ensemble averaging pulsed laser Raman data from a temporally fluctuating medium. Average density measurements can still be performed if the Stokes bandwidth factor is made independent of temperature. Fairly wide bandwidths (Fig. 9) are required to eliminate the temperature dependence of the bandwidth factor, leading to lower S/N ratios than those previously calculated for narrow bandwidth. Temperature measurements are obscured however by averaging, and the data is no longer amenable to unambiguous interpretation. In this situation temperature measurements must be performed accurately with each laser pulse. Most practical combustion devices, of course, are highly turbulent to promote mixing of the fuel/air mixture. In summary then, for temperature measurements in turbulent media, individual channel Raman signal/noise ratios of at least ten appear required. For temperature measurements in stationary media and for density measurements in any situation, lower S/N are tolerable, generally above 0.01, but signal averaging over many pulses (generally more than one hundred) is required.

Practical Combustion Device Applicability

It is difficult to be categorical about the utility of spontaneous Raman scattering in regard to practical combustor diagnosis. There are undoubtedly measurement situations to which spontaneous Raman scattering can be successfully applied. For example, in exhaust regions and some secondary combustion zones where particulate loadings may be substantially lower than in the primary zone, Raman measurements are potentially possible. What has been attempted in the foregoing sections are Raman S/N calculations for both background luminosity and laser modulated soot incandescence employing a common value of radiation energy density typical of a hydrocarbon-fueled primary combustion zone. Recall that the Raman/laser modulated soot incandescence S/N ratio is independent of the specific dispersion characteristics for a given radiation energy density. The S/N calculations were made at favorably

high peak powers and focal fluxes. The latter were somewhat speculative in regards to gas breakdown, whose occurrence, of course, would obviate any measurement. For single pulse thermometry or detection of minority species quantities, laser modulated soot incandescence led to unacceptably low S/N ratios. For frequency doubled ruby lasers, fluorescent interferences are probable as well but more difficult to predict a priori without experimental investigation. The S/N ratio can be improved somewhat by noise sampling and subtraction and enhanced considerably by signal averaging. Signal averaging in turbulent, fluctuating media appears permissible only for density determinations, but, for low concentration species detection, an inordinate number of pulses would need be averaged over.

In regard to cost and probability of success, the following comments may be offered. The dye laser considered is the least expensive approach ($\sim$ \$10 K) but is faced with very low S/N. Experience at UTRC with such a laser confirms this conclusion. A 1 Joule frequency-doubled neodymium laser is quite expensive (\$140 K, Ref. 130), yields fairly good major constituent S/N in some but not all situations and can be operated at good repetition rates for diagnostics (10-20 pps). One Joule ruby lasers are cheaper (\$20-50 K , depending on mode quality desired) but are generally limited to a pulse/second at best. In the cases considered here, they were less attractive than 2X Nd. If frequency doubled, the 2X ruby appears slightly better than 2X Nd re particulate incandescence, may be worse vis-a-vis fluorescence and suffers, of course, from lower repetition rates. Furthermore, 2X ruby laser gas breakdown thresholds may be considerably lower than those for 2X Nd due to multiphoton ionization phenomena (2X ruby has a 3.6 ev photon energy). In summary, the costs for these potentially successful lasers are high, and the probability of success for spontaneous Raman scattering in these environments even for thermometry from majority species appears fair at best. For trace species measurements (i.e. $<$ 1000 ppm), the probability of success is poor over a broad range of combustor operating conditions. Thus spontaneous Raman appears to be a high risk approach for practical device diagnostics.

Clean Flame Diagnostics

Previously it was shown that trace species detectivity was quite limited even with high energy pulsed lasers and poor spatial resolution. For clean flames, the high peak Raman powers produced by pulsed lasers are of no special diagnostic advantage, except for turbulence studies where time resolved measurements are desired. From a collected Raman photon standpoint, there is no difference between a 10 pps, 1 Joule pulsed laser and a 10 Watt continuous wave laser. However cw lasers do possess the general advantages of lower cost, increased operational reliability, better linewidth and better beam quality. cw gas lasers are generally diffraction-limited permitting the use of multipass optical scattering cells to expediate photon collection. For conditions similar to the pulsed laser detectability limit calculations presented earlier, calculations of photon counting time versus NO concentration were made and are summarized in Fig. 14. Shown parametrically is gas temperature, measurement

CW LASER RAMAN NO COUNT TIMES

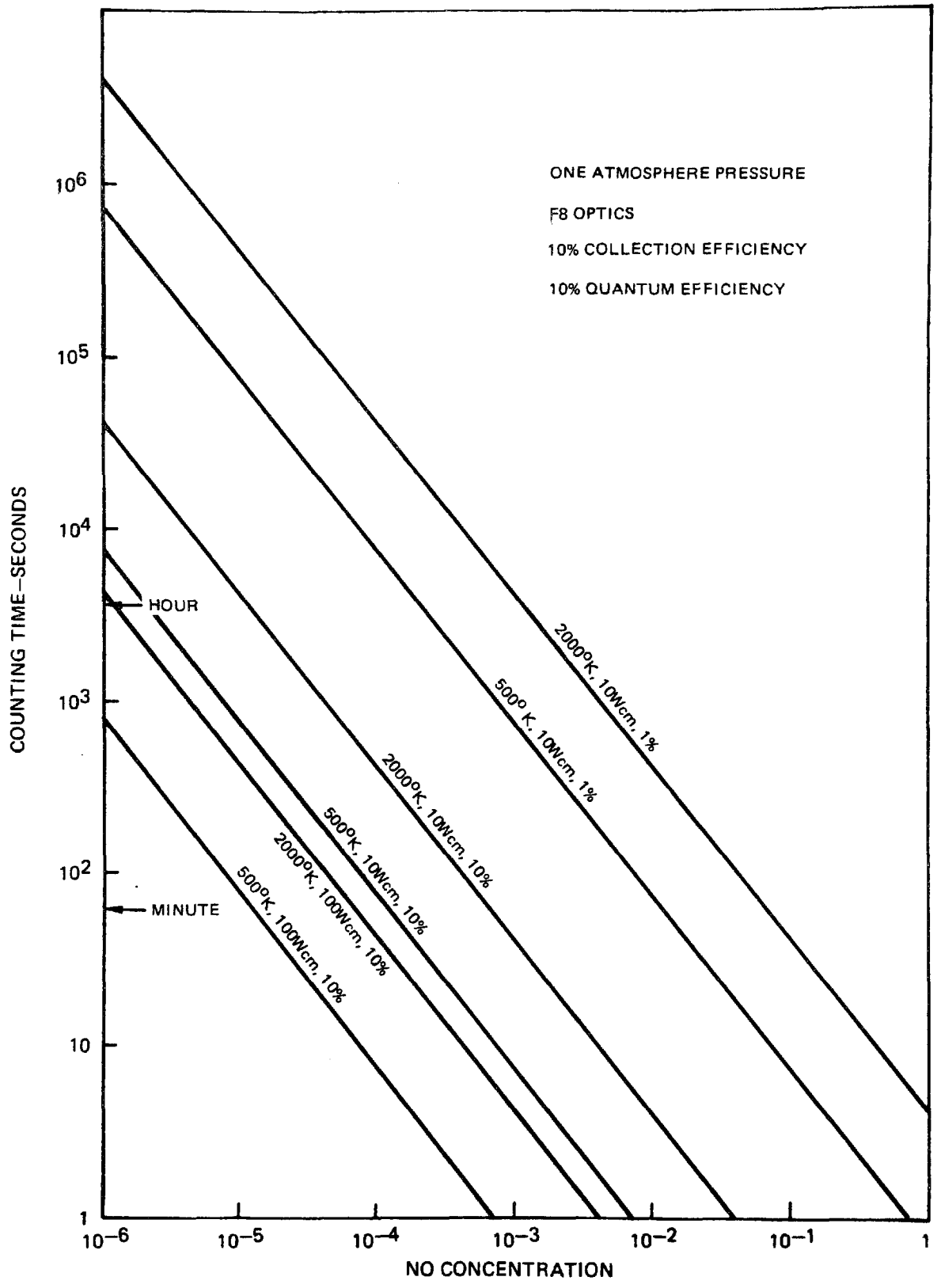

accuracy as determined by shot noise considerations, and laser power times pathlength product. For example, 10 Wcm may correspond to a 10 Watt laser over a 1 cm spatial resolution, one Watt over 10 cm, one Watt over 1 cm multipassed 10 times, etc. These calculations were made assuming unity bandwidth factor. From Fig. 13 it is seen that in a flame at 2000°K, species concentration measurements to 10 ppm with 10 percent accuracy could be made with a 5 watt argon ion laser, multipassed over a 1 cm path with a gain of 20 in about 7 minutes. Without a multipass approach or for measurements to greater accuracy, considerably longer times are required. Species concentration measurements much below 10 ppm would require inordinately long measurement periods and do not appear feasible.

Near-Resonant Raman Scattering

Review

Near-resonant Raman scattering, in principle, could lead to a substantial increase in the Raman cross sections, and, concomitantly, to great increases in the Raman intensities. In near-resonant Raman scattering, the laser frequency is tuned near an electronic resonance in the molecule being probed (see Fig. 1). Formerly resonance fluorescence and resonant Raman scattering were treated as separate physical processes. Current theories (Refs. 131, 132) hold that they are essentially the same physical process distinguished by the frequency difference between the absorption and laser lines. As the frequency difference, $\Delta\omega$, becomes small, the state liftetime ($1/\Delta\omega$) becomes long, i.e., if energy is not conserved in the transition to the excited state by an amount $\Delta\omega$, then via an uncertainty relationship, the lifetime of the molecule in the excited state is limited to $1/\Delta\omega$. Hence as the detuning $\Delta\omega$ decreases, the "scattering" changes from a nearly instantanous Raman-like process to a longer lived fluorescence emission process exactly on resonance. Although resonance Raman is a commonly used term, the nomenclature of Ref. 133, namely near-resonant Raman scattering, will be used here. That near resonance leads to greatly enhanced scattering is illustrated by the fact that the intensity of scattering for the induced transition $n \rightarrow m$ is given by (Ref. 9)

$$I_{nm} = \frac{64\pi^2}{3c^2} (\nu_o + \nu_{nm})^4 P_{nm}^2 \qquad (26)$$

where ν_o is the incident laser frequency and ν_{nm}, the frequency corresponding to the transition $n \rightarrow m$. P_{nm} is the induced electric moment matrix element given by

$$P_{nm} = \frac{1}{h} \sum_r \left(\frac{M_{nr}M_{rm}}{\nu_{rn}-\nu_o} + \frac{M_{nr}M_{rm}}{\nu_{rm}+\nu_o} \right) E \qquad (27)$$

where E is the electric vector of the incident light; r denotes any level of the complete set of the unperturbed molecule ; ν_{ri}, the frequency corresponding to the frequency difference of states r and i; and M_{ri}, the corresponding transition moment

Clearly when ν_o lies near a particular real absorption frequency ν_{rn}, the intensity of scattering will be significantly enhanced and so-called near-resonance Raman scattering is observed.

In liquid solutions, substantial increases, on the order of 10^6, in the Raman intensities have been reported in certain instances (Ref. 9). Until recently, relatively little had been done on near-resonant Raman scattering in gases. Many studies have concentrated only on spectral (Refs. 134, 135 and 136) and/or lifetime (Ref. 131) observations. Penney (Ref. 132), Robrish et al (Ref. 137) and Fouche and Chang (Ref. 138) have examined the degree of resonant enhancement attainable. Fouche and Chang, tuning across the 5145 Å argon ion laser line, report a ratio of the near-resonant Raman I_2 cross section to the ordinary Raman cross section of N_2 of $2.6(10^6)$, an enhancement of six orders of magnitude. It is interesting to note that the resonance fluorescence was three orders of magnitude stronger than the near-resonant Raman. It should also be pointed out that Williams et al (Ref. 131) showed that the change from a longer-lived fluorescence process to a short-lived Raman process occurred in just 2.3 GHz, which at 5145 Å corresponds to a detuning of only 0.02 Å. Robrish (Ref. 137) reports a resonantly enhanced I_2 cross section at 5466.36 Å in atmospheric pressure N_2, $4(10^6)$ greater than the N_2 spontaneous Raman cross section. In NO_2 they report a cross section of $5.6(10^{-27})cm^2/sr$ at 4547.8 Å, resonantly enhanced by about three orders of magnitude over those reported in Table V. Clearly, very narrow laser linewidths and very good laser frequency stability are required to avoid exciting potentially stronger fluorescence interferences. In high temperature flames with high water vapor concentrations, this may be less of a problem due to severe quenching of the fluorescence.

Whether such large enhancements can be expected in all cases is not clear. For example, Penney (Ref. 132) performed a calculation for the near-resonant enhancement of NO tuning into the $\gamma(0,0)$ band at 2265 Å and estimated a factor of only forty enhancement. In a similar calculation, Robrish et. al. estimated a near-resonant enhancement of $1.6(10^6)$ (Ref. 139). There has not yet been an experimental examination of near-resonant Raman in NO. Enhancement is a strong function of band strength and six orders of magnitude enhancement certainly may not be typical, e.g., NO_2. One additional advantage of tuning near strong bands, as Penney points out, is that it may permit operation at larger detuning, relaxing requirements on laser linewidth and stability. Penney points out another difficulty with molecular near-resonant Raman in contrast to atomic work. Namely, and this is particularly true at high flame temperatures, the fraction of molecules in the appropriate initial state can be very small. A similar situation is encountered in laser fluorescence diagnostics. Unlike Q branch Raman scattering, where the entire rotational ensemble can be sampled with appropriate detector bandwidth, in near-resonant Raman only a single transition is probed. Several lines could be simultaneously excited presumably but the degree of near-resonant enhancement would not be uniform, leading to unacceptable diagnostic nonlinearities.

Practical Applicability

Recall that in practical combustor flames, spontaneous Raman scattering appeared tenuous for the probing of even majority constituents. Near-resonant enhancement of several orders of magnitude would certainly alter this view. Unfortunately, the major species of interest such as N_2, O_2, CO and CO_2 possess strong absorption bands only at or below 2000 Å (see Tables III, IV) making them inaccessible to near-resonant enhancement. Near-resonant enhancement of minority species Raman cross sections is mitigated by three factors. First, by definition the low number densities associated with minority species offset the potential gains in cross sections so at best, enhanced minority species signals might be comparable to spontaneous Raman signals from major constituents. Second, the enhanced minority species signal is reduced by the laser energy compromises which result from the very narrow linewidth and spectral selectivity requirements of the laser source. Third, the requirement to probe a selected vibrational-rotational state as opposed to the entire band further decreases the generated signal. Thus, it is concluded that near-resonant enhancement of minority species Raman cross sections will not produce signal levels comparable to the spontaneous Raman signals from major species which were previously found lacking. Thus for the remote probing of practical combustion devices (high background luminosity, particulates) near-resonant Raman scattering does not appear particularly feasible.

Potential Applicability

In clean flames, near-resonant Raman scattering could permit probing of some molecules for which fluorescence is precluded or expedite photon collection in other cases. For example, in NO_2 where fluorescence is severely quenched under typical flame conditions (Ref. 55), near-resonant Raman may offer signal advantages over spontaneous Raman scattering. In molecules which dissociate upon absorption of light and, hence do not fluoresce, near-resonant Raman scattering may possibly be employed. In I_2 for example, near-resonance Raman was first observed at photon energies beyond the dissociation limit (Ref. 134) before it was observed below the limit (Ref. 138). In instances where photo-dissociation occurs, it is argued that, because of its extremely short lifetime, near-resonant Raman can be observed prior to molecular dissociation. Photon collection will only be expedited, of course, if the near-resonant enhancement achieved overcomes the sacrifices in laser energy and restricted state populations necessary to produce the effect.

LASER FLUORESCENCE

Introduction

Laser-induced fluorescence is a process, illustrated in Fig. 15, in which the laser wavelength is tuned to coincide with a molecular absorption, thereby causing the molecule to make a transition to an excited electronic state. Following absorption of the radiation, the excited molecule then returns to the ground state with emission of radiation. This fluorescence may be at the same wavelength as that of the exciting radiation, termed resonance fluorescence, or may be shifted in wavelength. In this latter case, the molecule returns to a vibrational state other than that from which it originated.

Laser-induced fluorescence has received considerable attention recently as a potential method of species concentration measurement. The technique is of interest both with regard to atmospheric and flame environments. Baardsen and Terhune (Ref. 37) and Wang and Davis (Ref. 38) have applied laser-induced fluorescence to detect OH in the atmosphere. In flames, the technique has been applied to CN by Jackson (Ref. 28), to CH by Barnes, et al (Ref. 27) and to C_2 by Jones and Mackie (Ref. 24) and Baronavski and McDonald (Ref. 25). The results of these latter works reflect the fact that the technique is still in its early stages of development with respect to flame and atmospheric probing. In particular, the flame measurements referred to are seen to be in fact demonstrations of feasibility. Up to the present time, concentrations have not been determined with good accuracy at ppm levels. Some of the specific problems associated with probing a turbulent reactive flow characteristic of a combustor have been discussed by Wang (Ref. 140). Wang reviews several different laser diagnostic techniques including laser-induced fluorescence. In regards to fluorescence, Wang concludes that low number density measurements are feasible, in principle, but that it may be difficult in practice to implement the technique for a complex chemical system owing to the spectroscopic and quenching data which are needed. Quenching corrections have always been a major problem in fluorescence diagnostics. Here the view is adopted that analytic quenching corrections to fluorescence data are feasible only in very well characterized flames, where temperature and major quenching species concentrations are known. In less well characterized, turbulent combustion media, such analytic corrections would, most likely, be very inaccurate. Accordingly, approaches are discussed herein, which obviate the difficulties and uncertainties associated with the need for quenching data and corrections. These approaches involve saturated laser-induced fluorescence whose importance with regard to species measurement was first realized by Piepmeier (Ref. 141) and more recently by Daily (Ref. 142).

There are several basic criteria which must be satisfied if fluorescence measurements are to be performed on a given molecule. The first of these is that the molecule must have a known emission spectrum. This is not always the case

MOLECULAR ABSORPTION/FLUORESCENCE

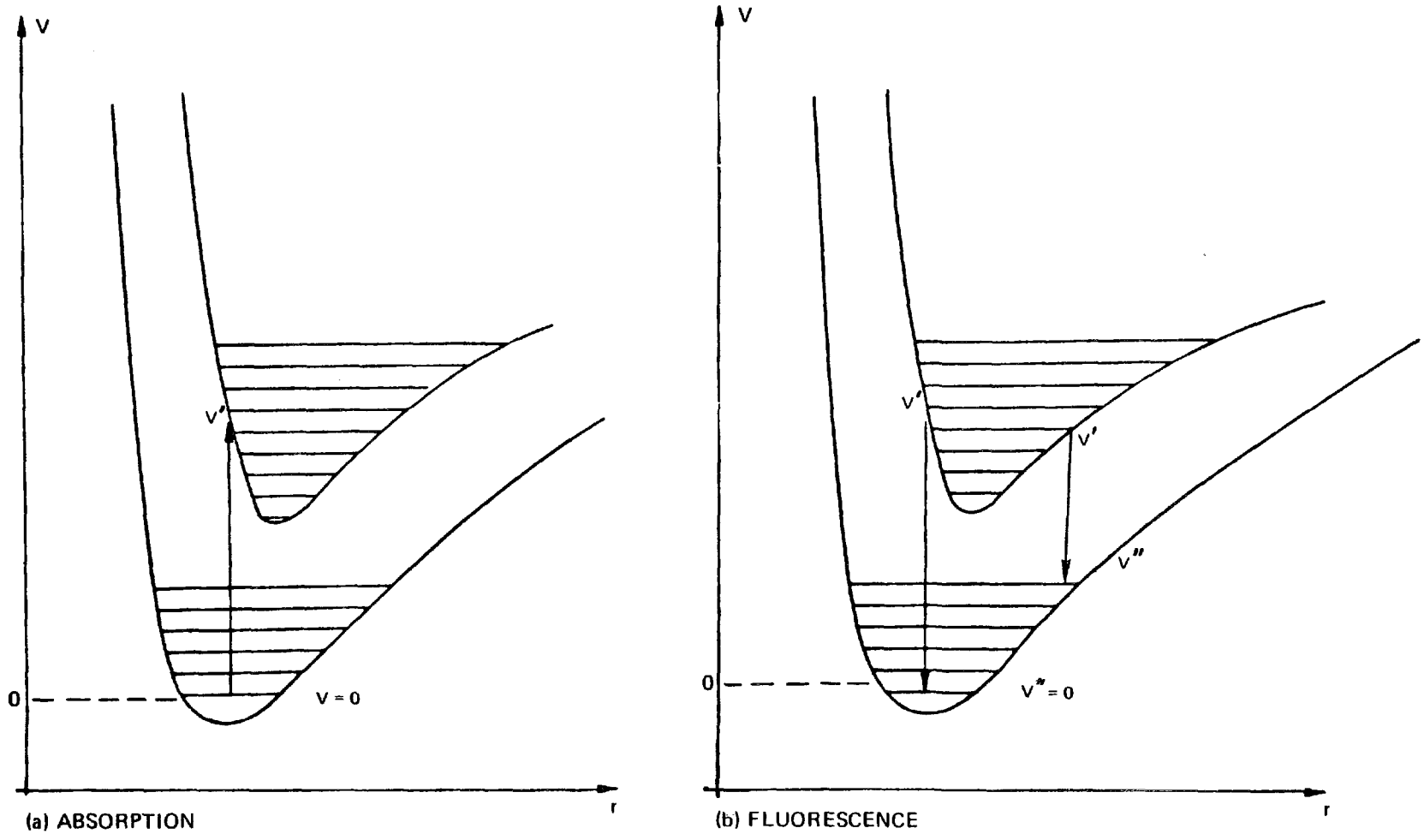

FIG. 15

since a molecule when excited to a given state may dissociate prior to the emission of a photon. Specific examples of this are given in Tables III and IV. In some cases assigning the absence of emission to predissociation is necessarily speculative since it may be difficult to rule out the presence of emission which is very weak and difficult to observe. Second, the molecule must have an absorption wavelength which is accessible to a tunable laser source. At the present time, the spectral range covered by tunable dye laser sources is roughly the interval from 2000 Å to 1.5 microns. In the case of the near UV wavelengths it is often necessary to frequency double the visible laser output to achieve the desired UV wavelengths. Several atoms and molecules, which are not amenable to laser-induced fluorescence techniques since the absorption occurs at wavelengths less than 2000 Å are listed in Table VII. A third requirement is that the rate of radiative decay of the excited state be known. This is simply due to the fact that the fluorescence power is proportional to this rate. Fourth, if other molecules are present, the excited state loss rate may be increased considerably over the radiative rate due to collisions involving the excited state and other molecules. The increase in total decay rate due to collisions is known as quenching. Historically, it is the requirement to correct the measured fluorescence power for quenching, prior to obtaining the species number density from the measurements, which has limited the applicability of the technique. The quenching correction involves knowing the partial pressures of all species present other than the one of interest, as well as the rates for deactivation of the excited state of the species of interest by all others present. In addition to this is the requirement that the dependence of these rate constants on temperature be known. Suffice it to say that all of this information is difficult if not impossible to obtain.

There are ways by which the difficulties associated with quenching may possibly be circumvented. These relate to saturation of the absorbing transition, achieved through the use of pulsed lasers with high spectral intensity. Saturation may be thought of as a condition for which a sizeable equilibrium population in the excited state is achieved. Daily (Refs. 142-144) has discussed saturation for the case of full saturation whereby the fluorescence power may be shown to be completely independent of quenching and incident laser spectral intensity. If full saturation is achieved, it is not necessary to know the partial pressures of other species present, nor is it necessary even that these be identified. A somewhat different approach has been taken by Baronavski and McDonald (Ref. 25). In this case, the requirement is for near saturation of the absorption. It may be shown that a measurement of fluorescence power versus laser spectral intensity yields the total quenching rate and number density provided that appreciable (but not complete) saturation is achieved. This is an important distinction in practice, since complete saturation may require unattainable laser spectral intensity.

The technique of partially saturated laser fluorescence is not without its difficulties. This technique involves measurement of fluorescence power as a function of laser spectral intensity. Accordingly, species concentration may not be determined

from a single laser pulse. This is of concern for measurements in a highly turbulent medium wherein temporal fluctuations of temperature and species concentration occur. At best then, a time-averaged concentration may be determined. Analysis is yet required to address the effects of signal averaging and to determine preferred measurement approaches. Measurement of the average species concentration also depends on knowing the flame temperature. This follows since the fluorescence power is representative only of the population of the particular vibration-rotation level of the molecule which absorbs the radiation. To compute the total population of the ground level of the molecule by use of an appropriate Boltzmann factor requires that temperature be known. Another potential difficulty with the saturation technique involves the multi-rotational level nature of molecules. Molecules with many rotational degrees of freedom are more difficult to saturate when collisional relaxation among rotational levels takes place in a time which is short compared with the time for relaxation of the excited state. For this reason it may be very difficult to saturate transitions in molecules such as NH_2 and NO_2.

Fluorescence Theory

Piepmeier's Approach

Three Levels

The three-level system which is treated in detail below is illustrated in Fig. 16. The analysis given follows Piepmeier (Ref. 141) closely. This system is appropriate, for example, to a case in which level 3 is near level 1 and collisional cross-relaxation occurs between them. The rate equations in this case are given by

$$\frac{dN_1}{dt} = -N_1 (b_{12} + Q_{13}) + N_3(Q_{31} + A_{31}) + N_2(A_{21} + Q_{21} + b_{21}), \quad (28a)$$

$$\frac{dN_2}{dt} = N_1 b_{12} - N_2(A_{21} + A_{23} + Q_{21} + Q_{23} + b_{21}) \quad (28b)$$

and

$$\frac{dN_3}{dt} = N_1 Q_{13} - N_3(Q_{31} + A_{31}) + N_2(A_{23} + Q_{23}), \quad (28c)$$

where N_1, N_2, and N_3 are the populations of levels 1, 2, and 3; A_{23}, A_{31} and A_{21}, the rates for radiative decay between the subscripted levels; Q_{13}, Q_{31}, Q_{21} and Q_{23}, the rates for collisional relaxation; and b_{12}, b_{21}, rates associated with stimulated absorption and emission, respectively. The lineshape is introduced in b_{12} through $b_{12} = \rho B_{12} g(\nu_F - \nu_L)$, where ρ is the laser energy density; B_{12}, the Einstein

FIG. 16

LASER–INDUCED FLUORESCENCE FOR THREE–LEVEL SYSTEM

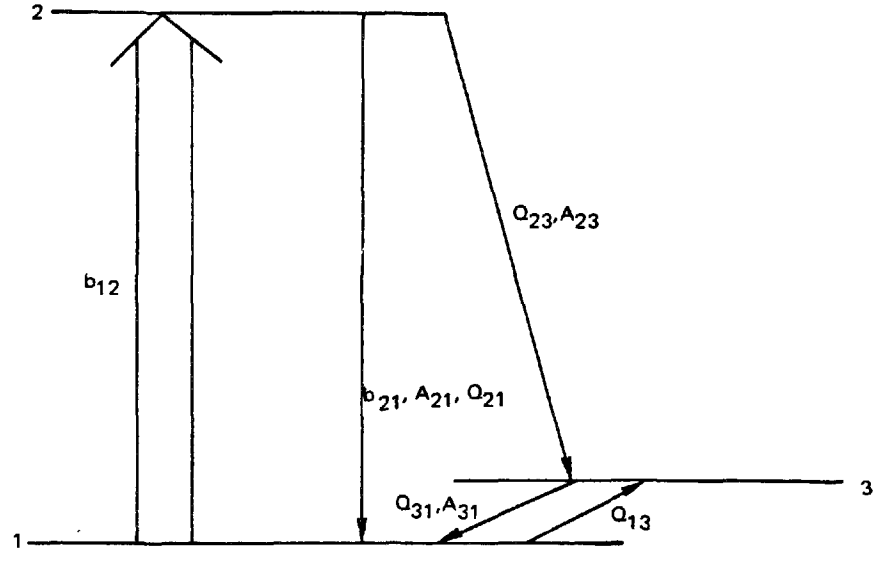

coefficient for stimulated absorption of radiation; $q(\nu_F - \nu_L)$ the lineshape factor. For the lineshape factor a Lorentzian profile is assumed hence

$$q(\nu_F - \nu_L) = \frac{(A_{21} + Q_C)}{4\pi^2(\nu_F - \nu_L)^2 + (\frac{A_{21}+Q_C}{2})^2} \tag{29}$$

where ν_F is the molecular frequency; ν_L, the laser frequency; Q_C, a net rate for all collision processes which interrupt stimulated emission. Omitting substantial algebraic detail, it may be shown that in the presence of the laser the fraction of molecules present in level 2 in the steady-state ($dN_1/dt = dN_2/dt = dN_3/dt = 0$) is given by

$$\frac{N_2}{(N_1+N_2+N_3)} = \frac{D\ \rho\ B_{12}/(1+L)}{4\pi^2(\nu_F - \nu_L)^2 + (\frac{A_{21}+Q_C}{2})^2 + D\ \rho\ (B_{21} + \frac{1+K}{1+L}\ B_{12})} \tag{30}$$

In Eq. (30), the parameters K, L, and D are given by $K = (A_{23} + Q_{23})/(Q_{31} + A_{31})$; $L = Q_{13}/(Q_{31} + A_{31})$; $D = (A_{21} + Q_C)/(A_{21} + A_{23} + Q_{23})$. Next account is taken of the thermal motion of the molecules in the gas, i.e., Doppler effect. It is assumed that despite the presence of the laser, the total population retains its Maxwell-Boltzmann distribution of velocities. The function which describes the Doppler-broadened frequency distribution is given by

$$N^0(\nu) = \frac{N^0}{1.064\Delta\nu_D}\ \exp\ [-(2(\nu-\nu_F)/\Delta\nu_D)^2\ \ln 2] \tag{31}$$

where N^0 is the total population appropriate to all frequencies, ν; $\Delta\nu_D$ the Doppler width associated with the molecular frequency, ν_F. It follows then that the fraction of molecules in level 2 with inclusion of the Doppler effect is given by

$$\frac{N_2}{N^0} = \frac{D\rho B_{12}}{1.064\Delta\nu_D(1+L)} \int_0^\infty \frac{\exp\ [-(2(\nu-\nu_F)/\Delta\nu_D)^2\ \ln 2]\ d\nu}{4\pi^2(\nu - \nu_L)^2 + (\frac{A_{21}+Q_C}{2})^2 + D\rho\ (B_{21} + \frac{1+K}{1+L}\ B_{12})} \tag{32}$$

The procedure for evaluation of the integral in Eq. (32) is known (Ref. 145). For the case $\nu_L = \nu_F$, the fraction of excited molecules is

$$\frac{N_2}{N^0} = \frac{1}{(1+L)[(g_1/g_2) + \frac{(1+K)}{(1+L)}]}\ (\frac{R}{1+R})\ F(a,R) \tag{33a}$$

In Eq. (33a), the parameters F(a,R), a and R are given by

$$F(a,R) = \pi^{\frac{1}{2}}\, a(1+R)^{\frac{1}{2}} \exp\,[a^2(1+R)]\ \mathrm{erfc}\,[a(1+R)^{\frac{1}{2}}] \tag{33b}$$

$$a = (\ln 2)^{\frac{1}{2}}\,(A_{21} + Q_C)/2\pi\,\Delta\nu_D \tag{33c}$$

and

$$R = \frac{D\rho(B_{21}+\frac{1+K}{1+L}\,B_{12})}{(\frac{A_{21}+Q_C}{2})^2}. \tag{33d}$$

The parameters g_1 and g_2 in Eq. (33a) are the degeneracies of levels 1 and 2, respectively. The term erfc in Eq. (33b) refers to the "error function". Tabulations of this function for various values of its argument are readily available (Ref. 145). The parameters a and R have a precise significance. The parameter a gives the ratio of the homogeneous to the Doppler width and, hence, characterizes the absorption lineshape. The parameter R is a saturation parameter. It gives the ratio of the rate for stimulated emission to the rate appropriate to de-excitation of the molecular excited state owing to radiative decay and collisions. The quantity F(a,R) approaches a value of unity for a and/or R large. Consequently, the more homogeneous the lineshape and/or the more intense the laser the less important is the factor F(a,R). In order to demonstrate the sensitivity of the factor F(a,R) to laser intensity, the quantity $[R/(1+R)]\,F(a,R)$ is plotted as a function of R in Fig. 17, for the case of homogeneous broadening ($a > 1$). The theory, as given by Piepmeier, is applicable to the case of strong homogeneous broadening. The parameter R is proportional to laser intensity, I_L. The fraction of molecules in the excited state may be obtained from Fig. 17 after multiplication of ordinate values by $\{(1+L)[(g_1/g_2) + (1+K)/(1+L)]\}^{-1}$. The latter factor is the limiting value of (N_2/N^O) in the case of R very large. This corresponds to full saturation of the molecular transition. It is worthwhile noting that in evaluating (N_2/N^O) the fluorescence power is also evaluated since it is proportional to N_2. The fluorescence power is given by

$$S_F = h\,\nu_F\,\frac{A_{21}}{4\pi}\;\Omega_c\,V_c\,(\frac{N_2}{N^O})\,N^O, \tag{34}$$

where Ω_c is the light collection solid angle; V_c, the sample volume; and h, Planck's constant. The exact shape of the curve in Fig. 17 is dependent on the magnitude of a. The practical implication of this is that the shape may be different for different temperature flame zones. If full saturation of the transition is not achieved, determination of species concentration by measurement of the fluorescence power requires knowing the Doppler and homogeneous widths of the transition as well as the rate constants. Even if full saturation is achieved and

FIG. 17

SATURATION FOR HOMOGENEOUS BROADENING

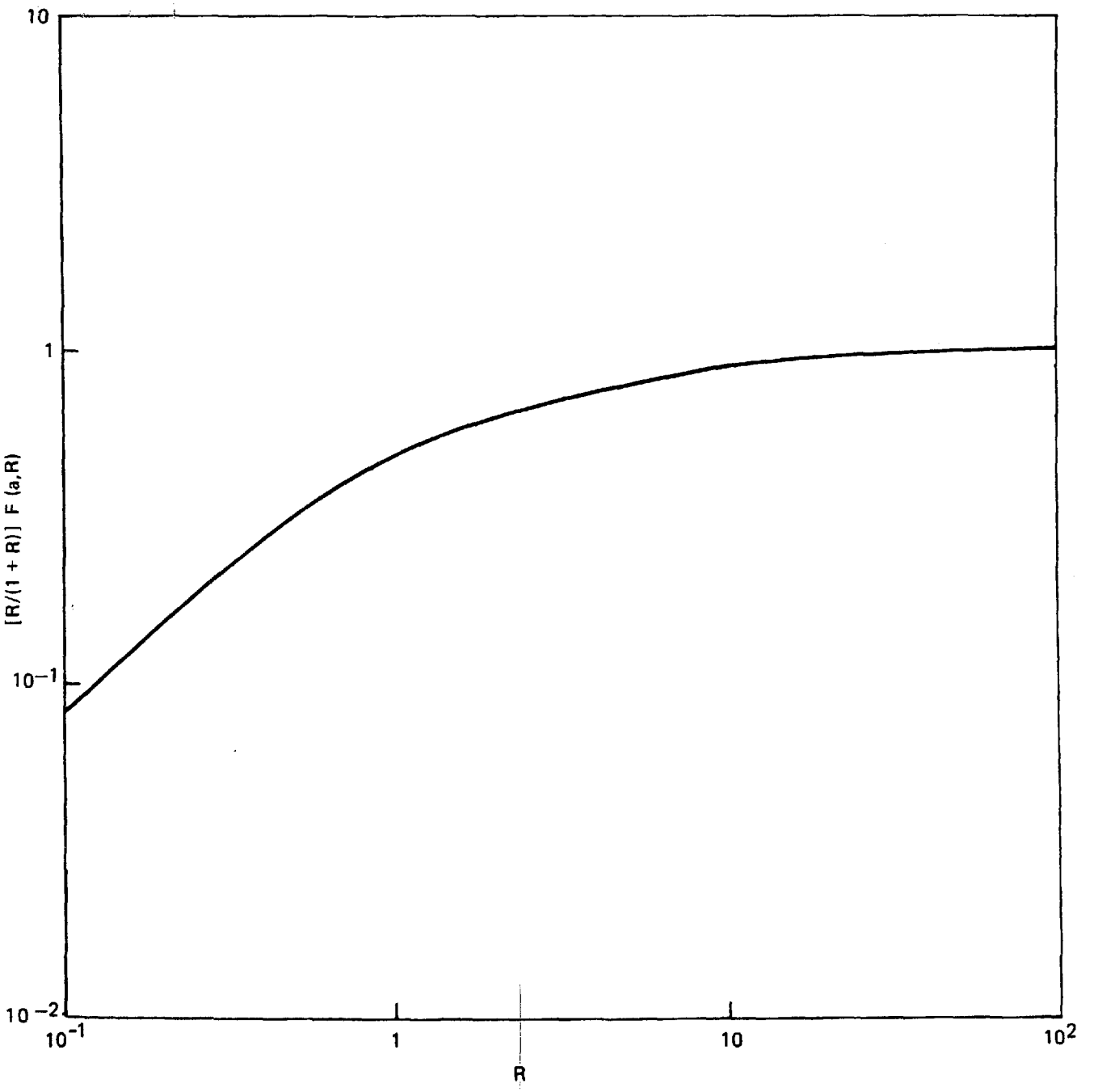

$[R/(1+R)]\ F(a,R) \rightarrow 1$, the rate constants still enter through the parameters K and L. Therefore, for a three-level system full saturation does not obviate quenching corrections if only fluorescence at ν_F is measured. In view of the above, the presence of an active third level is viewed as seriously complicating species measurements. A specific example, where effects such as these could be important, is for CN. Here it is known that, in addition to emission from the excited state $B^2\Sigma^+$ to the ground level $X^2\Sigma^+$, emission from $B^2\Sigma^+$ to $A^2\Pi$ has also been observed (Ref. 42). A second example involves the OH molecule where fluorescence occurs via $^2\Sigma^+(v' = 1) \rightarrow {}^2\Pi(v'' = 1)$ or $^2\Sigma^+(v' = 0) \rightarrow {}^2\Pi(v'' = 0)$, whereas the excitation corresponds to $^2\Pi(v'' = 0) \rightarrow {}^2\Sigma^+(v' = 1)$ (Ref. 39).

Two Levels

It is desirable to apply the above analysis to a two-level system. The reasons for this are as follows: (1) It is important to know whether the saturation behavior of a two-level system differs from that of a three-level system. If so this would provide a means of detecting the influence of a third level. (2) By performing a two-level analysis with inclusion of lineshape factors, a more ready comparison may be made between these results and the two-level results of Daily (Refs. 143-144) and Baronavski and McDonald (Ref. 25) which are discussed below. (3) The two-level model is the model one would hope to apply to species determination. The reason for this resides in the relative simplicity of the model, and the more direct interpretation of experimental results.

For a two-level system, the appropriate rate-equations are

$$\frac{dN_1}{dt} = -N_1 b_{12} + N_2(A_{21} + Q_{21} + b_{21}) \tag{35a}$$

and

$$\frac{dN_2}{dt} = N_1 b_{12} - N_2(A_{21} + Q_{21} + b_{21}). \tag{35b}$$

If a steady-state is assumed, it is readily shown that

$$\frac{N_2}{N_1+N_2} = \frac{D\rho B_{12}}{4\pi^2(\nu_F-\nu_L)^2 + (\frac{A_{21}+Q_C}{2})^2 + D\rho(B_{12}+B_{21})}, \tag{36a}$$

where

$$D = (A_{21}+Q_C)/(A_{21}+Q_{21}). \tag{36b}$$

If this result is compared with that given in Eq. (30) above, it is apparent that the two-level result may be inferred from the three-level result by setting L=K=0 and defining a new D as given in Eq. (36b). Accordingly, for a two-level system with lineshape analysis included, it follows that

$$\frac{N_2}{N^0} = \frac{1}{[(g_1/g_2)+1]} \left(\frac{R}{1+R}\right) F(a,R), \tag{37a}$$

in which

$$R = \frac{D\rho\,(B_{21} + B_{12})}{\left(\frac{A_{21}+Q_C}{2}\right)^2} \tag{37b}$$

The parameter a retains its earlier definition. It is apparent that there are not any significant differences between a two-level and a three-level system as regards the dependence of N_2/N^0 on a and R. When R is large the limiting value of (N_2/N^0) for a three-level system is $(1+L)[(g_1/g_2)+(1+K)/(1+L)]^{-1}$, whereas for a two-level system it is $[(g_1/g_2) + 1]^{-1}$. The ratio of degeneracies (g_1/g_2) is generally known. Consequently, if one succeeds in fully saturating a two-level system the details of the lineshape are not relevant and the fluorescence power is completely independent of quenching. As is shown in Eq. (34), the fluorescence power depends on A_{21} and N^0. Accordingly, N^0 may be determined without quenching corrections provided that A_{21} is known, which is often, but not always, the case.

Daily's Proposals

Two Levels

Daily has made two proposals for the measurement of species concentration via laser-induced fluorescence methods (Refs. 142-144). These are related in that, in both cases, saturation of the absorbing transition is shown to eliminate the need for quenching corrections to the fluorescence yield. The first proposal involves observing the temporal behavior of the fluorescence, while the second involves time-averaged measurement of the fluorescence power.

For the case in which the temporal behavior of fluorescence is monitored, Daily suggested excitation of the molecule with a laser pulse, abrupt turn-off of the pulse after equilibrium saturation is achieved, and temporal measurement of the subsequent fluorescent decay. In such a case, the fluorescence power may be shown to be given by

$$S_F(t) = S_F(t=0) \exp\,[-(Q + A_{21})t], \tag{38}$$

where S_F is the fluorescence power at time t; $S_F(t=0)$, the power at the time of laser cut-off. Accordingly, if the laser is turned-off abruptly, the time constant of the fluorescence decay gives $(Q + A_{21})$ and, hence, the quenching rate Q provided that A_{21} is known. In this way, the total quenching due to all other species present is determined directly, and reference to individual rates and partial pressures of other molecules is not required. If the absorption is fully saturated the number of molecules in the upper level may be seen to have a very simple relationship to the number in the lower level. This relationship is given by

$$N_2 \doteq [B_{12}/(B_{12} + B_{21})]N_1^{\,0} \tag{39}$$

It may be shown then that the number of molecules in the absorbing level is given by

$$N_1^{\,0} = [(g_1/g_2) + 1]\frac{(Q+A_{21})}{A_{21}}\,\frac{4\pi}{(hc/\lambda_F)}\int_0^\infty S_F(t)\,dt, \tag{40}$$

where λ_F is the fluorescence wavelength. The significance of this result may be summarized as follows: If the laser intensity is large so that Eq. (39) is valid and the temporal behavior of the fluorescence power is measurable, the number density $N_1^{\,0}$ may be determined from one trace of fluorescence versus time provided that g_1, g_2 and A_{21} are known. The number density is the area under the curve of $S_F(t)$. The quenching term Q is derived from the decay of the fluorescence.

It is important to remember that determination of the total number density of molecules in the ground level from $N_1^{\,0}$ is possible provided only that the gas temperature is known. This temperature must be measured separately. Further, A_{21} is not always known precisely. A practical difficulty, which one may encounter in a flame at 1 atm pressure, is that Q is large and hence, the decay so rapid that it is not possible to shut off the laser pulse abruptly enough to time-resolve the fluorescence. It is known that quenched excited molecular lifetimes in a flame can be as short as 10^{-12} sec (Ref. 25). In principle, a Pockels cell can function as a shutter with about a 500 picosecond response time, but this represents its limit of operation. Moreover, photomultipliers have response times which are typically tenths-of-nanoseconds at best. Accordingly, time resolving picosecond decay times is a formidable task.

Daily's second proposal deals with time-averaged measurement of the fluorescence power. In this case, the fluorescence power is given by Eq. (34). This is equivalent to measurement of the number of fluorescence photons emitted without reference to time resolution of the excited-state decay process. In the limit of small laser

spectral intensity $I_{L\nu}$, i.e., laser intensity per unit bandwidth, $I_L/c\Delta\nu_L$, it may be shown that $N_2^{(1)} = N_1^0 B_{12} I_{L\nu}/(Q_{21} + A_{21})$, whereas in the limit of large $I_{L\nu}$, $N_2^{(2)} = [1 + (g_1/g_2)]^{-1} N_1^0$. In the former case, the fluorescence is

$$S_F^{(1)} = h(c/\lambda_F) \frac{B_{12}}{4\pi} \Omega_c V_c \left(\frac{A_{21}}{Q_{21} + A_{21}}\right) I_{L\nu} N_1^0. \tag{41a}$$

Here it is apparent that $S_F^{(1)}$ depends on $I_{L\nu}$ and quenching Q_{21} through the factor $A_{21}/(Q_{21} + A_{21})$, which is commonly referred to as the fluorescence yield or Stern-Vollmer (Ref. 146) factor. This factor may be very small; it is not unusual for it to be of order 10^{-6} (Ref. 25), thereby severely limiting the fluorescence power. In the limit of large $I_{L\nu}$, however, use of $N_2^{(2)}$ yields

$$S_F^{(2)} = h(c/\lambda_F) \frac{A_{21}}{4\pi} \Omega_c V_c \frac{1}{[1 + (g_1/g_2)]} N_1^0. \tag{41b}$$

In this case, S_F is independent of quenching and laser spectral intensity. Accordingly, the sought for N_1^0 may be determined by measurement of S_F without any reference to quenching. This result is identical to that of Piepmeier for two-levels in the case that $R \gg 1$.

A practical difficulty is whether $I_{L\nu}$ can be made large enough that Eq. (41b) applies. This is discussed in detail further in the text. However, it is concluded that it is very difficult to saturate a transition fully such that Eq. (41b) may be used directly to infer N_1^0. This is due to practical limitations concerning achievable spectral intensities. A way around this difficulty has been suggested by Baronavski and McDonald (Ref. 25).

Three Levels

The preceding discussion was confined to a two-level system. Daily has considered a three-level system as well (Ref. 143). The principle conclusion is that species concentrations may be determined without reference to quenching in the three level case as well, providing that the absorbing transition is fully saturated and that measurements of fluorescent intensities at two wavelengths are made. Daily points out that this procedure is applicable to more complex systems although the separation of the increased number of fluorescence intensities may be more difficult. Again there remains the uncertainty as to whether it is possible to saturate the absorbing transition fully.

Baronavski-McDonald Approach to Species Measurements

Baronavski and McDonald have made use of Daily's proposals regarding saturated fluorescence (Ref. 25). A difference in their approach involves the recognition that it may be very difficult in practice to saturate a transition completely. Accordingly, their analysis is appropriate to a condition for which the degree of saturation is high but not complete, a condition more common in practice. The analysis applies to a two-level system. The fluorescence power in exact form is given by

$$S_F = h(c/\lambda_F)(A_{21}/4\pi)\Omega_c V_c \frac{N_1^0 B_{12}}{\left[\left(\frac{Q_{21} + A_{21}}{I_{L_\nu}}\right) + (B_{12} + B_{21})\right]} \qquad (42)$$

They then expand S_F about $(I_{L_\nu})^{-1}$ in a Taylor series. This results in an approximate expression for S_F given by

$$S_F \doteq h(c/\lambda_F)(A_{21}/8\pi)\Omega_c V_c \left[N_1^0 - \frac{N_1^0 (Q_{21} + A_{21})}{(B_{21} + B_{12})\, I_{L_\nu}}\right] . \qquad (43)$$

From Eq. (43), it is evident that S_F has a linear dependence on $(I_{L_\nu})^{-1}$. In a plot of S_F versus $(I_{L_\nu})^{-1}$, the intercept of the resulting straight line is essentially N_1^0, while the slope of the line depends on the quantity of $(Q_{21}N_1^0)$ from which the quenching rate can be determined. The accuracy of the N_1^0 measurement depends on knowing λ_F, Ω_c, V_c and A_{21}. The former three parameters can be obtained through suitable calibration. Uncertainty in the determination of N_1^0 then depends on the uncertainty in A_{21}.

Baronavski and McDonald applied the preceding method of analysis to the determination of C_2 concentration in an oxy-acetylene flame. A concentration of 10^{16} cm^{-3} was determined with a factor of 3 uncertainty. This latter uncertainty was due to lack of precise values for the apparatus parameters Ω_c and V_c. Inclusion of the uncertainty in A_{21} would result in still larger error in N_1^0. In determining the C_2 concentration, a value of 10^{-6} was obtained for the fluorescence yield factor $[A_{21}/(Q_{21} + A_{21})]$. This emphasizes the extreme importance of quenching in influencing the fluorescence intensity for a case in which the laser spectral intensity is far less than that required for saturation. The maximum laser power appropriate to the C_2 measurements above was about 10^3 Watts. This was achieved with a flashlamp-pumped dye laser. The laser was focused to a spot size of 0.1 mm, corresponding to an intensity of 1.3×10^7 Watts/cm^2. The beam divergence of such lasers is typically 1 milliradian at best. For measurement in a 1 meter diameter furnace, where the focusing lens could be as much as 50 cm removed from the sample

volume, the focal spot size would be about 0.5 mm, corresponding to an intensity of 5.2×10^5 Watts/cm^2. This would not suffice to saturate the C_2 transition sufficiently to permit implementation of the Baronavski-McDonald analysis procedure. For such furnace measurements to be feasible, laser powers on the order of 25 (10^3) Watts would be required.

Lineshape

The preceding discussions of the saturation properties of the fluorescence power are not applicable to arbitrary values of the laser spectral width $\Delta\nu_L$ relative to the molecular linewidth. The molecular linewidth is determined by contributions from collisional and Doppler broadening. If the pressure is high and temperature low, the lineshape is homogeneous. If the gas temperature is high and pressure low, the Doppler effect predominates and the lineshape is inhomogeneous. Cases occur wherein the two effects contribute almost equally to the linewidth. Figure 18 displays the homogeneous and inhomogeneous broadened linewidths for NO, where collisions of NO with water molecules primarily determine the homogeneous width, $\Delta\nu_H$. It is seen that for the temperature range $1000^oK < T < 2000^oK$, $\Delta\nu_H > \Delta\nu_D$ for $P_{H_2O} > 10$ torr. The Piepmeier analysis is appropriate to the case in which homogeneous broadening is present and the molecular linewidth exceeds the laser spectral width. Daily and Baronavski-McDonald treat the case where the laser spectral width exceeds the molecular linewidth. More detailed discussions of these subtleties are given by Greenstein (Ref. 147) and Killinger, Wang and Hanabusa (Ref. 39). Here discussion will be limited to pointing out the differences which occur for the two cases with regard to the manner in which the quenching influences the saturation of a two-level system.

If the laser spectral width exceeds the molecular linewidth, it is not difficult to show from the preceding discussions that

$$\frac{N_2}{N_1^0} = \frac{1}{[(g_1/g_2)+1]} \left(\frac{R'}{1+R'}\right) \tag{44a}$$

where

$$R' = \frac{(B_{12} + B_{21})\, I_{L\nu}}{(Q_{21} + A_{21})} \quad . \tag{44b}$$

In Eq. (44b), $I_{L\nu} = I_L/(c\Delta\nu_L)$ and R' is seen to be inversely proportional to the product $(Q_{21} + A_{21})\,(c\Delta\nu_L)$. It may be shown that for a two-level treatment following Piepmeier the saturation parameter is

$$R = \frac{(B_{12} + B_{21})\, I_L}{\left(\frac{Q_{21} + A_{21}}{2}\right)^2} \quad , \tag{45}$$

FIG. 18

DOPPLER AND HOMOGENEOUS LINEWIDTHS FOR NO

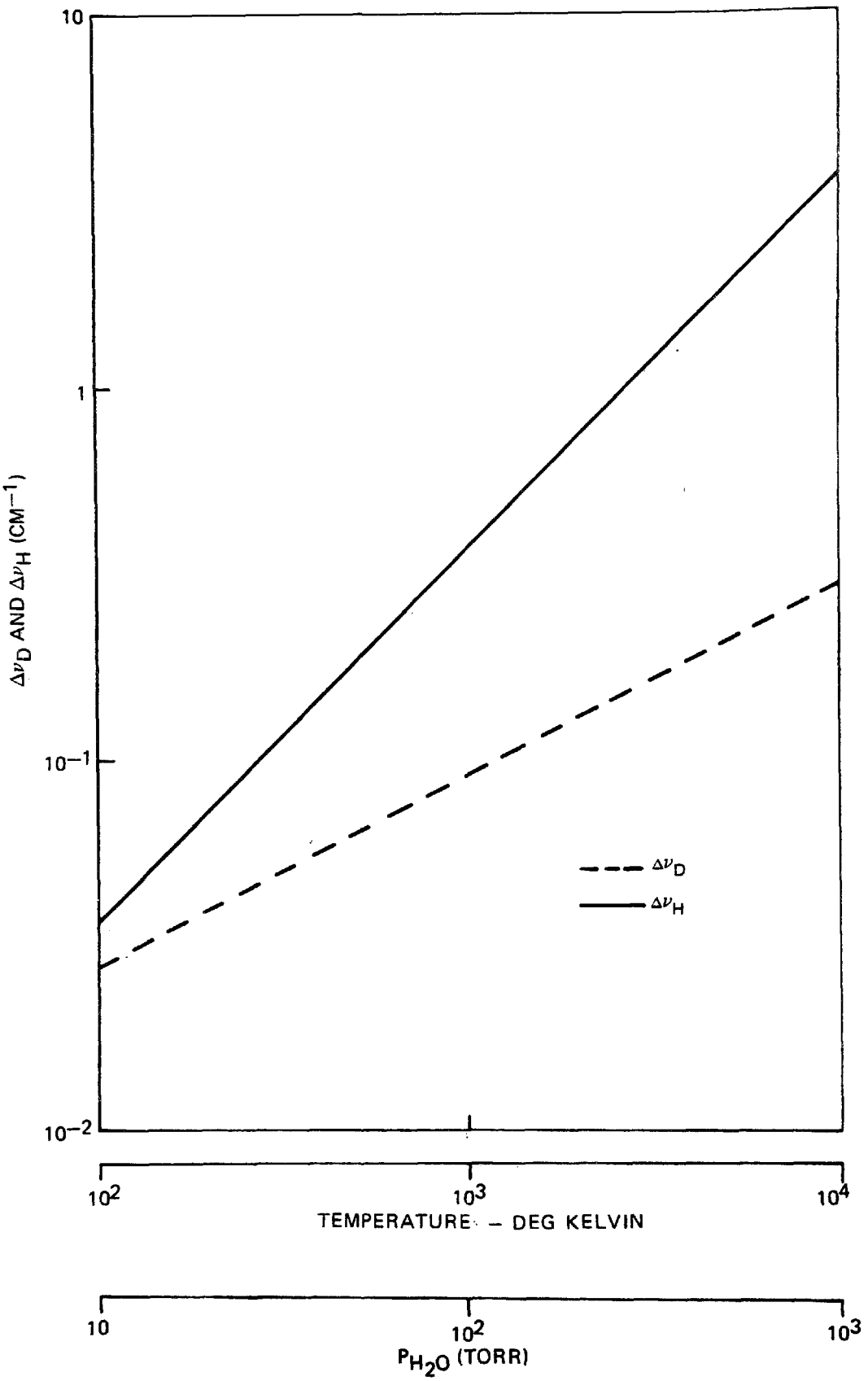

and R is seen to be inversely proportional to $(Q_{21} + A_{21})^2$. In general then, the two cases differ in the way the saturation parameter is defined, and for the case of Piepmeier the term F(a,R) is present. If the molecular lineshape is strongly homogeneous, F(a,R) is nearly unity in value and, hence, this distinction vanishes. However, even for a homogeneous lineshape the distinction exists between R and R'. Of course, should the intensity of the laser be so high that both [R/(1+R)] and [R'/(1+R')] have values of approximately unity, then all reference to lineshape and quenching becomes unimportant, and the two approaches agree as regards $(N_2/N_1{}^0)$. Hence, in applying a two-level model to species determination, it is apparent that not one model applies to all cases. The model selected must satisfy the existing relationships between the laser spectral width, homogeneous and inhomogeneous molecular width.

Multi-Level Saturation

The preceding models are strictly appropriate to systems where only two or three levels are present. If such models are applied to estimate the laser spectral intensity required to saturate a molecular transition, where many closely-spaced rotational levels are present, the saturation intensities estimated will be low. Multi-level saturation has been discussed by Christensen, Freed and Haus (Ref. 148) with reference to the CO_2 molecule and depends on rapid cross-relaxation among the rotational levels within the time of electronic deactivation of the molecule. In this way, the effective relaxation rate can be shown to be increased by the weighted relaxation rates of all the other tightly-coupled rotational levels. If there are M rotational levels populated at the gas temperature, the effective rate is $Q_{eff} = MQ$, thus resulting in an increase in the laser intensity required to achieve saturation. For a diatomic molecule, it is a straightforward matter to estimate M, which is the inverse of the number of molecules in a given J-state in relation to the total number of molecules present in a given vibrational state. Specifically, the parameter M is given by (Ref. 23)

$$M \doteq (N_J/N^o)^{-1} = \left[\left(\frac{hcB_e}{kT} \right) (2J+1) \exp -[J(J+1)hcB_e/kT] \right]^{-1} \quad (46)$$

where B_e is the rotational constant; k, Boltzmann's constant; T, the gas temperature; and J, the rotational quantum number of the excited level. An evaluation of M for a selected group of molecules is given in Table XIV. The J value is that which corresponds to maximum population in the Boltzmann distribution for 2600°K.

Two-Photon Spectroscopy

Attention has been given by others to species measurement via two-photon absorption of radiation (Ref. 149) which eliminates the need for frequency-doubling to achieve near UV wavelengths. A single visible source may be used. This technique is not given consideration here in that perturber concentrations and individual quenching rates are required. This requirement arises, since with

TABLE XIV

EFFECTIVE NUMBER OF ROTATIONAL LEVELS
(2600°K)

Molecule	J_{MAX} (Maximum Population)	M
CH	7	13
CN	21	36
NH	7	12
OH	6	11
NO	22	38

available laser sources, it is not possible to saturate a two-photon absorption with severe excited state quenching present. The two-photon absorption rate would have to be comparable to the single-photon rate required for saturation. This, however, is unlikely in the presence of quenching since the two-photon absorption cross-sections are approximately 10^{-6} - 10^{-7} of the single-photon cross-sections.

Signal to Noise Estimates

Signal Strength Calculations

Signal strength estimates are made for the molecules CH, CN, NH, OH and NO. These molecules have known emission spectra, absorption wavelengths accessible to tunable dye lasers and known lifetimes for radiative decay. The existence of quenching information concerning these molecules is, in principle, not relevant since quenching corrections may be determined experimentally using the Baronavski and McDonald approach. Attention is not given to the molecules NO_2 and NH_2. The molecule NO_2 has a relatively long lifetime for radiative decay of (2×10^{-5}) sec. Since the saturation parameter is inversely proportional to this lifetime, it is unlikely that it is possible to saturate the NO_2 transition at $\lambda_F(NO_2) \doteq 4000$ Å. The molecule NH_2 has a shorter lifetime for radiative decay of (5×10^{-7}) sec and a relatively long fluorescence wavelength, $\lambda_F(NH_2) \doteq 5700$ Å which makes it more favorable than NO_2 vis-a-vis saturation. The difficulty with NH_2 is analytic; namely, it is a strongly asymmetric molecule and this makes it difficult to compute M. For this reason detailed estimates for NH_2 are not made. However, it appears to be a molecule worthy of experimental study in order to determine if saturation can be achieved since $\lambda_F(NH_2) \doteq 5700$ Å which is a favorable wavelength regime for high power tunable dye lasers.

The saturation fluorescence analysis given by Baronavski and McDonald is applicable for the case in which $\Delta\nu_L > \Delta\nu_H$ as previously stated. For the diatomic molecules above, the absorption is homogeneously broadened in a flame environment and $\Delta\nu_H$ is determined by the electronic deactivation of the excited molecular state by collision with water vapor molecules. Water is taken here as the dominant broadening species in a flame due to its relatively high partial pressure and its efficiency as a quencher. In the case of the NO γ-bands for example, the homogeneous width, $\Delta\nu_H$ is 0.43 cm^{-1} computed using a quenching rate of 6.84 x 10^8 sec^{-1} $Torr^{-1}$ (Ref. 150) and a water vapor partial pressure of 120 Torr (Ref. 151). For the laser spectral width, a value of $\Delta\nu_L$ = 2.5 cm^{-1} is used in the computations; this value is consistent with the spectral width achieved recently with a flash-lamp-pumped dye laser (Ref. 152). Accordingly, the ratio of linewidths in this case is $\Delta\nu_L/\Delta\nu_H$ = 5.8 so that $\Delta\nu_L > \Delta\nu_H$ is satisfied. In the case of the γ-bands of NO and a temperature of 2600°K, it is readily shown that $\Delta\nu_D$ = 0.15 cm^{-1} or $\Delta\nu_D \ll \Delta\nu_H$.

The expression which is used to evaluate the fluorescence signal power is given by (Ref. 25)

$$S_F = h(c/\lambda_F)\,\frac{A_{21}}{8\pi}\,\Omega_c\,(L_c A_c)\,N_1^{\,0}\,\left(\frac{R}{1+R}\right), \tag{47a}$$

where the saturation parameter may be shown to be given by

$$R = (4\pi hc)^{-1}\,\frac{I_L}{c(\Delta\nu_L)}\,A_{21}\,\lambda_F^{\,3}\,\left(\frac{1}{Q + A_{21}}\right). \tag{47b}$$

The expression for S_F is equivalent to that given previously in Eq. (42). The degeneracies g_1 and g_2 in this case are assumed to be approximately equal. This is an adequate approximation for transitions involving moderately high vales of J.

For the signal estimates, an F/8 lens system for light collection is assumed corresponding to an Ω_c of 0.012 sr. For a 90° sampling geometry and unity magnification optical transfer (Fig. 4), L_c is equal to the aperture diameter A, here assumed to be 1 mm in diameter. Assuming a laser beam divergence of 1 milliradian and a 50 cm focal length lens, the cross sectional area, A_c, of the focused laser beam is $\pi/4$ (.05 cm)^2 or 1.96 (10^{-3}) cm^2. Hence the sample volume V_c is 1.96 (10^{-4}) cm^3.

The evaluation of the saturation parameter R would be straightforward were it not for the uncertainty regarding Q for the molecules CH, CN and NH. For these molecules, rates for electronic quenching by water vapor are unknown. The situation is somewhat better, however, for the molecules NO and OH. In the case of quenching of excited NO $^2\Sigma^+$, the rate is 6.84 x 10^8 sec^{-1} $Torr^{-1}$ (Ref. 150). This rate was measured at 300°K. The rate which corresponds to a temperature of 2600°K

is expected to be larger, but data at this or nearby temperatures are not available and calculation of the rate at 2600°K from first principles is difficult if not impossible (Ref. 153). In the case of OH, the rate for quenching of the $^2\Sigma^+$ excited state is 1.45×10^7 sec^{-1} Torr^{-1} (Ref. 154), a value considerably smaller than that for NO. Again, in the case of OH the rate is known only at the temperature of 300°K. The reason for the smaller rate in the case of OH is probably due to the fact that the dipole moment of OH is 0.95 Debye whereas for NO the dipole moment is much larger and equal to 7.47 Debye (1 Debye = 10^{-18} esu-cm). Thus, despite similar electronic structure of the excited state, the forces acting between NO and H_2O in a collision exceed those between OH and H_2O. In view of the lack of data and in order not to underestimate the intensity required to saturate transitions in CH, CN and NH, the procedure adopted here is to use, for the quenching rate in these cases, the larger of the two values above, namely the quenching rate for NO. Even this value may be too large however. In the work of Basco, Callear and Norrish, (Ref. 150), a value of 616(Å)^2 is given for the collision cross section for electronic relaxation of NO ($A^2\Sigma^+$) by NO ($X^2\Pi$). In the subsequent work of Callear and Pilling (Ref. 155), a value of 35(Å)^2 is given. No reference is made to the earlier work. The value of Callear and Pilling is in reasonable agreement with 25(Å)^2 and 18(Å)^2 as measured by Melton and Klemperer (Ref. 156) and Broida and Carrington (Ref. 36), respectively. This raises serious doubt concerning the correctness of the value given by Basco, Callear and Norrish. In addition, this may imply that the cross section given by these latter authors for relaxation by H_2O is also much too large, which would lower significantly the laser spectral intensity required for saturation of CH, CN, NH and NO. It is tempting to take a less pessimistic view and assume the rates associated with CH and NH are the smaller OH value since CH, NH and OH have comparable dipole moments. This is not done. However, it is important to keep in mind that estimates made below of laser spectral intensities required to saturate transitions in NH and CH may be high, and the resolution of this uncertainty resides in performing NH and CH saturation measurements.

In Table XV, the quantity $[R/(1+R)]$ is evaluated. The parameter M is introduced to account for an increase in Q to MQ due to the presence of M rotational levels in the excited electronic state. Accordingly, $[R/(1+R)]$ is calculated using Eq. (47b) except that Q is replaced by (QM). If $(QM)^{-1}$ is evaluated for NO, the result is $(QM)^{-1} \doteq (3 \times 10^{-13})$ sec. This appears at first sight to be a very short time; however, Baronavski and McDonald have measured quenched lifetimes on the order of 10^{-12} sec for C_2 molecules in an oxy-acetylene flame. Accordingly, the present estimate of $(QM)^{-1}$ for NO may not be unrealistic.

In Table XV, the transition is completely saturated in the case that $[R/(1+R)] \rightarrow 1$. It is apparent from the Table that for the laser intensity and spectral width given, substantial saturation is achieved for all molecules except NO. The reason for this is that R is proportional to λ_F^3 and A_{21}, and for NO, these parameters are small relative to other cases. This leads to the conclusion that despite its importance in combustion processes it may be difficult to measure NO in the manner described herein owing to difficulty in saturating the transition.

TABLE XV

SATURATION TERM IN FLUORESCENCE INTENSITY

$I_L = 10^8$ watts/cm^2, $\Delta\nu_L = 2.5$ cm^{-1}, T = 2600°K

Molecule	λ_F(Å)	M	R	[R/(1+R)]
CH	4315	13	0.82	0.45
CN	3883	36	1.8	0.64
NH	3360	12	0.46	0.32
OH	3064	11	8.0	0.89
NO	2270	38	0.10	0.09

In order to compute S_F from Eq. (47a), it is necessary first to evaluate N_1^0 This latter number density is distinct from the total number density of molecules N^0 present at 1 atm pressure and at 2600°K. It is well known that N_1^0 is given by $N_1^0 = N^0 f^V f^J$, where f^V and f^J are evaluated from appropriate vibrational and rotational partition functions (Ref. 23). For 2600°K, 1 atm pressure and a species concentration of 1 ppm, it follows that $N^0 = (2.84 \times 10^{12})/\text{cm}^3$. The product $f^V f^J$ for the molecules of interest is given in Table XVI along with the number density, N_1^0. The calculation is done for excitation from the level v = 0 and J = J(MAX).

TABLE XVI

NUMBER DENSITY OF ABSORBING MOLECULES

Concentration = 1 ppm @ 1 atm total pressure, T = 2600°K

Molecule	$(f_{v=0})(f_{J=JMAX})$	$N_1^0(\text{cm}^{-3})$
CH	6.2×10^{-2}	1.8×10^{11}
CN	1.9×10^{-2}	5.5×10^{10}
NH	7.0×10^{-2}	2.0×10^{11}
OH	7.7×10^{-2}	2.2×10^{11}
NO	1.7×10^{-2}	4.9×10^{10}

It is now possible to evaluate S_F in Eq. (47a) for the five molecules. Values of S_F are given for CN, OH and NO in Fig. 19. From these curves, it is possible to determine the minimum value of $I_{L\nu}$ required to saturate the transitions to an extent which permits evaluation of N_1^0 as described in preceding discussions. These values are given in Table XVII and are appropriate to R ≐ 1 for each molecule. Values are given in Table XVII for 12 Torr of H_2O as well, in order to stress that less water

FLUORESCENCE POWER VERSUS SPECTRAL INTENSITY

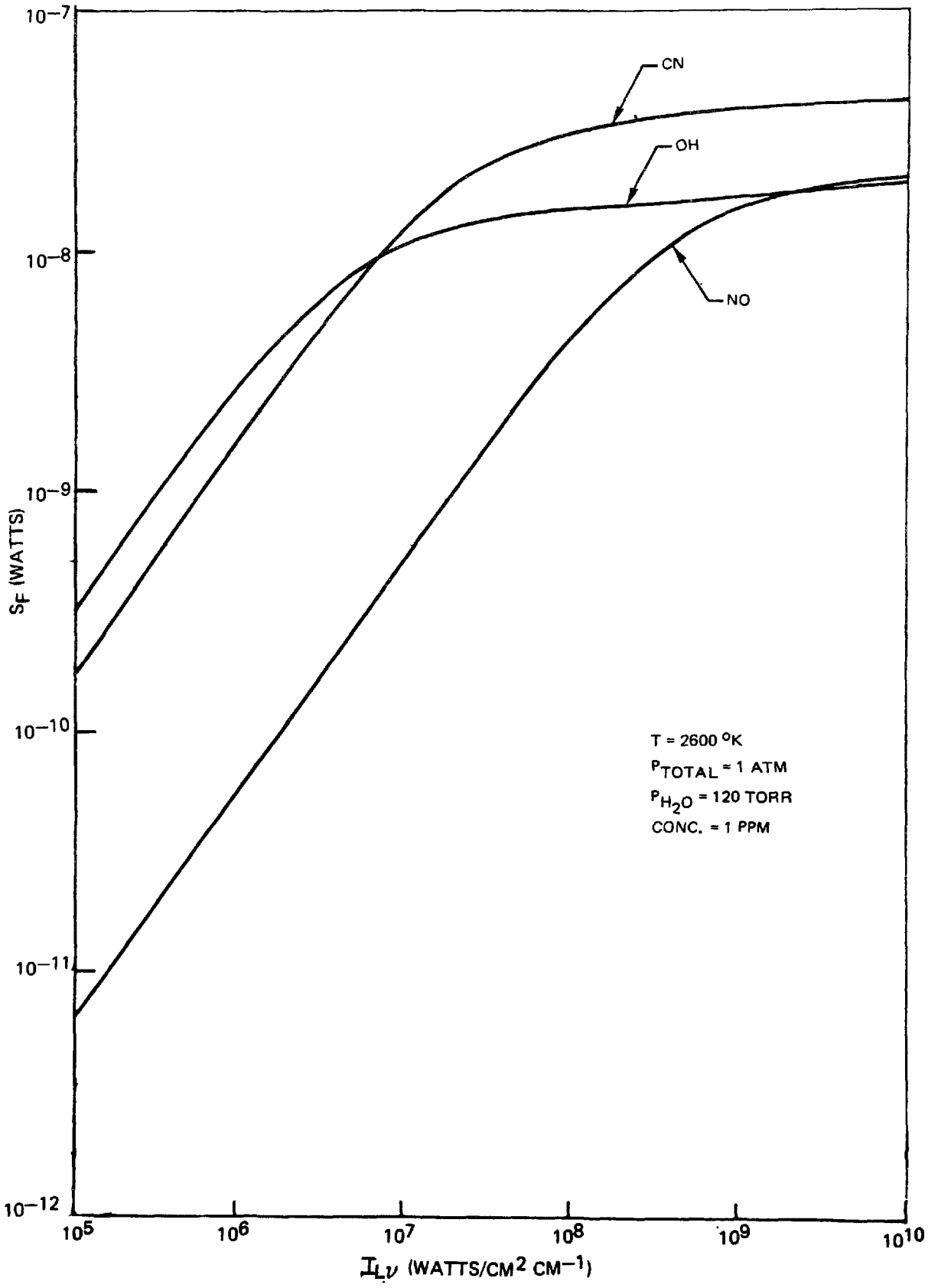

vapor lowers the threshold for saturation correspondingly. If a plot of S_F versus I_{L_ν} is made for a molecule such as CN at a temperature lower than 2600°K, namely at 1000°K, the value of $I_{L_\nu}^{SAT}$ is not changed markedly. In the case of CN at 1000°K, $I_{L_\nu}^{SAT} \doteq 1 \times 10^7$ watts/cm^2 cm^{-1}. Accordingly, calculations are presented in Fig. 19, only for the one temperature of 2600°K.

TABLE XVII

SATURATION LASER SPECTRAL INTENSITY

(T = 2600°K)

Molecule	λ_F(Å)	$I_{L_\nu}^{SAT}$ (12 Torr H_2O)	$I_{L_\nu}^{SAT}$ (120 Torr H_2O)
CH	4315	4×10^6 Watts/cm^2 cm^{-1}	4×10^7 Watts/cm^2 cm^{-1}
CN	3883	3×10^6	3×10^7
NH	3360	1×10^7	1×10^8
OH	3064	6×10^5	6×10^6
NO	2270	4×10^7	4×10^8

It is important to realize that for a molecule the fluorescence can occur in a large bandwidth. This is due to fast cross-relaxation among rotational levels which establishes rotational equilibrium in a time which is generally short compared to the electronic deactivation time. The emission occurs in a width influenced by B_e and T. As an approximate method of estimating this bandwidth, $\Delta\lambda_F$, the separation of the P- and R-branch maxima for a diatomic molecule is taken to be $\Delta\lambda_F$ which is equal to $2.36\sqrt{B_eT}$ (Ref. 23). Values of $\Delta\lambda_F$ for the 5 molecules are given in Table XVIII. These are important for the estimates below of species detection limits.

TABLE XVIII

FLUORESCENCE EMISSION BANDWIDTH

(T = 2600°K)

Molecule	λ_F(Å)	$\Delta\lambda_F$(Å)
CH	4315	85
CN	3883	25
NH	3360	56
OH	3064	49
NO	2270	8

Species Detection Limits

In order to set detection limits in ppm for the species, it is necessary to make estimates of the signal-to-noise ratio (S/N). This requires taking into account the various sources of noise. In this regard, three sources of noise are considered. The first of these is elastic scattering of the laser radiation by the particulates in the flame, namely Mie scattering. Mie scattering cross sections are given in Fig. 6. The second is the radiation energy density which is given in Fig. 3. The third source of noise is laser-modulated particulate incandescence.

The background due to Mie scattering depends on particulate properties, namely the number of particulates present, their size and refractive index. The Mie power occurs at the same wavelength as that of the incident radiation and may be estimated by use of

$$P_M = (d\sigma/d\Omega)(n_P V_c)\Omega_c I_L \qquad (48)$$

where $d\sigma/d\Omega$ is the differential cross section; n_P, the particulate number density. For 400 Å particles, 5000 Å laser radiation and 90° viewing, it may be shown that $d\sigma/d\Omega \doteq (4 \times 10^{-15})$ cm^2/steradian. If $n_P = 10^8/cm^3$, $I_L = 10^7$ Watts/cm^2, and V_c and Ω_c are as given earlier, the Mie power is calculated to be $P_M = 1.1\ (10^{-5})$ Watts. The very large Mie power precludes observation of the fluorescence exactly at the wavelength of the exciting radiation. Fortunately this does not constitute an unresolvable difficulty since fluorescence is emitted in a broad spectrum. Spectrometers with good discrimination are available and it is possible to observe shifted fluorescence.

For the radiant energy density a value is taken from Fig. 3 typical of that measured in the Rainbow furnace. For wavelengths of 4000Å or less, a region of particular interest in view of the fact that $\lambda_F \leq 4315$Å for the given molecules, a conservative value for the radiation energy density of 100 (10^{-9}) watts/cm3 Å steradian is assumed. For a detection bandwidth of 10Å, and the previously assumed viewing parameters, the background power is calculated to be $1.6(10^{-10})$ watts. In the discussion which follows concerning laser-modulated particulate incandescence, this radiant power is seen to be small.

It may be shown that the noise power due to laser modulated particulate incandescence is $6.9(10^{-9})$ Watts for a 10Å bandwidth, V_c and Ω_c as above and $\lambda = 6073$Å. This value is appropriate to 400Å particles in a concentration of $10^8/cm^3$, and was scaled from earlier calculations. Comparing it with the radiant power, it is apparent that the laser modulated incandescence is more than an order of magnitude more important than the background luminosity. The former is therefore used in the S/N calculations. The laser-modulated particulate incandescence wavelength dependence is determined by the black-body distribution function, namely $\lambda^{-5}\,[\exp(hc/\lambda kT) - 1]^{-1}$. Table XIX gives noise powers for the wavelengths of interest inferred from the value above at 6073Å using the black-body distribution function.

TABLE XIX

LASER MODULATED PARTICULATE INCANDESCENCE NOISE POWER LEVELS

$\bar{\Delta\lambda}$ = 10Å, Ω_c = 0.012 ster, V_c = 1.96 (10^{-4}) cm^3

Molecule	λ_F(Å)	Noise Power (Watts)
CH	4315	7.5(10^{-9})
CN	3883	6.9(10^{-9})
NH	3360	5.5(10^{-9})
OH	3064	4.4(10^{-9})
NO	2270	1.2(10^{-9})

With the values given in Table XIX, it is possible to compute S/N ratios for given species concentrations. An example of this is given in Fig. 20 for CN. In Fig. 20 a spectrometer efficiency of 30 percent and a 10^{-6} sec laser pulse width are assumed. Species detection limits are summarized in Table XX. In practical flames, the lower limit on species concentration is taken as that concentration which yields S/N ≥ 10. Limits are also given for the case of a clean flame. In this case, the view is adopted that the limit of sensitivity is set by the available number of photons. The values given correspond to about 150 photons at the cathode of a photomultiplier tube. This may be shown to yield about a 1 mV signal at the photomultiplier anode for a reasonable choice of gain, capacitance and quantum efficiency.

TABLE XX

DETECTION LIMITS FOR SPECIES MEASUREMENT

	Practical Flame		Clean Flame	
Molecule	ppm	# photons	ppm	# photons
CH	80	4.7 (10^4)	.26	150
CN	10	3.1 (10^4)	.05	150
NH	25	3.1 (10^4)	.13	150
OH	35	1.6 (10^4)	.32	150
NO	1	3.1 (10^3)	.05	150

From Table XX, it is apparent that saturated laser fluorescence appears capable of quite sensitive trace species detection for the molecules to which it is applicable. This is true even in practical flame situations. For example, if the S/N requirement is relaxed to unity, measurements below 10 ppm may be possible for all the species listed.

SIGNAL–TO–NOISE ESTIMATE FOR CN

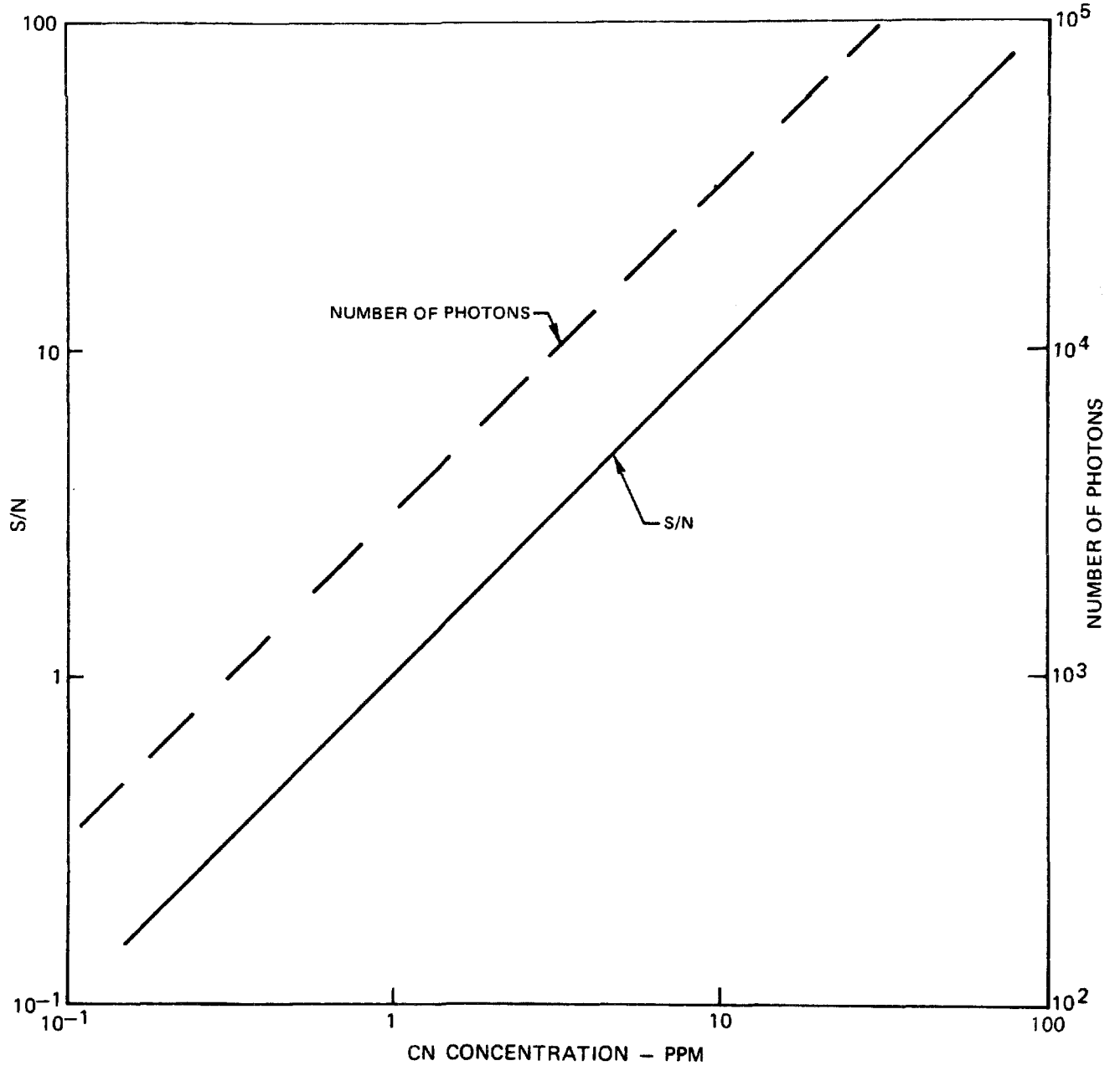

Apparatus Calibration

In order to determine a number density from a measurement of the fluorescence power, values for a number of parameters related to the measurement are required which are exclusive of the fluorescence power itself. Aside from fundamental constants, the following are required: (1) λ_F, fluorescence wavelength; (2) A_{21}, radiative decay rate; (3) Ω_c, light collection solid angle; (4) V_c, sample volume; (5) $I_{L\nu}$ (implies knowing laser intensity in watts, focused area in cm^2 and spectral width in cm^{-1}; and (6) ϵ, light collection efficiency. Quantities which lend themselves to measurement with some precision are λ_F and $I_{L\nu}$, although there may be some difficulty in determining the focused area precisely. For A_{21}, the usual procedure is to use the best value available in the published literature. For Ω_c, V_c and ϵ, the uncertainty in these values may be large; that is, these uncertainties are likely to be more significant than those for λ_F, $I_{L\nu}$ and A_{21}. For the preceding reasons, it is important to have a calibration procedure in order to be able to determine $\epsilon\Omega_c V_c$. A calibration procedure which does not require detuning λ_L away from λ_F is most desirable. One such procedure which fits these requirements very well is spontaneous Raman scattering from room air nitrogen. Since this latter process is non-resonant, it may be used at any wavelength corresponding to the molecule chosen. Therefore, resonance-fluorescence and spontaneous Raman emission may be observed at λ_F. This calibration procedure has been used successfully by Wang and Davis to measure OH concentration in air (Ref. 40). Indeed, in this latter case the spectrum of scattered light displayed Raman scattering from N_2, O_2 and water. The only requirement of this approach is that the Raman cross-section be known which it is to fairly good accuracy.

Required Temperature Measurements

In order to determine the total species population of interest, once the population of the initial level excited is determined from the fluorescence measurements, it is necessary to know the flame temperature. Since it may be necessary to pulse average the fluorescence measurements, and since fluctuations of temperature in a turbulent medium cause population changes, it is desirable to select a particular initial J-level for measurement which is least sensitive to changes in population due to temperature fluctuations. If this is possible, an average temperature, as determined, for example by CARS, may be used to compute the species concentration from the measured fluorescence power. This then would eliminate the need for simultaneous and instantaneous temperature measurements.

The particular J-value which achieves this end is determined by evaluating $\partial f_J/\partial T$ and equating the result to zero. f_J is the fraction of molecules in the state J and is given by (Ref. 23)

$$f_J = \frac{B_e hc}{kT} (2J+1) \exp - [B_e J(J+1)\, hc/kT]. \tag{49}$$

If this is done, the rotational level meeting this requirement is determined from

$$J^{*2} + J^* - (k/B_e hc)\bar{T} = 0, \tag{50}$$

where $\bar{T}$ is an average flame temperature. This is a quadratic equation with real roots and is trivial to evaluate. If J^* is evaluated for the CN molecule and for $\bar{T} = 2000^\circ K$, the result when rounded to the nearest integer is $J^* = 27$. This contrasts with the state of rotation associated with a population maximum of $2000^\circ K$ which is $J_{MAX} = 19$. In Fig. 21 , f_{J^*} and $f_{J_{MAX}}$ are plotted versus temperature for average temperatures of $2000^\circ K$ and $1400^\circ K$. For $\bar{T} = 1400^\circ K$, $f_{J^*} = 22$ and $f_{J_{MAX}} = 16$. In both cases, it is evident that f_{J^*} is significantly less sensitive to temperature excursions about $\bar{T}$ than $f_{J_{MAX}}$. Indeed, for 20% fluctuations in temperature for the case $\bar{T} = 2000^\circ K$, f_{J^*} changes by no more than 3.5% while $f_{J_{MAX}}$ can vary up to 10%. In view of the above, it is important to select for excitation the level J^*. Thus, despite temperature fluctuations it may be possible to determine reliably a concentration even for the case in which averaging of pulses is required by using the average temperature.

Summary

The significant conclusions of this section are: (1) Of all the molecules of interest in combustion processes, only a few are amenable to detection by laser fluorescence. (2) The laser spectral intensities which are required to saturate the molecular transitions are of order $(10^6\text{-}10^8)$ Watts/cm^2 cm^{-1}. In the case of OH the estimated spectral intensity is probably reliable. In the case of CH, CN, NH and NO the estimated saturation intensities may or may not be too high depending on the correctness of assumptions made concerning the relevant quenching rates. For these latter molecules, it is desirable to make laboratory measurements in order to determine the saturation laser intensities. (3) Laser modulated particulate incandescence is the principal background noise source. (4) The lower limits of detection sensitivity are determined by laser modulated particulate incandescence for practical flames and by photon considerations in clean flames. (5) Calibration of the fluorescence apparatus is best done by measurement of spontaneous Raman scattering from N_2 in air. (6) By proper choice of excitation level, it appears possible to employ an average temperature to avoid simultaneous temperature measurements and which might make averaging possible. (7) If saturation is achieved, detection limits are typically in the tens of ppm for the molecules considered in practical flames.

Practical implementation and systems considerations are discussed in a subsequent section.

CN FRACTIONAL POPULATION VARIATION WITH TEMPERATURE

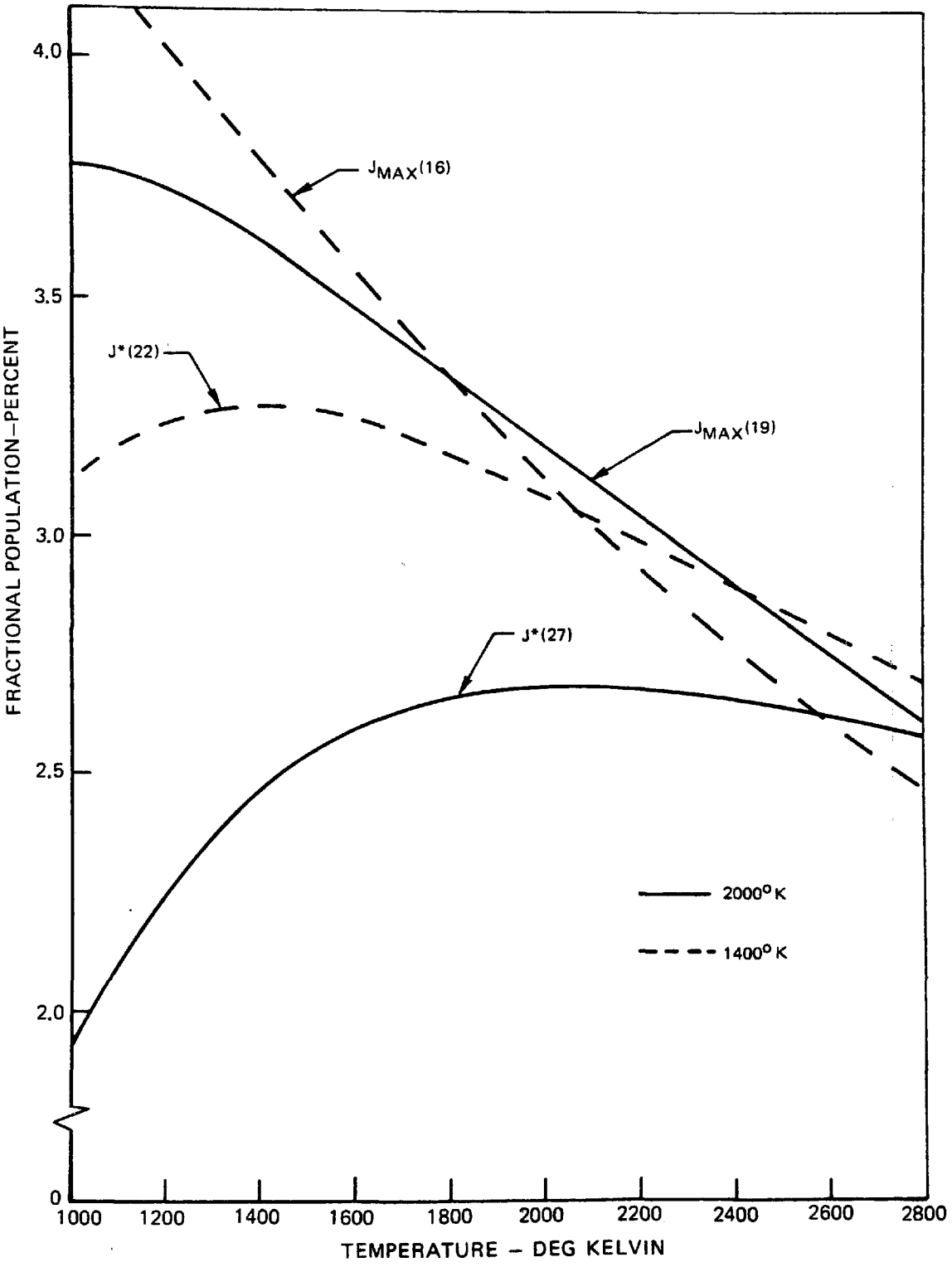

COHERENT ANTI-STOKES RAMAN SCATTERING (CARS)

Introduction

CARS techniques have recently come to prominance for combustion diagnostics based upon the investigations of Taran and his coworkers (Refs. 19, 157-160) at ONERA in France. The effect was originally discovered in the early sixties by Maker and Terhune (Ref. 161) and essentially remained in the province of nonlinear optics investigations until Taran's application of it for gas phase diagnostics. In the United States, Harvey and his coworkers (Refs. 162-165) have conducted numerous investigations into the technique. Barrett has demonstrated both CW CARS generation (Ref. 45) and pure rotational CARS (Ref. 166). Broadband CARS generation in a single pulse has also been obtained (Ref. 167). Publications describing investigations into the technique are appearing at an ever increasing rate and the technique apparently will have a major impact in molecular structure and biological studies. The technique has also been described as four wave mixing or three wave mixing, but use of the acronym CARS seems to be gaining broad acceptance.

Review

CARS is probably best understood by reference to Fig. 22 The explanations outlined in Refs. 160 and 162 will be followed. Incident pump photons at frequency ω_1 interact with photons at ω_2 (often termed the Stokes beam) through the third order nonlinear susceptibility $\chi^{(3)}(-\omega_3, \omega_1, \omega_1 - \omega_2)$ to generate a polarization component which produces radiation at the anti-Stokes frequency $\omega_3 = 2\omega_1 - \omega_2$. Note that the CARS signal is in a spectral region largely free of fluorescent interferences, i.e., anti-Stokes region. When the frequency difference $\omega_1 - \omega_2$ is close to the vibrational frequency of a Raman active resonance, the magnitude of the signal generated becomes very large as will be seen. Because of the requirement to conserve linear momentum, the anti-Stokes signal emerges as a diffraction-limited beam at an angle, θ', as shown in Fig. 22 . Consequently all of the CARS radiation can be collected. Contrast this with the situation pertaining in the normal Raman process where photons are scattered over 4π sr and are collected only over a limited solid angle, Ω. Furthermore, since CARS can be collected in an extremely small solid angle, discrimination against background luminosity and laser induced particulate effects is greatly facilitated. In actuality, the pump (ω_1) and Stokes (ω_2) beams need not be precisely aligned as shown in Fig. 22 since a certain amount of phase mismatch is tolerable, namely,

$$|\Delta k|\ \ell_c = \pi \tag{51}$$

where $|\Delta k|$ is the magnitude of the vector

$$\vec{\Delta k} = \vec{2k_1} - \vec{k_2} - \vec{k_3} \tag{52}$$

COHERENT ANTI–STOKES RAMAN SCATTERING (CARS)

(a) ENERGY LEVEL DIAGRAM

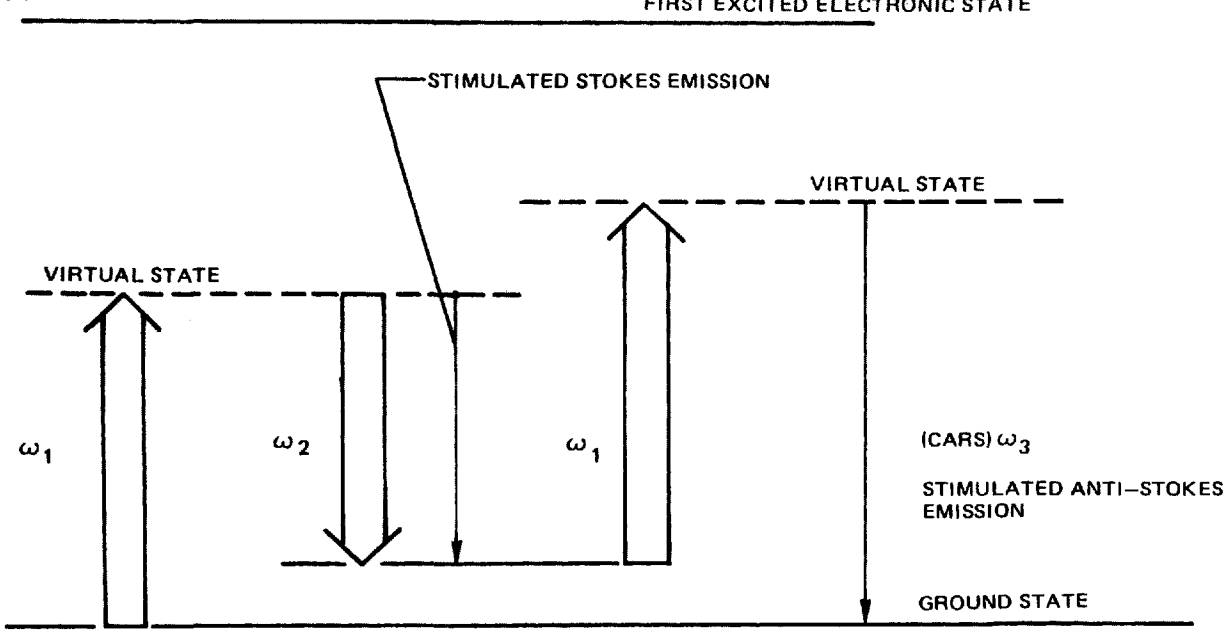

(b) PHASE–MATCHING DIAGRAM

$$2\omega_1 - \omega_2 = \omega_3$$

$$\vec{2k_1} = \vec{k_2} + \vec{k_3}$$

$$|\vec{k}| = \frac{\omega n}{c}$$

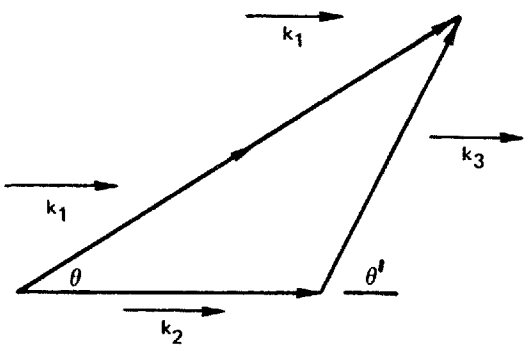

REF: BEGLEY, ET AL, APPL. . HYS. LETT., 25, 387 (1974)

FIG. 22

where $\bar{k}$ is the wave vector, $2\pi/\lambda$ and ℓ_c is the coherence length between ω_1 and ω_2. ℓ_c depends on the frequencies and the dispersion of the medium. For most gases in the visible the coherence length is on the order of tens of centimeters (Ref. 159) permitting colinear alignment of the pump and Stokes beams, while still satisfying the phase matching requirements.

The CARS intensity I_3 at ω_3 is expressible as

$$I_3 = \left(\frac{4\pi^2\omega_3}{c^2}\right)^2 I_1^2 I_2 |\chi|^2 z^2 \tag{53}$$

where I_i is the intensity at frequency ω_i; χ, the third order nonlinear susceptibility, and z, the distance over which the phase matched interaction occurs. The susceptibility can be written in terms of a resonant and nonresonant part, χ^{nr},

$$\chi = \chi' + i\,\chi'' + \chi^{nr} \ . \tag{54}$$

χ^{nr} is the contribution from electrons and remote resonances. The resonant susceptibility associated with a homogeneously broadened Raman transition, j, is

$$\chi' + i\,\chi'' = \frac{2c^4}{\hbar\omega_2^4} N \Delta_j g_j \left(\frac{\partial\sigma}{\partial\Omega}\right)_j \frac{\omega_j}{\omega_j^2 - (\omega_1-\omega_2)^2 - i\Gamma_j(\omega_1-\omega_2)} \tag{55}$$

where $\hbar$ is Planck's constant divided by 2π; N, the total species number density; Δ_j, the population difference between the levels involved in the transition; g_j, strength factor and equal to $(v_j + 1)$ for a Q line; $(\partial\sigma/\partial\Omega)_j$, the Raman cross section for the transition characterized by frequency ω_j; and, Γ_j, the Raman linewidth. From Eqs. (53) and (55), one can discern why CARS signals are so strong relative to spontaneous Raman scattering. CARS is an intensity dependent effect (in fact, third order in intensity), whereas spontaneous Raman scattering is not intensity but only power dependent. CARS varies as the square in number density, Raman only linearly. CARS varies as the square of the interaction length, Raman only linearly.

It is quite common in the CARS literature in the case of gases to replace Eq. (53) which is in terms of intensities, with an expression in terms of powers for colinear diffraction limited beams, namely

$$P_3 \approx \left(\frac{\omega_1}{\pi c}\right)^2 \left(\frac{4\pi^2\omega_3}{c^2}\right)^2 P_1^2 P_2 |\chi|^2 \tag{56}$$

Here the interaction occurs in a beam diameter, ϕ, and length, ℓ, of

$$\phi = \frac{4\lambda f}{\pi D} \qquad\qquad \ell = \frac{\pi\phi^2}{2\lambda} \tag{57}$$

where f is the focussing lens focal length; D, the beam diameter at the lens; and λ, the pump laser wavelength. The foregoing correspond to a diffraction angle, $4/\pi\,(\lambda/D)$ of 0.07 milliradians at 5320 Å and D = 1 cm. In actuality, most pulsed solid state lasers used for gas phase CARS work are not diffraction limited, but possess divergence angles on the order of 1 milliradian. Due to the cubic dependence on intensity of the CARS signal, the CARS signal generated for a given focal length lens will vary inversely as the sixth power of the divergence angle. In the example above this could lead to an overestimation of the CARS signal intensity by a factor of nearly seven orders of magnitude. Furthermore, with colinear beams the region over which the CARS is generated may exceed the desired spatial resolution. For example, in Table XXI below, the diffraction limited geometric parameters are displayed for varying focal length lenses.

TABLE XXI

CARS PROBE VOLUME

Focal length (cm)	Diameter (cm)	Length (cm)
10	6.11 (-4)	1.22 (-2)
100	6.11 (-3)	1.22
1000	6.11 (-2)	122

As can be seen with a one meter focal length lens which may be necessary in some measurement situations, the resolution would be about 1.2 cm and may exceed the resolution desired. In the signal estimates to be made here, the intensity formulations will be employed to show explicitly the spatial resolution and focal lengths employed.

CARS Signal Strength and S/N Calculations

Signal Magnitudes

If the detuning frequency, $\Delta\omega_j = \omega_j - (\omega_1 - \omega_2)$ is introduced, the resonant susceptability may be expressed as

$$\chi = K_j \frac{\Gamma_j}{2\Delta\omega_j - i\Gamma_j} \tag{58}$$

where

$$K_j = \frac{2c^4}{\hbar\omega_2^4} N \Delta_j g_j \left(\frac{\partial\sigma}{\partial\Omega}\right)_j \frac{1}{\Gamma_j} \tag{59}$$

On resonance $\Delta\omega_j = 0$, and $|\chi| = K_j$. Assuming the CARS beam to have the same cross sectional area as the Stokes beam, the CARS power is

$$P_3 = \left(\frac{4\pi^2\omega_3}{c^2}\right)^2 I_1^2 P_2 K_j^2 z^2 \qquad (60)$$

Consider an atmospheric pressure flame at 2000°K. For N_2, the rotational distribution peaks at J = 18 and Δ_j can be shown to be 0.029. Since the line strengths of the individual Q branch lines have only a weak dependence on J (i.e., most of the scattering arises from the trace of the polarizibility tensor, Ref. 9), the cross section for Q (18) is assumed to be the unresolved Q branch cross section. Assuming ω_1 to be generated by a frequency doubled neodymium laser at 5320 Å and assumed $\Gamma_j/2\pi c = 0.1$ cm^{-1} for the v = 0, J = 18 to v = 1, J = 18 transition (Ref. 160), K_j can be shown to be 2.48 (10^{-10}) cm^3/J. The doubled neodymium laser will be assumed to have a pulse energy of 0.1 J in 10 nanoseconds and a 1 milliradian beam divergence. For a 50 cm focal length lens, the pump intensity would be about 5(10^9) Watts/cm^2. For a 1 cm interaction length, one finds $P_3/P_2 \approx 5$ (10^{-8}) whereas Raman "efficiencies" are typically 10^{-14}. This represents "the orders of magnitude improvement in conversion efficiency" often ascribed to CARS. Assuming the Stokes beam to be 0.001 Joule in 10 nanoseconds at 6073 Å, the generated CARS power at ω_3 (4733 Å) is calculated to be 5 (10^{-3}) Watts for a 1 cm interaction length (spatial resolution). In 10 nanoseconds, this CARS power corresponds to about 10^8 photons. Note that this is the power generated from just a single line, i.e., Q(18) in the vibrational-rotational manifold.

For this calculation, N_2 was assumed to constitute 70 percent of the combustion mixture. At a density of 1000 ppm the generated signal would drop to 10^{-8} Watts or 240 photons, at 100 ppm to 10^{-10} Watts or 2 photons. At lower gas temperatures, the CARS signal would increase due to increases in gas number density and Δ_j, the latter arising due to a contraction in the rotational population distribution. As will be seen subsequently, however, minority species measurements involve much more than just photon yield considerations.

Signal to Noise Ratio

Using these power levels, S/N ratios can be estimated for both background luminosity and laser modulated particulate incandescence. As before, the latter is a more severe problem. The optical collection system will be assumed to possess an angular acceptance of 5(10^{-3}) radian (F = 200) corresponding to a solid angle of 2(10^{-5}) sr. The optical bandwidth will be assumed to be 1 Å. Assuming an aperture diameter of 0.05 cm (corresponding to the focal laser beam diameter) and coaxial collection (Fig. 4) the background luminosity collected is only 2.3 (10^{-13}) Watts, far below the CARS signal level, at even 100 ppm. For laser modulated incandescence the previously used dispersion of 400 Å dia, 10^8 cm^{-3} will be assumed to be heated

to a temperature of 6000°K over a 20 cm extent. Actually, due to the gradient in focal flux along the laser beams, the particles will not all reach 6000°K. The 20 cm extent corresponds to 2FA (Fig. 4) for an aperture of 0.05 cm and F = 200. For the $2(10^{-5})$ sr viewing solid angle, and a 1 Å bandwidth, the collected laser modulated incandescence is calculated to be $1.54\ (10^{-11})$ Watts, nearly an order of magnitude below the 100 ppm signal level. For an order of magnitude increase in number density, corresponding to the highest luminosity displayed in Fig. 3, the laser modulated incandescence would be comparable to the 100 ppm signal level for the conditions assumed. It appears then that both background luminosity and laser modulated soot incandescence should not pose serious noise problems for carefully designed CARS diagnostics.

Population Perturbations

Taran (Ref. 160) describes two potential perturbations in CARS diagnostics. The first is stimulated Raman gain wherein, because of too high an intensity at ω_1, the Stokes wave at ω_2 experiences gain and P_2 is no longer the initial power introduced. This effect is generally weak as the previous examination of stimulated Raman scattering demonstrated. The second effect involves a perturbation in Δ_j expressible as

$$\tau_\Delta^{-1} = \frac{1}{\Delta_j}\ \frac{\partial \Delta_j}{\partial t} = 2\left(\frac{4\pi c}{\hbar\omega_2^2}\right)^2 g_j \left(\frac{\partial\sigma}{\partial\Omega}\right)_j \frac{I_1 I_2}{\Gamma_j} \tag{61}$$

on line center. Clearly, since $\Delta_j(t) = \Delta_j(0)\ \exp\ (-t/\tau_\Delta)$, for the population distributions to be unperturbed, $\tau_\Delta \gg \tau_\ell$, where τ_ℓ is the laser pulse duration. Evaluating Eq. (61) for the previously assumed parameters in the signal strength calculations, i.e., $I_1 I_2 = 2.6(10^{17})\ W^2/cm^4$, τ_Δ is found to 750 (10^{-9}) sec, much larger than the laser pulse duration of 10 (10^{-9}) sec so that no perturbation occurs. For laser and Stokes focal flux products of $2(10^{18})\ W^2/cm^4$, a 10 percent population change will occur. Consequently the product of the laser and Stokes beam intensities should not exceed this value.

Medium Property Measurements

In this section some of the problems and limitations of the CARS technique will be examined. These will include interference effects which complicate the CARS spectrum and nonresonant contributions which limit species detection sensitivity.

Interferences

From Eq. (54) and noting that $P_3 \sim |\chi|^2$, the square of the absolute value of the susceptibility is given by

$$|\chi|^2 = \chi'^2 + 2\chi'\chi^{nr} + \chi^{nr2} + \chi''^2 \qquad (62)$$

χ' and χ'' have a functional dependence on the detuning frequency, $\Delta\omega = \omega_j - (\omega_1-\omega_2)$, similar to the real and imaginary parts of the refractive index about resonance as illustrated in Fig. 23. χ'' exhibits line shape behavior and χ' derivative behavior, i.e., χ' is positive or negative depending on the sign of $\Delta\omega$. In the absence of the nonresonant background, χ^{nr}, $|\chi|^2$ is equal to $\chi'^2 + \chi''^2$ and the CARS spectrum exhibits line shape behavior as the detuning is scanned through the resonance. However, in the presence of nonresonant background, the CARS spectrum will exhibit "anti-resonance" behavior when the $2\chi'\chi^{nr}$ term is negative. Far from resonance the CARS signal will be proportional to χ^{nr2}. As resonance is approached the signal will fall below this value as illustrated in Fig. 23 and then exceed this level when χ' becomes positive.

In the presence of multiple resonances, for example when probing a vibrational-rotational distribution with small rotational spacing, the susceptibility must be written as, recasting Eq. (58),

$$\chi = \sum_j K_j \frac{\Gamma_j}{2\Delta\omega_j - \Gamma_j} + \chi^{nr} \qquad (63)$$

Consider the case of two adjacent resonances, 1 and 2, when one is tuned to the first resonance, then $\chi_1' = 0$ and

$$|\chi|^2 = \chi_2'^2 + 2\chi'_2\chi^{nr} + \chi^{nr2} + \chi_1''^2 + 2\chi_1''\chi_2'' + \chi_2''^2 \qquad (64)$$

Hence, on line center of the first resonance, in addition to $\chi_1''^2 + \chi^{nr2}$ which would constitute the signal from a single resonance, there are additional "contributions" to the signal from the nearby resonance. The term $2\chi_2'\chi^{nr}$ may be a positive or negative contribution depending on the relative orientation of the two resonances. Thus unlike the Raman spectrum which, for the most part, mirrors the distribution of state populations, the CARS spectrum is much more complicated as evidenced by the distributions displayed in Ref. 160.

Thermometry

Temperature measurements have been performed from CARS measurements of flame N_2 by Taran (Ref. 160) from the rotational distribution of the Q branch under high resolution, and from the ratio of the CARS peaks from the ground and first vibrational states. The first technique gives greater accuracy, since, for high J values, there is little line overlap, the resonant susceptability is much larger than the nonresonant contributions and interference effects are small. This permits a straightforward temperature determination from the rotational population distribution. The second

CARS SPECTRA

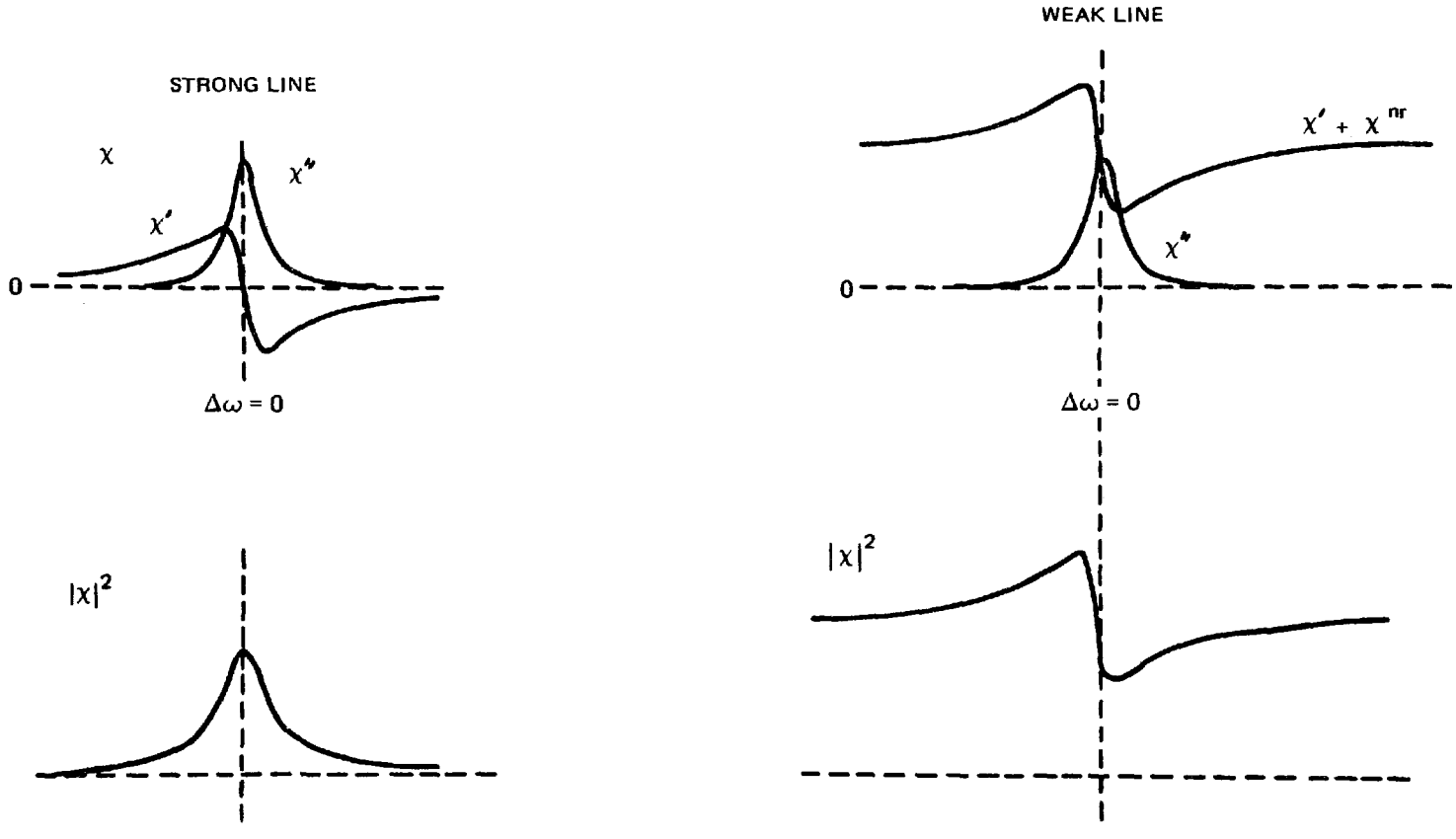

FIG. 23

technique is less accurate since, at high temperature, the high J valued Q branches from the ground vibrational state interfere with the first vibrational state signal.

Because of the complex nature of the CARS process, signal averaging in temporally fluctuating media will certainly obscure interpretation of the CARS spectrum leading to temperature measurement errors. In such cases, measurements will have to be performed with each laser pulse. This can be done with a device such as a multichannel spectrum analyzer (Ref. 168) or a pair of interference filters appropriately placed. In the case of the spectrum analyzer, considerable improvement in the state-of-the-art will be required before high resolution spectra can be captured accurately from a molecule such as N_2. To date the technique has been demonstrated only in CH_4 and H_2 (Ref. 167), where in the latter case, due to the very large rotational constant, i.e., $B_o \approx 60$ cm^{-1}, the CARS Q branch is well dispersed. The use of interference filters will require an elaborate CARS computer program with accurate linewidth, filter function, etc., input; this remains to be experimentally demonstrated.

Despite these spectral complications, CARS appears to be the best approach for thermometry in practical combustion devices. With moderately powerful, pulsed laser sources, collected CARS signal strengths significantly greater than background luminosity and laser modulated soot incandescence can be generated. However, interference free CARS generation has yet to be demonstrated in sooting flames. Of possible jeopardy in this regard are potential, nonlinear particulate interactions which shall be discussed later.

Species Concentration Measurements

For simplicity consider the case of a single resonance belonging to the species of interest immersed in a background diluent, e.g., N_2 in air fed combustors. Then Eq. (64) applies and on resonance may be written as

$$|\chi|^2 = N_S^2 \hat{\chi}_S''^2 + N_b^2 \hat{\chi}_b^{nr2} \tag{65}$$

where N_S is the species density of interest; N_b, the diluent or majority species density; and the caret notation on the susceptibilities indicates the per molecule susceptibility. From Eq. (65) it is clear that when the background contribution begins to dominate the susceptibility, species detection and measurement will be precluded. The nonresonant third order susceptibility has been measured for a number of gases (Ref. 169) and for atmospheric pressure N_2 is 1.35 (10^{-11}) cm^3/J. Recall that the previously calculated resonant susceptibility for the Q(18) line of N_2 at 2000°K was 2.48(10^{-10}) cm^3/J. On a per molecule basis one finds $\hat{\chi}_b^{nr} \approx 5(10^{-31})$ cm^6/J and $\hat{\chi}_S'' \approx 8.8(10^{-29})$ cm^6/J. Assuming the resonant susceptibility calculated for N_2 to be representative of any diatomic minority species, Eq. (55), the minority species resonant and nitrogen background nonresonant contributions are equivalent for a

minority species concentration of about 6000 ppm assuming N_2 to constitute the background. Actually, the foregoing illustration is greatly oversimplified and among other things neglects other Q line contributions to the total signal. Also for weak lines in a strong background, the CARS signal does not maximize at resonance; the CARS peak is actually shifted off resonance. For weak lines, the CARS spectrum resembles the real part of the resonant susceptibility as it in effect "modulates" the nonresonant background (Fig. 23). Nevertheless, the foregoing approach illustrates the fundamental limitation on minority species detectivity in the presence of other gases using CARS techniques. Namely, for very low minority species concentrations, the resonant susceptibility contribution from the species of interest (i.e., the signal) is masked by the nonresonant contribution of the background gases.

Without going into the details of the derivation, a more rigorous approach (Ref. 160) yields the minimum detectable species density as

$$N \geq |\chi^{nr}| \frac{\hbar \omega_2^4 \Gamma_j}{2c^4 \Delta_j g_j \left(\frac{\partial \sigma}{\partial \Omega}\right)_j} \frac{\alpha}{2\sqrt{n}} \qquad (66)$$

where α is the peak to peak fluctuation in the relative CARS signal magnitude, and n, the number of pulses averaged over. Using Eq. (66), a detailed calculation was performed for the case of CO detection. For a typical α of 0.3 (Ref. 160) and a single shot (i.e., n = 1) the minimum detectable CO concentration in a 2000°K flame was calculated to be 944 ppm. With the exception of light molecules such as H_2, typical minimum detectivities for heavier molecules using CARS are generally about 1000 ppm. As Taran points out, these must be considered order of magnitude estimates. For H_2 where the large rotational spacing leads to large values for Δ_j, and due to the narrow linewidths, detectivities to 10 ppm appear possible. Experimentally, Taran was able to detect H_2 in N_2 to about 100 ppm (Ref. 159). However, for most molecules of interest in combustion situations, CARS species detectability limits appear to be on the order of 1000 ppm. However, several variations of conventional CARS have been proposed to reduce or eliminate these background interferences and will be examined briefly in the next section.

CARS Variants

Variations of the CARS technique previously described have been proposed in an attempt to eliminate or suppress the nonresonant contributions of background gases. Most of the techniques to be outlined have only been demonstrated in liquids. Their application for combustion diagnostics has to be considered speculative at this point until such time that they are successfully demonstrated. Furthermore, they generally represent additional sophistication and, hence, additional complexity to an already complex technique.

Resonance Enhancement

The third order susceptibility has the form (Ref. 162)

$$\chi^3 \sim (\omega_1-\omega_a)(\omega_1-\omega_2-\omega_j + i\Gamma_j)(2\omega_1-\omega_2-\omega_b)^{-1} \qquad (67)$$

where ω_a and ω_b are electronic transition frequencies. Note that $\chi^{(3)}$ displays resonant enhancement as the input laser pump frequency, ω_1, or the anti-Stokes frequency, $\omega_3 = 2\omega_1-\omega_2$, approaches an electronic transition in the same manner that spontaneous Raman scattering shows near-resonant enhancement. By analogy with near-resonant Raman scattering, detectivities in the ppm range are anticipated (Ref. 170) but yet to be demonstrated. Besides the obvious difficulty of tuning to an electronic resonance (if accessible) there are fundamental questions as to whether the nonresonant background may not also be enhanced. Certainly the cross terms between the real part of the resonant susceptibility and nonresonant background will be enhanced.

Double Resonance CARS

In this approach demonstrated in liquids (Refs. 171 and 172) three beams at ω_0, ω_1 and ω_2 are introduced into the medium under observation. ω_1 and ω_2 are tuned as in the usual CARS arrangement to the resonance of interest. ω_0 is tuned in such a way that $\omega_0-\omega_2$ approaches a resonance from another constituent. For example, in a combustion application one might tune near N_2. Writing the susceptibility as $\chi = \chi_1 + \chi_2 + \chi^{nr}$ where the subscript 1 refers to the resonance being probed and 2 to the resonance being exploited, the square of the absolute value of the susceptibility is

$$|\chi|^2 = \chi_1'^2 + 2\chi_1'\chi_2' + 2\chi_1'\chi^{nr} + \chi_2'^2 + 2\chi_2'\chi^{nr} + \chi^{nr2} + 2\chi_1''\chi_2'' + \chi_2''^2 \qquad (68)$$

If $\omega_0-\omega_2$ are tuned in such a way that $\chi_2' < 0$, then cross terms such as $2\chi_2'\chi^{nr}$ and potentially $2\chi_1'\chi_2'$ can be used to cancel out the nonresonant contributions and contributions from the exploited resonances.

Using such a technique, the resonance curve of cyclohexane in a benzene background was enhanced nearly an order of magnitude above the background (Ref. 171). Such a technique, then, might result in an order of magnitude improvement in species sensitivity.

Polarization Techniques

Nibler, et al., (Ref. 173), demonstrated that the normal CARS spectrum could be altered significantly if the polarizations of the laser and Stokes beams are aligned or orthogonal. In Ref. 174, Song, et al., have shown that in a four color

CARS experiment that background contributions can be eliminated resulting in undistorted line shapes. This approach is similar to double resonance in that three beams are employed, ω_0, ω_1, and ω_2, but only ω_1-ω_2 need be tuned to the resonance under investigation. In a polarization orientation approach termed "asterisk", because the properly aligned polarization directions resemble a star, no detectable background was found for detection of 3 percent benzene in carbon disulfide. For conventional CARS, orthogonally oriented laser and Stokes beams are preferable with the CARS viewed parallel to the laser beam. However, this technique does not suppress background to the extent "asterisk" does.

Background Subtraction

Background subtraction techniques have been investigated using reference nonresonant samples (Ref. 175) but the noise reductions were more modest (factor of three) than expected. One could consider doing in-situ background subtraction using a three beam approach where ω_0-ω_2 is not tuned to a second resonance. Such an approach however cannot eliminate interference effects between the resonant and nonresonant susceptibilities, but might improve species detectivity accuracy depending on the photon levels involved. The subtraction accuracy or signal/noise improvement would be comparable to that calculated in Fig. 13. As before, subtraction accuracy on a single pulse is limited by photomultiplier tube shot noise effects.

Preferred Variant

Of all of the foregoing approaches, the polarization techniques appear most promising for near term investigations in terms of simplicity and potential benefit. These approaches have not been demonstrated as yet in gases and one can only conjecture as to what the improvement in species detectivity might be. One to two orders of magnitude may be possible, potentially permitting CARS species measurements in the 10 to 100 ppm range. Also of potential importance is the elimination of the anti-resonance effects leading to "clean" spectra which would facilitate simpler and more straightforward data reduction approaches, particularly, in regards to thermometry.

Practical Applicability

Based upon the preceeding considerations, CARS appears to possess high potential for successful application to practical combustion device probing. The calculated signal levels appear to be well in excess of the collected noise levels, such as background luminosity and laser modulated soot incandescence. These signal levels were produced by laser and Stokes intensities well below population perturbation, gas breakdown and stimulated Raman scattering thresholds. Potential jeopardies include phase mismatching induced by turbulence and nonlinear interferences generated

by interactions with particulates. The former effect is not anticipated to be serious in general. This conclusion is based upon the fact that LDV is performed rather routinely in modest sized turbulent combustors, and from the interference fringe examinations by Farmer in the EPA Rainbow furnace (Ref. 74). At worst, occasional interruptions in the CARS data rate might be anticipated. Analogous to the nonresonant majority species background interferences, nonresonant CARS generation from the soot particulates and the soot vaporization products could be problematical. With the laser intensities used in CARS, it is clear from earlier discussions of laser-soot interactions, that significant soot vaporization will occur during the time of the pulse (Ref. 88). Due to the density squared scaling of the CARS signal, the high pressure soot vapor species may produce serious nonlinear, nonresonant interference. CARS techniques have yet to be demonstrated in sooting flames; this represents an area in which further investigation is required to address this potential problem. In general the jeopardies appear modest.

The probability of successful thermometry appears to be high although data reduction may be more complex relative to Raman processes. Species concentration measurements appear likely with good chance of success to about the 1000 ppm level. Potential improvements in detectibility appear possible using polarization approaches or double resonance with probability of success for measurements in the 10-100 ppm range assessed as fair. For low density flame work, high peak power laser sources are absolutely required. Pump laser selection narrows quickly to either ruby or frequency doubled neodymium. From a systems standpoint the latter, although generally more expensive, appears preferable. 2X Nd lasers can be operated at a repetition rate generally an order of magnitude higher than ruby, at least 10 pps versus 1 pps. If a portion of the pump laser is split off to pump the Stokes beam dye laser, 2X Nd lasers at 5320 Å can pump very efficient dyes in the 5500-6500 Å region, while ruby lasers must work on lower efficiency near ir dyes. Furthermore, the coherent anti-Stokes radiation from 2X Nd resides in regions of higher photomultiplier tube quantum efficiencies than do those generated by ruby. These systems aspects will be addressed in more detail in the section on systems considerations.

SYSTEMS CONSIDERATIONS

To this point, attention has been addressed, separately for the most part, to the various aspects of the in-situ, point, combustion diagmostics problem, i.e., species spectroscopy, potential sources of noise, and the physics/capabilities of the various approaches under review. In this section, preferred measurement approaches employing the various scattering techniques previously reviewed will be described. An assessment of systems costs and the probability of success will be attempted. Some of the material has already been discussed in previous sections; it will be briefly summarized here for completeness as required. Areas of additional research/development to improve device performance and address technical uncertainties will also be described. Possible systems integration of the various techniques will also be discussed.

Raman Scattering

Spontaneous Raman

From a systems standpoint, spontaneous Raman scattering is the most attractive diagnostic technique for multiple species and temperature determinations since only a single, nonspecific wavelength laser is required. Data on a variety of molecular species of interest can be obtained simultaneously without the requirement to tune to a resonance as required in near-resonant Raman, CARS and laser fluorescence. Unfortunately, because of its inherent weakness, it is the technique least likely to succeed in most practical combustion systems. As previously discussed, for minority species measurements in practical combustors, its probability for success is perceived to be very poor. For majority species measurements and for thermometry, the probability of successful application ranges from fair to poor depending on the hostility of the particular combustor and combustion zone being probed. Therefore, in examining the systems aspects of spontaneous Raman scattering, attention will be directed toward major constituent measurements.

In Fig. 24, a laser Raman system for combustion diagnostics is displayed. Two possible optical routings of the laser beam are shown. In the scheme emphasized, coaxial scattering is shown. This has the advantage of permitting radial traverses at a given axial location in the combustor simply by translating the focusing lens, FL and collecting lens, CL in tandem. In the alternate routing, namely right angle viewing, measurements would typically be constrained to the center line regions without elaborate modification of the combustor housing. In coaxial viewing a port opposite the viewing window would be required for a suitable beam trap. Also the inlet window would have to be of a compound design to prevent collection of window fluorescence. By obscuring the central part of the collecting lens with a disk, O,

SPONTANEOUS RAMAN SCATTERING COMBUSTION DIAGNOSTIC SYSTEM

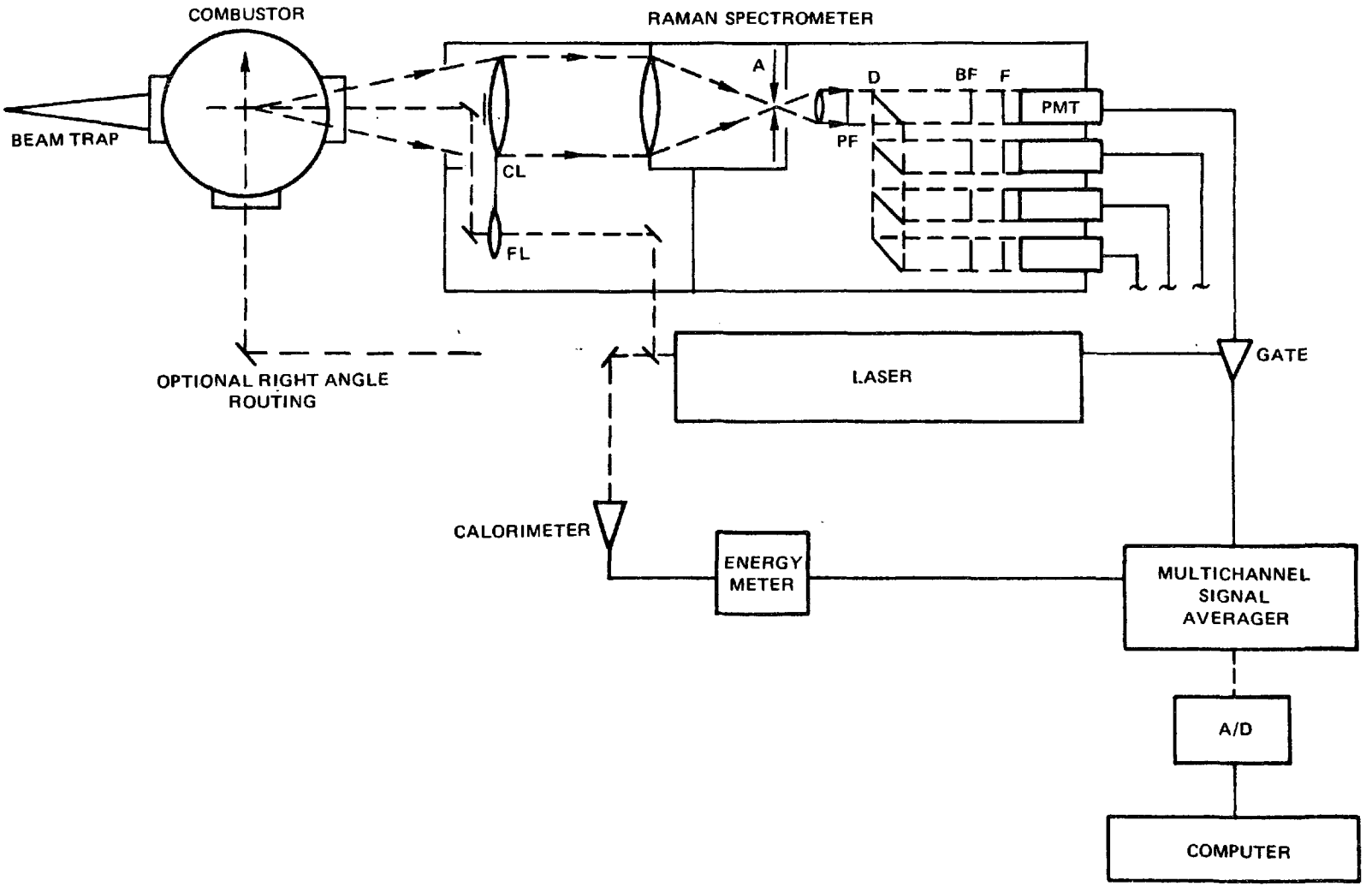

spatial resolution can be considerably enhanced as described in Ref. 176. The collected scattering is focused through the aperture A and recollimated. It passes through an optional polarization filter and is spectrally separated by a series of dichroic's D and passed through a series of blocking and narrow-band interference filters which isolate selected portions of the Raman spectrum. In Fig. 24, only four channels are displayed for simplicity, more or less could be present as desired. At least two channels would be employed for thermometry, ratioing the anti-Stokes to Stokes intensity bands from nitrogen, a commonly used technique (Refs. 112, 113, 119). Four channels may be used for thermometry if noise sampling and subtraction are necessary. Other channels would monitor Stokes bands from molecules whose number density is desired. Preferably, the filter bandpasses are made broad enough so that there is no bandwidth factor variation with temperature. If not, temperature corrections to the Raman density data would be required. Broad bandpasses lead, of course, to much lower S/N ratios. If the laser pulse energy stability is poor, the laser energy would be monitored on each pulse and used as a normalization factor for the density measurements. For thermometry, where band ratios are employed, this would not be necessary since the pulse energy divides out in forming the ratio. Calibration for thermometry is performed using a tungsten filament lamp whose temperature is known (standard source) or measured. Calibration for density measurements of N_2 or O_2 could be performed in room air. For gases such as CO_2 or CO, calibration would be performed from sample cells containing the gases at known pressure.

For an end use measurement system, a monochromator offers no advantage, since only a single constituent could be examined at a time. Although other constituents could be probed sequentially, this approach is rather inefficient since much information is lost (i.e., those spectral regions not being examined) with each pulse. A spectrograph could be employed together with a multichannel spectral analyzer, such as that used in Refs. 168, 177 or commercially available Ref. 178. Such an approach would be considerably more expensive than the use of multilayer dielectric filters and does not appear to possess any particular advantage.

Signal processing can range over an extended spectrum of cost and sophistication depending on the degree of automation and speed of data reduction required. Little or no information is gained by following the Raman scattering on a fast time scale (tens of nanoseconds or less) since this is considerably faster than the characteristic time for small scale turbulent fluctuations. Furthermore, real time photon statistics may preclude such dynamic measurements even if desired. Thus, the Raman scattering can be integrated in time using gated detection techniques and fed to an appropriate multichannel signal averager. For measurements employing just a few channels, commercially available boxcar averagers may be used. From there the averaged data can be received and reduced, or digitized and computer processed. Recall that signal averaging may not be tolerable in fluctuating media depending on the magnitude of the fluctuations and the parameter range of interest (Appendix II). Density measurements can be designed to avoid such averaging errors as discussed earlier, but problems may be encountered in thermometry.

The jeopardies to successful implementation of spontaneous Raman scattering reside primarily, as discussed extensively earlier, in laser induced or naturally occurring background noise in practical combustors. With the exception of a few details, the physics of spontaneous Raman scattering is well understood. Present, and for the most part commercially available, laser sources and instrumentation are completely adequate for Raman diagnostics of clean flames. For practical diagnostics, high peak power, solid state laser sources will be required, based upon the previously performed S/N calculations. These lasers, depending on specific types, are fairly expensive, ranging in price from $20K to $60K for several joule ruby lasers and several tenths Joule frequency doubled neodymium lasers, (depending on the mode quality and repetition rate desired, (Ref. 179)) to $140K for custom high energy (1.2 Joules) frequency doubled neodymium (Ref. 130). The Raman spectrometer may range in price depending on the number of channels from about $5K for an interference filter type to $25K for a commercial 1-meter double or triple monochromator inclusive of many desired options. Averagers may run from $3K-$6K for a single or double channel boxcar to $10-$15K for multiple input averagers. Miscellaneous items might be on the order of $5-$10K for mirrors, lenses, mounts, doublers, etc. Small computers, if desired, would add perhaps $15-$20K in capital cost plus peripherals and engineering for the interfacing. Since such equipment is optional, already available or present in the form of even larger computational facilities in many laboratories, costs beyond the averager will not be included in assessments of total cost. Not including engineering, design, etc., a system may run from a low of $35K to a high of $190K depending on the speed and number of channels desired. Similar figures were arrived at in Ref. 2. Note that the laser system is the dominant cost item.

In Table XXII, the assessment of spontaneous Raman scattering for practical combustion diagnostics is summarised. Based upon the previous signal/noise calculations for a variety of high peak power, pulsed laser sources, the probability of successful temperature and major species concentration measurements varies from fair to poor depending on fuel type and combustor operating conditions. Minority concentration measurements are deemed highly unlikely under most circumstances. Based upon systems costs of $35K to $190K, the "risk" of spontaneous Raman scattering is, therefore, perceived to be high. Risk is subjectively assessed and combines systems costs and probability of success judgments.

Before deciding affirmatively on a spontaneous Raman approach for a given diagnostic application, the medium to be studied should be well assessed in regard to the estimated magnitude and spectral character of background radiations, presence of particulates, turbulence levels and ranges of operation. Some of the above can be measured fairly inexpensively, and others can be estimated by reference to similar environments. In this manner, one should be able then to assess a priori the feasibility of a given measurement.

TABLE XXII

COMBUSTION DIAGNOSTIC SYSTEMS ASSESSMENT

	Probability of Success				
Technique	Temperature	Major Species	Minority Species	System Costs	Perceived Risk
Spontaneous Raman	Fair-Poor	Fair-Poor	Very Poor	$35K-$190K	High
Near-Resonant Raman	Poor	Not Applicable	Poor	$90K-$190K	High
Laser Fluorescence	Questionable	Not Applicable	Good	$90K-$120K	Moderate
CARS	Good	Good	Fair-Poor	$80K-$120K	Low-Moderate

Near Resonant Raman

Unlike spontaneous Raman scattering, wavelength specific and narrow linewidth laser sources are required to perform near-resonant Raman scattering diagnostics. From a systems standpoint, the approach and equipment required is very similar to that needed for laser fluorescence. Consequently, systems considerations will be treated in the fluorescence section.

Here only the probability of successful application will be reiterated. For major species measurements and thermometry from major species, the likelihood of a measurement is very unlikely at the present time due to the unavailability of high energy laser sources at or below 2000Å. For measurement of trace constituents, the probability of success is very low due to the lack of high energy laser pulses at the desired wavelengths and linewidth, the near-resonant enhancement achievable, and the small fraction of molecules in the appropriate initial state. Should the laser source picture change with advances in existing or with the development of new laser sources, the situation would have to be reassessed.

Laser Fluorescence

A laser fluorescence combustion diagnostics system is schematically diagramed in Fig. 25. It is quite similar in regard to major components to the laser Raman system just described. Unlike the Raman scattering system, however, only a single molecular species can be probed at a time using a single laser source and detector. It would be possible to combine a multiplicity of laser beams of different wavelengths, which could probe various molecules simultaneously using a multichannel detection scheme. Such a system would be considerably more complex, however. A laser is employed to induce fluorescence from the molecule under study. The fluorescence is collected either coaxially or at right angles to the incident laser beam (not shown). As before, coaxial scattering is preferred since it readily permits radial traverses of the combustor/furnace. The collected fluorescence is focused upon the entrance slit of a double monochromator. Unless the fluorescence is well shifted in wavelength, i.e., a hundred Angstroms or more, it is unlikely that interference filters could be employed to discriminate against the strong Mie/Rayleigh scattering. Good double monochromators on the other hand can possess as much as fourteen orders of magnitude rejection within 20 cm^{-1} of the laser line (Ref. 180). The fluorescence power incident on the photomultiplier can simply be integrated through a gate driven by a fast detector which monitors the laser pulse duration. The integrated signal can be digitized via a dc to frequency converter and read out on a frequency counter or sent to a computer for storage and/or processing. The data can also be normalized by the laser pulse energy as required. Other data treatment schemes, e.g., boxcar averagers, may also be employed. Depending on the magnitude of the temporal fluctuations, however, signal averaging may or may not be tolerable as discussed earlier.

LASER FLUORESCENCE DIAGNOSTIC SYSTEM

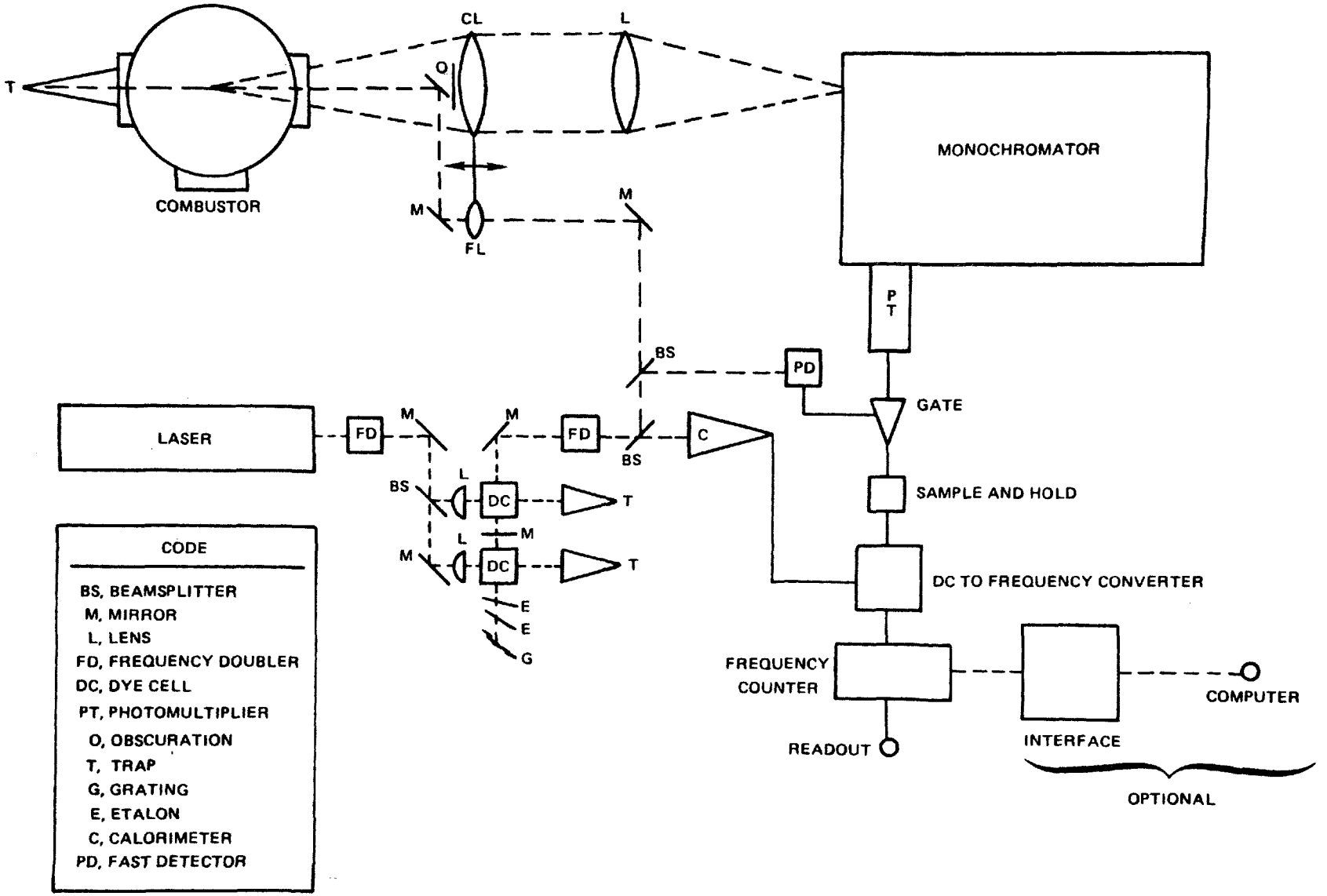

FIG. 25

The heart of a fluorescence diagnostic system resides in the laser source which must be tunable and have sufficient spectral intensity to saturate the molecular transitions of interest. For near-resonant Raman scattering which is always independent of quenching, the spectral power (i.e., power/bandwidth) is of prime importance. To obtain high spectral intensities, stringent requirements are then placed on pulse energy, duration, laser spectral width and beam quality. In this discussion, two general classes of dye lasers will be considered -- flashlamp-pumped and laser-pumped.

Flashlamp-pumped dye lasers (Ref. 181) generally deliver large pulse energies but suffer from relatively long pulse durations, typically several hundred nanoseconds. Good performance has been reported recently by Butcher and Sherman (Ref. 152) in regards to power and spectral condensation with a flashlamp-pumped dye laser followed by a flashlamp-pumped, two-pass amplifier. At a wavelength of 5400 Å and a 1 μsec pulse width, 0.5 joules pulse energy was obtained with a spectral width of 0.4Å (1.4 cm^{-1}). The beam divergence was 4 milliradians. Focusing the output into an ADP crystal led to a frequency doubling efficiency of 10 percent with a 50 millijoule output at 2700Å. For a 50 cm focal length lens, a spectral intensity of 1.2 (10^7) W/cm^2 cm^{-1} at 5400Å and 5.7 (10^5) W/cm^2 cm^{-1} at 2700Å is calculated. This performance in terms of spectral intensity exceeds that reported for two commercially available flashlamp-pumped systems (Refs. 182 and 183) by about an order of magnitude. The difference in spectral intensity is primarily attributable to lack of an amplifier in the commercial units. Based upon published laser dye energy scaling (Ref. 184), spectral intensities have been calculated at five other wavelengths corresponding to various absorptions of interest. These are summarized in Table XXIII. In those cases requiring frequency doubling, a 10 percent doubling efficiency was assumed, i.e., that achieved by Sherman and Butcher, and a factor of two included for the associated increase in freqeuncy bandwidth on doubling.

For laser-pumped dye lasers, three different laser source drivers will be considered, namely, pulsed nitrogen and various harmonics of ruby and neodymium. N_2-laser-pumped dye systems are characterized by pulse energies up to 1 millijoule at 4600Å for 10 mJ of pump energy in a pulse of approximately 5-7 (10^{-9}) sec duration (Ref. 185). Although this peak power of 1.4-2 (10^5) watts is comparable to flashlamp-pumped dye lasers, the N_2 laser pumped dye laser possesses a lower beam divergence angle, on the order of 1-1.5 milliradian and lower bandwidth, 0.6 cm^{-1}. This leads, of course, to higher spectral intensities, namely, 1.2 (10^8) watts/cm^2 cm^{-1} at 4600Å. Comparable performance is achieved at both 4315Å (CH) and 3883Å (CN). In Table XXIII, spectral intensities are also presented for N_2 laser-pumped dye lasers. The values listed correspond to what is commercially available, except for the NO value. In this case, the spectral intensity was achieved by use of two additional amplifier stages; a 2 percent frequency doubling efficiency was achieved (Ref. 186). The low spectral intensity values for wavelengths appropriate to NH and OH are due to low frequency-doubling efficiencies, typically between 1-4 percent.

Dye lasers can also be pumped with the second harmonic of ruby at 3472Å (Refs. 187, 188 and 189) or second harmonics of neodymium at 5320Å (Refs. 187 and 190). Pumping with the third harmonic of neodymium at 3546Å should also be possible. Conversion efficiencies are typically on the order of 15 to 20 percent. As in previous discussions, only neodymium lasers will be considered here because of their high pulse repetition rates. For the NH and OH wavelengths, the second harmonic would pump a dye laser which in turn would be frequency doubled. For CN and CH, the third harmonic would be used to pump a dye laser directly. For NO, the third harmonic pumped dye laser would be frequency doubled. A commercially available neodymium oscillator-amplifier system (Ref. 191) with 250 mJ at 5320Å and 70 mJ at 3546Å will be examined for illustrative purposes. For the molecules CH (4315Å) and CN (3883Å), pumping dye lasers with the third harmonic of neodymium at 3546Å should produce spectral intensities in excess of those produced by the 10 mJ N_2 laser at 3371Å, since the 3XNd has seven times the energy and peak power as the N_2 laser pump. Both systems have comparable beam quality and pulse duration. Hence, in Table XXIII, the spectral intensities are listed as > 1.2 (10^8) W/cm^2 cm^{-1}. For NH (3360) and OH (3064) the spectral intensities were calculated as follows. The 2XNd laser with 0.25 J and pulse duration of 10^{-8} sec was assumed to pump a dye laser in the 6000Å to 6600Å range with an efficiency of 15 percent. The dye laser was assumed spectrally condensed to 0.1Å (0.3 cm^{-1}) via intracavity dispersive elements (e.g., prisms, etalons) with 10 percent efficiency. The output was then frequency doubled using ADP or KDP crystals with 15 percent conversion to the second harmonic (Ref. 186). The NO spectral intensity value at 2270 was assumed achieved by frequency doubling via potassium pentaborate (KPB) the third harmonic pumped dye laser with 1 percent doubling efficiency (Ref. 192).

TABLE XXIII

LASER SPECTRAL INTENSITIES (Watts/cm^2 cm^{-1})
50 cm focal length lens

Molecule	Absorption Wavelength (Å)	Flashlamp-Pumped Dye	N_2 Laser Dye	Nd Laser Dye	Required to Saturate
CH	4315	5.6 (6)	1.2 (8)	> 1.2 (8)	4 (7)
CN	3883	2.8 (6)	1.2 (8)	> 1.2 (8)	2 (7)
NH	3360	5.6 (5)*	6.0 (5)*	1.0 (8)*	1 (8)
OH	3064	1.0 (6)*	3.8 (6)*	1.0 (8)*	4 (6)
NO	2270	4.4 (5)*	1.0 (6)*	7.0 (6)*	4 (8)

*Frequency doubling of dye laser output required

For Table XXIII several conclusions are apparent. At the large focal distances required in a practical measurement system, none of the laser systems can provide a high enough spectral intensity to saturate NO. The neodymium laser system appears preferable since it is capable of probing CH, CN, NH and OH subject to the assumptions made in arriving at the spectral intensity estimates. These were reasonable but yet to be demonstrated concurrently in an integrated setup. The N_2 laser pumped dye system is capable of saturating only two of the molecules, the flashlamp-pumped dye laser, none, in a practical situation. In a laboratory situation where shorter focal length lenses would be tolerable, e.g., 10 cm, both flashlamped-pumped and N_2 laser pumped dye lasers could saturate all the molecules listed except NO. NO appears difficult to probe in any flame situation with presently available or reasonably assumed tunable laser systems. This comment applies, of course, to probing NO via saturated fluorescence only. NO laser-fluorescence has already been examined in a sample cell at room temperature (Ref. 34).

In terms of cost, the laser fluorescence system using a neodymium laser system would be as follows. The neodymium driver with second and third harmonic capability would be about $45K (Ref. 191). The dye laser setup including grating, etalons, prisms, etc. is estimated at $10K. Commercial laser pumped dye systems begin at about this price, but may run two to three times this depending on accessories, capabilities, etc. The double monochromator is about $25K. A simple detection scheme might be about $5K from photomultiplier to readout. With miscellaneous items totaling $5K, the system would run between $90K and $125K, providing that a single molecule is probed at a time.

The major jeopardy with laser fluorescence probing is the validity and applicability of two level saturated fluorescence approaches to eliminate the effects of quenching. If such approaches are correct as reviewed previously, the ability to saturate the transition in question becomes of paramount importance. The saturation spectral intensities calculated above are approximate and rely upon low temperature quenching data. Experimental efforts should be directed toward investigations of the magnitudes of saturation spectral intensities and the validity of the simplified analytical approaches. If correct, the possibility of fluorescence measurements of selected species at ppm levels in practical environments appears to be good. Temperature measurements by spectral scanning are probably precluded in turbulent environments from consideration of the effects of signal averaging. Major species, i.e., N_2, CO, CO_2, O_2, are not possible due to the inaccessibility of their respective absorptions. In view of the lack of experimental confirmation of these approaches and high costs, they are viewed as being moderate in risk. Clearly, these assessments should be regarded as being preliminary.

CARS

For CARS diagnostics, a minimum of two laser sources is required as seen earlier, namely, "pump" and "Stokes" laser beams. For double resonance and/or polarization orientation approaches which suppress background, three beams are required. Some investigators have used one laser source and generated the Stokes beam via stimulated Raman scattering (Ref. 19). This scheme is limited to probing stable species from which stimulated Raman is readily produced and is not very versatile. A more flexible and, hence preferable, scheme is to employ a laser, part of which is split off to drive a tunable dye laser. In some cases, the laser may pump two dye lasers to produce both the pump and Stokes beams or the Stokes and the additional beam required in the three beam approaches. For gas phase diagnostics, either ruby or frequency doubled neodymium, because of their very high peak powers, appear preferable to pulsed nitrogen lasers. From a systems standpoint 2x Nd appears a better choice than ruby since the pulse repetition rate is generally an order of magnitude greater, 10 pps vs 1 pps typically, and more efficient laser dyes can be used with the 2x Nd. 2x Nd may be preferable to 2x ruby since gas breakdown thresholds are likely to be higher at 5320Å than 3472Å, in addition to repetition rate considerations.

In Fig. 26, a schematic diagram of a CARS system for diagnostics is displayed. Although the discussion herein will be specific to neodymium lasers, the approach would be basically the same for other laser sources. The neodymium laser radiation at 1.06μ is frequency doubled to 5320Å, the pump beam, and passes through a dichroic. The undoubled 1.06μ is split off and doubled again and employed to pump a tunable dye oscillator-amplifier combination. The dye oscillator is broadly tuned with a grating (or interference filter) and can be spectrally condensed as desired with etalons. The output from the oscillator-amplifier, the Stokes beam, is recombined with the pump beam and focused into the medium under observation. This can be done collinearly if the spatial resolution is satisfactory or at a slight angle for a more definite probing volume. At the output of the combustor, the laser pump and Stokes beams are split off by a dichroic or beamsplitter to generate a nonresonant reference signal in a cell typically containing an inert gas. The CARS signal at ω_3 is split off from any remaining pump and Stokes beams by prisms, can be additionally filtered for noise suppression and sent to a monochromator or spectrograph. In final applications form, the spectrograph may well be an interference filter device analogous to the Raman spectrometer previously suggested. The approach just described is essentially that employed by Harvey for CARS investigations (Ref. 173). For laminar flames, two approaches are possible. One is to spectrally condense the Stokes beam and tune it about resonance to generate the spectrum. The other is to produce a broadband dye spectrum and merely scan the spectrum. In the latter the signal is reduced since the Stokes intensity per unit spectral bandwidth is reduced. In turbulent flames, where the CARS data probably cannot be unambigously averaged, one records portions of the spectrum with interference filters to isolate bands of interest, or captures the entire spectrum (termed multiplex CARS by Taran) with an

CARS SYSTEM SCHEMATIC

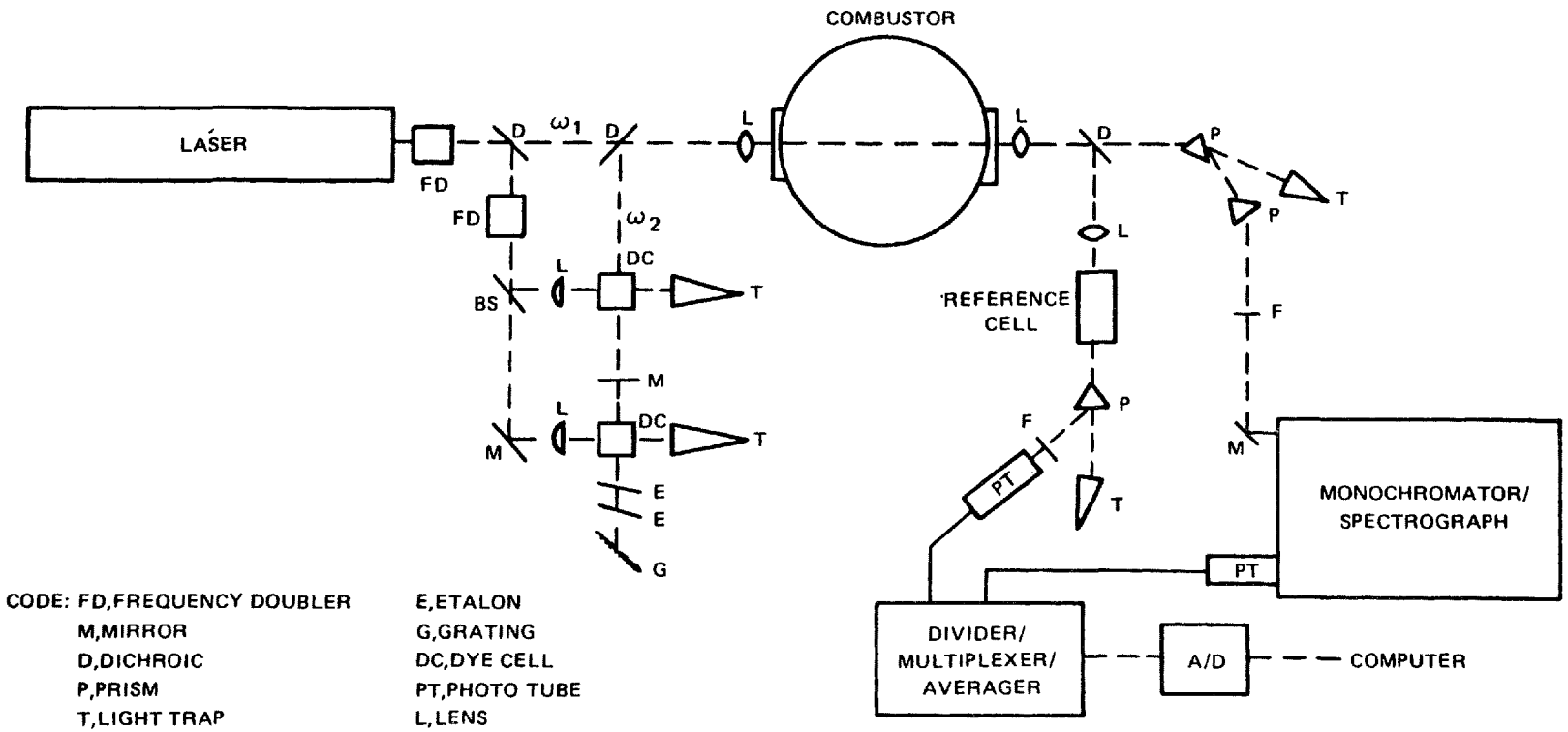

CODE: FD,FREQUENCY DOUBLER
M,MIRROR
D,DICHROIC
P,PRISM
T,LIGHT TRAP
BS,BEAM SPLITTER
E,ETALON
G,GRATING
DC,DYE CELL
PT,PHOTO TUBE
L,LENS
F,FILTER

FIG. 26

appropriate vidicon (Ref. 178), or intensified version thereof using the monochromator as a spectrograph. Because of amplitude and frequency instabilities from shot to shot, the magnitude of the CARS spectrum will fluctuate. These effects can be handled by generating a nonresonant reference signal, as shown, for normalization purposes. For multiplex CARS, the vidicon in the reference leg essestially captures the Stokes beam spectral distribution. The signals are then sent to appropriate electrical instrumentation. For steady work, this would include a ratio circuit, signal averager and recorder. For unsteady media investigations a multiplexer, divider, and multichannel readout would be used. In a final instrument, the data would probably be digitized and sent to a computer for data reduction, possibly by comparison with computer generated spectra.

Frequency doubled neodymium lasers with single transverse mode output at 10 pps and 0.2-0.3 J/pulse cost between approximately $40K to $60K depending on exact specifications and manufacturer (Refs. 191, 193 and 194). The dye oscillator/amplifier subassemblies including second doubler, mounts, optics, etc., would cost between $2K-$5K. The one meter double monochromator is approximately $20-$25K. The vidicons, depending on intensification required and instrumentation packages, would vary from $10K to $25K. For estimation purposes only one will be assumed to be necessary. Miscellaneous optics, filters, mounts and so forth are crudely estimated at $5K. Total systems cost using commercially available, already developed equipment, again exclusive of computer and peripherals, total between $80K and $120K.

For thermometry and majority species detection (> 1000 ppm), the probability of successful application in practical combustion devices appears good. For minor species measurements, the probability of success in the 10-1000 ppm range is deemed fair to poor, until demonstrated otherwise by double resonance or polarization oriented CARS techniques. Below 10 ppm, the probability of success is seen as very low, based upon both photon yield and nonlinear background interference considerations. The risk is thus perceived to be low to moderate (due to the high systems costs) for thermometry and major species detection, high for trace species measurements. Approaches employing interference filters and photomultipliers instead of double monochromators and multichannel spectrum analyzers are clearly desirable in regard to greatly reducing costs and should be an objective of future developmental works.

Jeopardies in the CARS area include potential nonlinear noise interactions with soot particulates, turbulence dephasing, and complex data reduction in general. For minority species concentration measurements, the feasibility of double resonance and polarization orientation CARS techniques is yet to be established for gas phase work. Future research efforts are required in these areas to assess the seriousness of these jeopardies. As with spontaneous Raman scattering, little in the way of laser or instrumentation development appears to be required.

Systems Integration

Based upon the systems review of the various diagnostic techniques together with their perceived probability of success, an integrated CARS-laser fluorescence measurement system is shown in Fig. 27. Shown is an approach which, in principle, would permit simultaneous CARS-fluorescence diagnostics. Due to the redundancy in equipment, considerable expense would be eliminated, however, by sequential or nonconcurrent measurements using the foregoing measurement approaches. By referring back to Figs. 25 and 26, the major subsystems of the CARS and laser fluorescence systems are readily recognizable. A single neodymium laser is frequency doubled or tripled to drive dye lasers in either an oscillator or oscillator/amplifier configuration as required. One dye subsystem generates the CARS Stokes beam, the other the fluorescence laser source which may or may not be frequency doubled as required. A multiple beam fluorescence system would be similarly configured. The laser beams are directed into the combustor/furnace as shown. CARS is, of course, detected and analyzed in the forward direction, while the laser induced fluorescence is collected coaxially at 180°. Hence, both measurement approaches could be utilized simultaneously, provided the combined focal flux does not exceed the combustor gas breakdown threshold. If the measurements are not performed simultaneously, then only one laser pumped dye subsystem and monochromator would be required. Clearly, if interference filters could ultimately be employed for spectral separation of the CARS and fluorescence signals, simultaneous measurements would be more feasible economically. An advantage of concurrent measurements is that the CARS could provide the correct temperature information required in the laser fluorescence data reduction. Recall that fluorescence measures the population only in a selected level of the ground state and temperature information is required to relate that one single state population to the total ground state or total species concentration. One must also take care to make sure that the fluorescence inducing laser beam frequency which is greater than the CARS pump and Stokes frequencies, is not resonantly separated from the latter. In such an instance, nonlinear (e.g., CARS) and spurious signals may be induced. In general this will probably not be a problem, and the integrated system illustrates the fact that the two diagnostic approaches are concurrently compatible.

INTEGRATED COMBUSTION DIAGNOSTICS SYSTEM

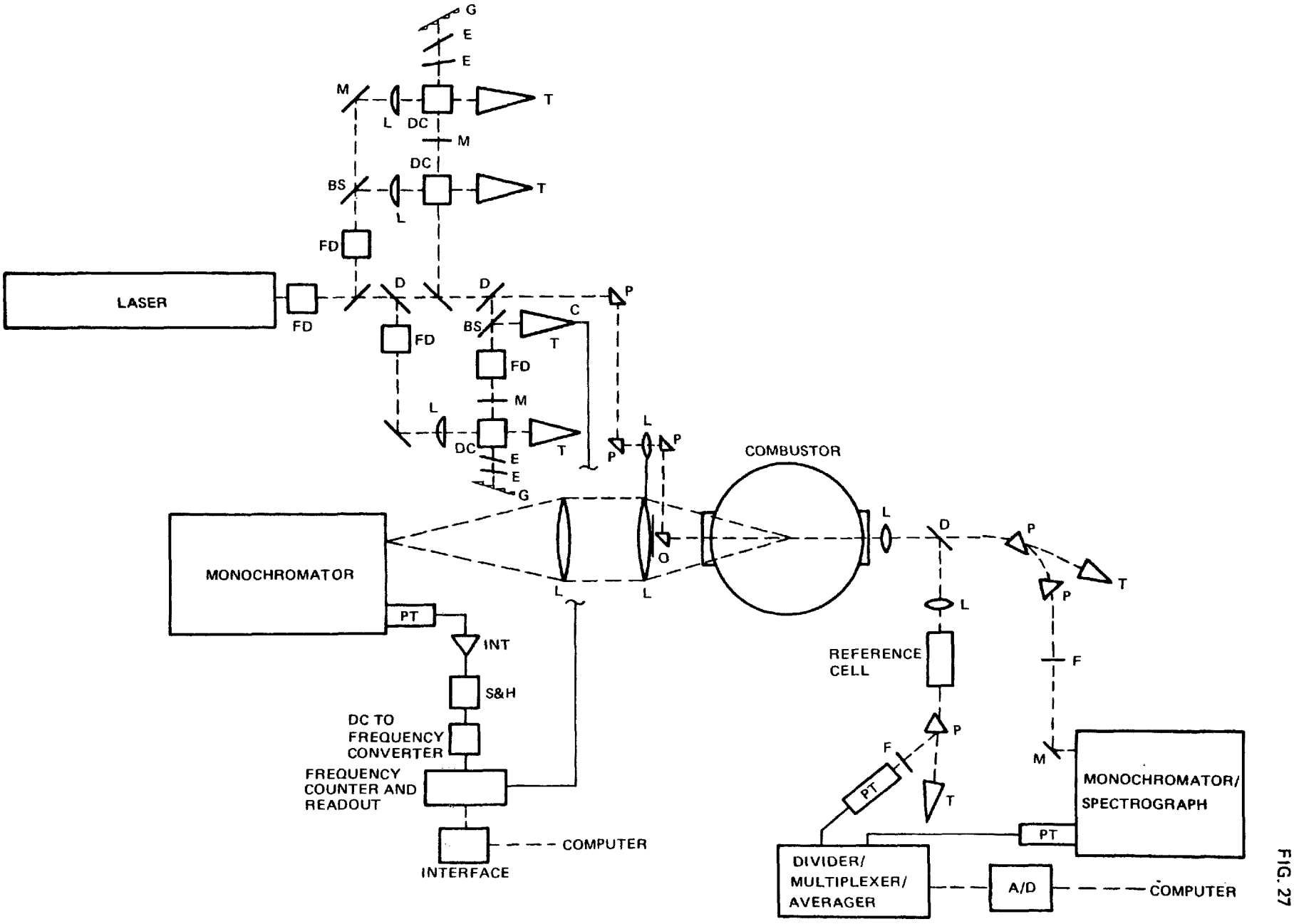

FIG. 27

CONCLUSIONS

On the basis of the foregoing discussions, the following general conclusions may be drawn.

(1) For most species of combustion interest, at least one of the diagnostic techniques investigated is applicable for point measurements of that constituent. The lone exception is the N atom which would have to be probed using either a lamp source absorption or fluorescence technique. Of course, depending upon which technique is relevant, sensitivity limits may vary widely, e.g., CARS is much less sensitive than saturated laser fluorescence.

(2) Practical combustion devices contain flames which are very hostile from an instrumentation viewpoint. High levels of spurious radiations, either naturally occurring or laser induced, must be overcome by the signal of interest. These effects, rather than shot noise, are generally the major determinants of signal/noise ratios. A host of other practical problems, e.g., gas breakdown, window damage, large distances to the measurement location, must also be confronted. Temporal fluctuations may well preclude signal averaging approaches to enhance signal/noise ratios. These effects should be closely examined in each measurement situation before a given measurement approach is adopted.

(3) Spontaneous and near-resonant Raman scattering appear generally incapable of probing hydrocarbon-fueled, primary combustion zones over a broad range of operating conditions. Application to exhausts and secondary combustion regions may be possible if particulate levels are not too high. For primary zone diagnostics, thermometry and major species concentration measurements appear problematical even with advanced state-of-the-art laser sources. Trace species concentration measurements are definitely precluded. Due to its advanced state-of-development, spontaneous Raman scattering should receive much near-term emphasis for fundamental combustion research in specially selected clean flame investigations.

(4) Saturated laser fluorescence has great potential for the measurement of selected species in low concentrations (ppm) in both practical and clean flames. The fluorescence signals will be independent of gas quenching effects if the absorption resonances can be saturated and if simple two and three level models are applicable. Considerable fundamental and applied research investigations are required to address these questions for this potential to be realized or dispelled.

(5) CARS is ideally suited for thermometry and major species concentration measurements in both practical and clean flame environments. Considerable research is nevertheless still required. Potential nonlinear laser-soot interaction effects need be addressed to either dismiss or reckon with them. Turbulence dephasing effects need to be systematically evaluated. Simplifications in gathering and treating CARS data are highly desirable. Species sensitivity limits in flames need

to be clearly established experimentally. Present estimates indicate sensitivity to be relatively poor for most molecules, i.e., on the order of 1000 ppm. CARS variants need to be assessed vis-a-vis their practical utility and capability in regards to lowering detectivity limits.

(6) Laser diagnostic techniques capable of point, in-situ diagnostic application to practical combustion media are quite expensive, generally in the $50K-$200K range for equipment alone and require skilled personnel for their operation. Considerable simplification of any diagnostic approach would be desirable to reduce system costs and personnel skill requirements.

REFERENCES

1. Hartley, D. L., Editor: The Role of Physics in Combustion. American Physical Society Summer Study Report, (1974).

2. Goulard, R., Editor: Combustion Measurements in Jet Propulsion Systems. Project SQUID Workshop Proceedings, December 1975.

3. Selected papers from the conference sessions are summarized in the forthcoming Measurements in Combustion Research, a volume in AIAA Progress in Aeronautics and Astronautics Series.

4. Byer, R. L.: Review, Remote Air Pollution Measurement. Opt. Quant. Elec., Vol. 7, pp. 147-177, (1975).

5. Lapp, M., C. M. Penney and J. A. Asher: Application of Light-Scattering Techniques for Measurements of Density, Temperature and Velocity in Gasdynamics. Technical Report prepared under Contract F33615-71-C-1867 for the Air Force Aerospace Research Laboratores, Dayton, Ohio, January 1973.

6. Harvey, A. B., J. R. McDonald and W. M. Tolles: Analytical Applications of a New Spectroscopic Tool: Coherent anti-Stokes Raman Spectroscopy (CARS). Progress in Analytical Chemistry, Plenum Press, to be published.

7. Robben, F.: Comparison of Density and Temperature Measurement Using Raman and Rayleigh Scattering. pp. 179-195 in Ref. 2.

8. Lapp, M. and C. M. Penney: Laser Raman Gas Diagnostics, Plenum Press, New York, (1974).

9. Szymanski, H. A.: Raman Spectroscopy, Theory and Practice, Plenum Press, New York, (1967).

10. Straughan, B. P. and S. Walker, Eds.: Spectroscopy, Vol. 3, Halsted Press, New York, (1976).

11. Sulzman, K. G. P., J. E. L. Lowder and S. S. Penner: Estimates of Possible Detection Limits for Combustion Intermediates and Products with Line Center Absorption and Derivative Spectroscopy Using Tunable Lasers. Comb. Flame, Vol. 20, pp. 177-191, (1973).

12. McGregor, W. K.: Absorption-Emission Measurements in Jet Engine Flows. pp. 107-109, in Ref. 2.

13. Jones, W. J. and B. P. Stoicheff: Inverse Raman Spectra: Induced Absorption at Optical Frequencies. Phys. Rev. Letts., Vol. 13, pp. 657-659, November 1964.

14. Lau, A., W. Wernicki, M. Pfeiffer, K. Lenz, and H. J. Weigmann: Possibilities and Limits of Inverse Raman Scattering. pp. 39-42, in J. P. Mathieu, Editor Advances in Raman Spectroscopy, Vol. I, Heyden and Son. Ltd, London, (1973).

15. Heiman, D., R. W. Hellwarth, M. D. Levenson and G. Martin: Raman-Induced Kerr Effect. Phys. Rev. Letts., Vol. 36, pp. 189-192, January 1976.

16. Bloembergen, N.: The Stimulated Raman Effect. Amer. J. Phys., Vol. 11, pp. 989-1023, November 1967.

17. Maier, M.: Applications of Stimulated Raman Scattering. Appl. Phys., Vol. 11, pp. 209-231 (1976).

18. Verdieck, J. F., S. H. Peterson, C. M. Savage, and P. D. Maker: Hyper-Raman Spectra of Methane, Ethane and Ethylene. Chem. Phys. Letts., Vol. 7, p. 219, (1970).

19. Regnier, P. R. and J. P. E. Taran: On the Possibility of Measuring Gas Concentrations by Stimulated Anti-Stokes Scattering. Appl. Phys. Letts., Vol. 23, pp. 240-242, September 1973.

20. Chabay, I., G. K. Klauminzer and B. S. Hudson: Coherent anti-Stokes Raman Spectroscopy (CARS): Improved Experimental Design and Observation of New Higher-Order Processes. Appl. Phys. Letts., Vol. 28, pp. 27-29, January 1976.

21. Schlossberg, H.: Fluorine Atom Probe Techniques for Chemical Lasers. Air Force Cambridge Research Laboratories Report, AFCRL-TR-75-0522, October 1, 1975.

22. Vriens, L.: Raman Scattering Cross Sections for Indium and Thallium Atoms. Optics. Commun., Vol. 11, p. 396, (1974).

23. Herzberg, G.: Molecular Spectra and Molecular Structure. I. Spectra of Diatomic Molecules, D. Van Nostrand Co., Inc., Princeton, NJ, (1950).

24. Jones, D. G. and J. C. Mackie: Evaluation of C_2 Resonance Fluorescence as a Technique for Transient Flame Studies. Combustion and Flame, Vol. 27, pp. 143-146, (1976).

25. Baronavski, A. and J. R. McDonald: The Application of Saturation Spectroscopy to the Measurement of C_2 $^3\Pi_u$ Concentration in Oxy-Acetylene Flames. Submitted to Appl. Optics.

26. Baronavski, A. P. and J. R. McDonald: Chem. Phys. Lett. in press.

27. Barnes, R. H., C. E. Moeller, J. F. Kirscher and C. M. Verber: Dye-Laser Excited CH Flame Fluorescence. Appl. Optics, Vol. 12, p. 2531, (1973).

28. Jackson, W. M.: Laser-Induced Fluorescence from CN Radicals. J. Chem. Phys., Vol. 59, p. 960, (1973).

29. Vear, C. J., P. J. Hendra, and J. J. McFarlane: Laser Raman and Resonance Fluorescence Spectra of Flames. J. Chem. Soc. Chem. Comm., p. 381, (1972).

30. Gaydon, A. G.: The Spectroscopy of Flames. Chapman and Hall Ltd., London, (1974).

31. Lee, L. C. and D. L. Judge: CS ($A\ ^1\Pi \rightarrow\ ^1\Sigma^+$) Fluorescence from Photodissociation of CS_2 and OCS. J. Chem. Phys., Vol. 63, p. 2782, (1975).

32. Suchard, S. N.: Spectroscopic Constants for Selected Diatomic Molecules, Air Force Report No. SAMSO-TR-74-82, the Aerospace Corp., Los Angeles, CA, (1974).

33. See Ref. 30, p. 353.

34. Zacharias, H., A. Anders, J. P. Halpern and K. H. Welge: Frequency Doubling in $KB_5O_8 \cdot 4H_2O$ and Application to NO A $^2\Sigma$ Excitation. Optics Comm. Vol. 19, p. 116, (1976).

35. Callear, A. B. and E. W. M. Smith: Fluorescence of Nitric Oxide. Trans. Far. Soc., Vol. 59, p. 1720, (1963).

36. Broida, H. P. and T. Carrington: Rotational, Vibrational and Electronic Energy Transfer in the Fluorescence of Nitric Oxide. J. Chem. Phys. Vol. 38, p. 136, (1963).

37. Baardsen, E. L. and R. W. Terhune: Detection of OH in the Atmosphere Using a Dye Laser. Appl. Phys. Lett., Vol. 21, p. 209, (1972).

38. Wang, C. C and L. I. Davis, Jr.: Measurement of Hydroxyl Concentrations in Air Using a Tunable UV Laser Beam. Phys. Rev. Lett., Vol. 32, p. 349, (1974).

39. Killingen, D. K., C. C. Wang and M. Hanabusa: Intensity and Pressure Dependence of Resonance Fluorescence of OH Induced by a Tunable UV Laser. Phys. Rev. A, Vol. 13, P. 2145, (1976).

40. Wang, C. C. and L. I. Davis: Ground State Population Distribution of OH Determined with a Tunable UV Laser. Appl. Phys. Lett., Vol. 25, p. 34 (1974).

41. Becker, K. H., D. Haaks and T. Tatarczyk: Monitoring of Radicals by a Tunable Dye Laser. Z. Naturforsch., Vol. 27a, pp. 1520-151 (1972).

42. Pearse, R. W, B. and A. G. Gaydon: The Identification of Molecular Spectra. Fourth Ed., Chapman and Hall, London (1976).

43. Herzberg, G.: Infrared and Raman Spectra of Polyatomic Molecules. D. Van Nostrand Co., Inc., Princeton, NJ (1945).

44. Cotton, F. A.: Chemical Applications of Group Theory. Wiley-Interscience, NY (1963).

45. Barrett, J. J. and R. F. Begley: Low-Power CW Generation of Coherent Anti-Stokes Raman Radiation in CH_4 Gas. Appl. Phys. Lett., Vol. 27, p. 129, (1975).

46. Weber, A., S. P. S. Porto, L. E. Cheesman, and J. J. Barrett: High-Resolution Raman Spectroscopy of Gases with CW Laser Excitation. J. Opt. Soc. Am., Vol. 57, p. 19, (1967).

47. Barrett, J. J. and A. Weber: Pure-Rotational Raman Scattering in a CO_2 Electric Discharge. J. Opt. Soc. Am., Vol. 60, p. 70 (1970).

48. Becker, K. H., V. Schurath and T. Tatarczyk: Fluorescence Determination of Low Formaldehyde Concentrations in Air by Dye Laser Excitation: Appl. Optics, Vol. 14, p. 310, (1975).

49. Bribes, J. L., R. Gaufres, M. Monan, M. Lapp and C. M. Penney: Raman Band Contours for Water Vapor as a Function of Temperature. Appl. Phys. Lett., Vol. 28, p. 336, (1976).

50. Itzkan, I. and D. A. Leonard: Observation of CARS Scattering from Liquid Water. Appl. Phys. Lett., Vol. 26, p. 106, (1975).

51. Halpern, J. B., G. Hancock, M. Lenzi and K. H. Welge: Laser-Induced Fluorescence from NH_2 (^2A). J. Chem. Phys., Vol. 63, p. 4808, (1975).

52. Gelbwachs, J. A., M. Birnbaum, A. W. Tucker, and C. L. Fincher: Fluorescence Determination of Atmosphere NO_2. Opto-Electronics, Vol. 4, p. 155, (1972).

53. Tucker, A. W., M. Birnbaum and C. L. Fincher: Atmospheric Determination of NO_2 by 442-nm Laser Induced Fluorescence. Appl. Optics, Vol. 14, p. 1418, (1975).

54. Brand, J. C., J. L. Hartwiek, R. J. Pirkle and C. J. Seliskar: The Resonance Fluorescence and Absorption Spectrum of NO_2. Can. J. Phys., Vol. 51, p. 2184, (1973).

55. Agarwal, Y., T. Hadeishi and F. Robben: Measurement of NO_2 Concentration in Combustion Using Fluorescence Excited by an Argon-Ion Laser. AIAA Paper No. 76-136. AIAA 14th Aerospace Meeting, Washington, D.C., January 26-28, 1976.

56. Okabe, H., P. L. Splitstone and J. J. Ball: Fluorescence of SO_2 in Air. J. Air. Pollut., Control. Assoc., Vol. 23, p. 514, (1974).

57. Fowler, M. C. and P. J. Berger: Feasibility Study of the Use of Resonance Scattering for the Remote Detection of SO_2. Report No. EPA-65Q/2-74-020, January 1974.

58. Zulner, W., E. Cieplinski and D. Hulm: Pulsed Fluorescent SO_2 Analyzer. Thermoelectron Corp. Watham, MA 02154.

59. Jahnke, J. A., J. L. Cheney and J. B. Homolya: Quenching Effects in SO_2 Fluorescence Monitoring Instruments. Environ. Sci. Tech., Vol. 10, p. 1246, (1976).

60. Nakahara, S., K. Ito, S. Ito, A. Fuke, S. Komatsu, H. Inaba and T. Kobayasi: Detection of Sulphur Dioxide in Stack Plumes by Laser Raman Radar. Opto-Electronics, Vol. 4, p. 169, (1972).

61. Hirschfeld, T., E. R. Schildkraut, H. Tannenbaum and D. Tannenbaum: Remote Spectroscopic Analysis of ppm-level Air Pollutants by Raman Spectroscopy. Appl. Phys. Letts. Vol. 22, pp. 38-41, January 1973.

62. Kobayasi, T. and H. Inaba: Spectroscopic Detection of SO_2 and CO_2 Molecules in Polluted Atmosphere by Laser-Raman Radar Technique. Appl. Phys. Lett., Vol. 17, p. 139, (1970).

63. Moore, C. E.: Atomic Energy Levels, National Bureau of Standards, Vol. I, (1949).

64. Anderson, R.: Compilation of Measured Lifetimes of Gaseous Diatomic Molecules. Atomic Data, Vol. 3, pp. 227-240, (1971).

65. Wiese, W. L., M. W. Smith and B. W. Glennon: Atomic Transition Probabilities. National Bureau of Standards, Vol. 1, and Vol. 2, (1966).

66. Herzberg, G.: The Electronic Spectra of Polyatomic Molecules. D. Van Nostrand Co., In., Princeton, N.J., (1966).

67. Ref. 30, Appendix of Molecular Constants.

68. Ref. 43, Section on Individual Molecules.

69. Inaba, H. and T. Kobayasi: Laser Raman Radar-Laser Raman Scattering Methods for Remote Detection and Analysis of Atmospheric Pollution. Opto-Electronics, Vol. 4, pp. 101-123, (1972).

70. Calculated from Ref. 69.

71. Penney, C. M., R. L. St. Peters and M. Lapp: Absolute Rotational Raman Cross-Sections for N_2, O_2 and CO_2. J. Opt. Soc. Am., Vol. 64, p. 712, (1974).

72. Fenner, W. R., H. A. Hyatt, J. M. Kellam and S. P. S. Porto: Raman Cross Sections of Some Simple Gases. J. Opt. Soc. Am., Vol. 63, p. 73, (1973).

73. Penney, C. M. and M. Lapp: Raman Scattering Cross-Sections for Water Vapor. J. Opt. Soc. Am., Vol. 66, p. 422, (1976).

74. Farmer, W. H. and H. R. Bevis: Observation of Large Flame Characteristics Relative to the Performance of a Laser Analyzer. Technical Report Under Contract EPA F406-74-C-0004, August 1973.

75. Handbook of Light Measurement Techniques. Gamma Scientific Inc., San Diego, CA, and W. H. Farmer, Spectron Development Laboratories, Tullahoma, TN, private communication.

76. D'Alessio, A., A. DiLorenzo, A. F. Sarofim, F. Beretta, S. Masi and C. Venitozzi: Soot Formation in Methane-Oxygen Flames. Fifteenth Symposium on Combustion. The Combustion Institute, Pittsburgh, PA, (1975).

77. Eckbreth, A. C.: Laser Raman Thermometry Experiments in Simulated Combustor Environments. AIAA Paper 76-27, January 1976.

78. Leonard, D. A.: Field Tests of a Laser Raman Measurement System for Aircraft Engine Exhaust Emissions. Technical Report AFAPL-TR-74-100, October 1974.

79. Aeschliman, D. P. and R. E. Setchell: Fluorescence Limitations to Combustion Studies Using Raman Spectroscopy. Appl. Spec., Vol. 29, pp. 426-429, (1975).

80. Bailly, R., M. Pealat and J. P. E. Taran: Raman Investigation of a Subsonic Jet. Opt. Comm., Vol. 17, pp. 68-73, April 1976.

81. Wright, M. L. and K. S. Krishman: Feasibility Study of In-Situ Source Monitoring of Particulate Composition by Raman or Fluorescence Scatter. EPA-R2-73-219, June 1973.

82. Gelbwachs, J. and M. Birnbaum: Fluorescence of Atmospheric Aerosols and Lidar Implications. Appl. Opt., Vol. 12, pp. 2442-2447, October 1973.

83. Nakamizo, M., R. Kammereck, and P. L. Walker, Jr.: Laser Raman Studies of Carbon. Carbon, Vol. 12, pp. 259-267, (1974).

84. Eckbreth, A. C.: Applicability of Laser Raman Scattering Diagnostic Techniques to Practical Combustion Systems. Project SQUID Technical Report UTRC-4-PU, October 1976.

85. Dalzell, W. H., G. C. Williams and H. C. Hottel: A Light Scattering Method for Soot Concentration Measurements. Comb. and Flame, Vol. 14, pp. 161-170 (1970).

86. Kunugi, M. and H. Jinno: Determination of Size and Concentration of Particles in Diffusion Flames by a Light Scattering Technique. 11th Symposium on Combustion, pp. 251-266 (1966).

87. Pagni, P. J., L. Hughes, and T. Novakov: Smoke Suppressant Additive Effects on Particulate Emissions From Gas Turbine Combustors. AGARD-CP-125, pp. 25-1-10, (1973).

88. Eckbreth, A. C.: Laser Modulated Particulate Incandescence. Submitted to the Journal of Applied Physics.

89. Jeunehomme, M. and R. P. Schwenker: Focussed Laser Beam Experiment and the Oscillator Strength of the Swan System. J. Chem. Phys., Vol. 42, pp. 2406-2408, April 1965.

90. Howe, J. A.: Observations on the Maser Induced Graphite Jet. J. Chem. Phys., Vol. 39, pp. 1362-1363 September 1963.

91. Mentall, J. E. and R. W. Nicholls: Spectroscopic Temperature Measurements on Laser Produced Flames. J. Chem. Phys., Vol. 46, pp. 2881-2885, April 1967.

92. Gerry, E. T. and D. J. Rose: Plasma Diagnostics by Thomson Scattering of a Laser Beam. J. Appl. Phys., Vol. 37, pp. 2715-2724, June 1966.

93. Kincaid, B. E. and J. R. Fontana: Raman Cross-Section Determination by Direct Stimulated Raman Gain Measurements. Appl. Phys. Letts., Vol. 28, pp. 12-14, January 1976.

94. Smith, D. C. and R. G. Meyerand, Jr.: Laser Radiation Induced Gas Breakdown. Chapter 11 in Principles of Laser Plasmas, G. Bekefi, Editor, Wiley-Interscience, New York, (1974).

95. Kato, K.: Laser-Induced Breakdown in Air Using Visible Dye Laser. Jap. J. Appl. Phys., Vol. 14, pp. 1409-1410, (1975).

96. Busher, H. T., R. G. Tomlinson, and E. K. Damon: Frequency Dependence of Optically Induced Gas Breakdown. Phys. Rev. Letts., Vol. 15, p. 847, (1965).

97. Lencioni, D. E.: Laser-Induced Air Breakdown for 1.06-μm Radiation. Appl. Phys. Letts., Vol. 25, pp. 15-17, (1974).

98. Smith, D. C. and R. T. Brown: Aerosol-Induced Air Breakdown with CO_2 Laser Radiation. J. Appl. Phys., Vol. 46, pp. 1146-1154, (1975).

99. Draggoo, V. G., C. Y. She, G. L. McAllister and D. F. Edwards: Effects of Laser Mode Structure on Damage on Quartz. IEEE J. Quant. Elec., Vol. QE-8, pp. 54-57, (1972).

100. Bass, M. and H. H. Barrett: Laser Induced Damage Probability at 1.06 and 0.69μm. pp. 58-69 in Laser Induced Damage in Optical Materials: 1972 ASTM Symposium, Boulder, Colorado, (1972).

101. Glass, A. J. and A. H. Guenther: Laser Induced Damage of Optical Elements - A Status Report. Appl. Opt., Vol. 12, pp. 637-649, (1973).

102. Bloembergen, N.: Role of Cracks, Pores and Absorbing Inclusions on Laser Induced Damage Threshold at Surfaces of Transparent Dielectrics. Appl. Opt., Vol. 12, pp. 661-664, (1973).

103. Brown, R. T. and D. C. Smith: Aerosol-Induced Thermal Blooming. J. Appl. Phys., Vol. 46, pp. 402-405, (January 1975).

104. Lederman, S.: Modern Diagnostics of Combustion. AIAA Paper 76-26, Presented at the 14th Aerospace Sciences Meeting, Washington, D.C., (1976).

105. Lapp, M. and D. L. Hartley: Raman Scattering Studies of Combustion. Comb. Sci. and Tech., Vol. 13, pp. 199-210, (1976).

106. Widhopf, G. F. and S. Lederman: Species Concentration Measurements Utilizing Raman Scattering of a Laser Beam. AIAA J., Vol. 9, pp. 309-316, February 1971.

107. Arden, W. M., T. B. Hirschfeld, S. M. Klainer and W. A. Mueller: Studies of Gaseous Flame Combustion Products by Raman Spectroscopy. Appl. Spect., Vol. 28, pp. 554-557, (1974).

108. Lapp, M., T. M. Goldman, and C. M. Penney: Raman Scattering from Flames. Science, Vol. 75, pp. 1112-1115, March 1972.

109. Setchell, R. E.: Time Averaged Measurements in Turbulent Flames Using Raman Spectroscopy. AIAA Paper 76-28, AIAA 14th Aerospace Sciences Meeting, Washington, D.C., January 1976.

110. Drake, M. C. , G. M. Rosenblatt: Flame Temperatures from Raman Scattering. Chem. Phys. Letts., Vol. 44, pp. 313-316, December 1976.

111. Stricker, W.: Local Temperature Measurements in Flames by Laser Raman Spectroscopy. Comb. and Flame, Vol. 27, pp. 133-136, (1976).

112. Lapp, M., C. M. Penney, and R. L. St. Peters: Laser Raman Probe for Flame Temperature. Project SQUID Technical Report GE-1-PU, April 1973.

113. Eckbreth, A. C.: Laser Raman Gas Thermometry. AIAA Paper 74-1144, AIAA/SAE 10th Propulsion Conference, San Diego, CA., October 1974.

114. Salzman, J. A., W. J. Masica and T. A. Coney: Determination of Gas Temperatures from Laser Raman Scattering. NASA TND-6336, May 1971.

115. Boiarski, A. A.: Gas Diagnostics Utilizing Laser Induced Raman Scattering. Aerospace Research Laboratories Report ARL 72-008, January 1972.

116. Smith, J. R.: A Rotational Raman Scattering System for Measuring Temperature and Concentration Profiles in Transient Gas Flows. Sandia Laboratories Report SAND 75-8224, March 1975.

117. Hickman, R. S. and J. H. Liang: Rotational Temperature Measurements in Nitrogen Using Raman Spectroscopy. Rev. Sci. Instr., Vol. 43, pp. 796-799, May 1972.

118. Salzman, J. A., and T. A. Coney: Remote Measurement of Atmospheric Temperatures by Raman Lidar. NASA TM X 68250, June 1973.

119. Lederman, S., and J. Bornstein: Specie Concentration and Temperature Measurements in Flow Fields. Project SQUID Technical Report PIB-31-PU, March 1973.

120. Bandy, A. R., M. E. Hillard and T. E. Emory: Evaluation of Raman Scattering as a Sensor of Temperature and Molecular Density. Appl. Spect., Vol. 27, pp. 421-424, November 1973.

121. Boiarski, A. A.: Shock-Tube Diagnostics Utilizing Laser Raman Spectroscopy Naval Surface Weapons Center Report NSWC/NOL/TR 75-53, April 1975.

122. Nelson, L. Y., A. W. Saunders, Jr., A. B. Harvey, and G. O. Neely: Detection of Vibrationally Excited Homonuclear Diatomic Molecules by Raman Spectroscopy. J. Chem. Phys., Vol. 55, pp. 5127-5128, November 1971.

123. Barrett, J. J. and A. B. Harvey: Vibrational and Rotational - Translational Temperatures in N_2 by Interferometric Measurement of the Pure Rotational Raman Effect. J. Opt. Soc. Am., Vol. 65, pp. 392-398, April 1975.

124. Bhagavantam, S.: Scattering of Light and the Raman Effect. Chemical Publishing Co., Brooklyn, NY, (1942).

125. Anderson, A.: The Raman Effect. Marcel Dekker, Inc., New York, (1973).

126. Smith, W. H.: A New Method for the Detection of Raman Scattering from Atmospheric Pollutants. Opto-Elec., Vol. 4, pp. 161-167, (1972).

127. Penney, C. M., L. M. Goldman and M. Lapp: Raman Scattering Cross Sections. Nat. Phys. Sci., Vol. 235, pp. 110-111, February 1972.

128. Photomultiplier Manual. RCA Technical Series, PT-61, (1970).

129. Hill, R. A. and D. L. Hartley: Focused Multiple-Pass Cell for Raman Scattering. Appl. Opt., Vol. 13, pp. 186-192, January 1974.

130. Laser Focus, Vol. 12, p. 92, October 1976.

131. Williams, P. F., D. L. Rousseau and S. H. Dworetsky: Resonance Fluorescence and Resonance Raman Scattering: Lifetimes in Molecular Iodine. Phys. Rev. Letts., Vol. 32, pp. 196-199, February 1974.

132. Penney, C. M.: Light Scattering and Fluorescence in the Approach to Resonance - Stronger Probing Processes. pp. 191-217, in Ref. 8.

133. Hilborn, R. C.: Theory of the Time and Frequency Dependence of Near-Resonance Raman Scattering and Quantum Beats. Chem. Phys. Letts., Vol. 32, pp. 76-81, April 1975.

134. Holzer, W., W. F. Murphy and H. J. Bernstein: Resonance Raman Effect and Resonance Fluorescence in Halogen Gases. J. Chem. Phys., Vol. 52, pp. 399-407, January 1970.

135. Marsden, M. J. and G. R. Bird: Resonance Raman Spectrum of Gaseous Nitrogen Dioxide (NO_2). J. Chem. Phys., Vol. 59, pp. 1766-1767, September 1973.

136. Rousseau, D. L. and P. F. Williams: Resonance Raman Scattering of Light From a Diatomic Molecule. J. Chem. Phys., Vol. 64, pp. 3519-3537, May 1976.

137. Robrish, P., H. Rosen and O. Chamberlain: Study of the Quenching of Inelastic Light Scattering Near An Isolated Resonance in I_2 Vapor. Phys. Letts., Vol. 51A, pp. 434-436, April 1975.

138. Fouche, D. G. and R. K. Chang: Observation of Resonance Raman Scattering Below the Dissociation Limit in I_2 Vapor. Phys. Rev. Letts., Vol. 29, pp. 536-539, August 1972.

139. Rosen, H., P. Robrish and O. Chamberlain: Remote Detection of Pollutants Using Resonance Raman Scattering. Appl. Opt., Vol. 14, pp. 2703-2706, November 1975.

140. Wang, C. P.: Laser Applications to Turbulent Reactive Flows; Density Measurement by Resonance Absorption and Resonance Scattering Techniques. Comb. Sci. and Tech., Vol. 13, pp. 211-227, (1976).

141. Piepmeier, E. H.: Theory of Laser Saturated Atomic Resonance Fluorescence. Spectrochimica Acta, Vol. 27B, pp. 431-443, (1972).

142. Daily, J. W.: Pulsed Resonance Spectroscopy Applied to Turbulent Combustion Flows. Appl. Opt., Vol. 15, pp. 955-960, April 1976.

143. Daily, J. W.: Laser Induced Fluorescence Applied to Turbulent Reacting Flows. Presented at the Western States Section Combustion Institute Meeting, (La Jolla, California, Fall 1976), Paper 76-24.

144. Daily, J. W.: Saturation Effect in Laser Induced Fluorescence Spectroscopy. (To be published).

145. Abramowitz, A. and I. A. Stegun: Handbook of Mathematical Functions. Dover, New York, (1965).

146. Mitchell, A. C. G. and M. W. Zemansky: Resonance Radiation and Excited Atoms. Cambridge University Press, (1971).

147. Greenstein, H.: Line-Width and Tuning Effects in Resonant Excitation. Opt. Soc., Vol. 65, pp. 33-40, January 1975.

148. Christensen, C. P., C. Freed and H. Haus: Gain Saturation and Diffusion in CO_2 Lasers. IEEE J. Quant. Elec., Vol. QE-5, pp. 276-283, June 1969.

149. Gelbwachs, J. A. and J. E. Wessel: Doppler-Free Two Photon Spectroscopy Applied to Molecular Electronic Transitions. (To be Published).

150. Basco, N., A. B. Callear and R. G. W. Norrish: Fluorescence and Vibrational Relaxation of Nitric Oxide Studied by Kinetic Spectroscopy. Proc. Roy. Soc. London, Series A, Vol. 260, pp. 459-476, (1961).

151. Fristrom, R. M. and A. A. Westenberg: Flame Structure. McGraw-Hill, New York, (1965).

152. Butcher, R. and L. Sherman: Second Harmonic Generation Using a Flashlamp Pumped Dye Laser. Presented at Laser Institute of America Conference (Electro-Optics '76), New York, September 14-16, 1976.

153. Polanyi, J. C. and K. B. Woodall: Mechanism of Rotational Relaxation. J. Chem. Phys., Vol. 56, pp. 1563-1572, February 1972.

154. Becker, K. H. and D. Haaks: Measurement of the Natural Lifetimes and Quenching Rate Constants of $OH(^2\Sigma^+, v = 0,1)$ and $OD(^2\Sigma^+, v = 0,1)$ Radicals. Zeit. für Naturforschung, Vol. 28a, pp. 249-256, (1973).

155. Callear, A. B. and M. J. Pilling: Fluorescence of Nitric Oxide. Trans. Faraday Soc., Vol. 66, pp. 1618-1634, (1970).

156. Melton, L. A. and W. Klemperer: Energy Transfer in Monochromatically Excited Nitric Oxide: $A^2\Sigma^+$ and $B^2\pi$. J. Chem. Phys., Vol. 59, pp. 1099-1115, (1973).

157. Regnier, P. R., F. Moya, and J. P. E. Taran: Gas Concentration Measurement by Coherent Raman Anti-Stokes Scattering. AIAA Paper 73-702, AIAA 6th Fluid and Plasma Dynamics Conference, Palm Springs, CA., July 1973.

158. Moya, F., S. A. J. Druet and J. P. E. Taran: Gas Spectroscopy and Temperature Measurement by Coherent Raman Anti-Stokes Scattering. Opt. Comm., Vol. 13, pp. 169-174, February 1975.

159. Regnier, P. R., F. Moya, and J. P. E. Taran: Gas Concentration Measurement by Coherent Raman Anti-Stokes Scattering. AIAA J., Vol. 12, pp. 826-831, June 1974.

160. Moya, F., S. Druet, M. Pealat, and J. P. Taran: Flame Investigation by Coherent Anti-Stokes Raman Scattering. AIAA Paper 76-29, AIAA 14th Aerospace Sciences Meeting, Washington, D. C., January 1976.

161. Maker, P. D. and R. W. Terhune: Study of Optical Effects Due to an Induced Polarization Third Order in Electric Field Strength. Phys. Rev., Vol. 137, pp. A801-A818, February 1965.

162. Begley, R. F., A. B. Harvey, and R. L. Byer: Coherent Anti-Stokes Raman Spectroscopy. Appl. Phys. Letts., Vol. 25, pp. 387-390, October 1974.

163. Harvey, A. B., J. R. McDonald and W. M. Tolles: Analytical Applications of a New Spectroscopic Tool: Coherent Anti-Stokes Raman Spectroscopy (CARS) in Progress in Analytical Chemistry. Plenum Press, in press.

164. Tolles, W. M., J. W. Nibler, J. R. McDonald and A. B. Harvey: A Review of the Theory and Application of Coherent Anti-Stokes Raman Spectroscopy (CARS). Appl. Spect., to be published.

165. Nibler, J. W., J. R. McDonald, and A. B. Harvey: CARS Measurement of Vibrational Temperatures in Electric Discharges. Opt. Comm., Vol. 18, pp. 371-373, August 1976.

166. Barrett, J. J.: Generation of Coherent Anti-Stokes Rotational Raman Radiation in Hydrogen Gas. Appl. Phys. Letts., Vol. 29, pp. 722-724, December 1976

167. Roh, W. B., P. W. Schrieber and J. P. E. Taran: Single-Pulse Coherent Anti-Stokes Raman Scattering. Appl. Phys. Letts., Vol. 29, pp. 174-176, August 1974.

168. Smith, J. R.: A Rotational Raman Scattering System for Measuring Temperature and Concentration Profiles in Transient Gas Flows. Sandia Laboratories Report SAND 75-8224, March 1975.

169. Rado, W. G.: The Nonlinear Third Order Dielectric Susceptability Coefficients of Gases and Optical Third Harmonic Generation. Appl. Phys. Letts., Vol. 11, pp. 123-215, August 1967.

170. Druet, S. A. J.: *Resonant Coherent Anti-Stokes Scattering in Gases. Proceedings* of the Fifth International Conference on Raman Spectroscopy. pp. 736-737, (1976).

171. Lotem, H., R. T. Lynch, Jr., and N. Bloembergen: Interference Between Raman Resonances in Four Wave Difference Mixing. Phys. Rev. A., Vol. 14, pp. 1748-1755, November 1976.

172. Lynch, R. T., Jr., S. D. Kramer, H. Lotem, and N. Bloembergen: Double Resonance Interference in Third-Order Light Mixing. Opt. Comm., Vol. 16, pp. 372-375, March 1976.

173. Nibler, J. W., J. R. McDonald and A. B. Harvey: Coherent Anti-Stokes Raman Spectroscopy of Gases. Proceedings of the Fifth International Conference on Raman Spectroscopy, pp. 717-725, (1976).

174. Song, J. J., G. L. Eesley and M. D. Levenson: Background Suppression in Coherent Raman Spectroscopy. Appl. Phys. Letts., Vol. 29, pp. 567-569, November 1976.

175. Molectron Corporation: Coherent Anti-Stokes Raman Spectroscopy (CARS) - Update. Applications Note No. 112, August 1976.

176. Eckbreth, A. C. and J. W. Davis: Spatial Resolution Enhancement in Coaxial Light Scattering Geometries. Appl. Opt., Vol. 16, pp. 804-806, April 1977.

177. Wilbrandt, R., P. Pagsberg, K. B. Hansen, and C. V. Weisberg: Fast [illegible] Raman Spectroscopy of a Free Radical. Chem. Phys. Letts., Vol. 36, pp. [illegible], October 1975.

178. OMA Catalog, T336-20M-7/75-PB. Princeton Applied Research Corporation, Princeton, N.J. 08540.

179. 1977 Laser Focus Buyers Guide. Vol. 12, January 1977.

180. Instruments SA, Inc., J-Y Optical Systems Div., Metuchen, N.J. 08840.

181. Snavely, B. B.: Flashlamp-Excited Organic Dye Lasers. Proc. IEEE, Vol. 57, pp. 1374-1390, August 1969.

182. Chromatix Corp., Mountain View, CA 94043.

183. Electro-Photonics Ltd., Belfast, Northern Ireland BT 17 9HN.

184. Phase-R Company, New Durham, NH 03855.

185. Molectron Corporation, Sunnyvale, CA 94086.

186. Wallenstein, R. and T. W. Hansch: Powerful Dye Laser Oscillator-Amplifier System for High Resolution Spectroscopy. Opt. Comm., Vol. 14, pp. 353-357, July 1975.

187. McFarland, B. B.: Laser Second Harmonic-Induced Stimulated Emission of Organic Dyes. Appl. Phys. Letts., Vol. 10, pp. 208-209, April 1067.

188. Bergman, A., R. David, and J. Jortner: A Powerful Broad Band Tunable Dye Laser. Opt. Comm., Vol. 4, pp. 431-434, February/March 1972.

189. Deutsch, T. F., and M. Bass: Laser-Pumped Dye Lasers Near 4000Å. IEEE J. Q. E., Vol. QE-5, pp. 260-261, May 1969.

190. Wallace, R. W.: Generation of Tunable UV From 2610 to 3150Å. Opt. Comm., Vol. 4, pp. 316-319, December 1971.

191. Quanta-Ray Corporation, Mountain View, CA 94043.

192. Dewey, H. J.: Second Harmonic Generation in $HB_5O_8 \cdot 4H_2O$ from 217.1 to 315.0 nm. IEEE J. Q. E., Vol. QE-12, pp. 303-306, May 1976.

193. General Photonics Corporation, Santa Clara, CA 95050.

194. International Laser Systems, Orlando, FL 32804.

APPENDIX I

RADIOMETRIC MEASUREMENT CONVERSION

Spectral radiance measurements (Ref. I-1) have been made on the EPA "Rainbow" furnace employing a Gamma Scientific Model 2020-31 radiometer (Ref. I-2). For optically thin flames, spectral radiation energy densities are preferable to account properly for instrument techniques which view some volume of the combustion device being probed. The spectral radiance in Watts/cm^2 sr Å can be converted to a spectral radiation energy density by dividing the former by the depth of field of the radiometer.

The radiometer consists essentially of a lens, variable aperture and detector as seen in Fig. I-1 designed in such a way that the viewing solid angle times source area product remains constant independent of radiometer to source distance. The acceptance angle α is fixed, but selectable in various increments. From simple geometric considerations the linear acceptance angle, α, is given by

$$\tan \frac{\alpha}{2} = \frac{d_a}{2q} \tag{I-1}$$

where d_a is the aperture diameter and q the image distance shown in Fig. I-1. For fixed acceptance angle, the radiometer is designed with a constant d_a/q ratio. The source area A_S viewed can easily be shown to be

$$A_S = \frac{\pi}{4} \left(\frac{pd_a}{q}\right)^2 \tag{I-2}$$

The collection solid angle, Ω, is

$$\Omega = \frac{A_\ell}{p^2} \tag{I-3}$$

where A_ℓ is the area of the field lens employed. Note that the product of source area times collection solid angle is

$$A_S\Omega = A_\ell \pi \tan^2 \frac{\alpha}{2} \tag{I-4}$$

and is constant, i.e., independent of p, for fixed α. Thus the radiometer can be calibrated and used to make spectral radiance measurements directly for any distance from the source being measured.

From the lower part of Fig. I-1, the depth of field of the radiometer can be found using simple thin lens and geometrical relationships and is given by

$$\text{dof} = 2p^2 \frac{\tan \alpha/2}{d_\ell} \tag{I-5}$$

RADIOMETER SCHEMATIC

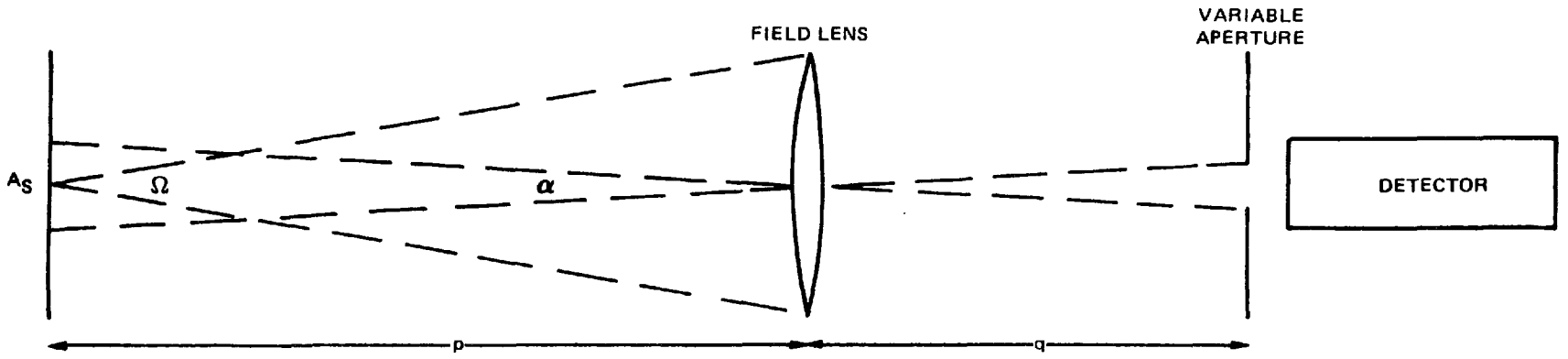

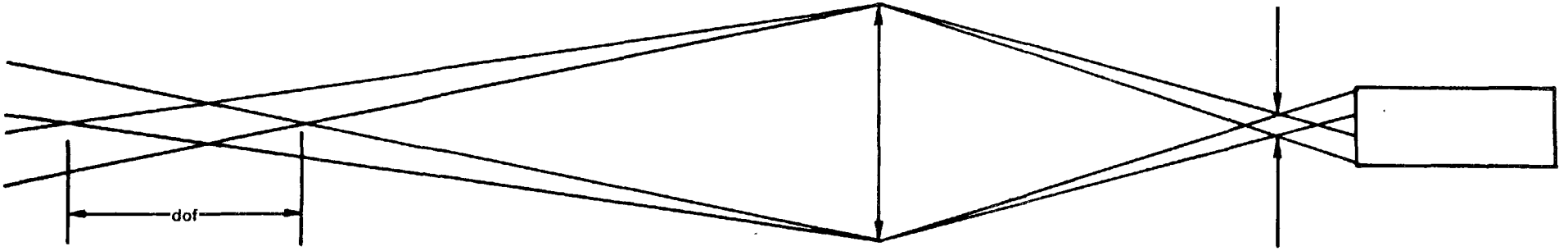

FIG.I-1

Note that the depth of field does depend on the radiometer to source distance. The radiometer employed had a minimum working distance of 1 meter. Since such a working distance is compatible with measurements from the side of the Rainbow furnace, this is the radiometer to source distance assumed for the side window measurements. For the measurements from the rear axial window, the minimum working distance was 140 cm. The measurements were made with an acceptance angle of 0.1°. The field lens employed in the radiometer was f/3.5 and 60 mm in diameter. For the side location, the depth of field was calculated to be 2.9 cm, for the rear axial work, 5.6 cm. The measurements reported in Ref. I-1 were divided appropriately by these numbers to obtain the radiation energy density at various locations in the furnace.

APPENDIX I

References

I-1. W. H. Farmer and H. R. Bevis: "Observation of Large Flame Characteristics Relative to the Performance of a Laser Analyzer." Technical Report under Contract EPA F 406-74-C-0004 (August 1973).

I-2. "Handbook of Light Measurement Techniques." Gamma Scientific Inc., San Diego, California.

APPENDIX II

AVERAGING CONSIDERATIONS FOR PULSED, LASER RAMAN SIGNALS FROM TURBULENT COMBUSTION MEDIA*

Introduction

The magnitude of temporal temperature fluxtuations is of great importance in the understanding and modeling of turbulent combustion phenomena, particularly in regards to pollutant formation (Refs. II-1, -2). Fluctuations are also relatable to the performance of combustors and to the lifetime of downstream turbine components (Ref. II-3). Thermocouples have been employed to measure fluctuations in turbulent (Ref. II-4) or oscillating flames (Ref. II-5). Laser Raman techniques (Ref. II-6) are anticipated to see widespread application in this area, particularly where the absence of a material probe will prove of great advantage, e.g., recirculating flows, extremely high temperatures. With pulsed lasers of sufficiently short duration, i.e. $< 10^{6}$ seconds, "instantaneous" temperature and species measurements can be made (Ref. II-7). By repeating these measurements a statistically significant number of times probability distribution functions can be assembled from which property averages and fluctuation magnitudes can be obtained.

In many instances, however, the Raman signal-to-noise (S/N) ratio is limited due to shot, background or laser induced noise (Ref. II-8) and accurate single pulse measurements are precluded. Signal averaging is usually then employed to enhance the S/N in an attempt to obtain time-averaged medium properties. However, such time averaging can lead to erroneous measurements. In Ref. II-9, Setchell examined the consequences of time-averaging Raman data generated by a continuous wave laser from a turbulent medium and identified those instances where averaging errors would arise. Similarly, an analysis has been presented of the effect of fluctuations on the accuracy of electron beam diagnostics (Ref. II-10). In this note the consequences of ensemble-averaging pulsed laser Raman data in a fluctuating environment will be treated. As will be shown, averaging can lead to measurement errors in medium properties, depending on the magnitudes and correlations of the fluctuations. In the first portion of the note, the case of averaging pulsed Raman data, exhibiting shot noise only, will be considered for both number density and temperature measurements. Preferred averaging approaches will be illustrated. Then the situation pertaining to averaging Raman data containing other sources of noise will be examined.

---

*Research supported by Project SQUID under subcontract 8960-20 and the Office of Naval Research under Contract N00014-75-C-1143.

Signal Averaging With Shot Noise

The number of Raman photons in the Stokes band, n_i^S (the superscript a will be used to denote the anti-Stokes region) generated by the ith laser pulse is given by

$$n_i^S = k^S N_i f^S(T_i) \epsilon_i \tag{II-1}$$

where N_i is the number density of the scattering species of interest at instant i; $f^S(T_i)$, the bandwidth factor; and ϵ_i, the energy of laser pulse i. The bandwidth factor is a temperature dependent term which accounts for the fraction of the scattering species in the appropriate initial quantum states for scattering to be observed. $f^S(T_i)$ depends on the spectral location and bandwidth (hence its name) of the spectrometer or interference filters employed; these dependences will not be explicitly denoted. k^S is a factor dependent on scattering cross section, geometry and optical collection efficiency and is constant from pulse to pulse. In Fig. II-1 bandwidth factors are displayed as a function of temperature for the anti-Stokes and Stokes Raman intensities for Gaussian shaped bandpasses (typical of interference filters) with bandwidths (FWHM) of 10, 50 and 100 Å. These were calculated for a laser operating at 5320 Å (e.g., frequency doubled neodymium) with an infinitesimally thin linewidth using the analysis described in Ref. II-11. Similar results would be obtained for triangular shaped bandpasses typical of monochromator slit functions (Ref. II-9). In Fig. II-2, the ratio of the anti-Stokes to Stokes bandwidth factors is shown as a function of temperature for bandwidths of 10, 50 and 100 Å. Of note is the near linearity displayed by the ratios at temperatures above 1250-1500°K.

The number of Stokes photoelectrons, S_i, generated by the Stokes photomultiplier can be expressed as

$$S_i = \eta^S m_i^S n_i^S \tag{II-2}$$

where η^S is the Stokes photomultiplier quantum efficiency and m_i^S, a factor to account for tube shot noise fluctuations. m_i^S will be Poisson distributed about unity (Ref. II-12) and can be written as

$$m_i^S = 1 + m_i^{S'} \tag{II-3}$$

where $\overline{m_i^S} = 1$, $\overline{m_i^{S'}} = 0$.

For an average photon flux from pulse to pulse of $\bar{n}$, the average number of photoelectrons created will be $\overline{\eta n}$. Here bars over symbols denote ensemble and not time averages. The actual number of photoelectrons will vary about the average from shot to shot with a variance given by $\sigma^2 = \overline{\eta n}$ (Ref. II-12). From the definition of the distribution variance, i.e. $[(p_i - \bar{p})^2]^{\frac{1}{2}}$, it can easily be shown that

$$\overline{m_i'^2} = \frac{1}{\overline{\eta n}} \tag{II-4}$$

FIG. II–1

BANDWIDTH FACTOR VARIATION WITH TEMPERATURE

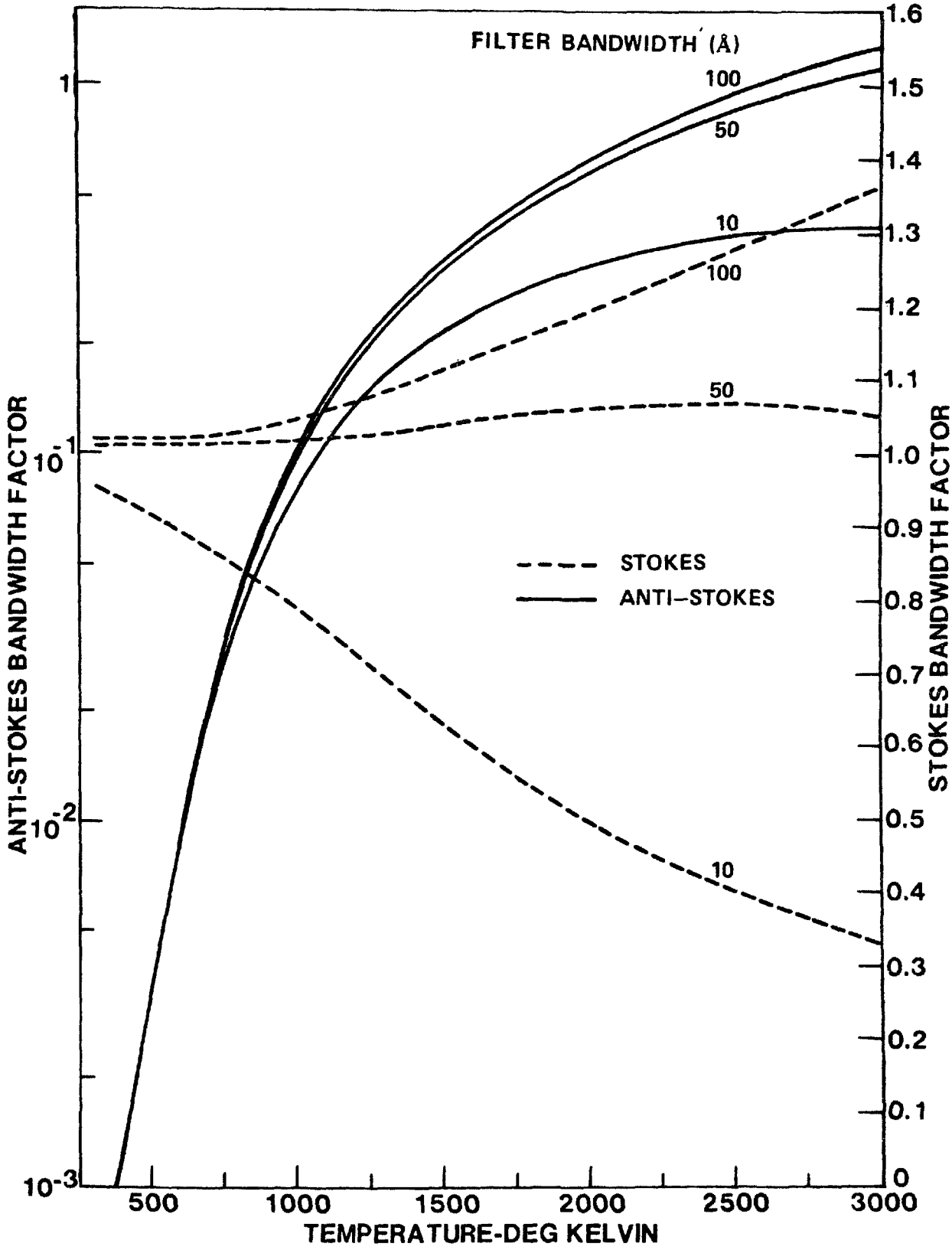

FIG. II–2

BANDWIDTH FACTOR RATIO VARIATION WITH TEMPERATURE

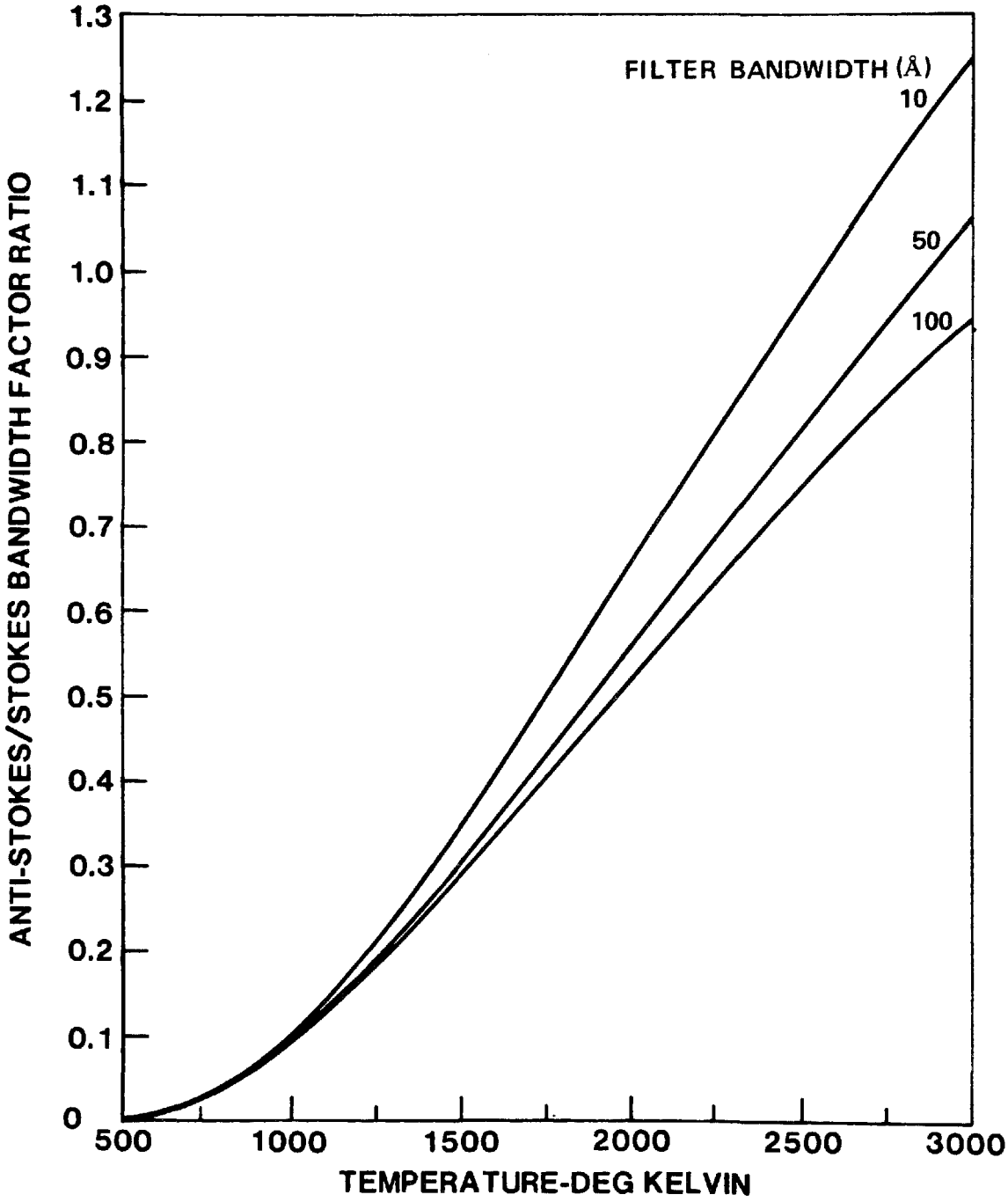

Density/Species Measurements

By combining Eqs. (II-1) and (II-2), the number density of the species of interest may be related to the measured number of Stokes photoelectrons

$$S_i = \eta^s m_i{}^s k^s N_i f^s(T_i) \epsilon_i \qquad \text{(II-5)}$$

By measuring the energy, ϵ_i, on each pulse, the number density can be measured to an accuracy dependent on the shot noise fluctuations and temperature. By proper bandwidth selection $f^s(T_i)$ can be made nearly independent of temperature (Fig. II-1) and the number density can be measured with an accuracy determined by the magnitude of the shot noise fluctuations. By signal averaging the energy normalized per pulse photoelectron yield, S_i^*, the average number density can be obtained

$$\overline{S^*} = \overline{\left(\frac{S}{\epsilon}\right)} \equiv \frac{1}{P} \sum_{i=1}^{P} \frac{S_i}{\epsilon_i} = \frac{\eta^s k^s f^s}{P} \sum_{i=1}^{P} N_i m_i{}^s \qquad \text{(II-6)}$$

Expressing N_i in terms of the mean and a fluctuation

$$N_i = \bar{N} + N_i' \quad \text{where } \overline{N_i'} = 0 \qquad \text{(II-7)}$$

and using Eq. (II-3)

$$N_i m_i{}^s = \bar{N} + N_i' + m_i{}^{s'} \bar{N} + N_i' m_i{}^{s'} \qquad \text{(II-8)}$$

Upon averaging

$$\frac{1}{P} \sum_{i=1}^{P} N_i m_i{}^s = \overline{(N_i m_i{}^s)} = \bar{N} \qquad \text{(II-9)}$$

the result following from the fact that $\overline{N_i' m_i{}^{s'}} = 0$. This arises due to the statistical independence of the number density fluctuations and shot noise fluctuations permitting $\overline{N_i' m_i{}^{s'}}$ to be separated to $\overline{N_i}\ \overline{m_i{}^{s'}}$ (Ref. II-13) which vanishes. Hence,

$$\left(\frac{\bar{S}}{\epsilon}\right) = \eta^s k^s f^s \bar{N} \qquad \text{(II-10)}$$

from which the average density is obtained after a suitable calibration.

Temperature Measurements

If the anti-Stokes to Stokes ratio is formed, the instantaneous number density and pulse energy cancel and a temperature measurement can be made from the ratio

$$R_i = \frac{k^a \eta^a f^a(T_i) m_i{}^a}{k^s \eta^s f^s(T_i) m_i{}^s} \tag{II-11}$$

with some error due to the shot noise term, $m_i{}^a/m_i{}^s$. Intuitively one might suspect these temperature measurement errors to cancel out over a large sample of measurements. However, this is not always the case. For example, consider the case of a laminar flame with constant (in time) temperature $\overline{T}$ at the measurement location. The ratio corresponding to this temperature will be denoted by R_o, i.e. $T(R_o) \equiv \overline{T}$. The measured ratio on any pulse will vary from R_o due to the shot noise fluctuations

$$R_i = R_o \frac{m_i{}^a}{m_i{}^s} = R_o + R_i' \tag{II-12}$$

The error in measured temperature from the true temperature can be obtained by expanding T about R_o

$$T(R_i) = T(R_o) + \frac{dT(R_o)}{dR} R_i' + \tfrac{1}{2} \frac{d^2T(R_o)}{dR^2} R_i'^2 \tag{II-13}$$

Expressing $m_i{}^a$, $m_i{}^s$ as in Eq. (II-3) and expanding $m_i{}^a/m_i{}^s$, R_i' can be shown to be

$$R_i' = R_o(m_i{}^{a'} - m_i{}^{s'} - m_i{}^{s'} m_i{}^{a'}) \tag{II-14}$$

for $m_i{}^{s'} \ll 1$. The maximum temperature error is approximately

$$\Delta T \simeq \frac{dT(R_o)}{dR} R_o \left(\frac{1}{\sqrt{\eta^s n^s T}} + \frac{1}{\sqrt{\eta^a n^a}} \right) \tag{II-15}$$

where m_i' has been assumed equal to the variance from Eq. (II-4) and the second drivative in Eq. (II-13) has been assumed equal to zero (Fig. II-2). The temperature measurement error at 2000°K for a 10 Å bandwidth can be estimated from Fig. II-2; $dT(R_o)/dR$ at 2000°K is approximately 1667 K deg. Assuming 1000 photons collected on both the anti-Stokes and Stokes channels and 10 percent quantum efficiencies, the maximum measurement error would be about 220°K, or $\pm$ 11 percent. If these erroneous measurements are averaged, substituting Eq. (II-14) into Eq. (II-13), one obtains

$$\overline{T(R)} = \overline{T} + \tfrac{1}{2} \frac{d^2T(R_o)}{dR^2} R_o{}^2 \left(\overline{m^{a'2}} + \overline{m^{s'2}} + \overline{m^{a'2} m^{s'2}} \right) \tag{II-16}$$

illustrating that shot noise fluctuations do not average out in general, but lead to an error in mean temperature for a non-zero second derivative. At high temperatures, the bandwidth ratios vary nearly linearly with temperature (Fig. II-2) resulting

in a very small or nonexistent second derivative. If the shot noise fluctuations are small enough so that the instantaneous ratios reside within the range of linearity, then averaging will yield the true average temperature even though each individual measurement is in error.

It should also be noted that in general $\bar{T}$ is not obtained from $\bar{R}$. Consider the situation of temperature measurements in a fluctuating medium with average temperature $\bar{T}$ where the instantaneous temperature can be measured quite accurately, i.e., shot and other noise being insignificant. Expanding R_i in a power series about $\bar{T}$

$$R_i = R(T_i) = R(\bar{T}) + \frac{dR(\bar{T})}{dT} T_i' + \frac{1}{2} \frac{d^2R(\bar{T})}{dT^2} T_i'^2 \qquad \text{(II-17)}$$

where $T_i = \bar{T} + T_i'$, T_i' being the deviation of temperature at any instant from the mean. Upon averaging one obtains

$$\bar{R} = R(\bar{T}) + \frac{1}{2} \frac{d^2R(\bar{T})}{dT^2} \overline{T_i'^2} \qquad \text{(II-18)}$$

Only in those cases where R is a linear function of T over the range of temperature fluctuations does $\bar{R} = R(\bar{T})$.

Very importantly it should be noted that the average temperature is not obtained from $\bar{A}/\bar{S}$ or equivalently $\bar{A}^*/\bar{S}^*$. $\bar{A}^*$ is obtained from

$$\overline{A^*} \equiv \left(\frac{\bar{A}}{\bar{\epsilon}}\right) = \frac{1}{P} \sum_{i=1}^{P} \frac{A_i}{\epsilon_i} = \frac{\eta^a k^a}{P} \sum_{i=1}^{P} N_i m_i^a f^a(T_i) \qquad \text{(II-19)}$$

Expanding $f^a(T_i)$ about $\bar{T}$

$$f^a(T_i) = f^a(\bar{T}) + \frac{df^a(\bar{T})}{dT} T_i' + \frac{1}{2} \frac{d^2f^a(\bar{T})}{dT^2} T_i'^2 \qquad \text{(II-20)}$$

and expressing density and temperature in terms of mean and fluctuating quantities one can show

$$\overline{A^*} = \eta^a k^a \left[\bar{N} f^a(\bar{T}) + \overline{N'T'} \frac{df^a(\bar{T})}{dT} + \frac{1}{2} \frac{d^2f^a(\bar{T})}{dT^2} \left(\bar{N}\overline{T'^2} + \overline{N'T'^2} \right) \right] \qquad \text{(II-21)}$$

This relation also derives from the fact that the shot noise fluctuations are statistically independent (i.e., uncorrelated) of fluctuations in medium properties (N', T'), so that terms such as $\overline{m_i^{a'} T_i'}$ are separable (Ref. II-13) to $\overline{m_i^{a'}}\ \overline{T_i'}$ and vanish. A similar relation pertains to $\bar{S}^*$; if the Stokes bandwidth factor is independent of temperature then Eq. (II-10) pertains and one obtains

$$\overline{A^*}/\overline{S^*} = \frac{\eta^a k^a}{\eta^s k^s f^s}\left[f^a(\bar{T}) + \frac{\overline{N'T'}}{\bar{N}}\frac{df^a(\bar{T})}{dT} + \frac{1}{2}\frac{d^2f^a(\bar{T})}{dT^2}\left(\overline{T'^2} + \frac{\overline{N'T'^2}}{\bar{N}}\right)\right] \qquad \text{(II-22)}$$

Hence the ratio of the separately averaged Raman band intensities depends not only on average temperature but also on the magnitude and correlation of the fluctuations in medium properties. Due to the exponential dependence of the anti-Stokes intensity (Fig. II-1) $\frac{df^a}{dT} > 0$ and $\frac{d^2f^a}{dT^2} < 0$, the last two terms in Eq. (II-22) tend to cancel the degree to which depends on the nature of the fluctuations.

Other Sources of Noise

There are diagnostic situations, particularly in relation to practical device probing, where despite limited bandwidth, polarization discrimination, high peak power and/or high focal flux diagnostic approaches (Ref. II-8) there are sources of noise, either naturally occurring or laser induced, present in the signal. Hence the number of Stokes photoelectrons for example, is then

$$S_i^* = \frac{S_i}{\epsilon_i} = \eta^s \frac{(n_i^s + n_i^{sn})}{\epsilon_i} m_i^s \qquad \text{(II-23)}$$

where n_i^{sn} are the number of "noise" photons in the Stokes bandpass. In this situation, the signal to noise ratio does not improve merely by averaging if the noise is more than a random occurrence. If another channel is placed in a spectral region adjacent to the Raman spectrum, the noise can be sampled assuming that it is fairly smooth spectrally. This is generally the case for laser modulated (Ref. II-8) or naturally occurring soot incandescence. The noise sampling channel will detect SN_i noise photoelectrons

$$SN_i^* = \frac{SN_i}{\epsilon_i} = \frac{\eta^s n_i^{sn} m_i^{sn}}{\epsilon_i} \qquad \text{(II-24)}$$

where for simplicity the quantum efficiency is considered the same for each tube. The desired "signal" can be obtained by subtracting the Stokes noise from the Stokes with the result

$$\mathscr{S}_i = S_i^* - SN_i^* = \frac{\eta^s n_i^s m_i^s}{\epsilon_i} + \frac{\eta^s n_i^{sn}}{\epsilon_i}(m_i^s - m_i^{sn}) \qquad \text{(II-25)}$$

the subtraction being imperfect due to the uncorrelated shot noise on each tube. Upon sufficient signal averaging, Eq. (II-25) becomes

$$\overline{\mathscr{S}} = \eta^s\left(\frac{\overline{n_i^s m_i^s}}{\epsilon_i}\right) + \eta^s\left[\left(\frac{\overline{n_i^{sn} m_i^s}}{\epsilon_i}\right) - \left(\frac{\overline{n_i^{sn} m_i^{sn}}}{\epsilon_i}\right)\right] \qquad \text{(II-26)}$$

Again due to the statistical independence of the shot noise and the signal photons, the $(\frac{n}{\epsilon})m$ term is separable and the first term simplifies to $\eta^s(\frac{n^s}{\epsilon})$. If the fluctuations in pulse energy are small permitting the denominator in the second term to be expanded, it can be shown that this term vanishes resulting in

$$\overline{\mathscr{S}} = \eta^s\overline{(\frac{n^s}{\epsilon})} = \eta^s k^s \bar{N} \left[f^s(T) + \frac{\overline{N'T'}}{\bar{N}} \frac{df^s(\bar{T})}{dT} + \frac{1}{2} \frac{d^2 f^s(\bar{T})}{dT^2} \left(\overline{T'^2} + \frac{\overline{N'T'^2}}{\bar{N}} \right) \right] \qquad \text{(II-27)}$$

As before if $f^s(T)$ is designed to be constant with temperature, the average number density can be obtained. A similar result would be obtained if the signal and noise channels were separately averaged, then subtracted.

Similarly $\overline{\mathscr{A}}/\overline{\mathscr{S}}$ can be shown to be independent of shot and background noise effects resulting in Eq. (II-22). $\overline{\mathscr{A}}/\overline{\mathscr{S}}$ is not a measure of average temperature alone but depends on the magnitude and correlation in the fluctuations.

If the ratio $\mathscr{A}_i/\mathscr{S}_i$ is formed first, the situation is analytically intractable. If $\mathscr{A}_i$ and $\mathscr{S}_i$ are expressed in a form (From Eq. II-25)

$$\mathscr{S}_i = \frac{\eta^s n_i^s m_i^s}{\epsilon_i} + RE \frac{n_i^{sn}(m_i^s - m_i^{sn})}{n_i^s m_i^s} \qquad \text{(II-28)}$$

where RE deontes the relative error, then $\mathscr{A}_i/\mathscr{S}_i$ can be cast into a form similar to Eq. (II-12) permitting an R_i' to be defined. Although the situation is still intractable, it was shown in the discussion following Eq. (II-12) that errors in a set of "instantaneous" "temperature" measurements would not average out and that an erroneous average temperature would result, Eq. (II-16), for a nonzero second derivative. Here an erroneous temperature measurement will result with each laser pulse except for the extremely rare instance when the shot noise on the four channels is the same. The measured averaged temperature will depart from the time average (averaging Eq. (II-13))

$$\overline{T(R_i)} - \bar{T} = \frac{dT(R_o)}{dR} \overline{R_i'} + \frac{1}{2} \frac{d^2T(R_o)}{dR^2} \overline{R_i'^2} \qquad \text{(II-29)}$$

depending upon $\overline{R_i'}$ (not necessarily zero in the background subtraction situation) and $\overline{R_i'^2}$. These terms will be dependent on the signal and noise levels in a particular situation.

Implications of Signal Averaging

There are a number of conclusions which can be drawn from the foregoing analyses. In measurement situations where the anti-Stokes and Stokes intensities cannot be determined to a high level of accuracy, the density and temperature measured at each instant will, of course, be erroneous. Quite importantly the average of these

erroneous measurements may not yield the true average, but may depart from the true average depending on the magnitude of the gasdynamic and shot noise fluctuations. Average density measurements appear possible in the presence of shot and/or background noise if the Stokes bandwidth factor is designed to be independent of temperature. In this case, the time averaged density is obtained from the averaged Raman data despite the character of the fluctuations. The situation with temperature measurements is less fortuitous. True average temperature can be obtained by signal averaging Raman data in the presence of shot noise only if: (1) the anti-Stokes to Stokes ratio is first formed, (2) by manipulation of spectral bandwidths and center frequencies, the anti-Stokes/Stokes ratio is made a linear function of temperature over the "temperature" range of interest. By "temperature" range is meant the temperature inferred from the measured anti-Stokes to Stokes ratio; this range may well be considerably larger than the actual physical temperature range. This would be the case for example when subtracting out large background interferences; and (3) the fluctuations in temperature are within the range of linearity. In this case the second derivative of the temperature with anti-Stokes to Stokes ratio vanishes prohibiting temperature fluctuation terms from accumulating during averaging. When fluctuations are very large, so as to extend beyond the range of ratio linearity as may be the case in practical combustor devices (Ref. II-3), accurate average temperature measurements cannot be made. When anti-Stokes and Stokes data are separately averaged, background can be subtracted on average and shot noise terms will average to zero. However, temperature inferred from the ratio of averaged anti-Stokes to averaged Stokes will not be the average temperature but will depart from the true average depending on the magnitudes and correlations of the fluctuations.

APPENDIX II

References

II-1. F. C. Gouldin: "Role of Turbulent Fluctuations in NO Formations," Comb. Sci. and Tech., Vol. 9, pp. 17-23 (1974).

II-2. W. P. Jones: "The Effect of Temporal Fluctuations in Temperature on Nitric Oxide Formation," Comb. Sci. and Tech., Vol. 10, pp. 93-96 (1975).

II-3. R. R. Dils and P. S. Follansbee: "Wide Bandwidth Gas Temperature Measurements in Combustor and Combustor Exhaust Gases," presented at the 22nd International Instrumentation Symposium of ISA, San Diego, CA (May 1976).

II-4. C. M. Ho, K. Jakus and K. H. Parker: "Temperature Fluctuations in a Turbulent Flame," Comb. and Flame, Vol. 27, pp. 113-123 (1976).

II-5. D. F. G. Durao and J. H. Whitelaw: "Instantaneous Velocity and Temperature Measurements in Oscillating Diffusion Flames," Contemp. Phys., Vol. 17, pp. 249-274 (1976).

II-6. M. Lapp and C. M. Penney: Laser Raman Gas Diagnostics, Plenum Press, New York (1974).

II-7. S. Lederman, M. H. Bloom, J. Bornstein, and P. H. Khosla: "Temperature and Species Concentration Measurements in a Flow Field," Int. J. Heat Mass Trans., Vol. 17, pp. 1479-1486 (1974).

II-8. A. C. Eckbreth: "Laser Raman Thermometry Experiments in Simulated Combustor Environments," AIAA Paper 76-27, 14th Aerospace Sciences Meeting, Washington, DC (January 1976).

II-9. R. E. Setchell: "Time Averaged Measurements in Turbulent Flames Using Raman Spectroscopy," AIAA Paper 76-28, 14th Aerospace Sciences Meeting, Washington, DC (January 1976).

II-10. S. S. Lazdinis: "Influence of Fluctuations in Electron Beam Diagnostics," AIAA J., Vol. 14, pp. 133-134 (February 1976).

II-11. A. C. Eckbreth: "Laser Raman Gas Thermometry," AIAA Paper 74-1144, AIAA/SAE 10 Propulsion Conference, San Diego, CA (October 1974).

II-12. Photomultiplier Manual, RCA Technical Series, PT-61 (1970).

II-13. W. B. Davenport and W. L. Root: Random Signals and Noise, McGraw-Hill, NY (1958)

TECHNICAL REPORT DATA
(Please read Instructions on the reverse before completing)

1. REPORT NO.	2.	3. RECIPIENT'S ACCESSION NO.
EPA-600/7-77-066		

4. TITLE AND SUBTITLE	5. REPORT DATE
REVIEW OF LASER RAMAN AND FLUORESCENCE TECHNIQUES FOR PRACTICAL COMBUSTION DIAGNOSTICS	June 1977
	6. PERFORMING ORGANIZATION CODE

7. AUTHOR(S)	8. PERFORMING ORGANIZATION REPORT NO.
A. C. Eckbreth, P. A. Bonczyk, and J. F. Verdieck	

9. PERFORMING ORGANIZATION NAME AND ADDRESS	10. PROGRAM ELEMENT NO.
United Technologies Research Center East Hartford, Connecticut 06108	EHE624
	11. CONTRACT/GRANT NO.
	68-02-2176

12. SPONSORING AGENCY NAME AND ADDRESS	13. TYPE OF REPORT AND PERIOD COVERED
EPA, Office of Research and Development Industrial Environmental Research Laboratory Research Triangle Park, NC 27711	Task 1 Final: 10/76-3/77
	14. SPONSORING AGENCY CODE
	EPA/600/13

15. SUPPLEMENTARY NOTES IERL-RTP project officer for this report is William B. Kuykendal, Mail Drop 62, 919/549-8411 Ext 2557.

16. ABSTRACT The report gives results of a detailed examination of four techniques for practical combustion diagnostics: spontaneous and near-resonant Raman scattering, laser fluorescence, and coherent anti-Stokes Raman scattering (CARS). For diagnosis of highly luminous, particle-laden flames (e.g., in hydrocarbon-fueled primary combustion zones), spontaneous and near-resonant Raman scattering appear to possess a low probability for successful application, even with advanced state-of-the-art laser sources. However, for clean flame diagnostic or probing of environments with modest particulate levels (e.g., some secondary combustion and exhaust/plume regions), spontaneous Raman scattering is very attractive due to its simplicity, high level of understanding, and advanced state of development. Laser fluorescence appears capable of species concentration measurements to 10's of ppm for selected molecules whose absorptions can be saturated. In this way, fluorescence magnitudes do not depend on quenching effects. CARS appears to be capable of successful thermometry and majority constituent measurements in practical flame environments, although some jeopardies need to be experimentally investigated. Potential detectivities in the 10-100 ppm range may be possible using sophisticated variants of the CARS technique.

17. KEY WORDS AND DOCUMENT ANALYSIS

a. DESCRIPTORS		b. IDENTIFIERS/OPEN ENDED TERMS	c. COSATI Field/Group
Air Pollution	Fluorescence	Air Pollution Control	13B 20F
Combustion	Exhaust Gases	Stationary Sources	21B
Flames	Plumes	Laser Fluorescence	
Measurement	Temperature Measurement	Particulates	14B
Raman Spectroscopy			
Coherent Scattering			20H
Lasers			20E

18. DISTRIBUTION STATEMENT	19. SECURITY CLASS *(This Report)*	21. NO. OF PAGES
Unlimited	Unclassified	173
	20. SECURITY CLASS *(This page)*	22. PRICE
	Unclassified	